PLANETARY GEARBOX CONDITION MONITORING BASED ON MODULATION ANALYSIS

GABALLA M ABDASALM ABDALLA

A thesis submitted to the University of Huddersfield in partial fulfilment of the requirements for the degree of Doctor of Philosophy

University of Huddersfield

March 2017

Abstract

The epicycle gearbox or planetary gearbox (PG) is a central power transmission systems of important machines such as helicopters and wind turbines which are mission critical and high cost systems. Condition monitoring (CM) has been explored extensively in recent years to avoid any unexpected interruptions and severe accidences caused by faults PGs. Although, considerable advancements in CM techniques, there still existed significant deficiency such as insensitivity, false diagnosis and high costs in implementing such techniques in industries. To improve CM techniques, therefore, this thesis focuses on an investigation of advanced signal analysis techniques such as higher order spectra (HOS) in order to achieve full characterisation of the nonlinear modulation processes of PG dynamics and thereby develop accurate diagnostic techniques.

The lumped mass model is established for modelling the dynamic behaviour of the PG under investigation, which allows the vibration behaviours to be understood for analysing different abnormalities such as tooth breakages and gear errors. This paves the way for subsequent data analytics and fault diagnostics using modulation signal bispectrum (MSB) that allows the vibration data to be examined through HOS, but it is significantly efficient in characterising the multiple and nonlinear modulations of PG dynamics alongside superior noise reduction performance.

Different degrees of misalignments in the PG drive system has been investigated and successfully diagnosed using MSB analysis of vibration measurements.. Moreover, the investigation included detection of tooth breakage faults of different severities in both the sun and a planet gear. The tooth faults were diagnosed using the recently developed MSB through accurately representation and estimate of residual sidebands induced by these faults. Consequently, MSB analysis produces an accurate and reliable diagnosis in that it gives correct indication of the fault severity and location for wide operating conditions.

Furthermore, these fault diagnosis practices allows the establishment of residual sideband analysis approach. These residual sidebands resulting from the out-of-phase superposition of vibration waves due to asymmetric, multiple meshing sources are much less influenced by gear errors than the in-phase sidebands due to faults or new occurrences of the symmetricity.

MSB can provide an accurate characterisation of the residual sidebands and consequently produces consistent diagnosis as confirmed by both simulation and experiment.

Acknowledgements

Firstly, the most important acknowledgement goes to God for being my main support, providing both guidance and light during my university career. Without Him I could never successfully achieve any of the opportunities I have been given in my life. All my achieved goals are thanks to Him.

I would like to express my sincere acknowledgment and deepest gratitude to my supervisor: **Prof. Andrew Ball,** for his contributions assisting me with my studies and for sharing his valuable knowledge in several key areas. Working for you is an honour, an experience that I will truly treasure. Thanks.

My thanks are also extended to **Dr. Fengshou GU**, who taught me how to question thoughts and express ideas. His patience and support helped me overcome many crisis situations and to finish my research work, I also owe thanks to him for providing me with the necessary support and supervision to make possible this big step of obtaining a PhD research degree.

Very special thanks and appreciation to my college friends for their continuous support and for the unforgettable moments we spent together during last four years.

My Doctor of Philosophy (PhD) journey would not have been possible without the support of my family. In particular I would like to thank my parents for encouraging me in all of my study stages and for inspiring me to follow my dreams, also for supporting me both emotionally and financially. I always knew that you believed in me and wanted the best for me. Thank you for teaching me that my job in life is to learn, to be happy and to know and understand myself, only then could I know and understand others. For both of you, Mom and Dad, thank you to my mother, ***Kinz***, my father ***Muftah***, and to my family ***Merahil, Ragad, Ahmad, Muftah and Retal***.

Statement of Originality

I hereby certify that all of the work described within this thesis is the original work of the author. Any published (or unpublished) ideas and/or techniques from the work of others are fully acknowledged in accordance with the standard referencing practices.

(Gaballa M Abdalla)

(October, 2016)

VITA

June 2001..... Bachelor of Mechanical (BSc)
Engineering Omar Al-Mukhtar University
Libya

March 2011..... Master of Mechanical (MSc)
Engineering and Design
University of Huddersfield
United Kingdom

FIELDS OF STUDY

Major Field: Mechanical Engineering

Focus on Condition Monitoring.

List of Publications

- Abdalla, G, Ball, A. and Gu, F. (2013) 'Fault Detection and Diagnosis of Ball Bearing Using Advanced Vibration Analysis Techniques. *In Proceedings of Computing and Engineering Annual Researchers' Conference 2013 (Poster): CEARC'13*. Huddersfield: University of Huddersfield. P.224. ISBN 9781862181212.
- Gaballa M Abdalla, Xiange Tian, Zhi Chen, Dong Zhen, Fengshou Gu and Andrew Ball, (2014) Misalignment Diagnosis of A Planetary Gearbox Based On Vibration Analysis, *The 21st International Congress on Sound and Vibration, Beijing, China, 13-17 July, 2014.*
- Fengshou Gu, Gaballa M Abdalla, Haijun Xu, and Andrew D. Ball A, (2014). A Novel Method for the Fault Diagnosis of a Planetary Gearbox based on Residual Sidebands from Modulation Signal Bispectrum Analysis. *COMADEM 2014, Brisbane Convention and Exhibition Centre, Australia 16-18 September 2014.*
- Xiange Tian, Gaballa M. Abdalla, Ibrahim Rehab, Fengshou Gu and Andrew D. Ball (2015). Diagnosis of Combination Faults in a Planetary Gearbox using a Modulation Signal Bispectrum based Sideband Estimator. *Proceedings of the 21st International Conference on Automation & Computing, University of Strathclyde, Glasgow, UK, 11-12 September 2015.*
- Tian, Xiange, Gu, Fengshou, Rehab, Ibrahim, Abdalla, Gaballa and Ball, Andrew (2015) A robust fault detection method of rolling bearings using modulation signal bispectrum analysis. *In: 28th International Congress of Condition Monitoring and Diagnostic Engineering Management (COMADEM 2015), 1st - 4th December 2015, Buenos Aires, Argentina.*

List of Contents

List of Figures

List of Tables

List of Abbreviations

AM	Amplitude modulation
CBM	Condition Based Monitoring
CIM	Computer Integrated Manufacturing
CM	Condition Monitoring
CF	Crest factor
CWT	Continuous Wavelet transforms
DAS	Data Acquisition System
DC	DC generator
DOF	Degree of freedom
Enc	Encoder
F	Force
FE	Finite element
FM	Frequency Modulation
F1	Small faults on sun gear
F2	Large faults on planet gears
FT	Fourier transforms
FFT	Fast Fourier transforms
GDM	Gear dynamic models
Hz	Hertz
IAS	Instantaneous Angular Speed
ICP	Integrated Circuit Piezoelectric Accelerometers
IEPE	Integral Electronic Piezoelectric Accelerometers
ISO	International Standard Organisation
kW	kilo-Watt
kHz	kilo-Hertz
MSB	Modulation Signal Bispectrum
MSB-SE	Modulation Signal Bispectrum and Sideband Estimator
MTTF	The mean-time-to-failure
NLTE	No-load transmission error

PG	Planetary Gearbox
PM	Preventive Maintenance
PPR	Pulse Per Revolution
PV	Peak value
RM	Reactive Maintenance
RMS	Root mean square
RPM	Revolution Per Minute
SDOF	Single degree of freedom
STFT	Short-time Fourier transforms
TSA	Time Synchronous Averaging
WT	Wavelet transforms
WVD	Wigner-Ville distribution
a	Acceleration
c	Carrier
g	Gravity =9.81 m/s^2
m	Modulation factor
m	Mass
p	Planet gear
r	Ring gear
s	Sun gear

List of Nomenclature

θ	Torsional angular displacement
$\dot{\theta}$	Torsional angular velocity
$\ddot{\theta}$	Torsional angular acceleration
C	Damping matrix
K	Mesh stiffness matrix
I_p	Moments of inertia of the planet
I_s	Moments of inertia of the sun
I_r	Moments of inertia of the ring
I_c	Moments of inertia of the carrier
T_s	Sun gear output torque
T_c	Carrier input torque
α	Pressure angle
α_r	Pressure angle of the ring –planet mesh
α_s	Pressure angle of the sun–planet mesh
q	Forced vibration response vector
ψ_n	Fixed angles which specified as Circumferential planet locations
ψ_{si}	Pressure angle of the sun-planet mesh
ψ_{pi}	Pressure angle of the ring-planet mesh
e_{rn}	Transmission error for ring-planet
e_{rpi}	Transmission error for sun-planet
e_{spi}	Transmission error for planet-ring
I_p	Moments of inertia of the planet
I_s	Moments of inertia of the sun
Z_r	Ring gear
Z_p	Planet gear
Z_s	Sun gear
N	The number of planet
i	Transmission Ratio
f	Frequency
m	Mass

r	Radius
d	Diameter
x, y	Translations
t	Time
k	Gear mesh stiffness
c	Gear mesh damping coefficient
spi	Gear pair of sun gear/planet gear
rpi	Gear pair of ring gear/planet gear
pi	*i th* planet gear
k_{sp}	Mesh stiffness between sun gear and planet gear
k_{rp}	Mesh stiffness between ring gear and planet gear
$k_p = k_r = k_s = k_c$	Bearing stiffness
k_{ru}	Torsion stiffness
f_s	Sampling frequency

CHAPTER ONE

INTRODUCTION, BACKGROUND AND MOTIVATION

The chapter begins with the background to the industrial applications of condition monitoring, followed by a description of maintenance strategies and their application to planetary gearbox condition monitoring, the chapter then describes the motivation for this research programme, and the overall aim and objectives of the research programme. Finally, the structure of the thesis is presented and the content of the remaining chapters is outlined.

1.1 Condition Monitoring Background

Condition monitoring (CM) is increasingly used in industry, especially in engineering departments, where it can reduce both maintenance cost and operational power consumed and also provide a significant improvement in the ongoing availability of plant (Svetlitsky 2012). CM involves the continuous or periodic assessment of the condition of a system or a component of equipment. Today these assessments can be achieved whilst the system is operational. CM allows fault detection and diagnosis and can provide an estimate of the expected time to system/component failure.

CM has many benefits, the most significant being:

- Reducing maintenance costs and avoiding unnecessary replacement of components.
- Improving system reliability and safety, with a consequent decrease in human injuries.
- Upgrading production quality at a lower cost price.
- Improving competitiveness and profitability.
- Predicting time to failure thus determining the remaining useful life of a component.
- Can be applied selectively, mainly to those machine components known to fail most frequently.

Integrating CM techniques can provide highly accurate criticality and failure-mode analysis to identify where improvements in machine availability and reductions in maintenance costs can be achieved (Lei, Lin et al. 2014). This approach involves selecting appropriate modes of CM, such as online or offline vibration monitoring and online or offline performance monitoring based on the criticality of the machine and its modes of failure. It can be used to optimise the CM system to effectively achieve specified objectives for the lowest total cost (Lei, Lin et al. 2014).

Criticality and failure mode analysis now also include consideration of total production output and manufacturing efficiency, since these aspects of plant operation are important to total operational costs and production output, hence bottom line profits of, for example, large-scale power generation facilities (Márquez, Tobias et al. 2012). The maintenance interval is determined by the condition of the machine. This is quite different to a scheduled maintenance programme, where a machine is serviced after a specific period of time

irrespective of its condition, and to a breakdown maintenance programme, where a machine is allowed to run until it fails. CM systems comprise of combinations of sensors and signal processing equipment that provide continuous indications of component (e.g. wind turbine) conditions based on techniques which include noise and vibration analysis, ultrasonic analysis, thermal imaging, lubricating oil analysis and strain measurement (Márquez, Tobias et al. 2012).

The vibration signals measured on the external surfaces of machines can contain vital information about internal processes and provide valuable information on the condition of the machine. When machines are in good condition their vibration frequency spectra have characteristic shapes, but as faults begin to develop the frequency spectra changes. Previous experience and fundamental vibration analysis provides the background and techniques that allow successful identification of the likely sources of modifications to the vibration signals produced by mechanical systems in the presence of wear and/or faults (Norton and Karczub 2003).

Whilst vibration analysis is the most commonly used CM technique (Irene Hamernick 2006), other techniques include; metallurgical failure and wear debris analysis, which are often used as supplementary diagnostic tools, and electrical current spectral analysis, which is sometimes used for the CM of electrical drives such as generators and large induction motors. Performance monitoring is able to provide additional information on plant deterioration due to fouling, leakage, wear and over-firing that cannot be readily assessed using more traditional CM techniques (Harris and Kotzalas 2006).

CM of industrial rotating machines has been an active field of research for best part of one hundred years (Harris and Kotzalas 2006). There is a real demand for reliable procedures that will allow relatively inexperienced users to detect and characterise fault conditions in an operating system without interrupting normal running. CM is the heart of predictive maintenance research; to produce a diagnostic procedure that will automatically and accurately detect and diagnose incipient faults in operational machines. Mechanical component faults generally progress through a series of degradation states before failure, if such running condition can be detected and characterised, then proactive as well as

corrective maintenance can be performed before a catastrophic failure occurs (N Tandona 1999; Komgom N. Christian 2007).

1.2 Impact and Procedures of Maintenance

For all production and manufacturing plant, a major portion of total operating costs is maintenance. Each year, nearly $60 billion is lost due to ineffective maintenance management (R. Keith Mobley 2002).Proper maintenance has a drastic effect upon the quality of the manufactured products, which is important in a highly competitive world market. US industry has been significantly adversely affected by low product quality and loss of production time due to ineffective maintenance management (Paz, Leigh et al. 1994).

Ineffective management mostly occurs due to the lack of ability to quantify factual data regarding requirements for maintenance and/or repair. Analysis of data trends provides a statistical prediction of when an item of equipment will fail and maintenance scheduling may be carried out accordingly. However, this may not be the most productive decision since the fault may develop much faster than predicted (leading to catastrophic failure) or much less than predicted which means the replacement will be carried out too soon (Mobley 2002; R. Keith Mobley 2002).

Until now, corporate management have not been able to quantify the importance of maintenance with regard to bottom line profit, production costs and product quality. Until about twenty years ago it was commonly believed that maintenance was a necessary evil, and it was impossible to reduce maintenance costs in any substantial way (R. Keith Mobley 2002). However today, technology allows computer based instrumentation and microprocessors to monitor systems, machinery and plant equipment to a degree that accurately determines machine failure, significantly reducing the negative effects of inefficient maintenance operations and unnecessary repairs, with a consequent increase in profitability (Mobley 2002).

1.2.1 Maintenance Management Methods

It is essential to consider the traditional management techniques as a first priority for understanding the predictive maintenance management programme. Two kinds of

maintenance management have been traditionally carried out on process and industrial plants, see Figure 1.1.

- Preventive maintenance.
- Corrective maintenance.

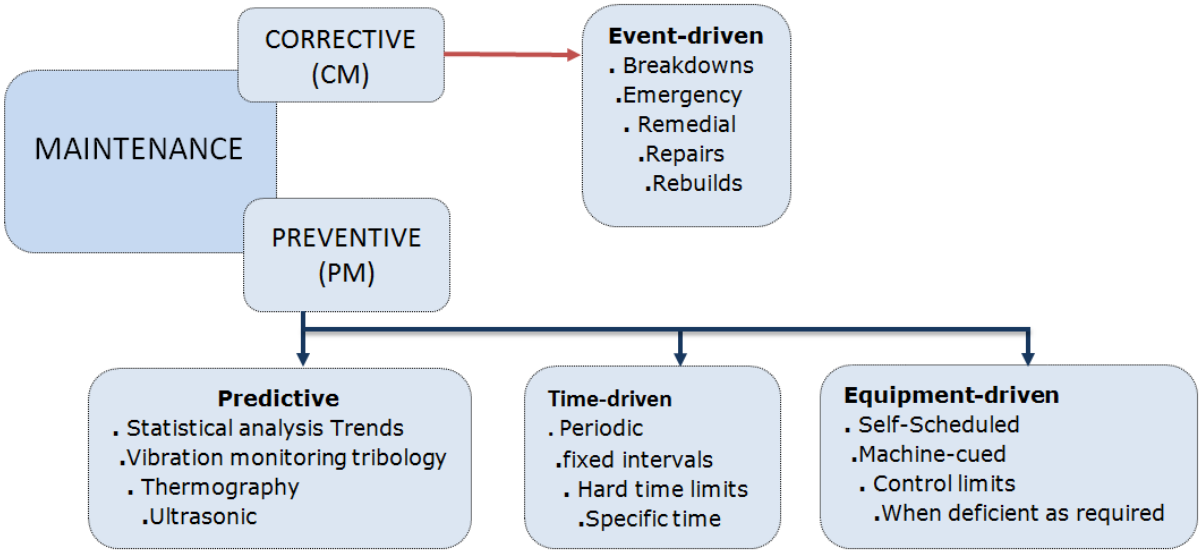

Figure 1.1 Traditional maintenance structure

1.2.1.1 Preventive Maintenance PM

Preventive maintenance has various definitions but the management programme for this kind of maintenance is time-based. Hours of operation or elapsed times are used for scheduling of the maintenance tasks. A typical machine's statistical life is shown in Figure 1.2. Probability of failure is indicated by the mean-time-to-failure (MTTF) or bathtub curve. During the first few weeks of operation, installation issues are the major reasons for high failure rate resulting in a lengthy period of low failure probability. Depending on the specific classification of the machine it is expected to degrade over a specified time frame according to preventive maintenance management programmes. Failure probability rises as the machine nears the end of its working life.

The MTTF is a basic statistic used for the scheduling of rebuilding or repairing machinery in preventive maintenance management (Mobley 2002; Ganguly, Kowar et al. 2012).

A thorough comparison between advantages and disadvantages of preventive maintenance must be made to fully understand its importance as summarised in Appendix A.

Generally, the use of condition monitoring and on-condition techniques is preferred to a programme where items of plant and machinery are replaced at fixed intervals.

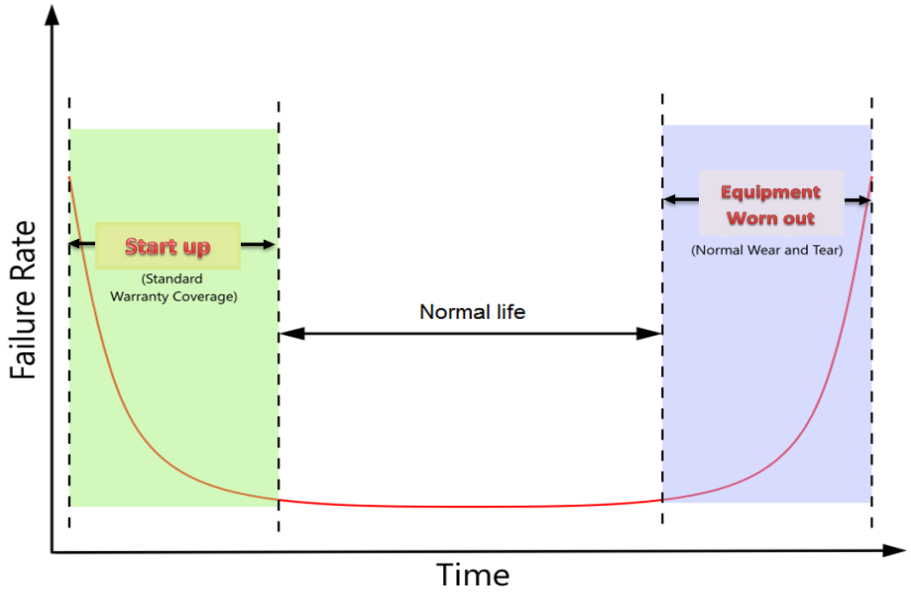

Figure 1.2 Mean time to failure (Bathtub curve) reproduced from (Hanson 2015)

1.2.1.2 Predictive Maintenance

There are various definitions for predictive maintenance. According to some workers, the monitoring of rotating machinery to predict and prevent any catastrophic failures is predictive maintenance. Some others state that it is the detection of developing issues such as through infrared images of electrical equipment like motors or switch gear (R. Keith Mobley 2002).

The actual mechanical condition is regularly monitored during predictive maintenance along with the operating efficiency and other machine train condition indicators. Through this process of system monitoring, the desired information can be extracted and it becomes possible to determine the maximum permitted repair time interval, minimising the costs associated with machine failures (R. Keith Mobley 2002).

As stated above, vibration monitoring is the most common of predictive maintenance techniques. Here, two basic phenomena are associated with the vibration signature analysis.

1- Certain common failure modes exhibit distinct vibration frequencies which can be isolated and identified.
2- In the presence of a fault there will be a change in the operating dynamics, which can be seen as a change in the amplitude of distinct vibration components within the signal.

These phenomena allow failure modes and their root causes to be identified allowing plant engineers and maintenance managers to attain optimum availability and reliability from their plants (Mobley 2002). Predictive maintenance can also be applied to improve the operating efficiency of non-mechanical plant equipment and systems as it includes process efficiency, non-destructive techniques and heat loss.

1.2.1.3 Corrective Maintenance

Maintenance is usually corrective as repairs are invariably required. Emergency corrections may, however, be reduced through efficient maintenance procedures. If there is an obvious problem, it can be detected easily. For example, a broken drive shaft will be easily identified by human operatives and the appropriate remedial actions taken. However, maintenance time is mostly taken up by diagnostic fault detection and troubleshooting, thus automatic diagnostic techniques are used to detect hidden defects and intermittent failures (Mobley 2002).The basic idea is to correct the defects at the lowest cost possible (Mobley 2002). Viable preventive maintenance makes it possible to detect and manage failure issues and causes before there is a breakdown.

1.2.2 Machinery Condition Monitoring and Diagnosis

Monitoring has been defined as the machine, system or process performance regulation. At the same time, diagnosis refers to the extraction of information regarding the issues related to the machine. The symptoms are assessed with regard to the system or the process, specifically suspicious symptoms along with their causes. Terms such as estimation, identification, in-process evaluation, online inspection, fault detection and fault prediction are used to describe such an activity.

For Computer Integrated Manufacturing (CIM) systems, diagnosis and monitoring are integrated. It is essential to control and monitor CIM systems continuously to ensure the processes and machines are operating efficiently. For instance, tool condition monitoring is essential for automated machining cells as scratched parts would be produced by broken or worn-out tools. However, it is difficult to monitor and diagnose the processes and machines due to their level of complexity. It is essential to include sensing, signal processing, cost-effective implementation and decision making techniques. A standard structure for engineering monitoring and diagnoses is shown in Figure 1.3. though of course, individual systems, processes and machines will differ (Leondes 2000).

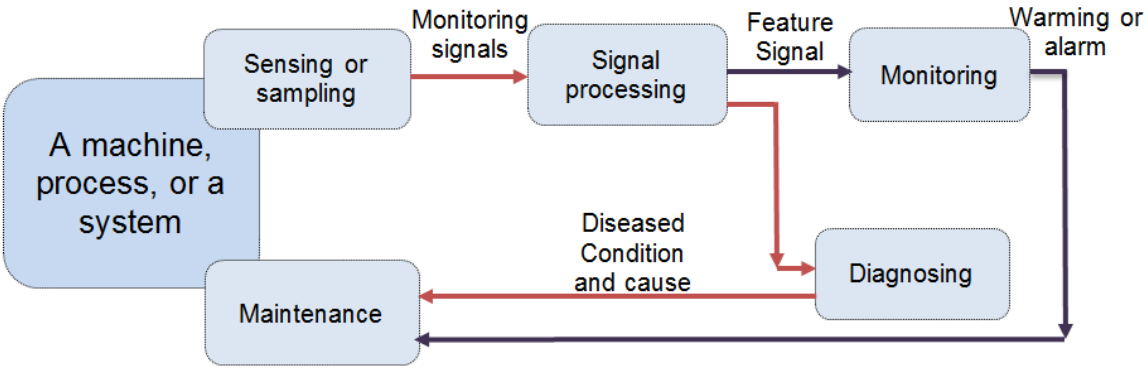

Figure 1.3 A Unified model for engineering monitoring and diagnosis

Figure 1.3 shows that the signal representing the system's health condition must be included in the system input as signals from the sensors. Noise affects these signals and signal processing is used to capture the features of the signals. The system conditions are estimated based on these feature signals. Because the required signal is often hidden in noise, it is usually impossible to attain feature signal critical information without signal processing (Adams 2009). It is possible to use several sensory signals based on the application of, for instance, vibration (displacement and/or acceleration), pressure, force, voltage, acoustic emission, audible noise, optic image, temperature and pressure.

The process of change in the machine condition is observed through a deterministic signal variation. As an illustration, the change may be due to electrical issues, even short circuiting, arising from an unwarranted increase in motor temperature. Alternatively the issues might be mechanical, a scratched bearing or a broken gear tooth.

Not only noise but also process working conditions affect the measured sensor signals. In the latter case the load on a motor and rotational speed may be the variations in process working conditions. Here, power supply fluctuation can be included as part of the noise disturbances. Using signal processing, the noise disturbances and effects of working conditions can be reduced. With graphical representation, there can be complicated arabesques, which represent the hidden signals that indicate all necessary information. The features from the signal can be captured using signal processing and used to characterise the condition of the system (Leondes 2000; Adams 2009; Lei, Zuo et al. 2010).

1.2.3 Planetary Gearbox Condition Monitoring

Condition monitoring and fault detection of gear transmission systems have attracted considerable attention in recent years due to the desire to minimise bottlenecks in production and to reduce the extent of secondary damage caused by failures (Bajrić, Sprečić et al. 2011). However, most investigations and researchers have focussed on fixed-axis gearboxes in which the gears are designed to rotate around their own fixed centres. Much less research has been done on condition monitoring of planetary gear sets. This is largely due to the relative complexity of planetary gear sets (Lynwander 1983; Wang, Wang et al. 2014).

Planetary gears are fundamentally different from fixed-axis gearboxes; an elementary planetary compound gear system is shown in Figure 1.4. The gear system contains a ring gear, a sun gear that rotates around its own centre, and several planet gears that not only rotate around their own centres but also revolve around the centre of the sun gear. With such a complex gear transmission structure, planetary gearboxes exhibit unique behaviours which invalidate fault diagnosis methods that work well for fixed axis gearboxes (Lei and Zuo 2009; Zhou, Wu et al. 2012).

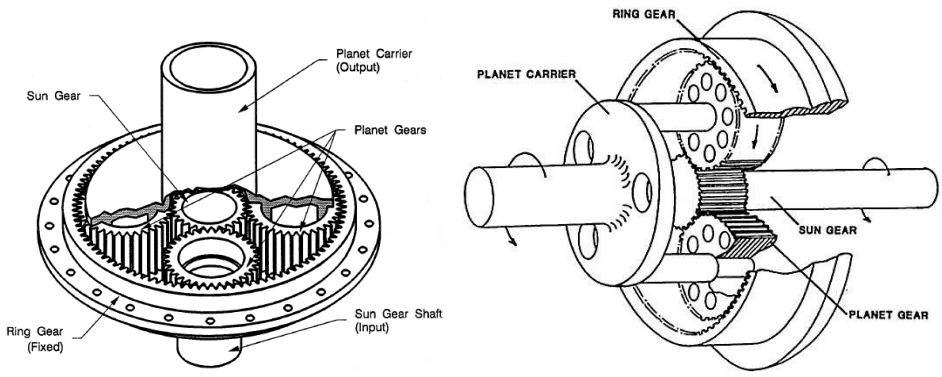

Figure 1.4 Planetary gear set reproduced from (D. Vijayaraghavan 2005)

The common planetary gear system configuration is where the drive shaft rotates the sun gear and the planet gears, held by the carrier-mesh with the sun and ring gear. The planetary gear set can be configured to have certain gears fixed or rotating, depending on the requirements of the application. This allows variation of the gear ratios and torque characteristics. In many applications, the sun gear is driven by the input shaft. In comparison with parallel shaft gearboxes, planetary gearboxes have substantial advantages such as compactness, large torque-to-weight ratio, reduced noise and vibration due to relatively smaller and stiffer components, diminished loads on shaft bearings over parallel shaft drives, improved reliability and more efficient power transfer (Lynwander 1983).

Planetary gear sets are recognised as particularly compact and efficient mechanisms and are used in a wide variety of machinery applications these include wind turbines, see
, automobiles, helicopter and aircraft engine transmissions, see Figure 1.6, as well as robotics, gas-turbine gear boxes, heavy machinery, marine and industrial power transmission systems.

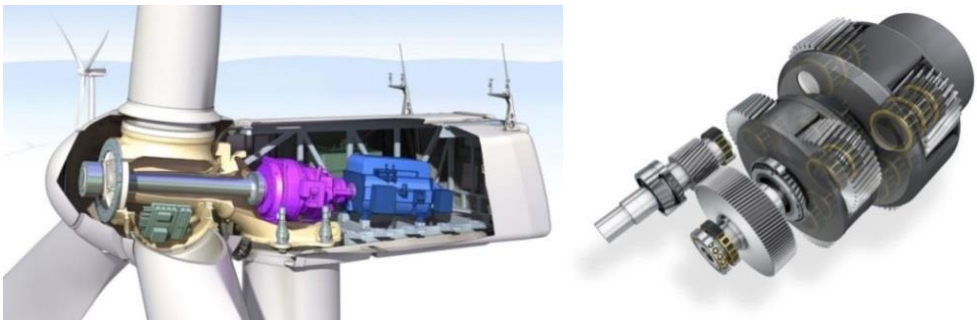

Figure 1.5 Wind turbine planetary gearbox reproduced from

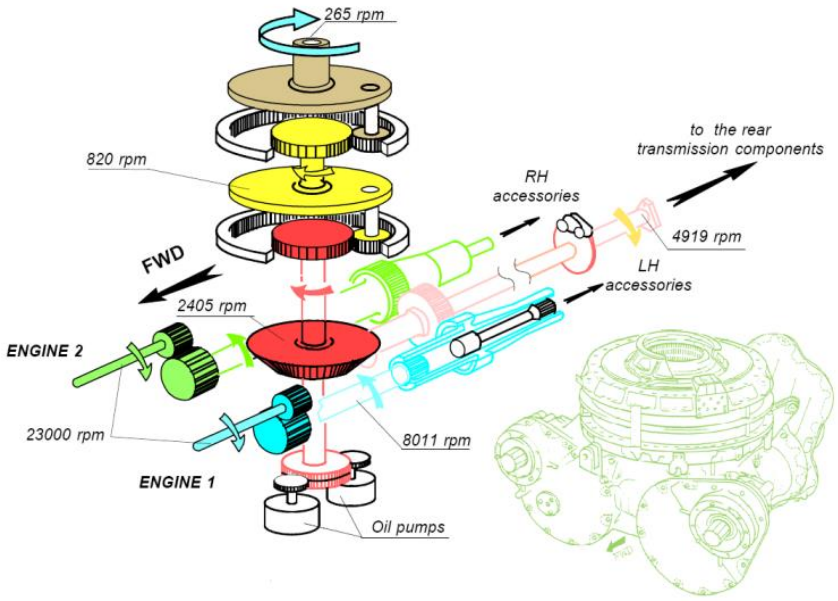

Figure 1.6 Super puma main gear box drawing reproduced from (G-Redl 2012)

1.3 Motivation of Research

Planetary gearboxes are widely used in the power transmissions of critical machines such as helicopters, automobiles, aircraft engines, heavy machinery and marine vehicles. Numerous researches have been carried out for developing condition monitoring techniques. However, to date there have not been any that are sufficiently accurate and reliable enough to meet industrial requirements. This gap is mainly due to the high complicity of the dynamic responses associated with planetary gearbox and interferences of noises in the measured vibration signals. (Parker, Lin et al. 2001). General design guidelines are needed to minimise planetary gear vibration, however, with regard to noise and vibration issues in planetary gear systems, designers tend to trust empirical experience and cut-and-dry methods rather than an engineering understanding (Lewicki, LaBerge et al. 2011; Walter Bartelmus 2011).

Early work focused on analytical models of spur gears, studying the relationship between natural frequencies and system parameters, but by the 1970's Cunliffe, et al.,(Cunliffe, Smith et al. 1974), were exploring the characteristic vibration modes of a 13 degree of freedom (DOF) PG with a fixed carrier (Botman 1976). Each gear has three degrees of freedom (one rotational and two translational). August and Kasuba, (August and Kasuba 1986) showed how a nine DOF lumped-parameter model, without translation of the planet gears, could be

used to compare the performance of fixed versus floating sun gears. This research will attempt to introduce dynamic excitations in a planetary gearbox. Then for the ease of implementation, the lumped mass model with an 18 degree of freedom is focused on for modelling the planetary gearbox under investigation, which allows the vibration behaviours to be understood for analysing different abnormalities tooth breakages, and gear errors and paves the way for subsequent data analytics and fault diagnostics.

Because of the criticalness of planetary gearbox associated applications, condition monitoring of planetary gearbox has received significant attention by many researchers. As shown in the general review paper by Leia et al (Lei, Lin et al. 2014), considerable works have been carried out on the investigation of vibration characteristics for monitoring various faults including gear pitting, crack and wear. In addition, many different signal processing methods in the time domain, frequency domain, time-frequency domain and advanced intelligent methods have been applied to analyse the complicated vibration signal for defining accurate and reliable diagnostic features.(McFadden and Smith 1985; Patel and Darpe 2009; Hong, Dhupia et al. 2014). However, it has been found that most of these works have developed the diagnostic parameters based on apparent vibration components which have large amplitudes in a spectrum and relate to fault dynamics. Especially, studies in (Hong, Dhupia et al. 2014)have shown that only the in-phase sideband components are useful for diagnosing different types of planetary gearbox faults.

In this research project, initial activities will investigate whether vibration signatures generated by the planetary gearbox is able to provide useful information for gearbox CM for a planetary gearbox operating under different loads and speed. The rest of thesis will investigate a novel approach to pattern recognition and fault detection using advanced signal processing.

Moreover, this research project will attempt to use the vibration signals, which are collected from the planetary gearbox under different load conditions and shaft speeds, to investigate the condition monitoring of the planetary gearbox with faults of different severities seeded into the sun and planet gears. Investigating the effect of varying degrees of misalignment by attempts to fill at least some gaps by investigating the misalignment on the vibration spectra of a planetary gearbox system, and to develop more reliable methods for diagnosing this fault

and the modulation signal bispectrum (MSB), will use because it is particularly effective in capturing the weak modulations in PG signals for fault detection and diagnosis (Gu 2011). Moreover, the effect of operational conditions and transmission paths on the vibration signals will be examined using vibration signals recorded at different shaft speeds, from 20%, 30% and 40% of the full speed 1450 rpm of the AC motor and under different loads from 0%-25%-50%-75% and 90% of the full load for each speed. Any one of the carrier, ring, or sun can be selected as the input or output component and the power will be transmitted through multiple paths of the planet meshes.

1.4 Research Aim and Objectives

1.4.1 Aim

In this research the aim is to achieve more accurate detection and diagnosis of common faults on a planetary gearbox transmission system through an exploitation of advanced signal modelling and processing techniques that can be applied to the vibration signals perceived on the gearbox housing. These techniques will be advanced during various phases including in-depth understanding vibration generation and characterisation, experiment verification and evaluation, noise reduction, signal analytics and feature optimisation. To achieve this aim, this research is carried out with a number of primary objectives which are depicted in Section 1.4.2.

1.4.2 Objectives

- **Objective 1**: To familiarise and understand planetary gearbox structures and basic dynamics and then establish a planetary gearbox test rig capable of reviewing gear vibration fundamentals and gear common failure modes.
- **Objective 2**: Review existing condition monitoring and vibration signal analysis techniques and assess the performance of generally used diagnostic techniques in terms of early fault detection of planetary gearbox.
- **Objective 3**: To familiarise vibration measurements based on the planetary gearbox test rig, which includes gaining full skills of gear fault creation, experiment implementation and data processing.

- **Objective 4**: To measure vibrations from the planetary gearbox for evaluating vibration gearbox fault diagnosis methods. Also to investigate the influences of common faults, such as shaft misalignment and gear tooth defects with different severities in both the sun and planet gears.
- **Objective 5**: To gain an understanding of the existing mathematical models for the dynamic analysis of planetary gearboxes. Subsequently, to establish a more realistic dynamic model and simulate vibration responses under different fault conditions and with inclusion of manufacturing errors in order to acquire an indepth undertsnading of vibration characterstics.
- **Objective 6**: To apply conventional signal analysis techniques, for example, power spectrum and time synchronous average (TSA), and then exploit advanced signal processing methods such as Modulation Signal Bispectrum MSB and improved MSB such as the MSB-based sideband estimator (MSB-SE), to obtain fault information in measured signals with noise and interferences.
- **Objective 7**: To investigate and obtain a set of vibration features for detection and diagnosing different gearbox faults including shaft misalignments, sun gear faults and planet gear faults under different loads.
- **Objective 8**: To provide guidelines and recommendation for future researches in this field.

1.5 Thesis Outline

This thesis is comprised of nine chapters as summarised below:

Chapter 1: presents a brief review of condition monitoring and maintenance procedures. Included are maintenance management methods such as preventive maintenance and corrective maintenance and the reasons why condition monitoring of this important industrial device needs to be improved. Certain techniques are suggested for detection and diagnosis of faults. Finally, the specific aims and objectives of this work plan have been stated.

Chapter 2: introduces the basic layout of the planetary gearbox, which has been used in this research work. The main advantages of the planetary gearbox over the parallel axis gearbox are given and the, gear classification, common failures, gear vibration and signal

modulation (both amplitude modulation (AM) and frequency modulation (FM) are discussed. There is also a literature review of planetary gearboxes and planetary gearbox characteristic frequencies also vibration sources which review previous work on planetary gearbox fault diagnostics.

Chapter 3: presents current dynamic models of planetary gears such as the hybrid model, finite element model (FE) and lumped parameter model. This includes sun gear and a planet bearing containing a localised defect, used to determine vibration signatures of planet and sun gears with seeded faults. Theoretically predicted vibration signatures of planet and sun gear faults are validated against experiments.

Chapter 4: presents a literature review of condition monitoring techniques for geared transmission systems based on measured vibration signals, including conventional techniques for processing the signals based on statistical analysis of the time domain for fault detection, and its limitations. Also included is frequency domain analysis including the use of the short time Fourier transform (STFT), conventional bispectrum and modulation signal bispectrum (MSB). The chapter also explains the modulation signal bispectrum and sideband estimator (MSB-SE).

Chapter 5: chapter begins with an overview of the planetary gearbox test rig used to carry out the investigations. Vibration measurement sensors, the transducers used to perform the various experiments and the data-acquisition system are described, and the specification of each component of the test rig is listed. Finally, the experimental and data collection procedures for all the experiments are listed and summarised.

Chapter 6: describes shaft misalignment in planetary gearboxes, reviews how it can happen and how the misalignment of a planetary gearbox can be diagnosed by vibration analysis. Tests will be carried out sequentially for three levels of seeded misalignment and how misalignment can be diagnosed using low-frequency components of the measured vibration signal. However, it is shown that MSB produces a more accurate and reliable diagnosis and gives a correct indication of the fault location and severity for all operating conditions.

Chapter 7: in this chapter, the detection and diagnosis of different severities of tooth defect faults seeded into the sun gear is reviewed under different operating conditions. A novel

approach is used to monitor sun gear faults (tooth breakage) F1-as small and F2- as large faults respectively, using vibration sensors mounted on the case of the planetary gearbox. The result shows that, by using the modulation signal bi-spectrum and sideband estimator (MSB-SE), the seeded faults can be detected with a good degree of accuracy. This method is found to produce accurate and consistent diagnostic results for sun gear faults with different levels of fault.

Chapter 8: the detection and diagnosis of planet gear faults (tooth breakage) for different operation conditions are reviewed. The method developed in Chapter Seven for sun gear faults is extended to planet gear faults (tooth breakage) F1-as small and F2- as large faults respectively, and it is again found that, by using the modulation signal bispectrum and sideband estimator (MSB-SE), the seeded faults can be found with a good degree of accuracy. This method is found to produce accurate and consistent diagnostic results of planet gear faults for different levels of fault.

Chapter 9: summarises the key conclusions of this research. The objectives are reviewed and a summary of the author's knowledge and the novel aspects of the research are presented. This chapter also provides suggestions and recommendations for future work, which directly follows from this research.

CHAPTER TWO

LITERATURE REVIEW OF PLANETARY GEARBOXES AND PLANETARY GEARBOX CHARACTERISTIC FREQUENCIES

This chapter begins with a review of gear types and their common failures see Section 2.1, and a review of different types of planetary gearboxes, in which the planetary gearbox used in this research stud, is described in Section 2.2.3 and then gives a brief overview of vibration sources in planetary gear systems in Section 2.3. Finally, in Section 2.4 a brief literature review of planetary gearbox condition monitoring research is presented.

2.1 Gear Types and Their Common Failures

There is a huge number of gear types used in industries throughout the world. One of the main differences between individual gears is their performance characteristics.

2.1.1 Gear Classification

The gears can be classified into one of three types according to the relative geometry of the shafts; Parallel, Intersecting and Non-parallel and non-intersecting.

1- Spur gears, helical gears and herringbone gears are gears that mesh in the same plane and transmit power of rotary motion between parallel shafts. The main advantages of parallel shafts are:

- They offer maximum power transmission, high efficiency and low noise.
- They have a greater load carrying capacity and so are used in higher horsepower applications and where long-term operational efficiency is important.

2- Intersecting shafts are usually mutually perpendicular and suitable gears include bevel, worm and spiral gears. These gears are widely used in hand drills, locomotives, automobiles, marine applications and all rotorcraft drive systems, many as planetary gearboxes. However, it is important to note that some of these are non-reversible, when a worm gear is turned, the meshing spur will also turn, but attempting to rotate the spur will not cause the worm gear to turn.

3- Gears suitable for non-parallel and non-intersecting shafts are hypoid gears, crossed helical gears and worm gears (A. Bhatia 2012).

Moreover, here some of the more common types used in industry are introduced.

2.1.1.1 External and Internal Spur Gear

Figure 2.1 shows spur gears; the first is an external spur gear where the shafts supporting each gear must be permanently parallel. Thus, the shaft bearings and their supports must be accurately mounted for alignment and be of the required strength.

In the same way Figure 2.1 (b) shows internal spur gear set which is an important component in planetary gearbox. Again the shafts supporting each gear must remain parallel. The internal spur system provides a stronger drive and a greater area of contact than external spur gears. The internal planetary gear system can provide a low speed and large torque source into a small space or small volume, thus, both the input and output shafts rotate in the same direction (Anaheim 2015).

(a) External spur gear reproduced from (Industries 2015)

(b) Internal spur gear reproduced from (Industries 2015)

Figure 2.1 Spur gears

2.1.1.2 Helical Gears

Helical gears as in Figure 2.2 are cut at angles which allow for gradual contact between each of the helical gear teeth. This arrangement provides a smooth and quiet operation. The helical nature of the teeth creates an extended length of tooth contact compared to spur gears and the load is distributed over a greater tooth area. Thus gearboxes using helical gears are used for power transmission with both parallel and mutually perpendicular shafts (Anaheim 2015).

Figure 2.2 Helical gearbox (reproduced from (Anaheim 2015)

2.1.1.3 Worm Gear

As shown in Figure 2.3 worm gears sets are used for applications where a large reduction in rotational speed is required between the driving and driven shafts. Worm gears are suitable to transmit power between two shafts that are at right angles to each other but non-intersecting. In this type of gear the pressure angle of this thread is about 14.5^0 to 30^0 (see below). As the lead angle of the worm increases, the greater the pressure angle is on the side of the thread (A. Bhatia 2012; 2015).

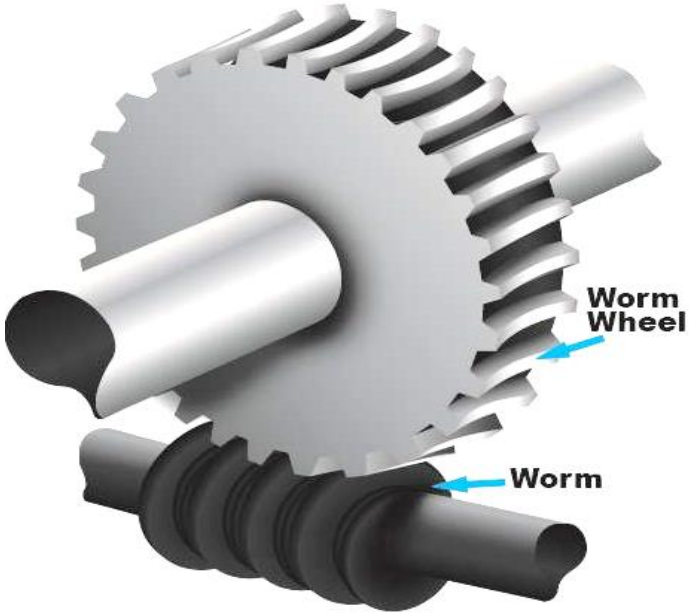

Figure 2.3 Worm gears reproduced from (Anaheim 2015)

2.1.1.4 Bevel Gears

Bevel gears, as seen below in Figure 2.4, cannot be used for parallel shafts and are used for power transmission between two mutually perpendicular shafts they can be noisy at high speeds. There are two types of bevel gears, either straight or spiral teeth. Spiral bevel gears have curved and oblique teeth providing high-performance, high speed applications. Straight bevel gears have straight and tapered teeth and are used in applications requiring slower speeds (Anaheim 2015).

(a) Spiral bevel gears (b) Straight bevel gears

Figure 2.4 Bevel gears reproduced from (Anaheim 2015)

2.1.2 Common Gear Failures

Gears have failed when they can no longer efficiently do the job for which they were designed. The causes of failure may range from excessive wear to catastrophic breakage. Gear tooth damage can be caused by a variety of factors including inadequate lubrication, inappropriate operating conditions or specifications, material insufficiencies and manufacturing or installation problems. Effective lubrication of gear systems is of critical importance because it prevents direct tooth contact (Yesilyurt 2003). Figure 2.5 shows the different gear failure mode classifications which is a summary of (Winter and Placzek 1989).

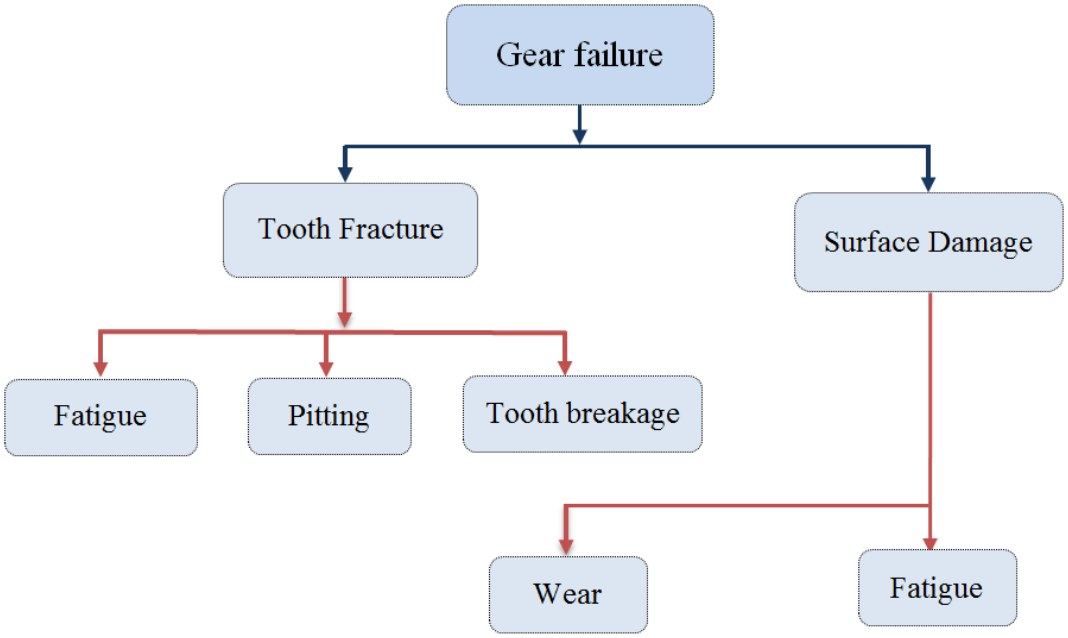

Figure 2.5 Gear failure modes reproduced from (Winter and Placzek 1989)

The rapid cyclic bending of gear teeth as they are subjected to high loads leads to metal fatigue. The greatest forces occur at the base of the tooth which can become a site at which fatigue cracks start. Once started the cracks propagate and the tooth can become distorted, increasing the load on adjacent teeth. The crack spreads from the initial defect site progressively, until fractional or total tooth failure, often taking part of the adjacent teeth (M.M.Mayuram 2015). Overloading of the gears or subjecting them to impact forces can exacerbate tooth fracture processes.

The main three steps of fatigue are:

1. Initial crack initiation.

2. Progressive crack growth across part of the tooth width.

3. Final sudden fracture of the remaining cross-section.

Some of the tooth fractures caused by a change in the amplitude of the tooth meshing vibration are pitting damage, tooth breakage and corrosion wears.

2.1.2.1 Pitting

Tooth pitting damage is a surface fatigue failure of the gear tooth as shown in Figure 2.6. It occurs when contact stress is greater than the fatigue tolerance limit and after a certain period of operation, with repeated variation of the load, small areas of gear metal on the tooth surface fatigue and drop off (Cheng Zhe 2011).

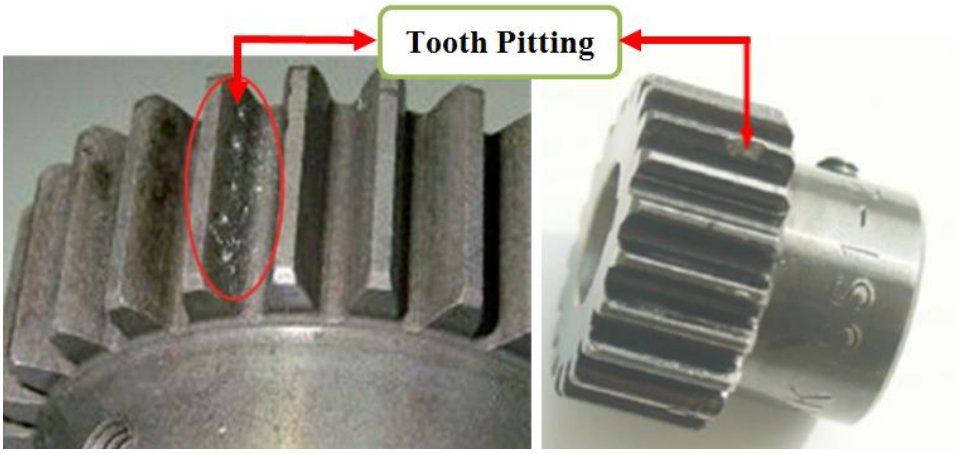

Figure 2.6 Typical tooth pitting reproduced from (Cheng Zhe 2011).

2.1.2.2 Tooth breakage

Once a tooth has fractured it will cause a change in the amplitude of the tooth meshing vibration, as will pitting damage, tooth breakage and corrosion wear. Tooth breakage, also known as a chipped tooth, is considered the most dangerous type of gear failure because the broken-off parts of the tooth can often lead to disablement of the drive and damage of other gearbox components such as the shaft, bearings and gears. Figure 2.6, illustrates tooth breakage that can occur due to overload or impact. However, the most common cause is bending fatigue due to repetitive loads on the gear teeth, as discussed above (F Elbarghathi 2012).

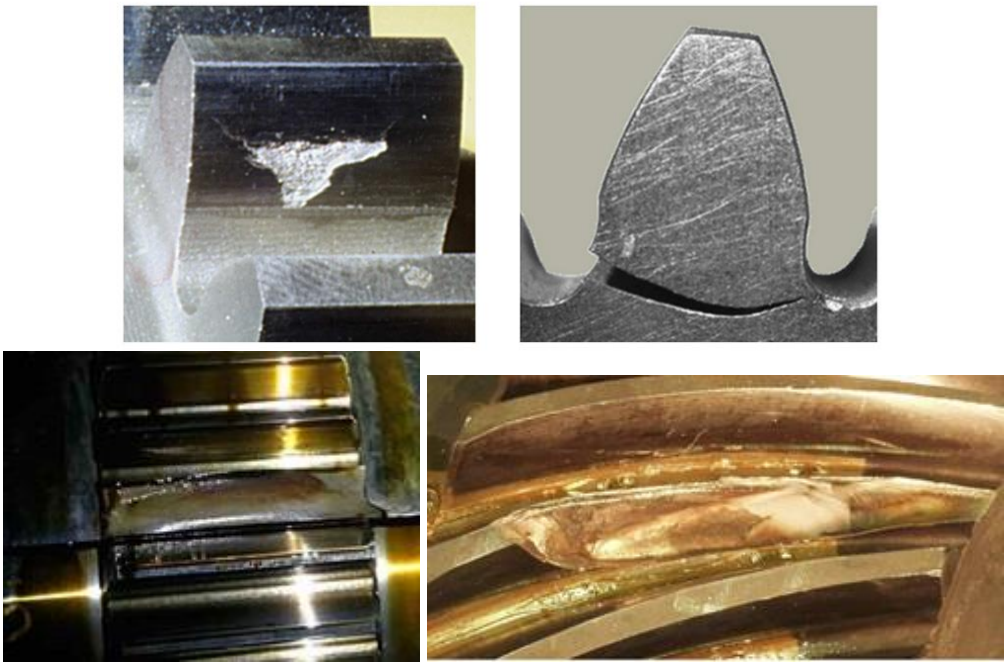

Figure 2.7 Different type of tooth breakage reproduced from (Dipl.-Ing. I. Boiadjiev 2015).

2.1.2.3 Wear

Wear in gears is that naturally damage and inevitable occurs as a result of normal gear contact, some of the wear as follow:

Corrosion wear, is produced by corrosion of the tooth surface due to the presence of corrosive elements. To avoid this type of wear an anti-corrosive should be used.

Scoring wear, originates when gears are subjected to excessive surface pressure, continuous high speed or failure of lubrication. All these factors will result in the generation of excessive heat.

Abrasive wear, generally results from foreign particles, such as dirt or dust entering between the teeth which causes damage to the tooth surface (Yesilyurt 2003).

2.1.3 Misalignment

Poor machine alignment can reduce the working life of a machine by as much as 30%. However, misalignment not only reduces machine life it can result in unexpected downtime which is extremely expensive for industry not only in terms of increased maintenance costs and replacement parts, but also of lost production. Misalignment rarely occurs during the

initial installation but can occur during re-assembly of the machine after maintenance. Given the importance of good alignment of coupled shafts, it is of concern that industry does not possess an extensive understanding or the appropriate tools for detecting and diagnosing misalignment. A survey of the literature reveals some important points regarding misalignment (John 2006; Ganeriwala, Li et al. 2008).

- Misalignment in the machines produces significant vibration levels.
- A machine might be having parallel misalignment without showing significant (2X) vibration levels.
- Misalignment effects in the machines are strongly influenced by speed.
- Fixable or soft coupling is more forgiving and will produce less vibration levels.
- Profiling of a single point from the vibration spectrum (for a given operating condition) is not a reliable indication of machinery misalignment.

Figure 2.8 shows the principle types of misalignments between coupled shafts, parallel, angular and axial. It is essential to have as part of the CM system, a procedure in place for ensuring that coupled shafts are correctly aligned (Ganeriwala, Li et al. 2008; Heney 2013). However, some commercial companies are producing couplers which are less stiff and allow some flexibility reducing the reaction load of the misalignment transmitted between the coupled shafts and this, it is claimed, will increase the life of the machine or mechanical system (Ganeriwala, Li et al. 2008; Heney 2013).

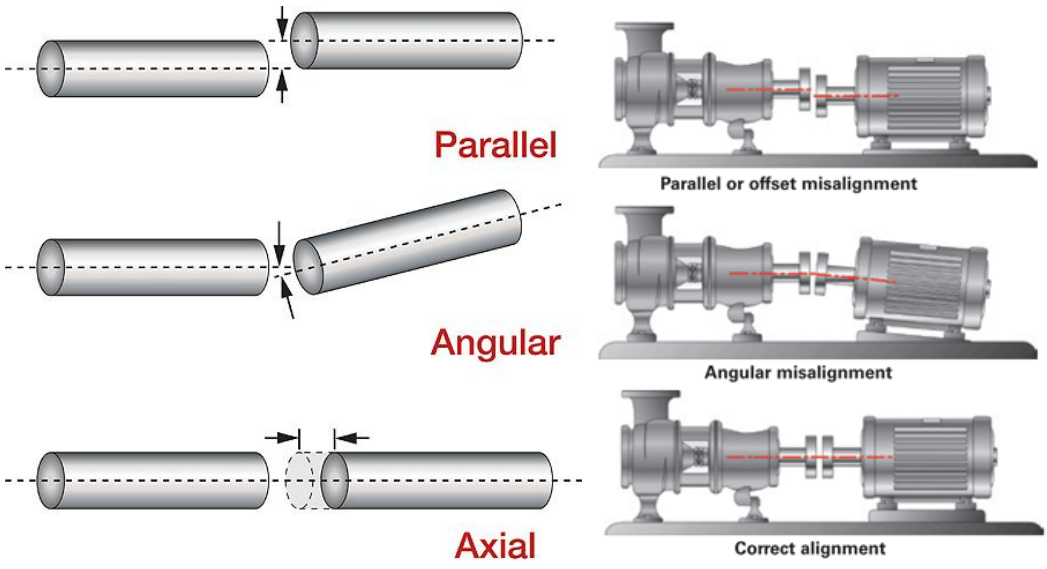

Figure 2.8 Types of misalignment reproduced from (Parker 2010; Bonanomi 2015).

- **Pressure Angle**

The pressure angle is the angle formed by a line through the points of contact of two adjacent mating teeth and the geometric tangent to the base circle at the pitch point. When two gears are meshing they must have the same pressure angle to mesh properly.

There are two common pressure angles used in gears, the first one is 14.5^0 and the second one is 20^0. The latter is of interest in this research. The major advantage of the 20^0 angle is that the tooth is wider at the base and consequently is stronger than the tooth with an angle of 14.5^0. Additionally, a 20^0 pressure angle helps to reduce undercutting, which usually begins when the number of teeth is less than 18 but may become excessive if the number of teeth is less than 14. On the other hand, teeth with a pressure angle of 14.5^0, tooth undercutting begins when the number of teeth is less than 32 and become excessive if the number is less than 22 (2015).

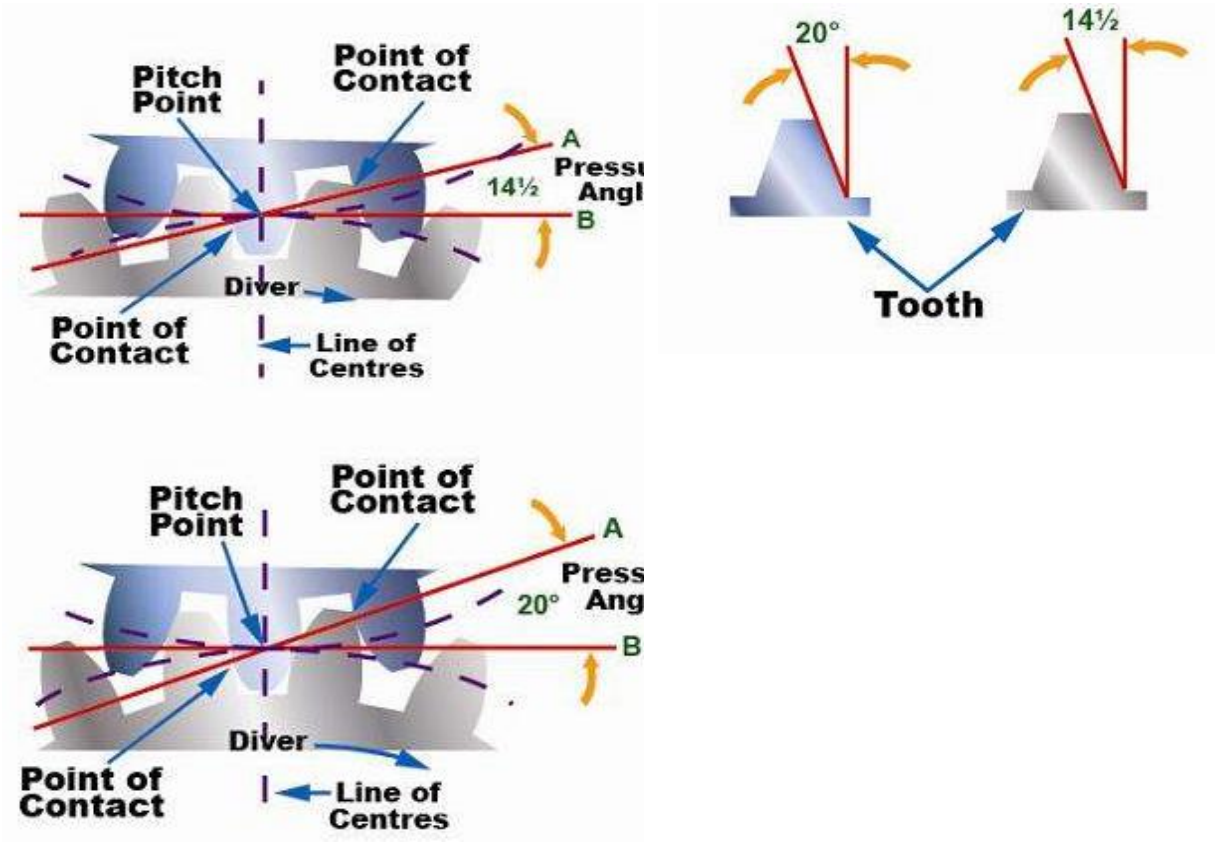

Figure 2.9 .Concept of pressure angle reproduced from (2015)

2.2 Planetary Gearboxes and Advantages

The planetary or epicycles gearbox (PG) is shown in Figure 2.10 and it can be seen that multiple, so-called planet gears mesh with and rotate around a central sun gear. Occasionally there is only one planetary gear, but there can be as many as required. The planet gears mesh with and rotate inside an internal ring gear. The planet gears are attached to a planet carrier which rotates around the same centre as the sun gear but at a different speed.

The major advantage of using a planetary gearbox is that large speed and torque ratios are obtainable with a compact gearbox. Moreover, the fact that the input and output shafts lie along the same axis means that the incoming shaft supplying the drive to the gearbox and the outgoing shaft from the gearbox align with each other. This means that equipment can be mounted on the same central axis without an offset as would be the case with a non-aligned gearbox. This characteristic of the planetary gearbox can considerably simplify a machine's design. It is also well known that planetary gearboxes have low noise and vibration characteristics (de Smidt 2009; Smidt 2009).

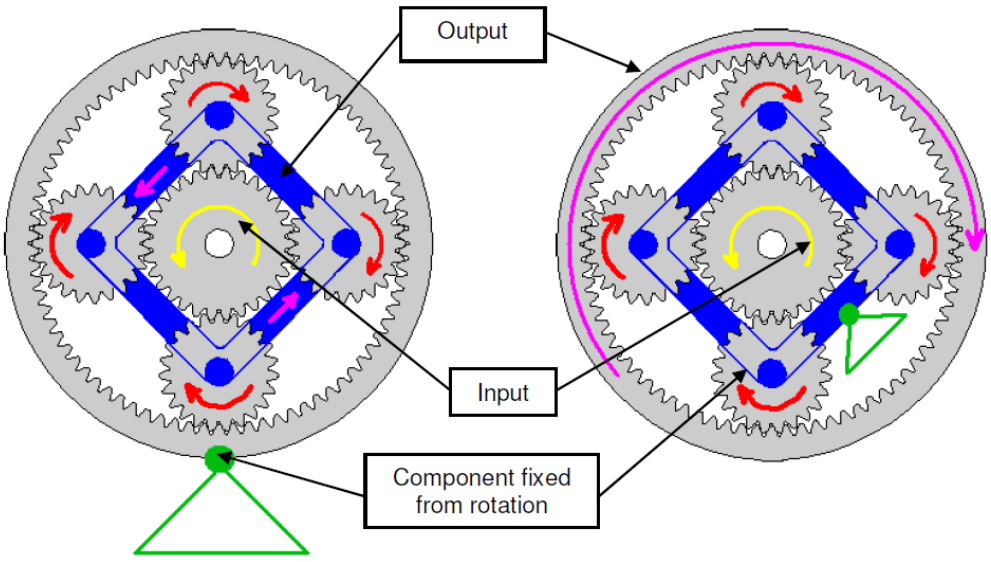

Figure 2.10 Different operational applications of planetary gear system

The planetary gearbox can operate in a number of different modes of which two are shown in Figure 2.10. The planetary gearbox components; sun, planet and ring (or carrier) gears are constantly in mesh and either the planet carrier, sun gear or ring can be used as the input with

either of the other components being used as the output. Other configurations using one input and two outputs or two inputs and one output are possible. The right hand side gearbox in Figure 2.10 has the planet carrier fixed with the sun gear as input and ring gear as output. The left hand side gearbox in the same figure has the ring gear fixed with sun gear again as input but with the planet carrier as output. Generally, in most applications the sun gear is used as an input with the planet carrier being used as an output and the ring gear kept stationary or at a standstill, which is the system to be used in this study (Smidt 2009).

A planetary gearbox has the ability to provide different speed and torque ratios from the same planetary set, depending on which is the input gear, which the output, and which remains stationary. This ability of the planetary gearbox makes it ideal for use in automatic vehicle transmissions, helicopters and wind turbines, as well as other assemblies such as all-wheel drive transfer cases and axle differentials. Planetary gear boxes are also extensively used in lifting applications where high speed to torque conversion is required in a small space. Industry makes extensive use of the many possible applications for planetary gearboxes and thus needs to be able to accurately monitor them (Smidt 2009).

2.2.1 Planetary Gearbox Installation

As stated above, planetary gearing or epicyclical gearing provides an efficient means of obtaining a compact design of power transmission because driving and driven shafts are parallel to each other. This means that there are many suitable applications, including:

- Increasing or decreasing the speed of the driven component.
- Change in direction of rotation of the output.
- Torque increase or decrease.

It is often said that the planetary gearbox is similar to the solar system, see Figure 2.11. The planet pinion gears are fixed on shafts in the carrier body assembly and each turn on their own axis whilst rotating around the centrally positioned sun gear. Figure 2.11 also clearly shows that the planet pinion gears mesh with the inside gear teeth of the ring gear (Odesie 2015). When power is applied to drive the sun gear, the planet carrier or the ring gear, the

entire planetary gear system will rotate as a unit. A restraining force applied to one of the other two planetary members will hold that item stationary.

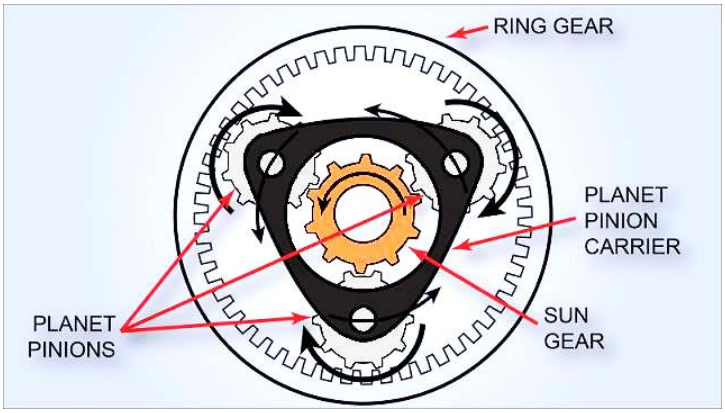

Figure 2.11 Planetary gearbox reproduced from (Odesie 2015).

When power is applied to one of the components of the planetary gearbox and a brake mechanism is applied to stop a second member from rotating, the remaining part will become a power output source as illustrated in the following examples.

1- The first case is shown in Figure 2.12, where the sun gear is driven and a brake applied to the ring. The rotation and movement of the planet pinions, which are meshed with the inner ring, force the planet gear carrier to rotate in the same direction as the sun gear, but in this case at a slower speed. This arrangement is used in applications where a decrease in rotational speed is required (Odesie 2015).

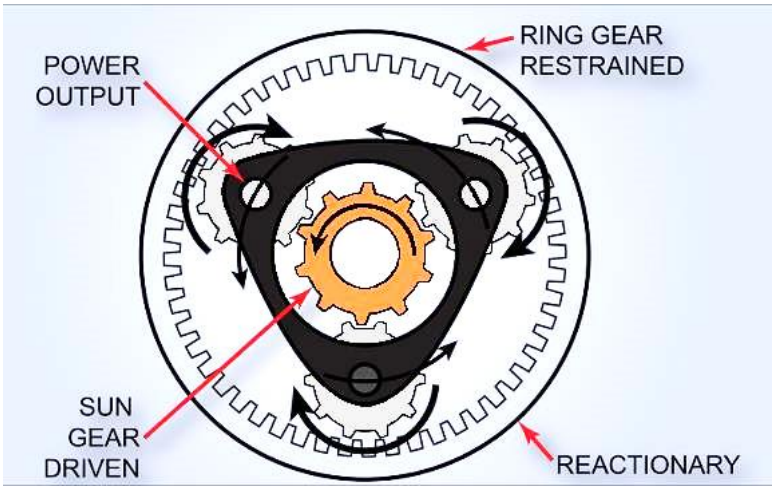

Figure 2.12 Planetary gearbox movement M1 reproduced from (Odesie 2015).

2- In the second case, see Figure 2.13, it is the planet carrier which is driven and as previously, the ring gear has a brake applied. The planet pinions revolve around the ring gear, forcing the sun gear to rotate in the same direction but at a higher speed. This arrangement is used in applications where an increase in rotational speed is required

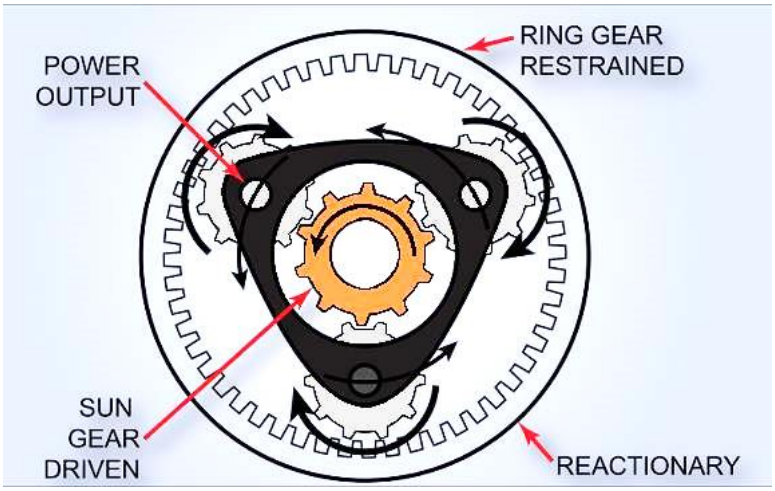

Figure 2.13 Planetary gearbox movement M2 reproduced from (Odesie 2015).

In industrial application there are six common applications of planetary gears that provide change of rotational speed and/or change of rotational direction and/or change of applied torque. The six applications are listed in Table 2.1 (Odesie 2015). Including the case studied in this research which is highlighted.

Table 2.1 Application of planetary gearbox

Driver	Driven	Held	Result
Sun	Carrier	Ring	Larger reduction Low speed
Sun	Ring	Carrier	Low reverse
Carrier	Ring	Sun	Overdrive
Carrier	Sun	Ring	Fast overdrive
Ring	Sun	Carrier	Reverse overdrive
Ring	Carrier	Sun	Speed reduction. Gear Reduction, Direction Change or Speed Increase Combinations

2.2.2 The advantages and disadvantages of planetary gears over parallel axis gears

Planetary gearboxes have many advantages over parallel axis gears; these include a larger transmission ratio, simpler construction, compactness and smooth running all of which have been advantageous in a wide number of applications.

- Higher power intensity: Due to common input torque between similar parallel sun gears, higher power densities (power-to-volume ratio) are obtained. Thus, planet and ring gears can be smaller and lighter than conventional gears for the same process.
- A number of speed ratios: Various input-to-output speed or torque ratios can be obtained through employing the same gear set simply by varying the input, output and reaction (fixed) members. By using different power flow settings, the highest possible amount of power can be amplified, merely by enhancing the number of parallel paths, for instance, the number of pinions in the planetary gear set. Efficiency and self-adaptability: Efficiency is offered through the use of coaxial parts, an arrangement that also provides the attribute of self-adaptability. If some of the main members (usually the sun gear) are allowed to float, the sensitivity of the gear set to different manufacturing defects can be reduced (Ligata 2008).
- Comparatively easier to build due to the use of smaller gears , as compared to parallel gear systems, allowing for more precise manufacturing
- Increased productivity: The power losses caused by tooth friction are reduced by decreasing the tooth load and pitch line rate. In the same way, bearing losses are reduced by using smaller bearings along with decreasing the radial forces on the central members (Lynwander 1983).

On the other hand, planetary gears may have undesirable dynamic behaviour resulting in, for example, much greater noise and vibration levels (Wang, Wang et al. 2014). Regardless of the benefits provided by planetary gearbox, there are numerous drawbacks which should be considered during any design analysis:

- Owing to the number of connected gears, they produce significant levels of noise during operation.
- Some of the constituent members have to withstand considerable loads due to the numerous interconnections, which can lead to significant failures. The compact gear

setting give rise to tooth failure, which poses significant level of damage as a fractured tooth can have a negative influence on the transmission system.

- Equal sharing of load between all the planets in the planetary gear system is deemed as a perfect setting. However, practically, the variations in network consistency and manufacturing faults may produce noise and vibration as well as contact and structural exhaustion of the gears (Ligata 2008; Wang, Wang et al. 2014).

2.2.3 Basic Layout of a STM Planetary Gearbox

The planetary gearbox supplied and manufactured by STM Power Transmission Ltd, was as presented in Figure 2.14, consisting of three planet gears namely, sun gear, ring gear and carrier. The technical specifications of the planetary gearbox are given in Table 2.2. The planet carrier is floating and fixed to the output shaft by means of splines which allow it to move axially as required. The planet gears are hardened and use the inside of the ring gear as the inner bearing race. Loose needle bearings are then inserted between the planet gear and the planet gear shaft with the shaft itself being the other race of the bearing. More drawing and specifications are listed and summarised in Appendix B.

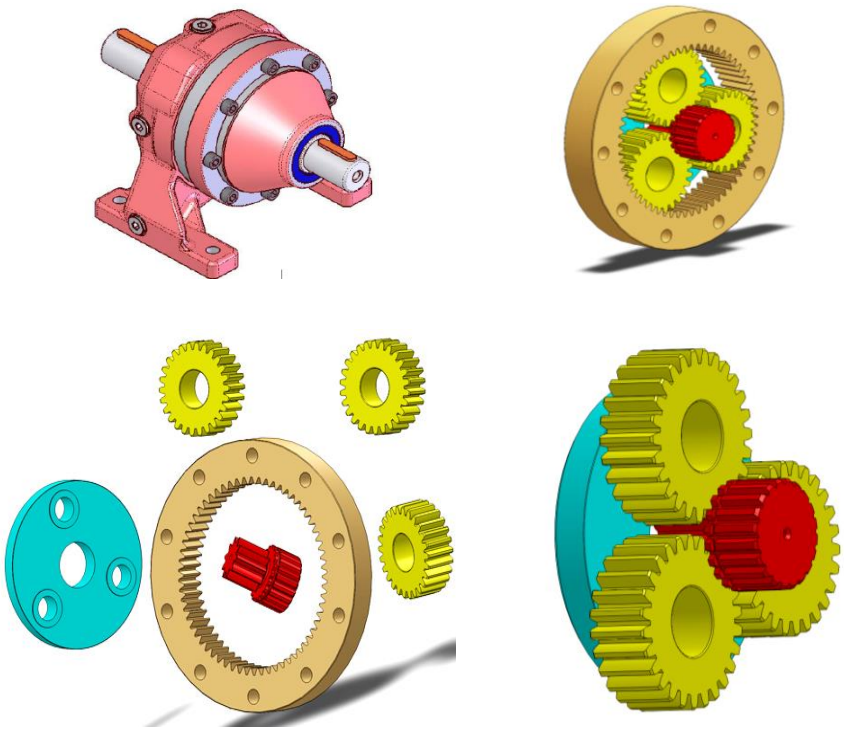

Figure 2.14 Planetary gearbox

In general fault detection and diagnosis can be carried out by examining the change of these characteristic frequencies in the frequency domain. However, it is often very difficult to identify and quantify these components because of the effects of interferences between higher order of harmonics and the attenuation and distortion of different wave transfer paths. These components are often found in the frequency range around the meshing frequencies at which the characteristic components are modulated

2.2.4 Planetary Gearbox Characteristic Frequencies

The characteristic frequencies of the planetary gearbox will be defined in terms of shaft rotation frequencies, gear meshing frequencies and frequencies of local gear faults. The latter are critical for identification of faults in gears. The derivation of these characteristic frequencies is based on the gear transmission structures of the planetary gearbox with the ring gear at standstill and the sun gear moving and where the carrier is driver and the sun gear is the driven as shown in Table 2.3. In this test rig the motor speed should not be accessed up to 50% of max speed 1450 rpm. This means that the max speed is 1450 rpm at 100% and up to 40% ≈ 580 rpm, see Figure 2.15.

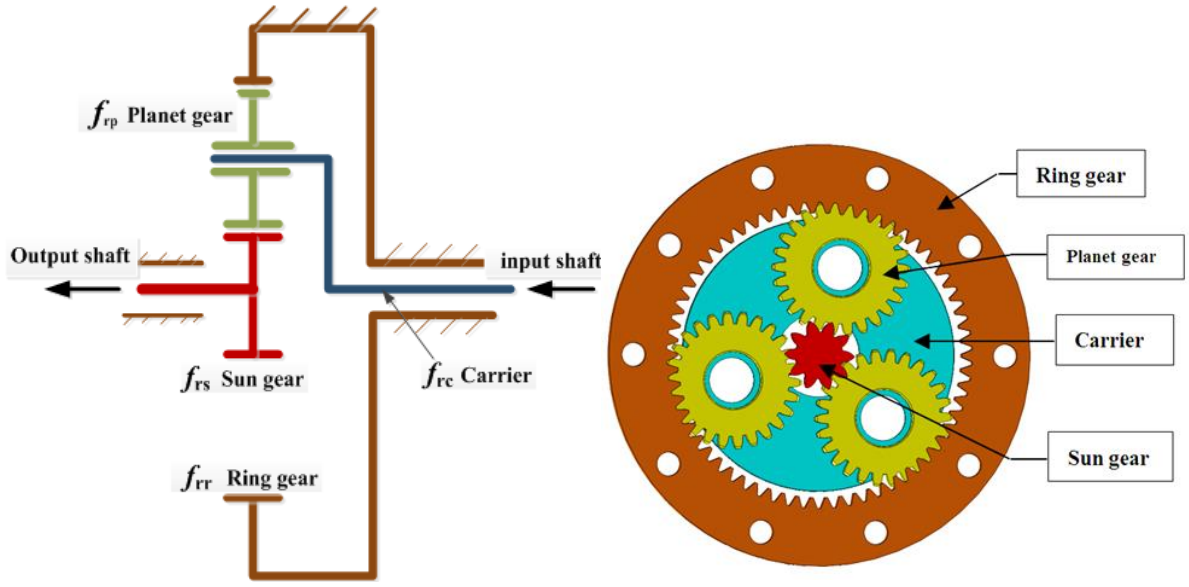

Figure 2.15 Schematic of a planetary gearbox with the standstill ring gear

Table 2.2 Planetary gearbox parameters

Nº	Gear	Teeth
1.	Ring	62
2.	3x Planets	26
3.	Sun	10
4.	Output Shaft Diameter	42 mm
5.	Input Shaft Diameter	38 mm
6.	Gear Ratio	7.2
7.	Maximum Torque	670 Nm
8.	Maximum input speed	2800 rpm
9.	Maximum output speed	388 rpm

According to this, transmission configuration is when the carrier is the driver and the sun gear is driven. Vibration characteristic frequencies for the case of error-free gears with elastic deformation are listed in Table 2.3.

Table 2.3 Planetary gearbox characteristic frequencies

v_1	Sun Gear RPM (Output speed)	RPM		1160
Z_R	Ring Gear Teeth			62
Z_P	Planet Gear Teeth			26
Z_S	Sun Gear Teeth			10
v_2	Carrier Rotation Speed (Input speed)	RPM		161
n_3	Ring Gear Speed	RPM		0
f_{rs}	The Sun gear rotational frequency	Hz		49.95
f_{rp}	The Planet gear rotational frequency	Hz		1.78
f_{rr}	The Ring gear rotational frequency	Hz		0
f_{rc}	The carrier rotational frequency	Hz		0.372
f_m	The meshing frequency	Hz		166.5
i	Gear box ratio			7.2

The transmission ratio is(Bartelmus and Zimroz 2011);

$$i = 1 + \frac{Z_R}{Z_S} = 1 + \frac{62}{10} = 7.2 \tag{2.1}$$

The calculated transmission ratio of 7.2 agreed with the ratio provided by the gearbox manufacture (STM Power Transmission Ltd).

By assuming that, the test rig motor is running at 40% of full motor speed.

Then:

$$n_1 = 1450 * 0.4 = 580\,rpm$$

By using the helical gearbox ratio (3.6) which is used in the test ring as reduced the speed then increased by planetary gearbox ratio which is (7.2), then the calculation will be as follow;

$v_1 = \frac{580}{3.6} \times 7.2 = 1160\,rpm$, which is the output shaft rotational speed or sun gear speed.

$v_2 = \frac{580}{3.6} = 161 rpm$, which is the input shaft rotational speed or carrier speed.

$$f_s = \frac{161}{60} = 2.68\,Hz$$

Then the carrier rotational frequency:

$$f_{rc} = \frac{v_1 z_S}{60(z_S + z_R)} = \frac{(161*10)}{60(10+62)} = 0.372\,Hz \qquad (2.2)$$

The planet gear frequency:

$$f_{rp} = \frac{4 v_1 z_S z_R}{60\left(z_R{}^2 - z_S{}^2\right)} = \frac{4*161*10*62}{60*(3844-100)} = 1.78\,Hz \qquad (2.3)$$

The sun gear frequency:

$$f_{rs} = \frac{v_1 z_R K}{60\left(z_s + z_R\right)} = \frac{1160*62*3}{60(72)} = 49.94\,Hz \qquad (2.4)$$

The pass frequency of the planet gears:

$$f_{P-P} = f_{rr} = K * f_{rc} = \frac{v_1 z_S K}{60\left(z_S + z_R\right)} = \frac{1160*10*3}{60\left(62+10\right)} = 8.05\,Hz \tag{2.5}$$

And the meshing characteristic frequency:

$$f_m = \left(f_{rs} - f_{rc}\right) z_S = \frac{v_1 z_R z_S}{60\left(z_S + z_R\right)} = \frac{1160*62*10}{60(10+62)} = 166.5\,Hz \tag{2.6}$$

where: f_{rs} is the sun gear speed; $i = 1 + Z_R / Z_S$; is the transmission ratio. z_R z_P and z_s denote the number of teeth for the ring, planet and sun gear respectively; and K the number of planet gears (Bartelmus and Zimroz 2009; Walter Bartelmus 2011).

2.3 Vibration Sources in Planetary Gear box

Vibration excitations in a planetary gearbox are generally associated with:

1) Variation of the instantaneous mesh stiffness due to changes in contact length along tooth flanks.
2) Various geometrical and mounting errors of rotating parts.
3) External load fluctuations.
4) Transmission errors.

For instance, consider the situation of variations in the input and/or output torque. The dynamic response to time varying input torque is generally easier to analyse than that induced by mesh stiffness, parametric excitation and geometrical errors, which are the main topics examined in this thesis.

2.3.1 Mesh Deflections and Mesh Stiffness

A number of analytical methods can be found in the literature to estimate mesh stiffness. Contact deformations are generally determined using the Hertzian theory and its variants. For structural deflections, Weber, later Weber and Banascheck and Tavakoli and Houser (Tavakoli 1986) and Lin et al considered a tooth as a cantilever of variable cross section whose bending displacements can be determined by equating the work done by that of the external force to the strain energy in the beam. The tooth root and base are modelled as an elastic half plane subjected to a tangential and a normal force. Extensions and variants of the

methodology were introduced by Attia and Cornell (Cornell 1981) among others. The individual deflections are then superimposed on the pinion and the gear teeth and the resulting displacement in the direction of force leads to the mesh stiffness.

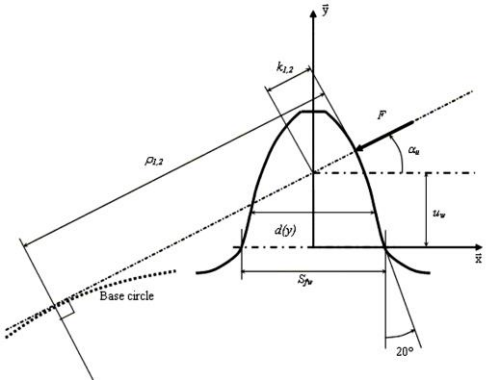

Figure 2.16 Parameters for Weber's formulae

2.3.2 Tooth Shape Errors and Mounting Errors

Significant errors such as tooth profile deviations, position errors, run out and thickness errors are to some extent present in all gears because of machining inaccuracies, thermal distortions after heat treatments, assembly errors etc. which, in practice, cannot be wholly avoided.

Such errors may induce partial or total contact losses, motion transfer and the load sharing amongst the paths of transmission in multi- mesh gears.

The classic tooth shape errors are listed and briefly described below:

1) ***Pitch error****:* which is usually separate into:
   - The individual pitch errors defined as the deviation of the actual measured pitch value between any adjacent tooth surface from and the theoretical circular pitch.
   - The pitch variation error as measured between any two adjacent teeth. In an ideal case, the pitch variation error will be zero.
   - The accumulated pitch error: The difference between the sum of the theoretical pitch over any number of tooth intervals and the sum of the actual pitch measurements over the same tooth interval.

2) ***Thickness errors:*** Thickness error is the amount by which the circular tooth thickness at the pitch circle differs from the nominal amount.

3) ***Tooth profile errors:***

Tooth profile error is the summation of the difference between the actual tooth profile and the correct involute curve which passes through the pitch point. Measurements are made perpendicular to the actual profile. Note that tooth modifications are not considered as part of profile errors.

2.3.3 Mounting or Positional Errors

2.3.3.1 Planet Positional Errors

In planetary gear systems, planet position error is defined as the error in the location of the planet centres. This is decomposed into radial and tangential position errors. It has been shown that radial errors slightly change centre-distances, pressure angles etc. but are far less influential than tangential errors which strongly modify planet load sharing (Harris. 1985).

2.3.3.2 Tooth Shape Modifications

Intentional profile and lead modifications are frequently used in order to improve the load distribution and dynamic properties of gears. Both profile and lead deviations can be used to compensate for elastic deflections and reduce mesh excitations.

Tip relief is a modification of a gear tooth's profile whereby a small amount of material is removed near the tip (or possibly the root) of the tooth. Such profile modifications are commonly applied in order to prevent shocks at engagement causing tooth deflections and to obtain a satisfactory tooth load distribution along the path of contact. Profile relief is characterised mainly by the degree of modification at tooth tip or root and by its length, as measured either along the profile or the path of motion on the base plane (Harris. 1985).

2.3.4 Transmission Errors

The concept of transmission error (TE) was first introduced by Harris in 1958 in relation to the study of the dynamic tooth forces generated in a pinion-gear pair. Harris realised that for high speed applications the problem was one of continuous vibrations rather than a series of

impacts as had been thought previously. Harris showed that the measure of departure from perfect motion transfer between two gears, which is the definition of TE which was strongly correlated with the excitations and dynamic responses. TE is classically defined as the deviation in the position of the driven gear relative to the position that the driven gear would occupy if both gears were geometrically perfect and rigid (P. Velex 2006).

No-load transmission error (NLTE) is directly related to geometrical errors and, for example, can be linked to the results of a single flank gear tester. Typically, the gear is mated with a master gear on a fixed centre distance apparatus and set in such a way that only one side of a tooth makes contact, the gears are rotated through this single flank contact action, and the angular transmission error of the driven gear is measured.

Transmission error under load is similar to NLTE but incorporates elastic deflections. From a practical viewpoint, one separates the quasi-static transmission error under load (TEs) and the dynamic transmission error under load (DTE). TE is currently used as an indicator of the excitations and noise level in a transmission and, as demonstrated by Velex and Ajmi (P. Velex 2006), it captures most of the mesh excitation for a single stage gear as long as linear behaviour prevails.

2.4 Review Performance of Condition Monitoring Research for P G

Because of the multiple load paths possible with of planetary gearing, the power transmitted is divided between several planet meshes. Of course, planetary stages can also be linked together efficiently to achieve high reduction ratios in a compact space. Because of the relatively small size of planetary gearboxes, they offer significant envelope or wrapper and weight savings. There are strong trends toward increasing utilisation of planetary gearboxes for industrial applications (Crowther, Ramakrishnan et al. 2011).Thus, improving the reliability of planetary gearbox components is important for industry to reduce the cost of maintenance and improve efficiency due to smaller, stiffer components. Since the output shaft axes and input shaft axes are concentric, they are effective in transmitting torque (Crowther 2011).

(McFadden and Smith 1985), discussed modifications of the vibration Condition Indices to better accord with the condition of a planetary gearbox. They proposed a Normalized

Kurtosis, Crest Factor, Energy Ratio, Sideband Level Factor (SLF), Sideband Index (SI) Zero-Order Figure of Merit and a Fourth-Order Figure of Merit (FM4e). The test data used was obtained from the main transmission of a UH-60A Blackhawk helicopter at different torque settings. After careful evaluation and interpretation of the CIs, it was reported that SI and SLF are efficient only in high torque conditions. No definite conclusions were drawn for the low torque condition and the CIs for the on-aircraft vibration data could not detect the seeded faults.

(McFadden 1987; McFadden 1991) developed a technique to calculate the time domain averages of gear tooth meshing vibration for both the sun and the planet gears individually. He found that most of these worked as diagnostic parameters only when the vibration components related to the fault dynamics had large peaks which stood out on the spectrum.

(McFadden and Howard 1990), used signal processing to isolate periodic waveforms in a noisy signal from a planetary gearbox. This worked well and the meshing frequency of interest was successfully isolated from the entire vibration of a large gearbox. To detect impairment different signal processing methods were used. The related motions of the planet gears to the sun and ring gears meant more than one interaction was taking place amongst and between the various parts of the planetary gearbox, which restricted the usefulness of the signal averaging processes. A complex indicator of the vibration from every planet gear mesh was displayed when the vibration measurement from a single accelerometer attached to the exterior of the gearbox was harmonised with either the sun gear or planet gears. It was found that in the system with eight planet gears, each gear contributed $1/8^{th}$ of the initial signal and any fault had to advance significantly to be identified.

(Kahraman 1994) proposed a simplified rotational lumped-parameter model, providing closed-form expressions for the torsional natural frequencies in terms of system parameters. Kahraman developed the model to include all six rigid body degrees of freedom of each gear component in order to fully analyse the three-dimensional motion expected in a helical gear system. He also investigated the effects of mesh phasing on the dynamics of equally spaced planet systems in helical planetary gears, using a 2-D rotational and translational model to explain the unique modal properties of a planetary gearbox. He claimed to have described all

meshing phase relationships in planetary gears and their instability effects on the dynamic behaviour of spur planetary gears.

(Kahraman 2001), is developed torsional dynamic models of compound gearboxes to predict the free vibration characteristics. Assuming the position of planet gears were axis-symmetrical to the axis of rotation he divided the natural modes of vibration into three groups; a rigid body mode, symmetric planet modes and axis-symmetric overall modes.

(Lin and Parker 2002) investigated the parametric instabilities arising from variations in the mesh stiffness in two planetary gearboxes, one with equal planet spacing and the other with opposed planet spacing. All the vibration modes were classified into one of three categories: rotational, translational, and planetary modes. Despite the large number of variations possible, most models focus on the planar rotational and translational motion of each gear. Here fixed and floating sun gears were compared using a nine degree of freedom lumped-parameter model without translation of the planet gears. Torsional, flexural, and axial displacements of the gear components were also considered using a model for a planetary gearbox having spur or helical gears.

(Decker and Lewicki 2003) evaluated vibration-based diagnostic metrics for the detection of a gear crack in its earliest stages. A faulty tooth with a notch in the fillet region was seeded onto an OH-58 Main Rotor Transmission of one of the spiral bevel pinion teeth and the system ran to failure. A visual inspection was performed at relatively frequent intervals, but even using an x60 microscope cracks detected by the CM systems were too small to be seen. Accelerometer location was found to be critical for the early detection of the fault, but some traditionally popular metrics such as RMS of the vibration signal were not effective. The most effective metrics, which were able to detect and diagnose the fault successfully, were those designated M6A and FM4. The equations for calculating both of these measures are given in the paper; M6A is a variation on kurtosis, the sixth moment is used and normalised in a similar manner to kurtosis. FM4 is non-dimensional metric and is found by dividing the fourth statistical moment about the mean by the square of the variance of the difference.

(Keller and Grabill 2003) also investigated the possibility of detecting a crack fault in the planetary carrier plate in the main transmission of a UH-60A Blackhawk helicopter using

standard Condition Indicators obtained using TSA vibration signals, but modified for use with planetary gears. These new CIs included modified Energy Ratio, normalised Kurtosis, Crest Factor and Sideband Index. None of the diagnostic parameters were able to detect a crack in on-aircraft conditions at low torque levels, and only the sideband index and sideband level factors could detect the presence of a fault under test cell conditions.

(Meltzer and Ivanov 2003), used time-frequency analysis to study the faults in the run-up and run-down testing of passenger car gear drives. Three stages of planetary gearbox are included in these drives, in each of which there were three planet gears. The vibration signal sample is tuned by an incremental sender and ordinary impulse generator. The data collected by the impulse generator (which is called data) underwent time-frequency analysis facilitated by use of the Fourier-spectrum. The detection and diagnosis of tooth flank faults in machines with non-uniform rotational speed was carried out by analysing the signals obtained from the incremental sender with a variety of smoothing kernels in the Choi-Williams distribution. Work was carried out to identify new ways of including the time-frequency approach in these analyses, the advantage being; elimination of the need for an incremental sender for the determination of the rotational angle, and easier detection and identification of faults in the system. In addition, implementing this approach would substantially reduce the equipment required for monitoring a planetary gearbox.

(Yuksel and Kahraman 2004) studied the influence of surface wear on gear tooth and mesh dynamic forces and its effect on the dynamic behaviour of a typical planetary gearbox with fixed planet carrier. This paper modelled the planetary gear train (PGT) to study the deflection and stresses due to tooth surface scoring and pitting. Using Ansys14.5 and with considerable analytical analysis the authors claim to have achieved their objective. The authors developed two models, the first being a lumped-parameter mathematical model and the second a finite element model.

(Wu, Saxena et al. 2004), analysed the vibration signal obtained from the planetary gears in the main transmission of a UH-60A Blackhawk helicopter, both in a test cell and under on-aircraft conditions. The aim was to detect a crack fault in planetary carrier plate, using a new method to analyse raw vibration data, using a Harmonic Index in the frequency domain which is defined as the sum of the amplitudes of all sidebands of a particular gear meshing

harmonic and Intra-Revolution Energy Variance in the wavelet domain and which is defined as the variance of the energy around a specific gear meshing harmonic. It was found that the Harmonic Index and Intra-Revolution Energy Variance were able to differentiate the data acquired from the faulty and healthy planetary gears and therefore is potentially useful. Raw data was used rather than Time Synchronous Averaged data, because raw data was said to provide more accurate results in relation to the already available planetary gearbox data. The collected TSA could be used in the collection of new data.

(Patel and Darpe 2009), investigated the influence of different types of misalignment on machine vibration behaviour. Effects of parallel and angular misalignment on the vibration behaviour of a coupled rotor were investigated. It was found that not only were the expected lateral, torsional and axial vibrations observed, but that misalignments can couple vibrations in torsional, bending and longitudinal modes.

Many signal processing approaches applied are with insufficient consideration in characterising the modulation characteristics although the modulation effects in planetary gearbox is acceptable as one of the most important sources of vibration due to defects in gears. Especially, both AM and FM are taken into account in developing vibration signal models in reference but the effect on spectrum structure has not been examined in analysing the measured signals for misalignment fault.

(Guo and Parker 2010) A gear tooth can come into simultaneous contact on both its drive-side and back-side (so-called tooth wedging), generating elevated non-linear forces in the gear's bearings and risking bearing failure. The major causes of tooth wedging are translational vibrations in the presence of backlash and nonlinearities in the bearing clearance. This work studied tooth wedging behaviour in a planetary gear. A 2-D lumped-parameter model was developed to include tooth wedging and bearing clearances. It was found that tooth wedging had a substantial effect on the forces applied to the planet bearings. A method to predict tooth wedging based on geometric interactions was developed and successfully tested.

(Crowther 2011) state that the National Renewable Energy Laboratory Gearbox Reliability Collaborative (NREL_GRC) Programme is one sample of industries working together to

improve understanding of the planetary gearbox and explore and disseminate reasons for early failure. Off-axis stresses in planet gears and bearings were investigated and it was shown how misalignment of planet pins varies with the rotation of the planetary set with consequent time-varying stresses and load distributions in the planet gears and bearings which strongly affected the fatigue life of the gearbox components. Redesign of the bearing arrangement and optimisation of the planet tooth geometry reduced the misalignment, gave better load distribution and significantly reduced time-varying contact stresses.

(Gu, Shao et al. 2011) used bispectrum analysis to identify and quantify induction motor faults in a two stage reciprocating compressor. A modified bispectrum based on the amplitude modulation features of the motor current signal was developed to consider both lower and higher sidebands, and this was found to characterise the current signal more accurately. The result showed that conventional bispectrum analysis does not adequately represent the motor current with amplitude modulation (AM) features because conventional bi-spectrum analysis cannot include two or pairs of sideband simultaneously and also, the random variation of sideband phases.

(Lei, Lin et al. 2014), reviewed the monitoring and fault diagnosis of planetary gearboxes. They noted that considerable work has been carried out investigating the vibration characteristics of gearboxes. Using advanced signal processing methods, vibration monitoring had been used successfully to identify faults such as gear pitting, cracks and wear. However, it was reported that little research has been done in developing methods for monitoring misalignment which is deemed as the second most commonly observed disturbance source in rotor systems.

(Xiange, Abdallaa et al. 2015) developed a new method for diagnosing combinations of faults in planetary gearboxes, such as sun gear and bearing faults. The vibration signature as measured on the gearbox housing is very complicated, because of the multiple paths travelled from any one source to the housing surface, high levels of background noise, and the multiple different modulations of synchronised excitation sources. A modulation signal bispectrum based sideband estimator (MSB-SE) was used to achieve a sparse representation of the content of the complex signals. MSB analysis proved effective in suppressing random

noise and decomposing the nonlinear modulation components in the measured vibration signals. The sideband amplitudes extracted by MSB-SE were related to characteristic frequencies, which provide reliable and acceptable information on the planetary gearbox faults which caused the sidebands.

2.5 Summary

This chapter presents a literature review of planetary gearboxes, see Section 2.1, and explained the basic layout of a standard planetary gearbox used in this research. The characteristic frequencies were calculated in Section 2.1.2. Subsequently, Section 2.2 described the common types of gear failures found in industry and then gave a brief overview of vibration sources in planetary gear systems in Section 2.3. Next, both signal amplitude modulation (AM) and frequency modulation (FM) was discussed. Finally, Section 2.5 provided a literature review on the identification of faults in planetary gearboxes by researchers who have successfully detected and diagnosed different types of faults such as misalignment and tooth breakages on both sun and planet gears in the planetary gearbox.

CHAPTER THREE

DYNAMIC MODELLING OF A PLANETARY GEARBOX FOR THE DETECTION OF GEAR TOOTH FAULTS

This chapter starts with an introduction to dynamic excitations in a planetary gearbox and various modelling techniques such as the lumped parameter, finite element and Hybrid models that are being employed for gear dynamic analysis. Then for the ease of implementation, the lumped mass model with a introduce modelling the planetary gearbox under investigation see Section 3.3, which allows the vibration behaviours to be understood for analysing different abnormalities, tooth breakages and gear errors and paves the way for subsequent data analytics and fault diagnostics. It must be noted that the presence of sidebands in the vibration signal of the PG become more prominent and much more complex when manufacturing errors are taken into consideration. The planetary gearbox fault characteristic frequencies for gears (sun, planet, and ring gears) are different.

3.1 Introduction

Planetary gearboxes are widely used in critical applications, as a result, the CM of PGs has received considerable attention from many researchers, as has analytical analysis and dynamic modelling of PGs (Cunliffe, Smith et al. 1974; Botman 1976).

Early work focused on analytical models of spur gears, studying the relationship between natural frequencies and system parameters, but by the 1970's Cunliffe, et al, (Cunliffe, Smith et al. 1974) was exploring the characteristic vibration modes of a 13 degree of freedom (DOF) PG with a fixed carrier. This was accompanied by experiments that measured input torque and planet pin loads. Botman studied the vibration modes of an 18 DOF system and the effects of planet pin stiffness on the natural frequencies (Botman 1976). Many researchers have followed his lead in modelling the gear meshes with linear springs and the gear bearings with two translational springs.

Each gear has three degrees of freedom (one rotational and two translational). August and Kasuba, (August and Kasuba 1986) showed how a nine DOF lumped-parameter model, without translation of the planet gears, could be used to compare the performance of fixed versus floating sun gears. Saada and Velex demonstrated that the torsional, flexural, and axial displacements of the gear components for planetary systems with spur or helical gears could be successfully represented in a model

3.2 Types of Dynamic Models

In analysis of PGs, a mathematical model is an important tool for fault diagnostics. Simulation using a model can be very valuable for gaining a deeper understanding of complex interactions between transmission components in a dynamic environment and hence improving machine diagnostics. Three types of models have been used to explain planetary gearbox dynamic behaviour and performance:

- Finite element (FE) approaches. These are considered dependable for the modelling of larger structural component parts but are considered slow and not well adjusted to the refined modelling required for tooth contact.

- Lumped parameter models give clear and reliable diagnostic for gear systems but have a restricted number of DOFs.

- Hybrid models merge the lumped parameter and finite element approaches.

3.2.1 Lumped Parameter Models

Lumped parameter models consider the system being modelled as a distribution of discrete, inter-acting elements whose combined behaviour approximates the behaviour of the system being considered. The physical dimensions of the individual objects must be small relative to the wavelengths of any vibrations being considered, which is usually valid for, the modelling of metal gears. A great advantage of the lumped parameter model is that the variables of interest are functions of time only, so the problem is reduced to solving a set of ordinary differential equations (Bilbao, S and Smith, J., (2014) Discrete-Time Lumped Models, Stanford University). The lumped-parameter model makes a number of simplifying assumptions; for example, the temperature distribution remains more or less constant which eliminates complex differential heat equations.

Gears are normally represented as rigid cylinders each with a given mass, connected to the remainder of the system by arrangements of springs and dampers, representing tooth/gear body stiffness etc. Subject to given forces this system models the movement of the gear with time and with contact conditions such as misalignments, instantaneous contact losses, tooth breakages, etc.

The 13 DOF-model of Cunliffe, et al.,(Cunliffe, Smith et al. 1974), one of the earliest, was developed for the analysis of the natural frequencies and modes in a single stage train with a fixed carrier. Jarchow and Vonderschmidt (Jarchow and Vonderschmidt 1981), developed a model with three planets taking into account manufacturing errors and mesh stiffness variations which may cause vibrations. A two dimensional transverse-torsional model with constant stiffness was used by Botman (Botman 1976) to study, numerically, the influence of carrier rotation and planet bearing stiffness on the system's natural frequencies with emphasis on the role of axis-symmetric modes on the generation of severe vibrations. Dynamic loads and the contributions of gear errors and misalignments were discussed later by Botman and Ma (Ma and Botman 1985) using a development of the same model.

August and Kasuba, (Kasuba 1984), constructed a torsional model for a basic epicycles gear system with two extra transverse DOF to allow for sun gear displacements. Kahraman (Kahraman 1994) proposed a purely torsional model for three-dimensional PGs in order to predict the natural frequencies of the planetary gear trains. A similar model, restricted to torsional degrees of freedom, was later used by Kahraman to analyse compound planetary gears typical of automotive gearboxes (Antony 1988; Kahraman 2001). Parker, et al (Antony 1988; Kahraman 2001),investigated the possibility of suppressing instabilities, and consequential structural vibration modes at the natural frequency properties of compound planetary gears and mode shape sensitivity (Kiracofe and Parker 2007). The effects of tooth contact losses and nonlinear phenomena were successfully modelled by Ambarisha and Parker (Ambarisha and Parker 2007). Tao and HaiYan (Sun and Hu 2003) established a two dimensional lumped parameter model that included rotational and transverse (horizontal and vertical) DOFs for the sun gear.

This research will investigate the dynamic behaviour of PGs with three planet gears held by a carrier, a sun gear and a fixed ring gear.

3.2.2 Finite Element Models

At an early stage in the development of the numerical modelling of PG behaviour Hidaka, et al. (Hidaka 1977) explained that better load sharing between the planet gears in real gear sets made possible by bendable ring-gears, are not fully catered for by lumped parameter models.

As finite element models justify several impacts such as mesh rigidity and pressures, sustenance and spline situations and gear blank deflections, they state the inadequacies of the lumped parameter models. On the downside, chance of in-depth studies is restricted by computational requirements since most FE models are quasi-static or static studies.

Hidaka, et al.,(Hidaka 1977) considered deflections of the ring-gear for different tooth loads and load sharing characteristics using a 2-D FE model. Numerous 3-D static evaluations and tests were undertaken on an instrumented experimental gear by Kahraman and colleagues (Kahraman and Vijayakar 2000; Bodas and Kahraman 2004; Wu and Parker 2008), and Wu and Parker (Kahraman and Vijayakar 2000; Bodas and Kahraman 2004; Wu and Parker 2008). These researchers highlighted the massive effect the flexibility of the interior gears

and positional errors in the planet gears had on load distribution between the various meshes. Subsequently, better associations with the calculated strains on the ring-gear were obtained using a more refined 3-D version of this PG model.

New FE models developed by Kahraman and colleagues (Yuksel and Kahraman 2004; Kahraman, Ligata et al. 2010) carried out a dynamic 2-D examination of tooth profile differences, in the form of manufacturing errors, wear, and changes in the tooth profile that copied rim deflections and spline settings deliberated seeded into the system. Wu and Parker (Wu and Parker 2008) developed a model of a planetary gear where the gear meshes were represented by linear springs. The sun, carrier and planet gears were treated as rigid bodies, and the ring gear modelled as a thin elastic body. The supports and bearings of the gears were modelled as two perpendicular springs of equal stiffness. The bearings and supports of the ring gear were treated as elastic. The planets are assumed to be identical and equally spaced.

An exclusive FE contact examination technique was used by Parker et al., Helsen, et al. who developed a 6-DOF multi-body model where the elements connecting rigid components were modelled using discrete spring-damper relationships. Here, the major contributions to flexibility were assumed to originate with gear meshing, splines and bearings, see Figure 3.1. Helsen, et al., concentrated their studies on modelling the behaviour of a generic gearbox with two helical and one planetary gear stages.

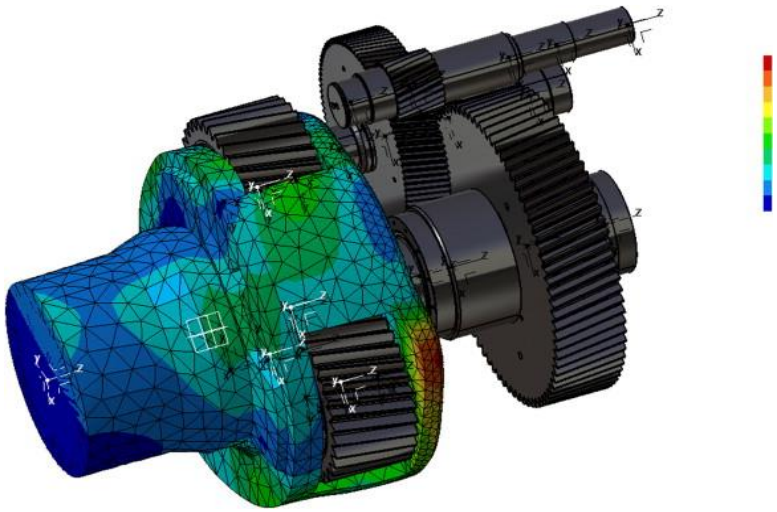

Figure 3.1 Planet carrier mode in wind turbine

3.2.3 Hybrid Models

Kahraman and his colleagues used a blend of 2-D FE analytical methods to develop a model which considered each individual gear as a deformable body to predict loads, stresses and deformations of the gears (Kahraman and Vijayakar 2000; Bodas and Kahraman 2004). A hybrid continuous discrete model was used by Parker, et al, (Parker and Wu 2010) to investigate the vibration modes predicted for planetary gears when considering the elastic properties of the ring-gears. Another modelling approach, using a hybrid style combined with FE and lumped parameters was presented by Abousleiman and Velex (Abousleiman and Velex 2006). It was claimed that the model achieved good simulation of the 3-D dynamic behaviour of PG gears by combining the lumped sun and planet gears with the shaft elements. The equations of motion were solved using time-step integration and a contact algorithm. Several quasi-static and dynamic results were provided which illustrated the possibilities of the model to account for ring-gear deflections. The number of DOFs remained restricted and a contact algorithm can be grouped with a time-step integrator to resolve the immediate tooth load distributions when a substitute structuring method is adopted to manufacture the components with linear performance, and the different meshes are controlled openly.

3.3 Dynamic Models of Planetary Gears

Dynamic models of PGs have been carefully studied by, for example, Cunliffe et al.(Cunliffe, Smith et al. 1974), who explored the characteristics of vibration modes in a 13 DOF PG with a fixed carrier, simultaneously performing experiments that measured input torque and planet pin loads. Botman (Botman 1976), studied the modes of an 18 DOF system and the effects of planet pin stiffness on the natural frequencies. Like many later researchers, he modelled the gear meshes as linear springs and the gear bearings as two translational springs.

Each gear has three degrees of freedom (one rotational and two translational). August and Kasuba, (August and Kasuba 1986), used a lumped parameter model without translation of the planet gears to compare the performance of fixed versus floating sun gears. Saada and

Velex (Saada and Velex 1995), considered the torsional, flexural, and axial displacements of gear components to develop a model for planetary systems with spur or helical gears.

Kahraman proposed a simplified rotational lumped parameter model, providing closed-form expressions for the torsional natural frequencies in terms of system parameters (Kahraman 1994). Kahraman later developed a more complex model that included all six rigid body DOF for each gear component to analyse the full 3-D motion expected in a helical system (Kahraman 1994). He then investigated the effects of mesh phasing on the dynamics of equally spaced planet systems in helical PGs. Lin and Parker used a two-dimensional rotational and translational model to explain the unique modal properties of a planetary system with equal planet spacing (Lin and Parker 1999). They extended this work to include diametrically opposed planet spacing studying parametric instability due to mesh stiffness variation, and the effect on the dynamic behaviour of spur planetary gears of mesh phasing relationships (Lin and Parker 2000). They categorised all vibration modes into three types: rotational, translational and planet, each with its own distinct characteristics.

Bahk and Parker (Bahk and Parker 2011) used these model and computational methods to investigate nonlinear behaviour in an equally spaced spur PG. Wu and Parker (Wu and Parker 2008) removed the assumption of a rigid ring gear, considering its elastic deformation and the subsequent effects on the modal properties. There are similar mode type categories associated with a full three-dimensional model and compound planetary gears (Wu and Parker 2008; Eritenel and Parker 2009; Guo and Parker 2010; Cooley and Parker 2012).

Dong, et al., (H. Dong 2015) recently reported on a torsional-translational coupled nonlinear dynamic model to represent a PG gear train with three planet gears which included not only gear elastic deformation but also manufacturing and assembly errors. The latter were presented as equivalent to the line of action of gear pairs. The authors claimed their model provides a guideline for design of PG.

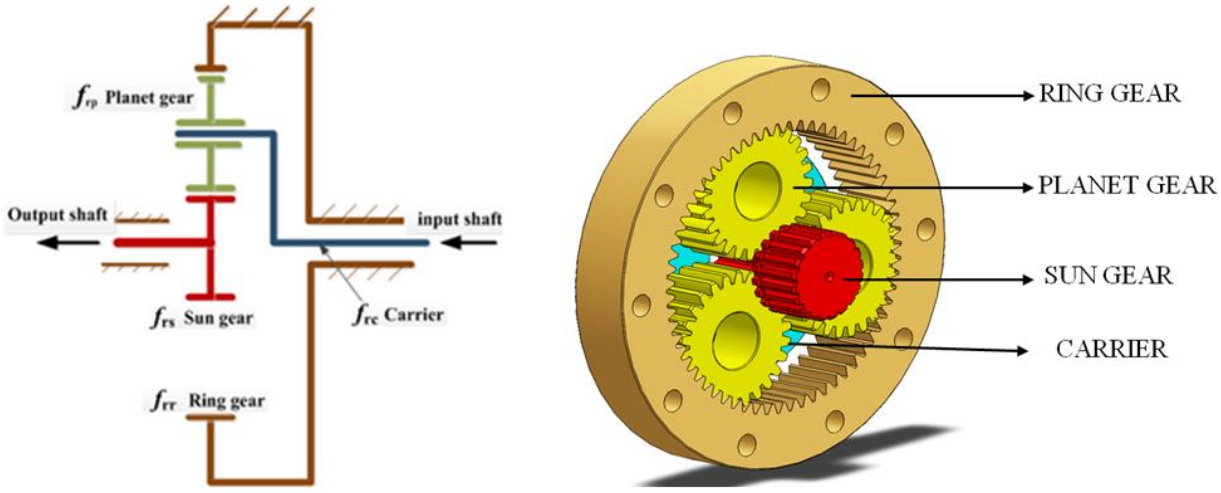

Figure 3.2 Schematic of a planetary gearbox with standstill ring gear

The PG supplied and manufactured by STM Power Transmission Ltd is represented in Figure 3.2. It is the basis for a model of a single stage PG consisting of three planet gears, one sun gear, one carrier and one gear wheel or ring which is at standstill. The technical specifications of the PG are given in Table 3.1 , and Table 3.2.The planet carrier is floating and fixed to the output shaft by means of splines, which allow it to move axially as required. The planet gears are hardened and use the inside of the planet gear as the inner bearing race. Loose needle bearings are then inserted between the planet gear and the planet gear shaft with the shaft itself being the other race of the bearing (Abdalla, Tian et al. 2014).

Table 3.1 Dimensions of the planetary gearbox

Gear	Teeth
Ring	$z_r = 62$
3 x Planets	$z_p = 26$
Sun	$z_s = 10$
Transmission Ratio	7.2

Input torque:

T_c=360 Nm

$T_S = T_c/7.2 = 360/7.2 = 50$ Nm.

Both T_S, T_c; are Clockwise.

Table 3.2 Data for the planetary gear configurations presented in this work

Parameter		Sun	Planet	Ring	carrier
Mass	kg	0.29	0.34	3.64	2.00
Module/Addendum	mm	2.25	2.25	2.25	…..
Outside diameter	mm	29.5	62.0	178.0	130.0
Inside diameter	mm	……	27.1	137.3	40.00
Base diameter	mm	21.143	54.972	131.087	130..0
Pitch diameter	mm	22.5	58.5	139.5	…..
Face width	mm	25.0	24.0	26.0	18.0
Tooth thickness	mm	4.75	4.43	4.28	……
Moments of inertia I_s, I_P, I_r, I_c	$kg.m^2$	2.10×10^{-4}	2.9×10^{-4}	5.05×10^{-4}	4.93×10^{-3}
I/r^2	kg	0.14	0.17	0.82	1
pressure angle		$\alpha_r, \alpha_s =$	$\alpha = 20^o$		
Mesh stiffness	N/m	$k_{sp} = k_{rp} = k_m = 5\times10^8$			
Bearing stiffness	N/m	$k_p = k_r = k_s = k_c = 10^8$			
Torsion stiffness	N/m	$k_{ru} = 10^9$	$k_{su} = k_{cu} = k_{pu} = 0$		

3.3.1 Lumped-Parameter Analytical Model

Figure 3.3 shows the model representation of a spur gear in the PG. This is a cross-sectional view of one stage, showing the PG lumped-parameters in two dimensions. The gear and bearing mesh are modelled as a nonlinear spring and damping with periodically varying stiffness acting along the line of action for the gear. The periodic variation in mesh stiffness is due to the change in the number of teeth in contact as the gears rotate (Ambarisha and Parker 2007).

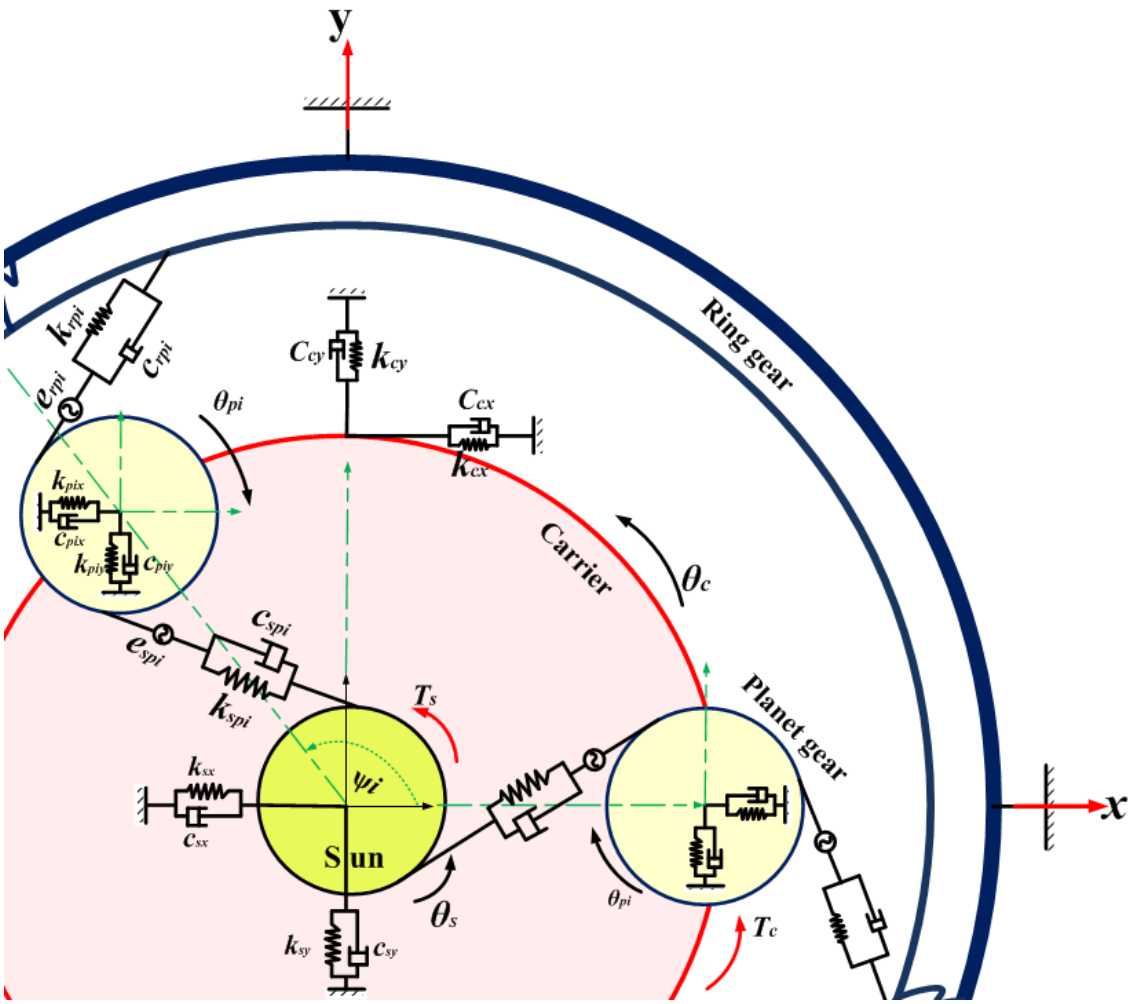

Figure 3.3 Dynamic model of a planetary gearbox (Fan, Wang et al. 2016)

3.3.2 Dynamic Motion Equations of the Model

Dynamic models of PGs have been carefully studied by, for example, Cunliffe et al.(Cunliffe, Smith et al. 1974), who explored the characteristics of vibration modes in a 13 DOF PG with a fixed carrier, simultaneously performing experiments that measured input torque and planet pin loads. Botman (Botman 1976), studied the modes of an 18 DOF system and the effects of planet pin stiffness on the natural frequencies. Like many later researchers, he modelled the gear meshes as linear springs and the gear bearings as two translational springs.

Each gear has three degrees of freedom (one rotational and two translational). August and Kasuba, (August and Kasuba 1986), used a lumped parameter model without translation of

the planet gears to compare the performance of fixed versus floating sun gears. Saada and Velex (Saada and Velex 1995), considered the torsional, flexural, and axial displacements of gear components to develop a model for planetary systems with spur or helical gears.

The dynamic equations of motion for the spur planetary system in a 18 DOF with N planets, as presented in Figure 3.3, can according to the Newton's second law and following Fan et al (Geramitcioski and Trajcevski 2002; Fan, Wang et al. 2016) and Geramitcioski and Trajcevski (Geramitcioski and Trajcevski 2002), be written in terms of rotational kinetic energy as:

Carrier;

$$(I_c / r_c^2)\ddot{u}_c(t) + \sum_{i=1}^{N} C_{pi}(t)\dot{\delta}_{nti} + \sum_{i=1}^{N} k_{pi}(t)\delta_{nti} = T_c / r_c \tag{3.1}$$

$$\begin{aligned}(m_c + N*m_p)\ddot{x}_c(t) + \sum_{i=1}^{N} C_{pi}(t)\dot{\delta}_{nri}\cos\psi_i + \sum_{i=1}^{N} K_{pi}(t)\delta_{nri}\cos\psi_i - \sum_{i=1}^{N} C_{pi}(t)\dot{\delta}_{nti}\sin\psi_i \\ - \sum_{i=1}^{N} K_{pi}(t)\delta_{nti}\sin\psi_i + c_c\dot{x}_c(t) + k_c x_c = 0\end{aligned} \tag{3.2}$$

$$\begin{aligned}(m_c + N*m_p)\ddot{y}_c(t) + \sum_{i=1}^{N} C_{pi}(t)\dot{\delta}_{nri}\sin\psi_i + \sum_{i=1}^{N} K_{pi}(t)\delta_{nri}\sin\psi_i + \sum_{i=1}^{N} C_{pi}(t)\dot{\delta}_{nti}\cos\psi_i \\ + \sum_{i=1}^{N} K_{pi}(t)\delta_{nti}\cos\psi_i + c_c\dot{y}_c(t) + k_c y_c = 0\end{aligned} \tag{3.3}$$

Ring;

$$(I_r / r_r^2)\ddot{u}_r(t) = 0 \tag{3.4}$$

For the ring gear rotational, the equation = 0, due to the ring gear in fixed with the gear house.

$$m_r\ddot{x}_r(t) - \sum_{i=1}^{N} C_{rpi}(t)\dot{\delta}_{rni}\sin\psi_{ri} - \sum_{i=1}^{N} K_{rpi}(t)\delta_{rni}\sin\psi_{ri} + c_r\dot{x}_r(t) + k_r x_r = 0 \tag{3.5}$$

$$m_r\ddot{y}_r(t) - \sum_{i=1}^{N} C_{rpi}(t)\dot{\delta}_{rni}\cos\psi_{ri} - \sum_{i=1}^{N} K_{rpi}(t)\delta_{rni}\cos\psi_{ri} + c_r\dot{y}_r(t) + k_r y_r = 0 \tag{3.6}$$

Sun;

$$(I_s / r_s^2)\ddot{u}_s(t) + \sum_{i=1}^{N} C_{spi}\dot{\delta}_{sni} + \sum_{i=1}^{N} k_{spi}\delta_{sni} = T_s / r_s \tag{3.7}$$

$$m_s\ddot{x}_s(t) - \sum_{i=1}^{N} C_{spi}(t)\dot{\delta}_{sni}\sin\psi_{si} - \sum_{i=1}^{N} K_{spi}(t)\delta_{sni}\sin\psi_{si} + c_s\dot{x}_s + k_s x_s = 0 \tag{3.8}$$

$$m_s\ddot{y}_s(t) - \sum_{i=1}^{N} C_{spi}(t)\dot{\delta}_{sni}\cos\psi_{si} + \sum_{i=1}^{N} K_{spi}(t)\delta_{sni}\cos\psi_{si} + c_s\dot{y}_s(t) + k_s y_s = 0 \tag{3.9}$$

Planet 01;

$$(I_{p1} / r_{p1}^2)\ddot{u}_{p1}(t) - C_{rp1}(t)\dot{\delta}_{rn1} - K_{rp1}(t)\delta_{rn1} + C_{sp1}(t)\dot{\delta}_{sn1} + K_{sp1}(t)\delta_{sn1} = 0 \tag{3.10}$$

$$\begin{aligned} &m_{p1}\ddot{x}_{p1}(t) - [C_{rp1}(t)\dot{\delta}_{rn1} - K_{rp1}(t)\delta_{rn1} + C_{sp1}(t)\dot{\delta}_{sn1} + K_{sp1}\delta_{sn1}]*\sin\alpha \\ &- K_{p1}\delta_{nr1} + c_p\dot{x}_{p1}(t) + k_p x_{p1} = 0 \end{aligned} \tag{3.11}$$

$$\begin{aligned} &m_{p1}\ddot{y}_{p1}(t) - [C_{rp1}(t)\dot{\delta}_{rn1} - K_{rp1}(t)\delta_{rn1} + C_{sp1}(t)\dot{\delta}_{sn1} + K_{sp1}(t)\delta_{sn1}]*\cos\alpha \\ &- K_{p1}\delta_{nr1} + c_p\dot{y}_{p1} + k_p y_{p1} = 0 \end{aligned} \tag{3.12}$$

Planet 02;

$$(I_{p2} / r_{p2}^2)\ddot{u}_{p2}(t) - C_{rp2}(t)\dot{\delta}_{rn2} - K_{rp2}(t)\delta_{rn2} + C_{sp2}(t)\dot{\delta}_{sn2} + K_{sp2}\delta_{sn2} = 0 \tag{3.13}$$

$$\begin{aligned} &m_{p2}\ddot{x}_{p2}(t) - [C_{rp2}(t)\dot{\delta}_{rn2} - K_{rp2}(t)\delta_{rn2} + C_{sp2}(t)\dot{\delta}_{sn2} + K_{sp2}(t)\delta_{sn2}]*\sin\alpha \\ &- K_{p2}(t)\delta_{nr2} + C_p\dot{x}_{p2} + k_p x_{p2} = 0 \end{aligned} \tag{3.14}$$

$$\begin{aligned} &m_{p2}\ddot{y}_{p2}(t) - [C_{rp2}(t)\dot{\delta}_{rn2} - K_{rp2}(t)\delta_{rn2} + C_{sp2}(t)\dot{\delta}_{sn2} + K_{sp2}(t)\delta_{sn2}]*\cos\alpha \\ &- K_{p2}\delta_{nr2} + c_p\dot{y}_{p2} + k_p y_{p2} = 0 \end{aligned} \tag{3.15}$$

Planet 03;

$$(I_{p3} / r_{p3}^2)\ddot{u}_{p3}(t) - C_{rp3}(t)\dot{\delta}_{rn3} - K_{rp3}(t)\delta_{rn3} + C_{sp3}(t)\dot{\delta}_{sn3} + K_{sp3}(t)\delta_{sn3} = 0 \tag{3.16}$$

$$m_{p3}\ddot{x}_{p3}(t)-[C_{rp3}(t)\dot{\delta}_{rn3}-K_{rp3}(t)\delta_{rn3}+C_{sp3}(t)\dot{\delta}_{sn3}+K_{sp3}(t)\delta_{3}]*\sin\alpha \\ -K_{p3}\delta_{nr3}+c_{p}\dot{x}_{p3}+k_{p}x_{p3}=0 \quad (3.17)$$

$$m_{p3}\ddot{y}_{p3}(t)-[C_{rp3}(t)\dot{\delta}_{rn3}-K_{rp3}(t)\delta_{rn3}+C_{sp3}(t)\dot{\delta}_{sn3}+K_{sp3}(t)\delta_{sn3}]*\cos\alpha \\ -K_{p3}\delta_{nr3}+c_{p}\dot{y}_{p3}+k_{p}y_{p3}=0 \quad (3.18)$$

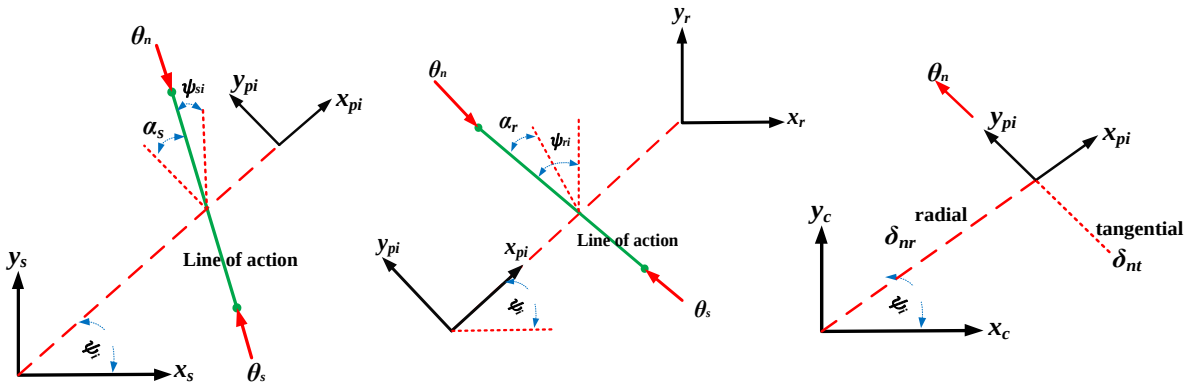

(i) (ii) (iii)

Figure 3.4 Kinematics sketches showing relative deflections of component

where;

The ψ_i is the circumferential position planet gear pi around the sun gear centre as follow;

$\psi_1=0$ Initial value for sun-planet mesh pressure angle, then the angular position $\psi_{si}=\psi_i-\alpha_s$, and the pressure angle of the ring – planet mesh $\psi i=\psi_i-\alpha_r$.

The (δ), represents the compressions of the elastic elements between the sun and planet gears and between ring and planet gears and can be defined as;

Sun-planet mesh:

$$\delta_{sni}=y_s(t)\cos\psi_{si}-x_s(t)\sin\psi_{si}-x_{pi}(t)\sin\alpha_s-y_{pi}(t)\cos\alpha_s+\theta_s(t)+\theta_{pi}+e_{spi} \quad (3.19)$$

$$\dot{\delta}_{sni}=\dot{y}_s(t)\cos\psi_{si}-\dot{x}_s(t)\sin\psi_{si}-\dot{x}_{pi}(t)\sin\alpha_s-\dot{y}_{pi}(t)\cos\alpha_s+\theta_s(t)+\theta_{pi} \quad (3.20)$$

Ring-planet mesh:

$$\delta_{rni} = y_r(t)\cos\psi_{ri} - x_r(t)\sin\psi_{ri} - x_{pi}(t)\sin\alpha_r + y_{pi}(t)\cos\alpha_r + \theta_r(t) - \theta_{pi} + e_{rpi} \quad (3.21)$$

$$\dot{\delta}_{rni} = \dot{y}_r(t)\cos\psi_{ri} - \dot{x}_r(t)\sin\psi_{ri} - \dot{x}_{pi}(t)\sin\alpha_r + \dot{y}_{pi}(t)\cos\alpha_r + \dot{\theta}_r(t) - \dot{\theta}_{pi} \quad (3.22)$$

Planet bearing tangential:

$$\delta_{nti} = y_c(t)\cos\psi_i - x_c(t)\sin\psi_i - y_{pi}(t) + \theta_c(t). \quad (3.23)$$

$$\dot{\delta}_{nti} = \dot{y}_c(t)\cos\psi_i - \dot{x}_c(t)\sin\psi_i - \dot{y}_{pi}(t) + \dot{\theta}_c(t). \quad (3.24)$$

Planet bearing radial:

$$\delta_{nri} = y_c(t)\sin\psi_i + x_c(t)\cos\psi_i - x_{pi}. \quad (3.25)$$

$$\dot{\delta}_{nri} = \dot{y}_c(t)\sin\psi_i + \dot{x}_c(t)\cos\psi_i - \dot{x}_{pi}. \quad (3.26)$$

In Figure 3.4 (i) and Equation (3.19) we synthesised the sun and planet deflections in the direction of the line of action for sun-planet meshes. In Figure 3.4 (ii) and Equation (3.21) we derived the ring and planet deflections in the direction of the line of action for ring-planet meshes. Similarly, Equation (3.25) shows the planet bearing interfaces with the carrier as obtained from Figure 3.4 (iii).

3.3.3 Matrix Format

Vibration differential equation for a rotational and translational model with *N* planet can be expressed as:

$$M\ddot{q} + C\dot{q} + Kq(t) = F(t) \quad (3.27)$$

Where;

M , is the mass matrix. C , is the damping matrix. K , is the stiffness matrix. $\ddot{q}, \dot{q}, q$, are the acceleration, velocity and displacement of the vibration motion, $F(t)$ is the force vector of externally applied load or torque (Lin and Parker 1999; Inalpolat and Kahraman 2010).

The inertia matrix;

$$M = \left\{ \frac{I_c}{r_c^2}, \frac{I_r}{r_r^2}, \frac{I_s}{r_s^2}, \frac{I_p}{r_{p1}^2}, ..., \frac{I_p}{r_{pN}^2}, m_c + Nm_p, m_r, m_s, m_{p1}, ..., m_{pN}, m_c + Nm_p, m_r, m_s, m_{p1}, ..., m_{pN} \right\}^T \quad (3.28)$$

$$q = \left\{\theta_c, \theta_r, \theta_s, \theta_{p1}, ..., \theta_{pN}, x_c, x_r, x_s, x_1, ..., x_p, y_c, y_r, y_s, y_{p1}, ..., y_{pN}\right\}^T \quad (3.29)$$

The matrices are defined in the Appendix for both the damping C and mesh stiffens K.

3.4 Modal Properties

By using an average value to replace the time varying tooth stiffness and leaving the damping terms, differential equations can be simplified in a matrix form as;

$$\mathbf{M}\ddot{\mathbf{q}} + \mathbf{K}(t)\mathbf{q}(t) = 0 \quad (3.30)$$

where, ***M*** is the mass matrix, ***K*** represents the stiffness

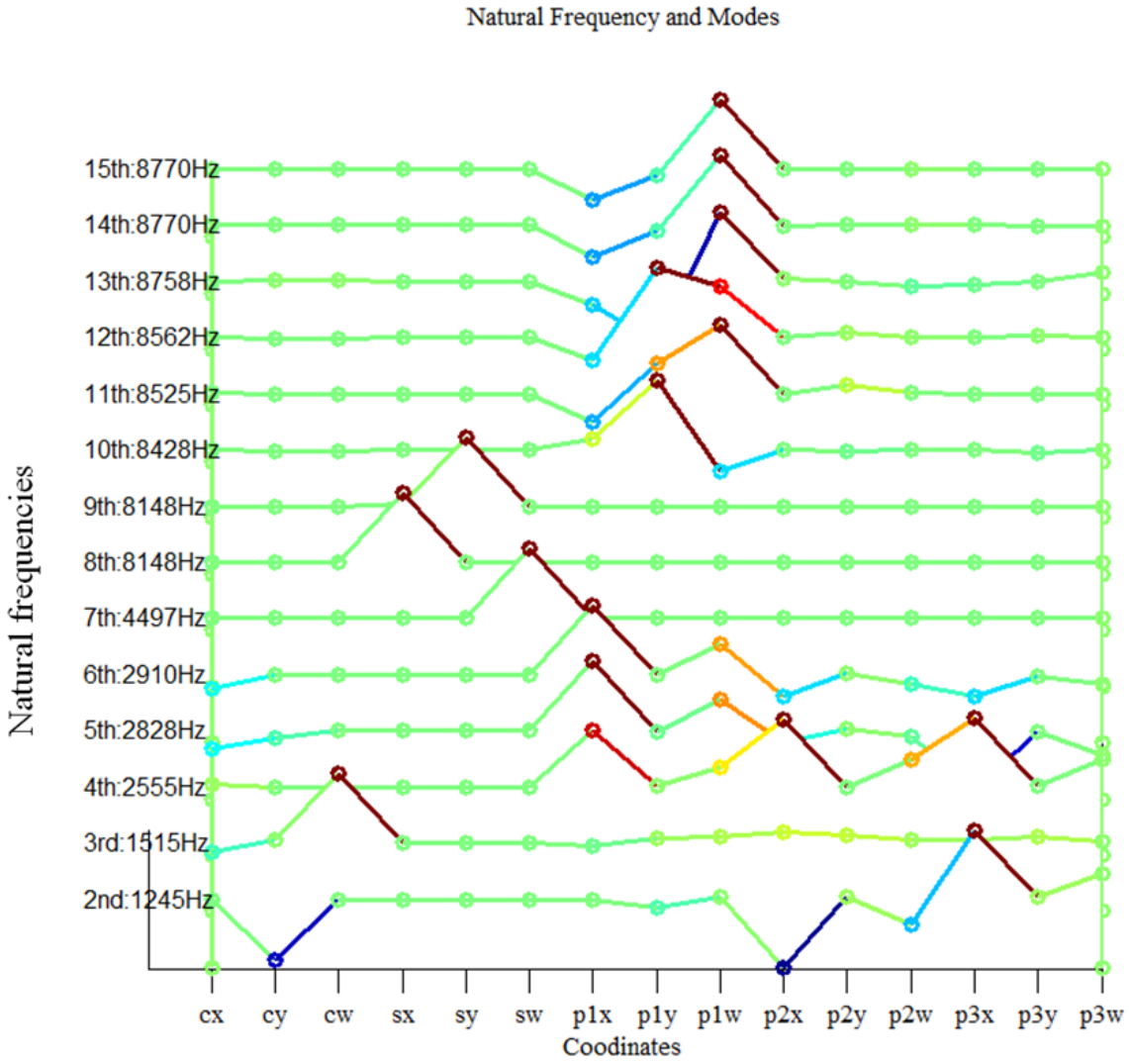

Figure 3.5 Natural frequency of the gearbox system

By solving the associated eigenvalue problem for the above matrix equation, natural frequencies and corresponding mode shapes can be obtained that are essential for the dynamic investigations of the PG gearbox and its vibration responses.

For the presented model here, there are six translational modes, five torsional modes and three planetary modes (Lin and Parker 1999).

As shown in the figure the lowest natural frequency is at 1245Hz, which is well above the meshing frequencies of underlying studies.

3.5 Numerical Analysis of Vibration Responses to Different Gear Faults

A significant number of studies have been carried out on the dynamic modelling of PGs to develop effective signal processing methods for detection and characterisation of complicated weak fault signals contaminated by noise (Jardine, Lin et al. 2006).

PG vibration spectrum sidebands are highly sensitive to the degree of the fault in the gears (sun, planet and ring), and have proved to be very useful for tooth fault detection and localisation. However, the amplitude and frequency modulation of the vibration signal will be affected not only by faults that develop within the PG, but will also be affected by manufacturing errors which invariably occur in real PG systems and generate complex sidebands in the vibration spectrum.

The lumped parameter model considered here for a typical PG system (three planets, one sun and one ring gear) with manufacturing and other errors was established, see Figure 3.3. In the PG model the influences of such faults as tooth breakages and consequent tooth impacts are analysed and effects on the time-varying mesh stiffness and dynamic forces are derived. Numerical methods were used to predict likely response spectra of the PG with and without tooth faults and other errors (Gui, Han et al. 2014).

3.5.1 Modelling for a Healthy Planetary Gear System

Figure 3.6 shows a healthy case in both *x* and *y* directions for the time and frequency domains. The first predicted mesh frequency f_m clearly appears at 156 Hz, and its harmonics

are seen at 312 and 468 Hz. The figure represents the case with no faults present and the sidebands at $nf_m \pm f_{rc}$ are without error effects.

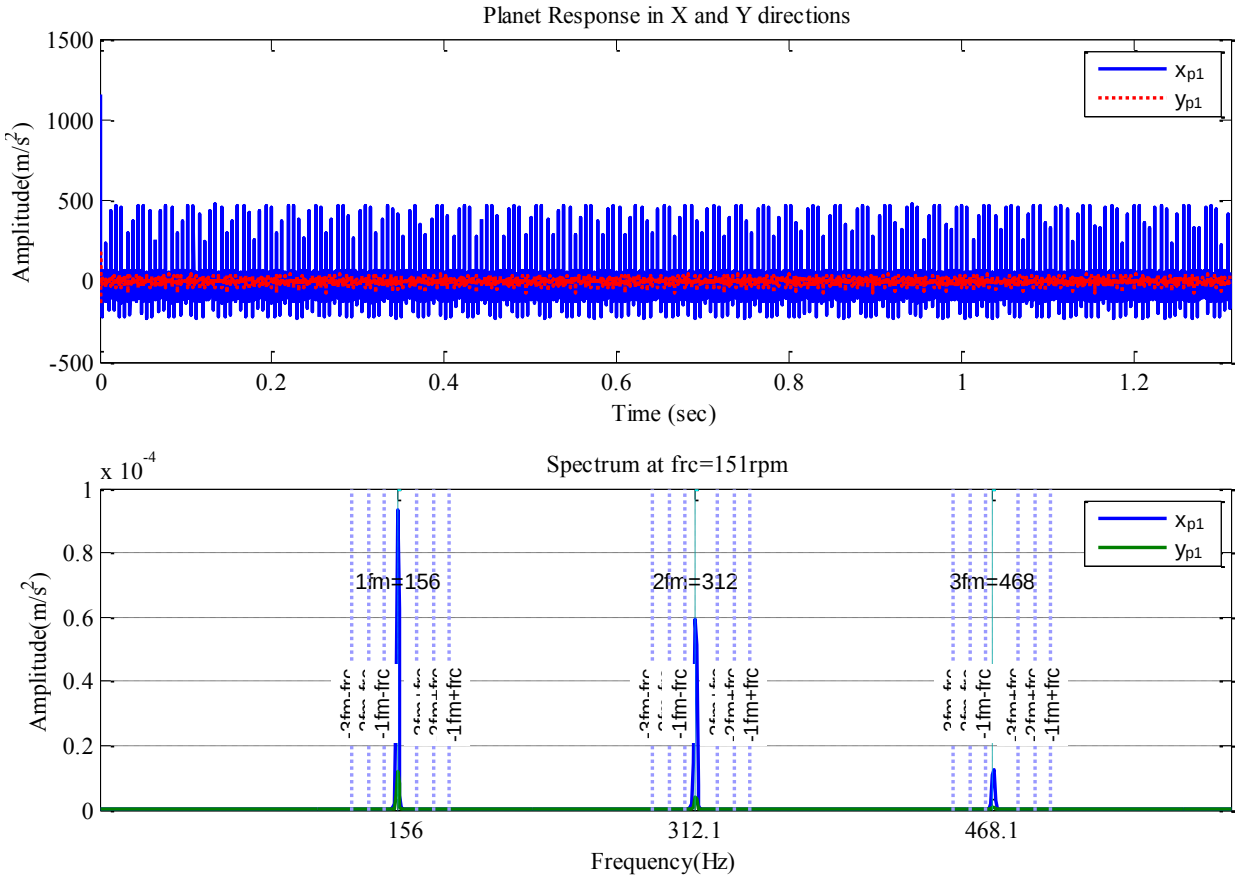

Figure 3.6 Simulated vibration signal for X direction and Y direction in time and frequency domain with no faults present

Figure 3.7 shows the predicted dynamic force between sun and planet gears and mesh stiffness of the sun–planet gear and planets- ring gear interactions. This is shown to be healthy example; there are no tooth faults to influence the dynamic forces between neither gears nor the mesh stiffness. The first predicted mesh frequency f_m clearly appears at 156 Hz, and its harmonics are seen at 312 and 468 Hz. The figure represents the case with no faults present and the sidebands at $nf_m \pm f_{rc}$ are without error effects.

However, the s-pn is the contact between the sun gear and planet gears where; n=1, 2, 3.

r-pn is the contact between the ring gear and planet gears where; n=1,2,3.

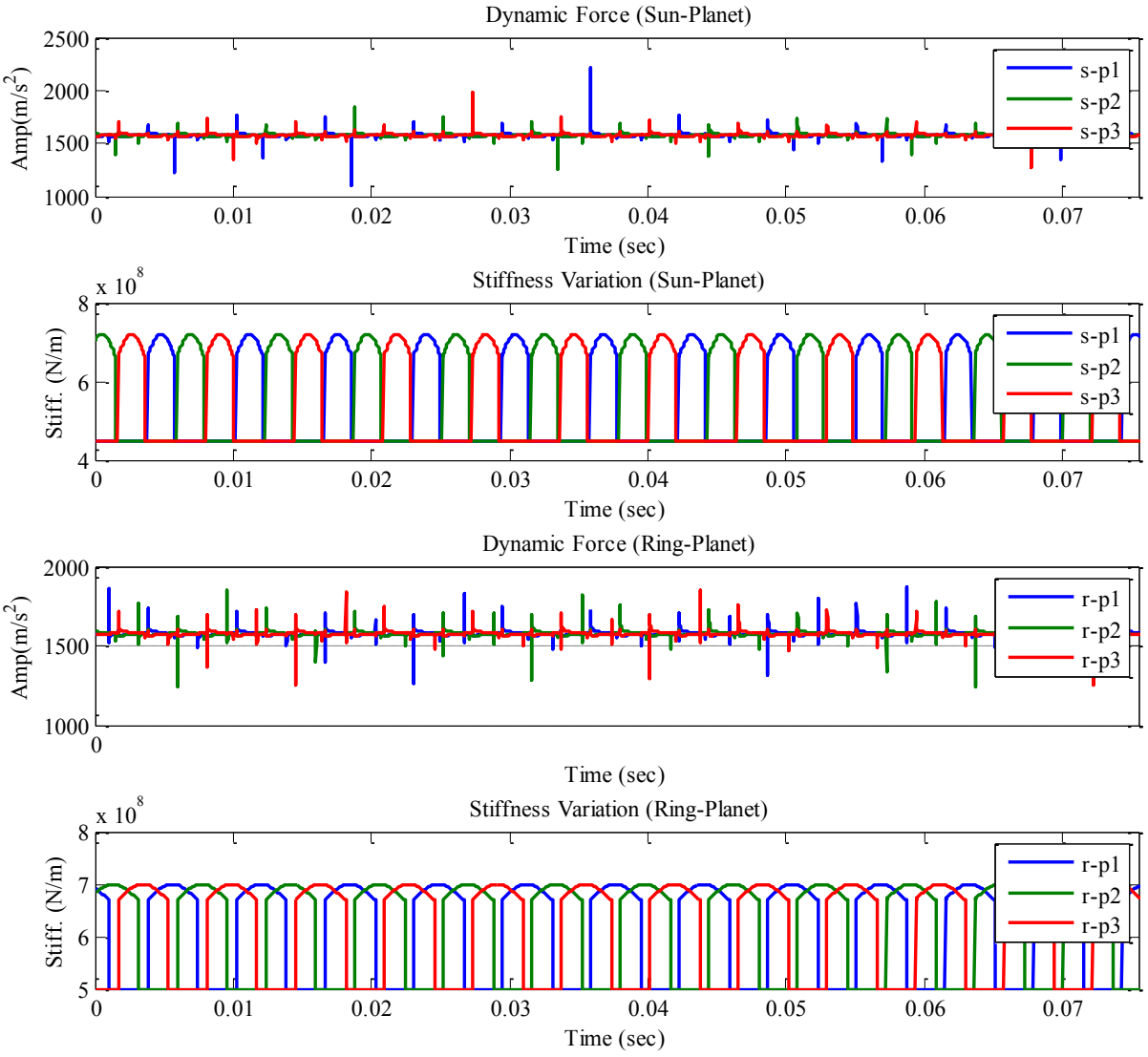

Figure 3.7 Both mesh stiffness and dynamic force for healthy sun-planet and ring-planet

Figure 3.8 shows the predicted mesh frequency (156 Hz) and harmonics (312 and 468 Hz) for healthy sun-planet and/or planet-ring contacts. Also shown are the summations at frequencies f_m, $2f_m$ and $3f_m$, it is clear they appear with the same amplitude of mesh frequency and as the amplitude decreases the sidebands are minimal.

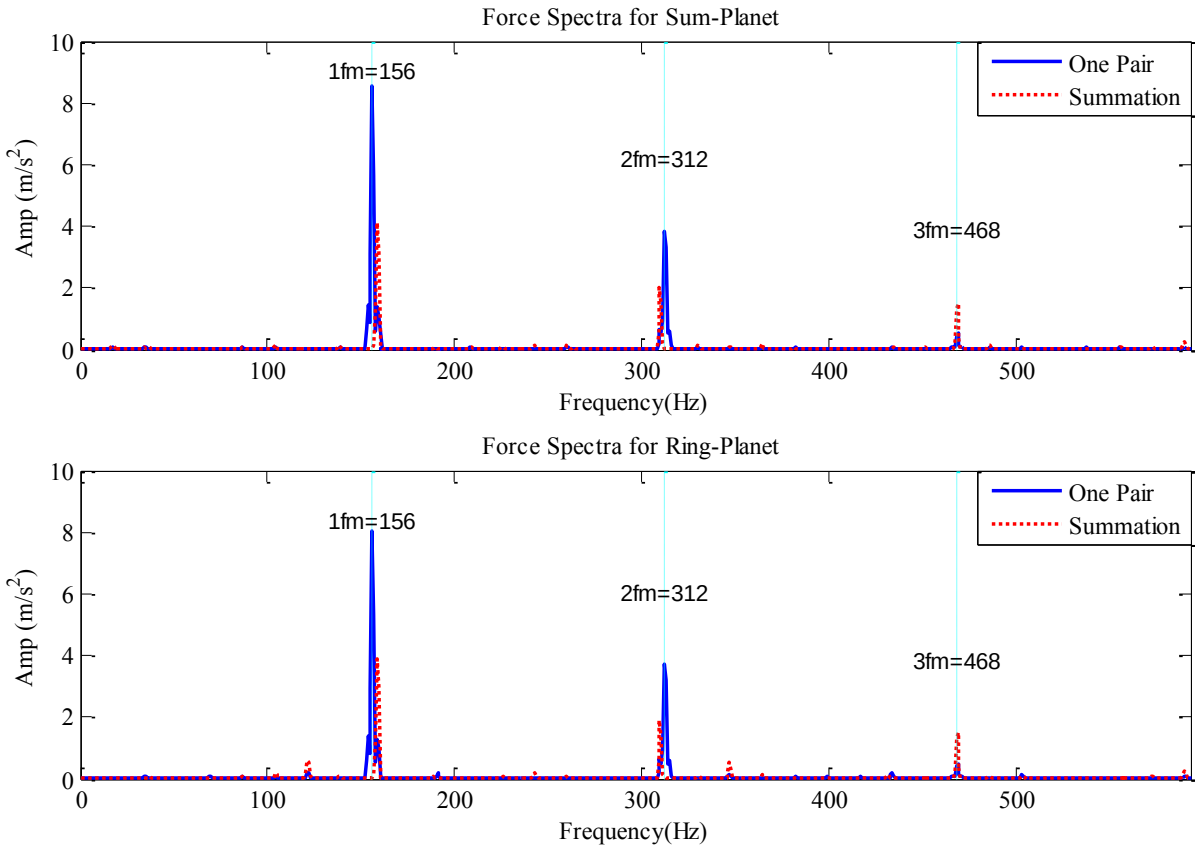

Figure 3.8 Simulated vibration signal of healthy sun and planet gear

3.5.2 Modelling of Sun Gear Fault

Figure 3.9 shows response of vibration signal tooth breakage fault in the sun gear in both x and y directions for time and frequency domain. The mesh frequency is again predicted to be 156 Hz but with a higher amplitude than that of the healthy case. The second harmonic appears at 312 Hz and is also greater than that of the healthy case. The third harmonic at 468 Hz appears to be much the same as for the healthy case but now is of the same amplitude as the sidebands which have appeared around f_m and $2f_m$, as a result of the introduction of the fault.

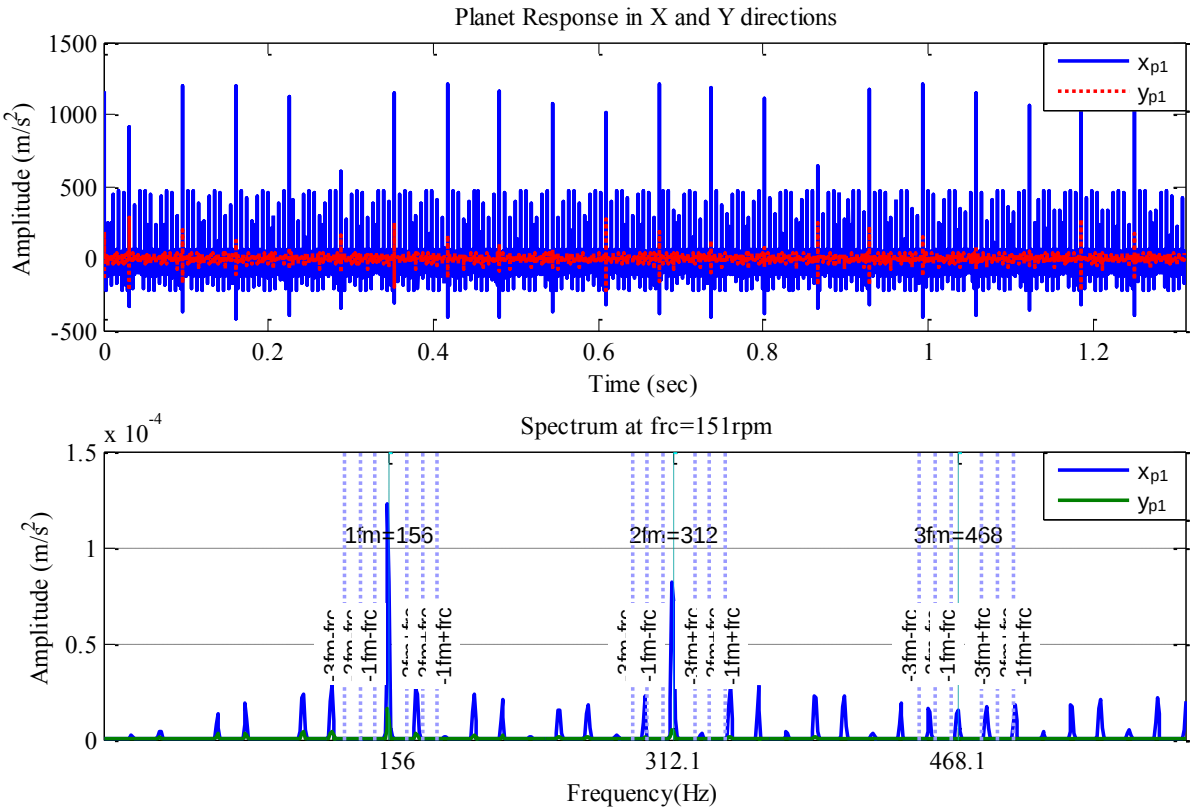

Figure 3.9 Vibration signal for X direction and Y direction in time and frequency domains with one tooth fault in sun gear

Figure 3.10, again shows the predicted dynamic force between sun and planet gears and mesh stiffness of the sun, planet gear and planets- ring gear interactions, but now a tooth breakage fault is included in the model. In the force/time plot there are the same numbers of peaks but now a much larger peak can be seen, representing the greater impact forces that are generated. The mesh stiffness plot for the sun–planet gears clearly shows the sun gear tooth fault. Because the planet-ring gear interactions contain no faults, obviously the tooth fault has no influence on mesh stiffness between planet and ring gears.

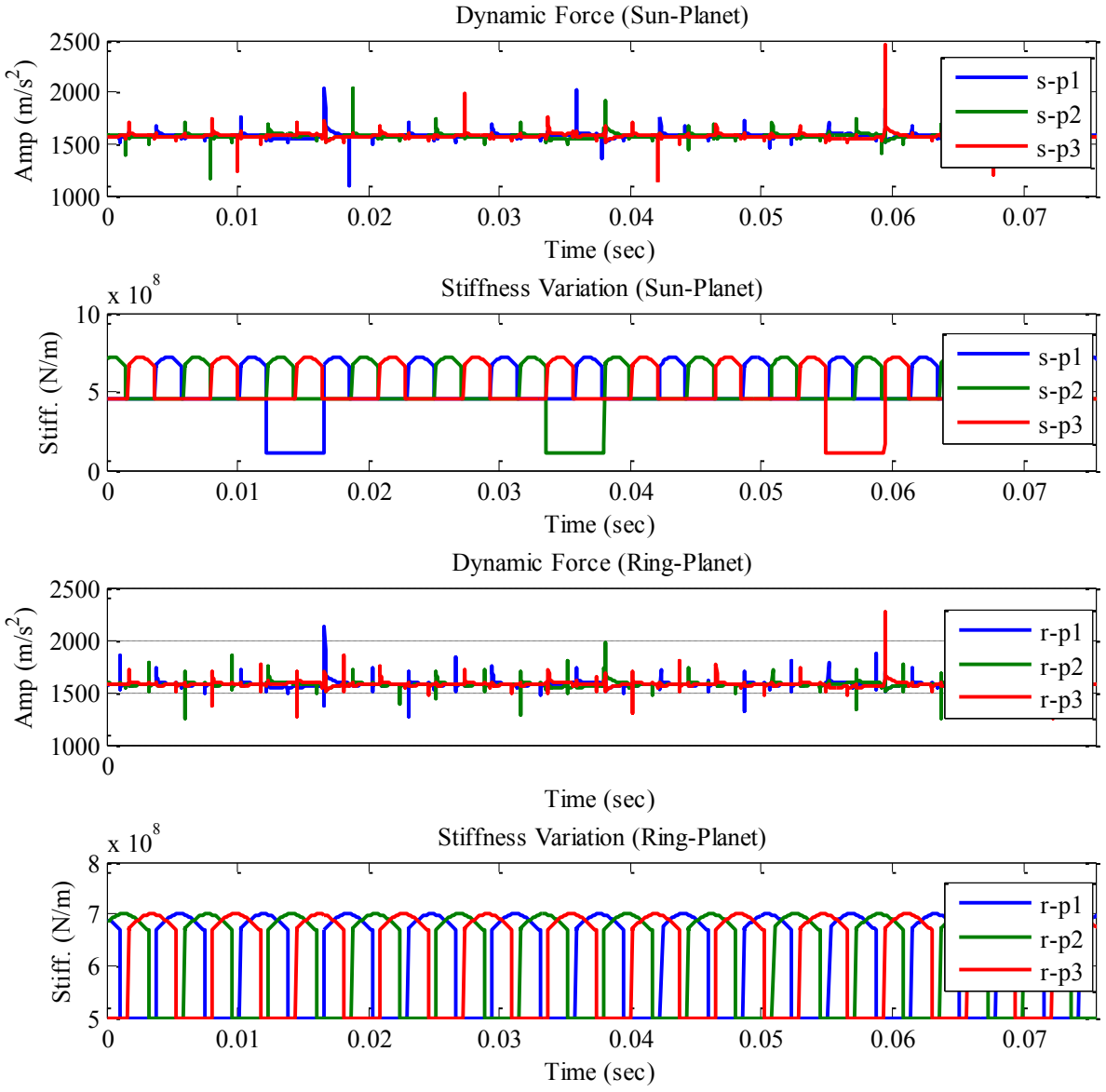

Figure 3.10 The sun-planet and ring-planet mesh stiffness with one tooth fault in sun gear

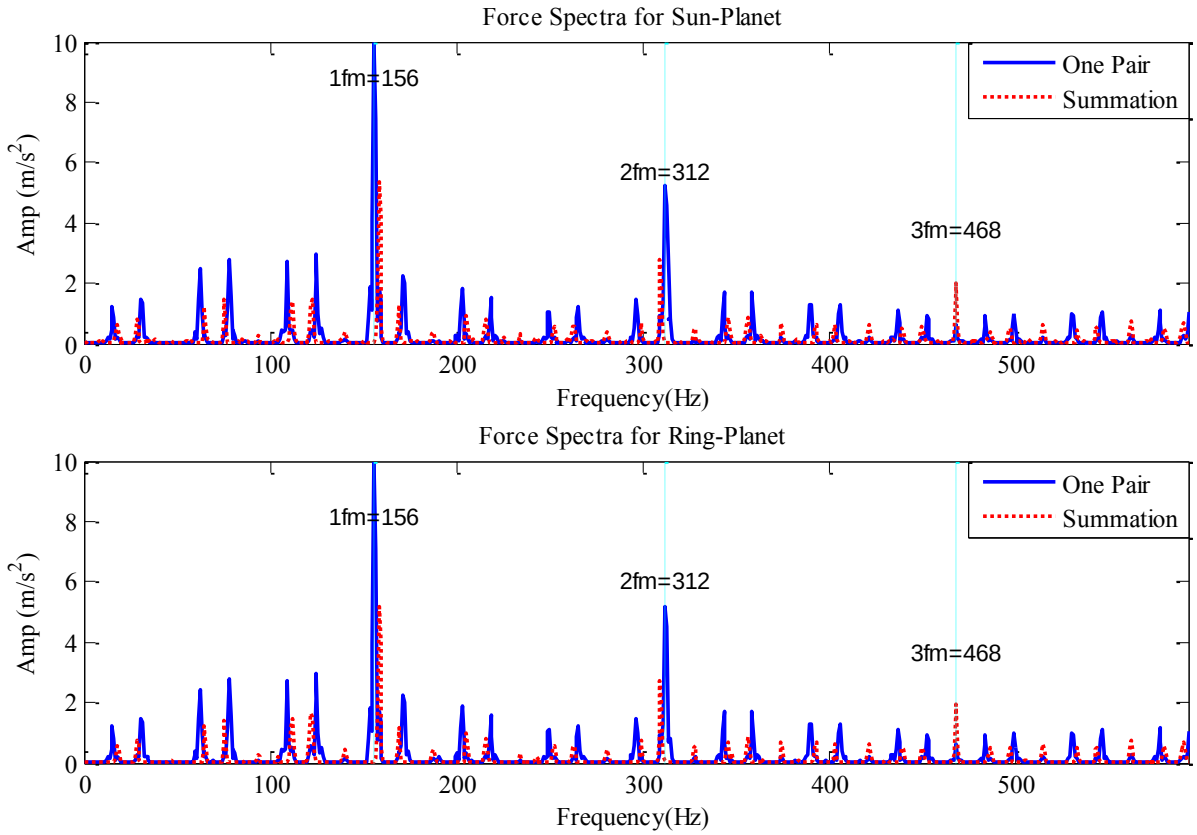

Figure 3.11 Simulated vibration signal for sun planet mesh with one tooth fault on sun gear

Figure 3.11, shows mesh frequency in the fundamental remain at 156n Hz, but has greater amplitude in the presence of a fault. This is also true for the second and third harmonics, $2f_m$ and $3f_m$.However, of most importance for this research is the presence of the sideband due to the introduction of the fault. These sidebands appear around each of f_m , $2f_m$ and $3f_m$ but are most clearly visible around f_m .

3.5.3 Modelling of Planet Gear Fault

The next stage in the simulation process was to revert to a healthy sun gear and introduce a single tooth fault into one of the planetary gears Figure 3.12 shows the predicted time domain amplitude response and the frequency domain acceleration response in both x and y directions for a planetary gear with single tooth fault. The first mesh frequency f_m is clearly visible at 156 Hz, and also at the second harmonic, $2f_m$ at 312 Hz. It is also possible to

observe the presence of small sidebands similar to those that appeared in Figure 3.9 due to the presence of a sun gear tooth fault.

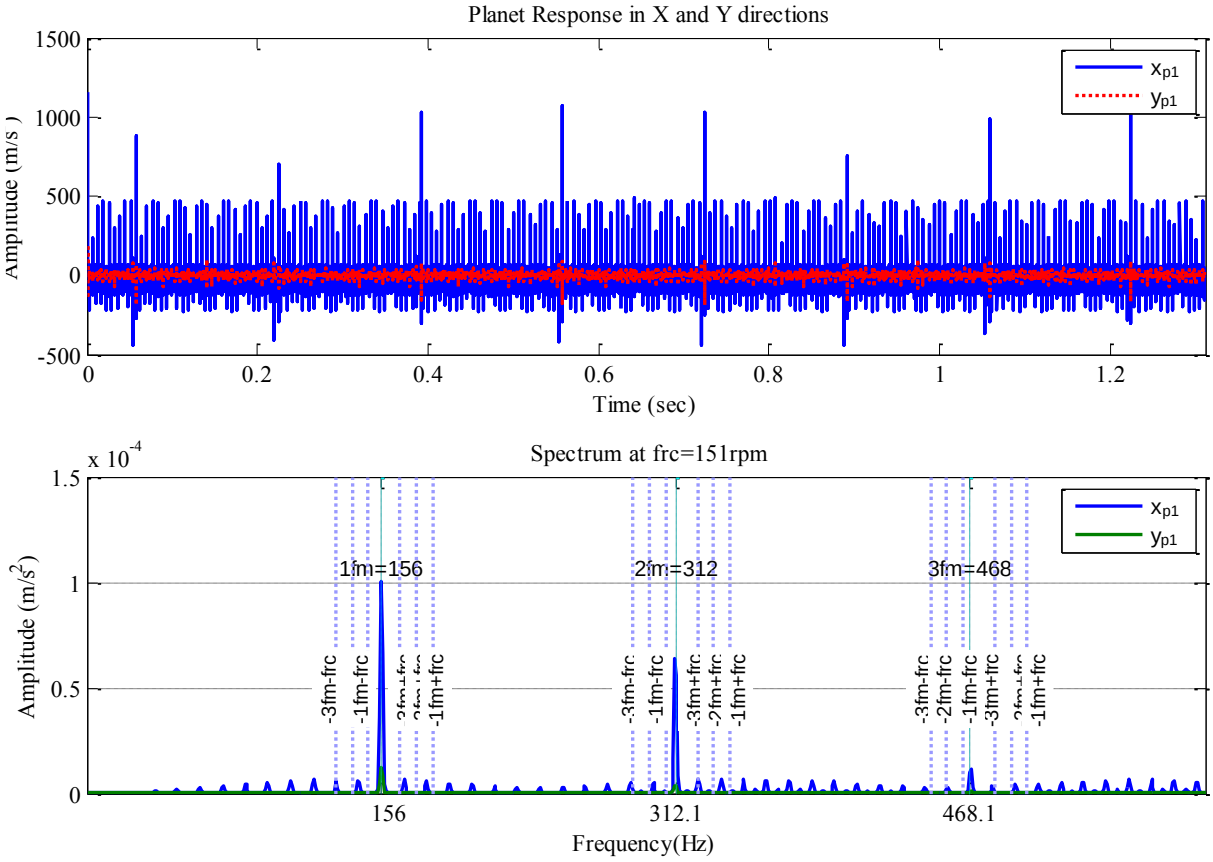

Figure 3.12 Simulated vibration signal for X and Y direction in time and frequency domains with a single tooth fault in one planet gear

Figure 3.13 shows the time domain signal for the dynamic force and stiffness for the sun gear and planet gear for a single tooth fault in one of the three planet gear faults. Tooth breakage is modelled to show the influence of tooth faults on gear mesh frequency, and also the impact of dynamic force generated. The mesh stiffness of the sun–planet gears are clearly presenting with planet fault gears and planets- ring gears showing no faults, illustrating there is no influence of tooth faults on mesh stiffness, and the impact of dynamic force between gears is with sun gear tooth faults.

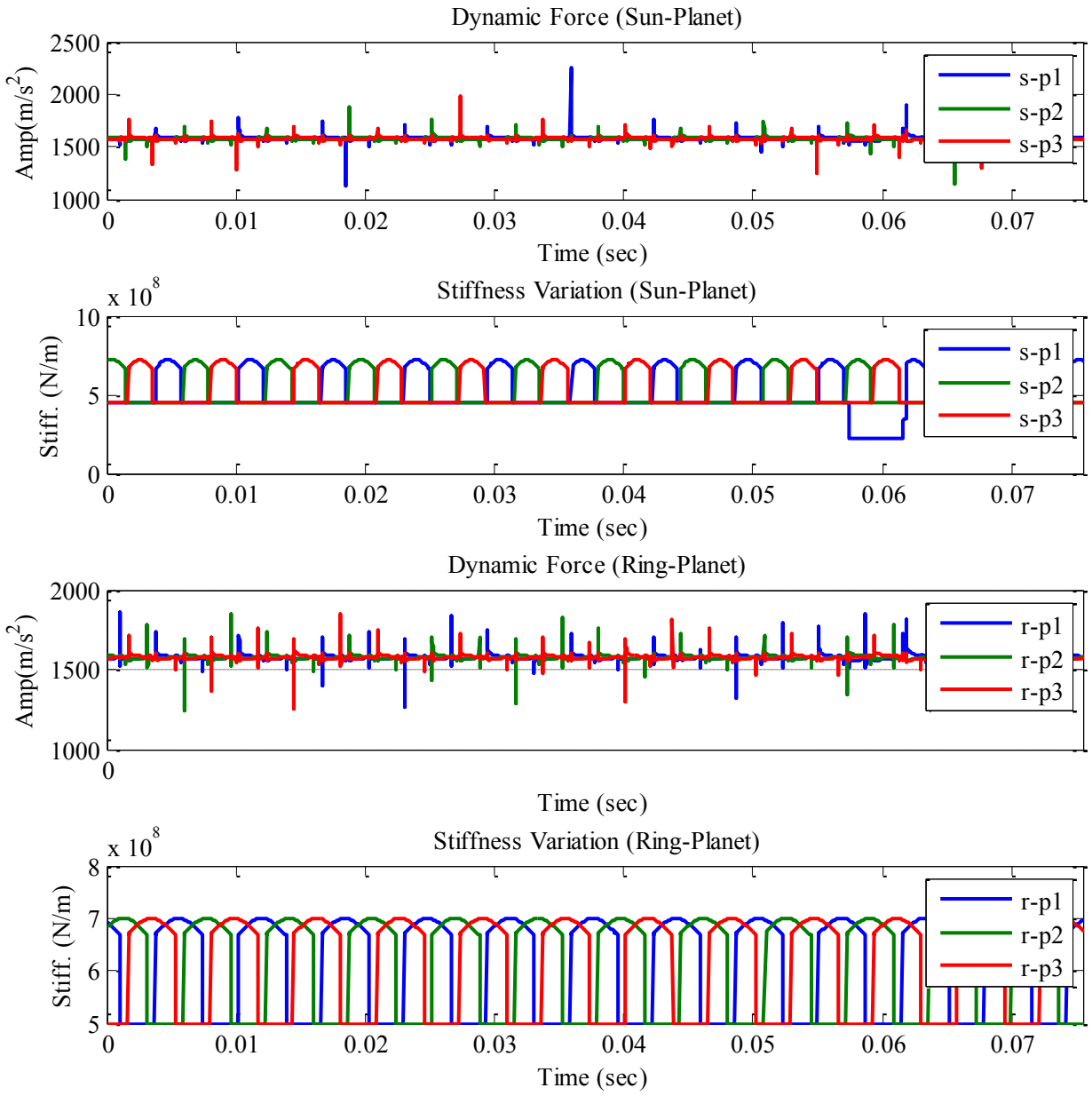

Figure 3.13 Sun-planet and ring-planet mesh stiffness with one tooth fault in planet gear

Figure 3.14 shows the mesh frequency for sun-planet and planet-ring gears occurs at f_m = 156 Hz with the second and third harmonics at 312 Hz and 468 Hz, respectively. The introduction of small amplitude sidebands around the fundamental meshing frequency and its harmonics due to the introduction of the tooth fault in the planet gear is clear.

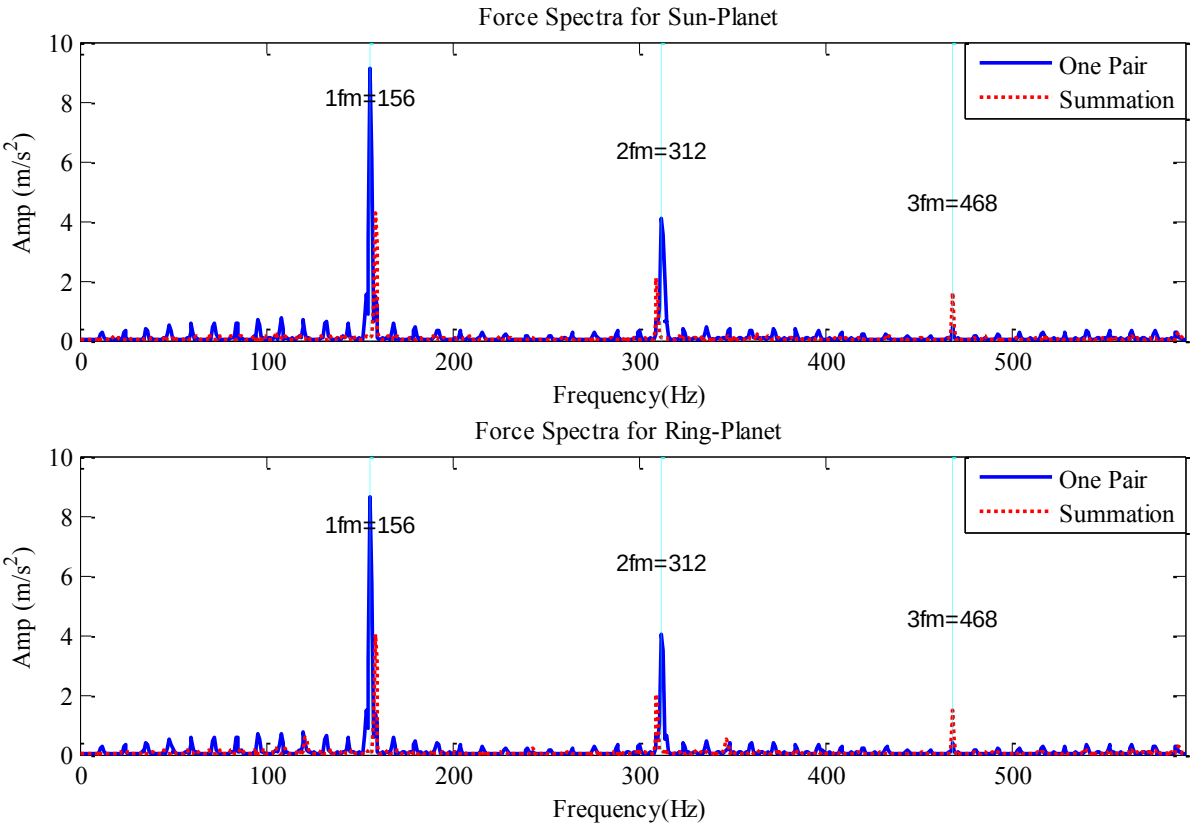

Figure 3.14 Sun-planet and ring-planet mesh stiffness with a tooth fault in one planet gear

3.5.4 Modelling of Ring Gear Fault

Figure 3.15 shows the response of vibration signal to a tooth breakage fault in the ring gear in both x and y directions in both time and frequency domains. The mesh frequency f_m is clearly at 156 Hz and the second harmonic, 312 Hz.

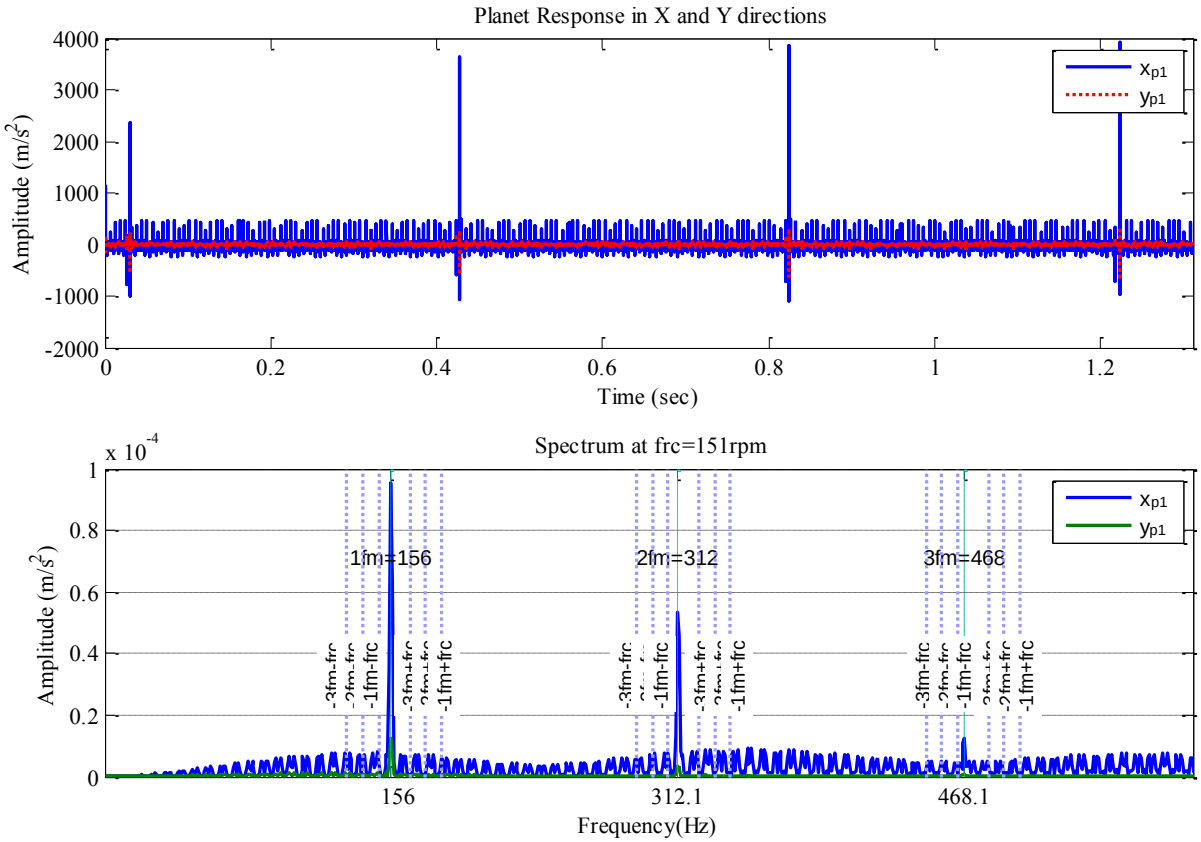

Figure 3.15 Simulated vibration signal for X and Y direction in time and frequency domains with a signal tooth fault in the ring gear

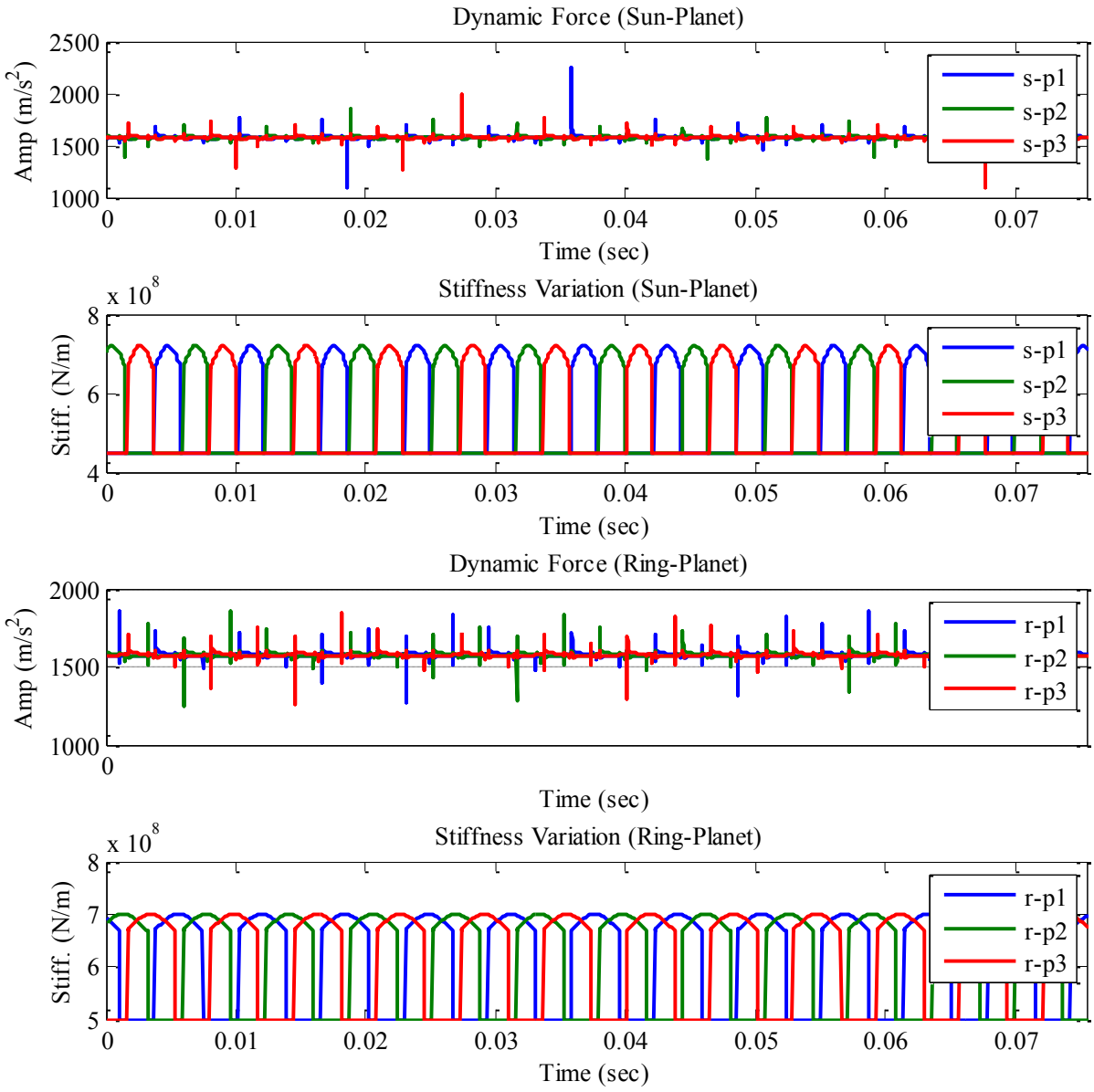

Figure 3.16 Sun-planet and ring-planet mesh stiffness with one tooth fault in ring gear

Figure 3.16 shows the simulated time domain signal for the dynamic force and stiffness between the sun and planet gears, and between ring and planet gears for a single tooth fault in the ring gear. Comparison with Figure 3.7, the no fault case, reveals remarkable similarities which suggests the tooth faults have little or no effect on mesh stiffness, or dynamic force impact.

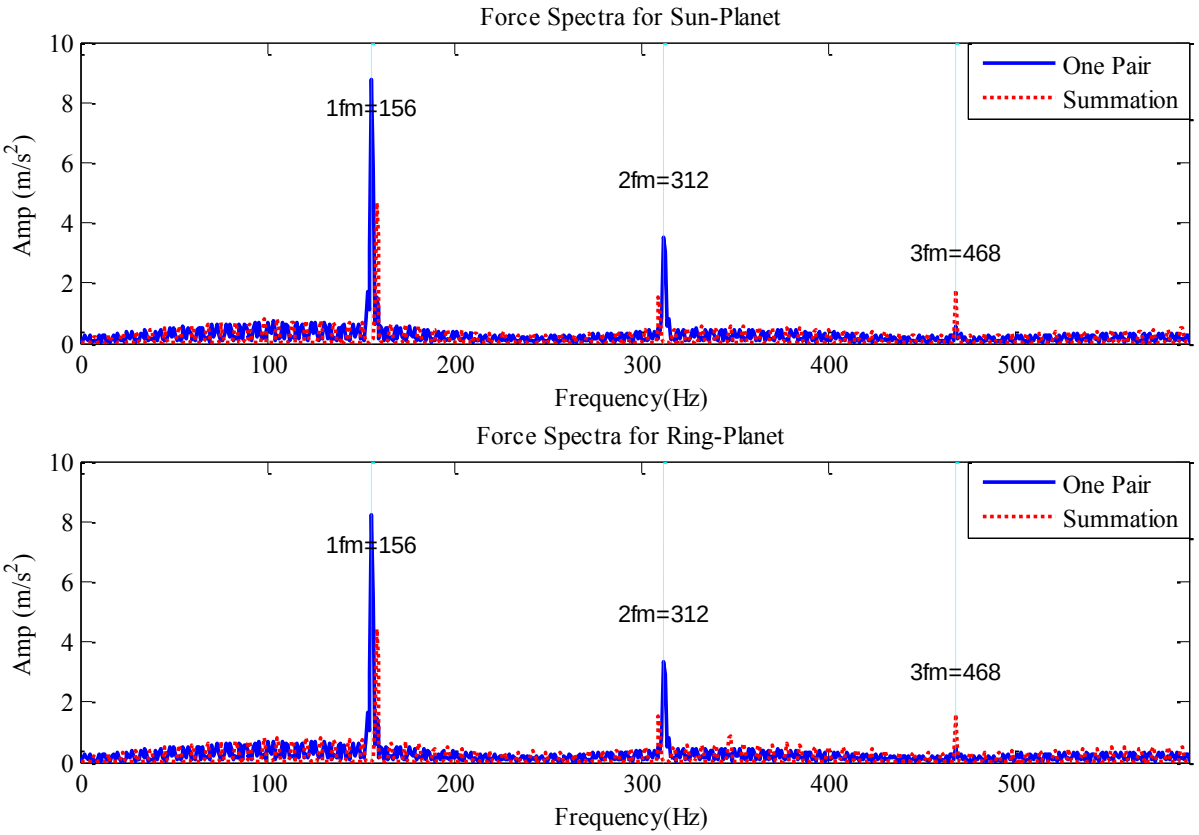

Figure 3.17 Sun-planet and ring- planet mesh stiffness with tooth fault in ring gear

3.6 Numerical Analysis of Vibrations with Faults and Errors

3.6.1 Modelling a Healthy Planetary Gear System

The parameters of the PG used in this model are listed in Table 3.2. The figure shows the vibration/force spectrum of planetary gearbox without error and faults in the frequency domain, with up to the third harmonic of the mesh frequency (3 x 156 = 468 Hz). Around the mesh frequency can be seen that there are no significant sidebands around mesh frequency f_m and its harmonics.

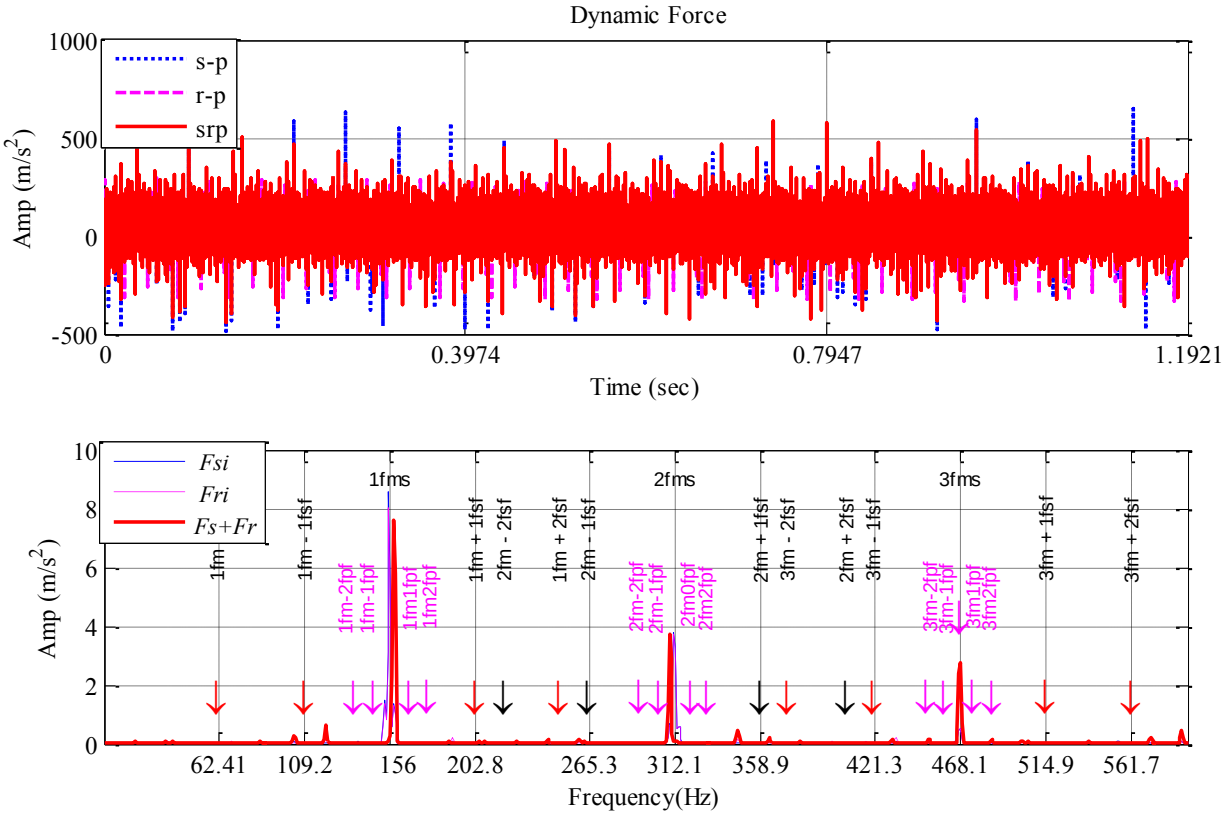

Figure 3.18 The time and frequency domains for the planetary gear set without faults or manufacturing errors

3.6.2 Sun Gear with Fault and Errors

Figure 3.19 shows that there are peaks in the amplitude of the time domain signal from the PG which are much higher than that of the healthy gear set case. This is due to impacts generated by the sun gear fault and the error. In the frequency domain, the peaks occur at the mesh frequencies; f_m =156 Hz, and the second and third harmonics. Sidebands peaks are clearly visible, clustered around the three major peaks at f_m, $2f_m$ and $3f_m$.

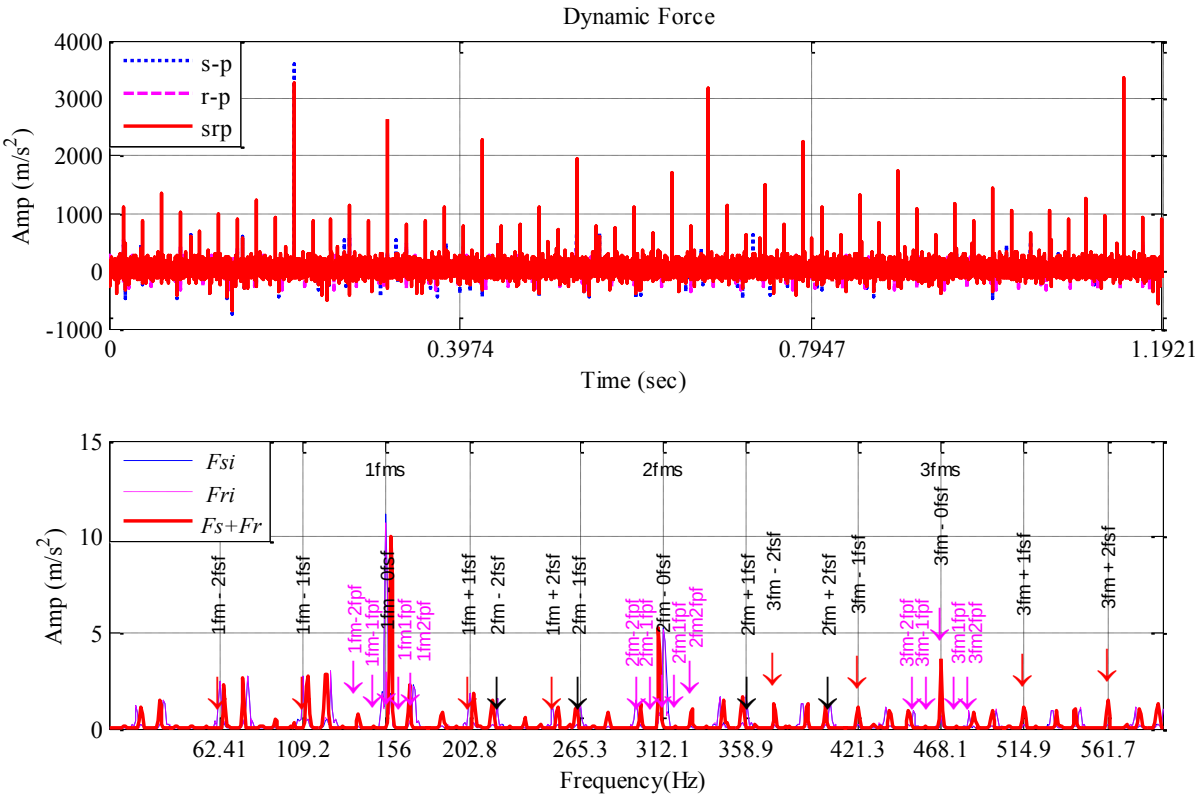

Figure 3.19 The predicted vibration spectrum of the planetary gear set with sun gear fault and error

The sidebands, which are not present for a healthy gearbox see Figure 3.18, are located symmetrically around the first three mesh frequencies as shown by the arrows in Figure 3.19. It can also be seen that these peaks indicate that the gearbox has significant manufacturing errors.

The planetary gearbox components which locate symmetrically around the 1st and 2nd mesh frequencies at $1f_m \pm 1f_{sf}$, $1f_m \pm 2f_{sf}$, $2f_m \pm 1f_{sf}$ and $2f_m \pm 2f_{sf}$, illustrated by the arrows, are clearly visible whilst, the high amplitude sidebands such as those around the third mesh frequency at $3f_m \pm 1f_{sf}$ and $3f_m \pm 2f_{sf}$ that are supposed not to appear for a healthy planetary gearbox, these peaks indicate that the gearbox has significant manufacturing errors.

3.6.3 Planet Gear with Fault and Errors

Figure 3.20 shows that the amplitude of the time domain signal with the presence of a single tooth fault in one of the planet gears, together with a manufacturer's error is much higher than that the healthy PG, see Figure 3.18. The spectrum of planetary gearbox in the frequency range up to the third harmonics of mesh frequency f_m, with planet gear fault and error is influenced by the planet gear faults. Error at the sidebands peaks are clearly visible around the spectrum of the planet gear faults, which are caused by the influence of planet gear fault on mesh stiffness and additional impact of dynamic force. Therefore, the sidebands of the planetary gearbox are comparatively simple if the errors are not included in the planetary gear box, see Figure 3.18.

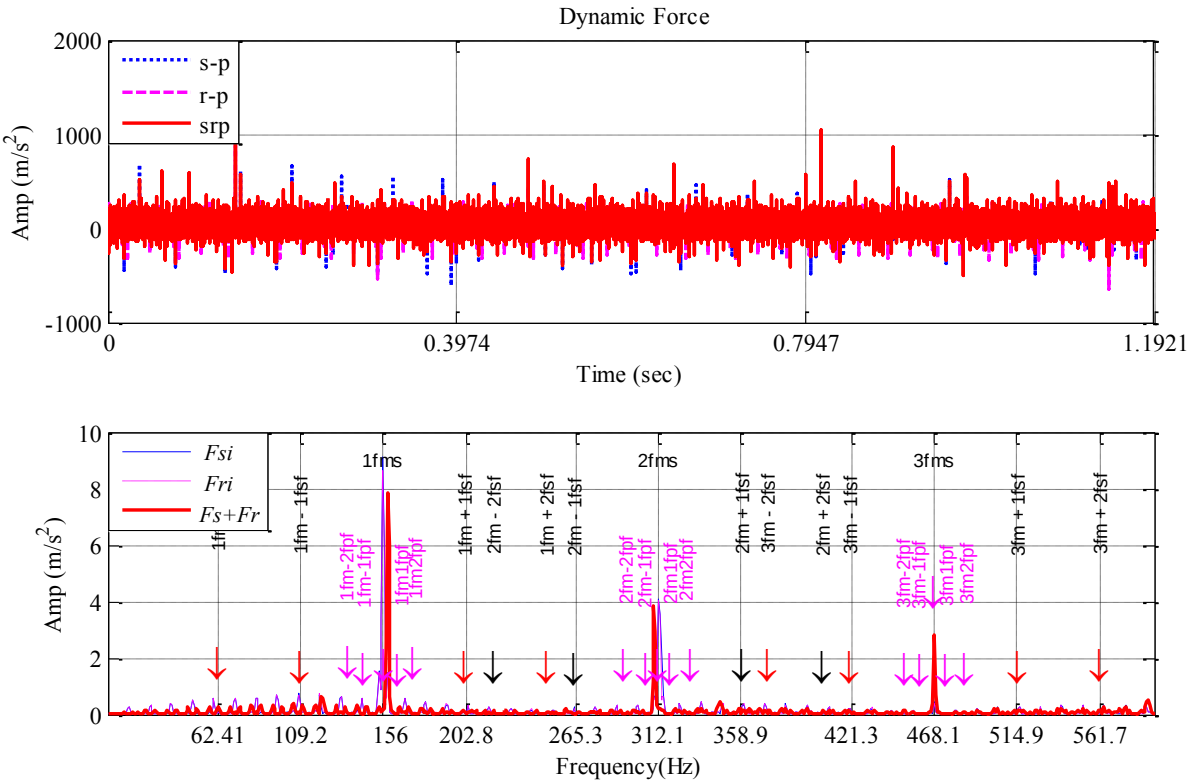

Figure 3.20 The spectrum of the planetary gear set with error and planet gear fault

3.6.4 Ring Gear with Fault and Errors

Figure 3.21shows that the amplitude of the time domain signals with the presence of a single tooth fault in the ring gear together with a manufacturer's error. The presence of peaks is of much higher amplitude than observed with the healthy PG and is immediately obvious, see Figure 3.18.

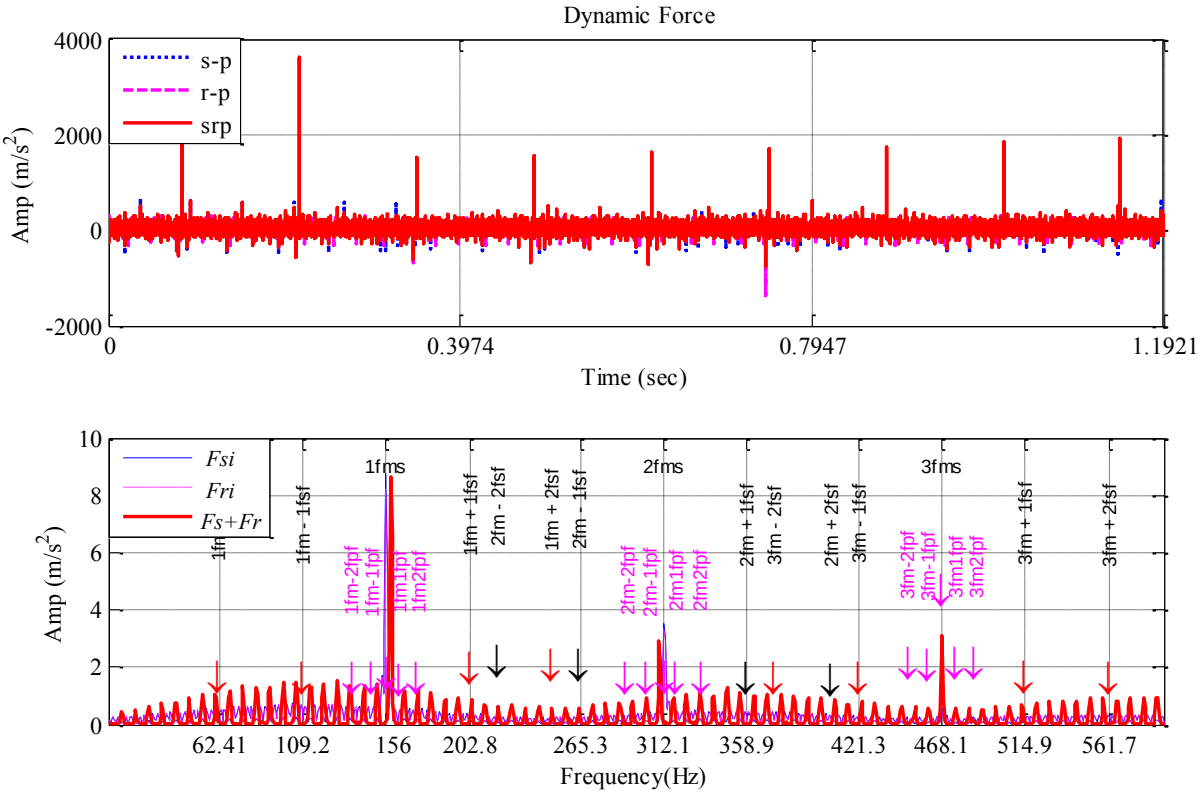

Figure 3.21 The spectrum of the planetary gear set with error and ring gear fault

The mesh frequency influenced by the ring gear faults and error showing the sidebands peaks are clearly appeared around the spectrum of the planet gear faults, ring gear fault on mesh stiffness and additional impact of dynamic force. Therefore, the sidebands of the planetary gearbox are comparatively simple if the errors are not included in the planetary gear box as seen in the Figure 3.18.

3.7 Summary

This chapter has presented a mathematical model of PG box with three planets, one ring and one sun gear; see Section 3.4, to simulate the vibration signals produced by the gears. Detection, diagnostics and localisation of PG tooth fault have been investigated numerically. Detailed comparisons of numerical results, see Sections 3.6 and 3.7, have shown that fault characteristic frequencies can be obtained after considering the gear manufacturing errors Additionally, it must be noted that the presence of sidebands in the vibration signal of the PG become more prominent and much more complex when manufacturing errors are taken into consideration. The planetary gearbox fault characteristic frequencies for gears (sun, planet, and ring gears) are different.

CHAPTER FOUR

LITERATURE REVIEW OF DATA ANALYSIS TECHNIQUES OF ROTATING MACHINERY

This chapter presents a literature review of condition monitoring (CM) techniques. It focuses on the vibration signal generated by rotating machinery and relevant signal processing techniques and both amplitude and frequency modulation is explained. Various commonly used statistical parameters are overviewed for gear condition monitoring. It also provides an overview of the more common techniques used for machinery CM with comment on their usefulness for planetary gearbox fault detection. Finally this chapter explains the modulation signal bispectrum (MSB) and MSB based sidebands estimation, which will be the main signal tools in this research and are being investigated extensively for monitoring the condition of geared transmission systems.

4.1 Introduction

Vibration due to both rotating shafts, and machines with components with an oscillatory back and forth movement is a common phenomenon and for such systems, vibration measurement and analysis is accepted as one of the most useful CM techniques (Shin and Hammond 2008) Such an approach is particularly used when monitoring rotating machinery where vibration is caused by factors such as eccentricity, misalignment, imbalance, and reaction to an external force. One of the most common elements damaged by vibration in rotating machines is the bearings and this can lead to unexpected failures. It is important to monitor bearings, as unanticipated failures can lead to severe loss of production and/or high replacement and maintenance costs (Davies 2012).

4.2 Condition Monitoring Techniques

Industrial plant can be considered well-organised economically when the machines and equipment are effectively maintained. Through an effective maintenance system, it is possible to predicted beforehand the appropriate measures to be applied to preserve investment, maintain effective plant operations and production continuity (IAEA-TECDOC 2007).

Within an industrial setting, the gearbox is considered essential equipment. Power or rotary motion is transferred by suitable gear systems from one shaft to another with a specific ratio and with high levels of efficiency if the gears have no faults. However, gear performance declines if it is subjected to such defects as pitting, cracks due to bending fatigue, abrasive wear or scuffing. In such circumstances it is not possible to transmit the motion or power as required and, if maintenance is ineffective; such defects may grow until fatal to the production process. Thus, it is essential to understand the importance of gearbox CM in reducing failures and making sure production operations run smoothly. CM to detect machinery faults can be classified in seven categories and these are briefly described below (Davies 2012; Márquez, Tobias et al. 2012).

- ***Visual, Aural and Tactile Inspection***

Trained operatives use their human senses to monitor machines and gearboxes. She/he will look at, listen to and touch the machine and can detect changes in, for example, the machine temperature or the level of vibration. This technique is flexible and provides instant assessment of the general condition of a working system. The main disadvantage of the human sense method is that it requires experience and skill and can show different conclusions depending on the individual inspector. However, these basic techniques can be enhanced by the use of devices such as microphones or stroboscopes (Özturk 2006). Generally, the cost of this method is very low compared with alternative CM techniques and it has proved very useful for detecting faults like cracks, corrosion, overheating and leakage (Drury and Watson 2002).

- ***Performance Monitoring***

The monitoring of operational parameters like speed, torque and force can be used to detect any kind of deterioration. The malfunction of the machine is observed if there is significant deviation from the desired operational parameters (Rao 1995). The definition of Performance indicators is "Performance indicators are at the heart of a performance monitoring system, it defines the data to be collected to measure progress and enable actual results achieved over time to be compared with planned results. Therefore, they are an indispensable management tool for making performance-based decisions about program strategies and activities."(Roberto Mosse 1996).

- ***Thermal Monitoring***

Temperature measurement is widely used in industrial environments and encompasses a wide variety of applications. Industry has developed a large range of sensors and devices to handle this demand.(Wang 2008).

A fault normally causes heat generation or process temperature variation which can be identified through this monitoring technique. Thermal sensors such as thermal cameras, thermometers, thermocouples and thermographic paints can be used to measure the temperature(Rao 1995).

- ***Wear Debris Monitoring***

The normal force between to surfaces moving against each other causes wear to take place. Wear can be minimised through lubrication with a suitable lubricant present in the desired quantity. However, wear will be exacerbated if there is excessive loading, or inadequate lubrication or the lubricant is contaminated. A clean and controlled working environment should be present within operational parameters, but because lubricant helps extract wear debris from the contacting surfaces, that debris material can itself be a cause of surface wear.

Magnetic plugs may be used for lubricant monitoring which helps assess the ferrous debris build-up. Spectrometric and photographic analysis of the oil, rate of debris accumulation and its composition, and particle shape can pin-point a damaged component or failure mode. Such a technique may not be applied for fatigue cracks since very few metallic particles are shed during failure (Rao 1995; Dempsey, Morales et al. 2002).

- ***Current Monitoring***

Motor current signal analysis (MCSA) is a non-intrusive method for detecting mechanical problems in machinery driven by an electric motor. It is a technique based on measuring and analysing the electric motor supply current. Changes in the mechanical load on the motor, affect the current in ways that correspond to the change in load. These current variations can be detected and monitored remotely and can be used for machine CM (IAEA-TECDOC 2007).

- ***Acoustic Emission Monitoring***

When there is structural damage within a mechanical component, acoustic emission is produced. The sound signal residual can be monitored and changes in both the time and frequency domains assessed to detect and diagnose the presence of faults. At times, it is not possible to use this method of acoustic monitoring due to a low signal-to-noise ratio (Özturk 2006; Márquez, Tobias et al. 2012).

- ***Vibration Monitoring***

For machine CM, vibration monitoring is widely used compared with other CM techniques because the vibration signal contains high levels of information (Davies 2012).Vibration within the machine operation is caused by forces and motion generation which are transmitted from one component to another. There will be a change in monitored vibration characteristics if a fault develops. Faults such as inappropriate clearances, unbalanced components, faulty bearings and gears, bent or eccentric shafts and misaligned components can be detected through vibration monitoring.

4.3 Signal Modulation

As shown in the simulated vibrations in Chapter3, the gear vibration signal exhibits clear modulation features. For more understanding of modulation, a more systemic review is made on the subject. Modulation is the process of changing amplitude or frequency or phase of a carrier wave in accordance with the intensity of the signal. Accordingly, there are three basic types of modulation, namely:

1- Amplitude modulation.
2- Frequency modulation.
3- Phase modulation.

In the above mentioned types, the first two, for example, Frequency modulation (FM) and Amplitude modulation (AM) are the most significant and common types of modulation and will be discussed in this chapter. The section following discusses the process by which the time-domain vibration signal under observation gets modulated due to a fault in the gear. The process of demodulation is used to extract the data from the modulated signal by eliminating the carrier from the processed signal; this greatly helps in obtaining the required information related to the fault and system from the carrier as well as the primary signal.

Both types of modulation are depicted in Figure 4.1 from (Chang 2002). When a carrier signal undergoes frequency modulation (FM), the frequency of the carrier signal varies in accordance with the amplitude of the modulating signal which is also known as the data signal, but the amplitude of the carrier signal does not change. On the other hand, when the

signal is amplitude modulated, the amplitude of the signal varies in proportion to the amplitude of the modulating signal (data signal), the frequency of the signal does not vary. The presence of noise in instrumentation or measurement processes mainly has an impact on the signal amplitude and thus effects AM more than it does FM (Chang 2002; Glatzel, Sadewasser et al. 2003).

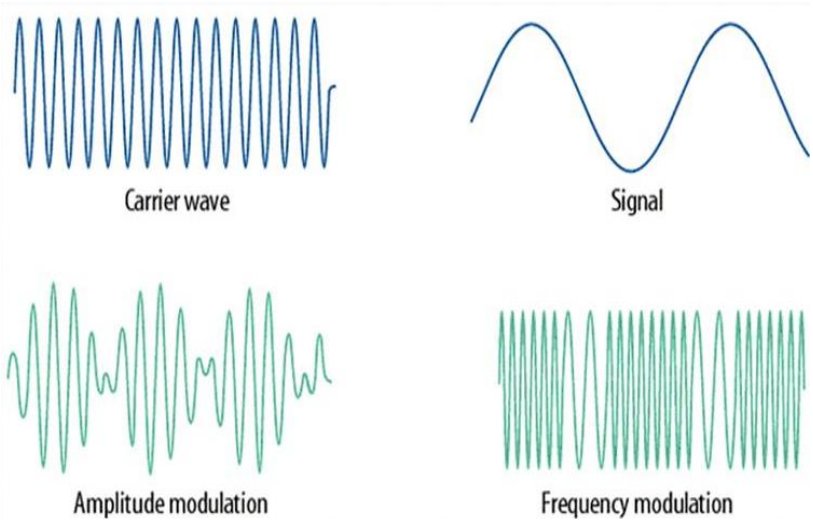

Figure 4.1 Amplitude and frequency modulation

4.3.1 Amplitude Modulation

Amplitude modulation is referred to as the process in which the high frequency carrier wave's amplitude varies in proportion with the signal intensity. This principle is illustrated in Figure 4.1. The modulated wave's frequency, the carrier frequency, remains constant and the amplitude changes in proportion to the signal intensity.

A modulator is used for carrying out Amplitude modulation. The audio electrical signal and constant amplitude carrier wave is depicted in Figure 4.2 (*i*) and (*ii*) .Thus, the amplitude modulated wave is illustrated in. Figure 4.2 (*iii*) showing the signal and the amplitude of negative and positive half cycle of carrier wave vary in conformity. An increase in the carrier wave's amplitude is seen when the signal is advancing in the positive cycle whereas a decrease in the amplitude is observed during the signal's negative half-cycle. A few important facts related to amplitude modulation are mentioned below:

1. The change in the amplitude of carrier wave is at signal frequency fs.

2. The amplitude of carrier wave varies in proportion to the signal intensity.(Broberg, Runnemalm et al. 2013).

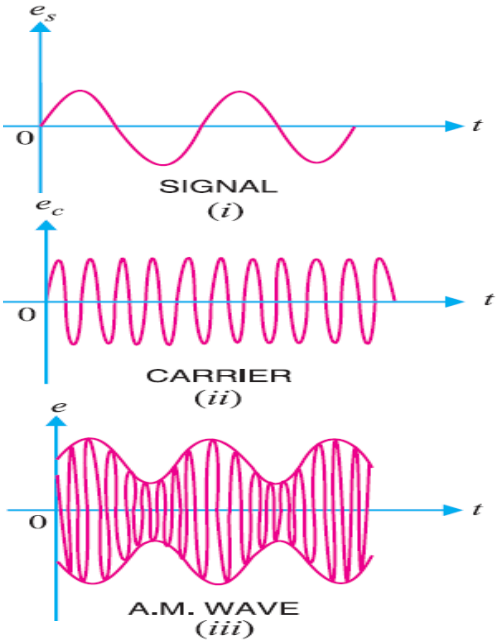

Figure 4.2 Principle of amplitude modulation

4.3.1.1 Limitations of Amplitude Modulation

Although theoretically highly effective, amplitude modulation suffers from the following drawbacks:

I. ***Low efficiency.*** The power of the sidebands in AM is low and this is where the signal is contained and hence useful power. For instance, the power of the sideband is only one third of the AM wave's total power when the 100% modulation takes place. Therefore, AM modulation has lower efficiency.

II. ***Noisy reception.*** As discussed earlier, deviation in the carrier amplitude carried the signal in an AM wave. However, all the different noises as natural and man-made noises present are basically electrical amplitude disturbances. The signal at the receiving end usually becomes noisy because of the fact that the radio receiver is incapable of distinguishing between noise amplitude variations and amplitude variations in an AM wave.

III. ***Small operating range.*** The operating range of transmitters using this method is small because AM has lower efficiency. This means that the distance over which messages can be sent is small. (Broberg, Runnemalm et al. 2013; S. Bhatia 2015).

4.3.2 Frequency Modulation

Frequency modulation (FM) is defined as the phenomenon by which the carrier wave's frequency varies in proportion to the signal intensity, no change in the carrier amplitude is observed. Figure 4.3 (a-iii) illustrates that the change in carrier wave's frequency is in accordance with the signal's instantaneous amplitude. This means that at times when amplitude of signal is zero, at *A*, *C*, *E* and *G* no change in the carrier frequency is observed. Minimum carrier frequency (represented by widely spaced cycle) is observed when the signal reaches negative peaks like in the points at the point *D*. Maximum carrier frequency is observed when the signal amplitude reaches its positive peaks as at points *B* and *F*.

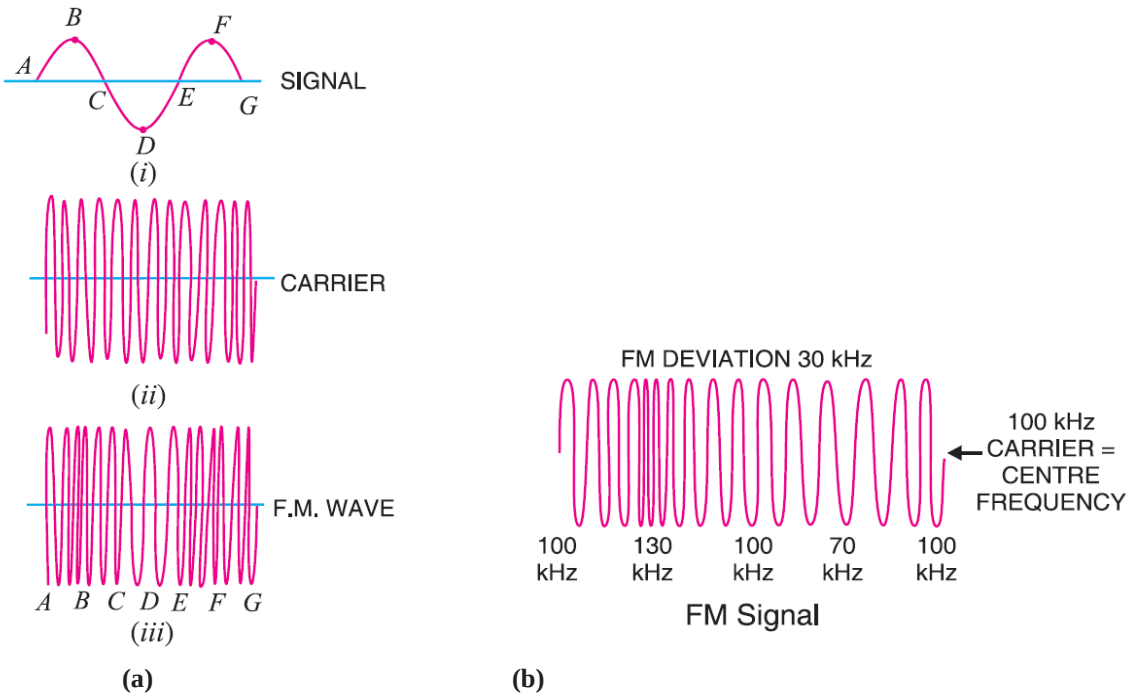

Figure 4.3 Frequency modulation (FM) signal

Frequency modulation is shown in Figure 4.3 to understand this process more clearly numerical values have been assigned, the carrier frequency (Fc) is considered as 100 kHz, see Figure 4.3 (b). This is known as the ***centre frequency*** because the frequency of the FM signal varies below and above the carrier frequency (S. Bhatia 2015). Modulating signal amplitude affects the frequency deviation or the degree of frequency variation from Fc. The relation between frequency deviation and signal amplitude is direct; therefore, maximum frequency deviation is observed when the signal voltage is at its peak. The peak signal

voltage produces maximum frequency deviation and in Figure 4.3 the maximum frequency deviation is 30 kHz.

Referring to Figure 4.3, it can be seen that:

- The carrier frequency is not modulated when the signal amplitude is zero.
- The amplitude of the signal determines the frequency deviation from F_c.
- Frequency deviation in the carrier is not effected by the frequency of the signal.

Advantages: some of the benefits of FM in comparison to AM are:

- A large operating range can be obtained.
- The transmission efficiency is relatively high.
- The reception is relatively noise free as noise expresses itself mainly as amplitude disturbances, thus noise signals are rejected by the FM receiver.
- The reception is relatively high-fidelity (S. Bhatia 2015).

Comparison of FM and AM

The table below shows the comparison of FM and AM

Table 4.1 Comparison of FM and AM

Nº	Amplitude Modulation (**AM)**	Frequency Modulation **(FM)**
1.	Modulation changes the carrier amplitude.	Modulation has no effect on the carrier amplitude.
2.	Modulation does not affect the carrier frequency.	The carrier frequency changes with modulation.
3.	The variation in the amplitude of the carrier depends on the modulating signal strength.	The variation in the frequency of the carrier depends on the modulating signal strength.
4.	For AM signal to be free from distortion, the modulation factor (m) should not be more than 1	Modulation index (mf) can have a value greater than 1.

4.4 Vibration Analysis Method

All types of mechanical equipment have their operation based on either rotational or linear motion, the vibration profile or signal is generated by the forces induced by these movements. Analysis of the vibration signal is very useful to diagnose faults and predict time to failure at an early stage and hence help to prevent the failure of the machine. Vibration analysis is a useful technique to achieve good operating conditions and efficiency of machines; this method is used for many, many applications including monitoring of machine rotation which includes gears, bearings, loose part detection, quality control etc. (Wowk 2000; Özturk 2006).

This kind of data is presented in the form of curves, the most commonly used for gear fault detection and diagnosis is based upon time domain, frequency domain and joint time-frequency domain analysis (Wowk 2000; Shin and Hammond 2008).

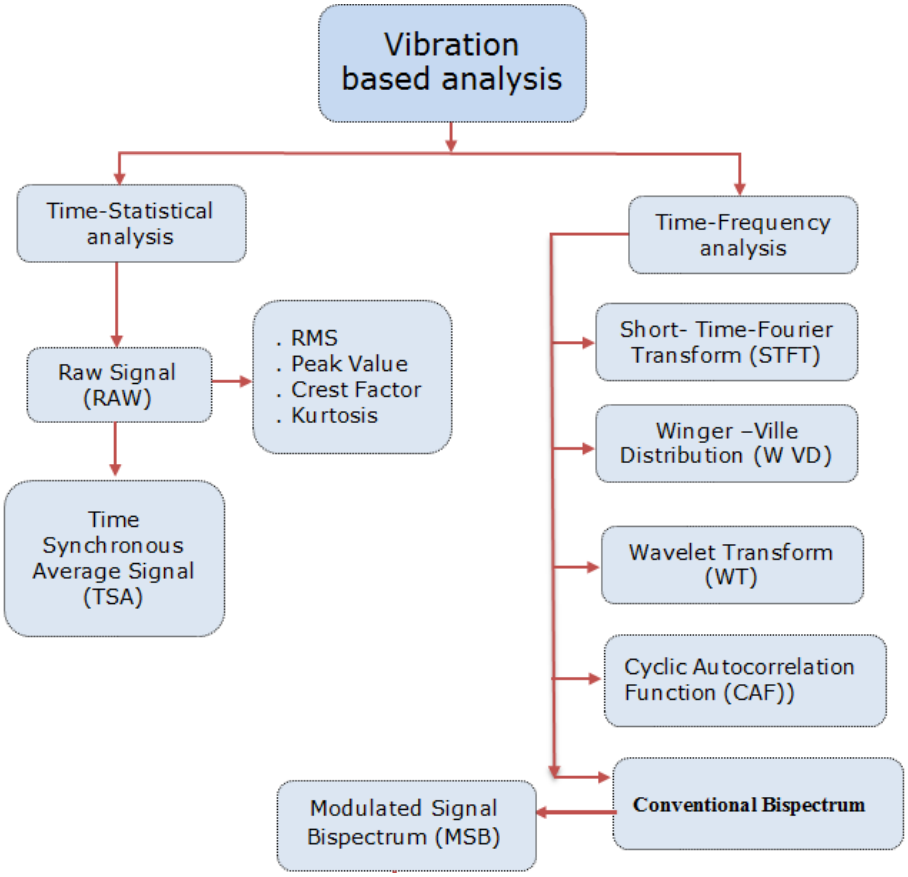

Figure 4.4. Classification of Vibration-Based Analysis Techniques and Parameters

Figure 4.4 shows the vibration-based analysis normally used for gear fault detection. There are several feature functions of the signals such as Kurtosis and RMS that can be calculated at different pre-processing stages. Both diagnostics and prognostics are important aspects in a CM programme. Diagnostics deal with fault detection which deals with identifying the fault, what it is, where it is, and may also assess the severity of the fault, and prognostics deal with fault prediction which assesses the severity of the fault and predicts a likely time to component failure. The main goal of these techniques is to minimise the cost and time in machine repairs and more importantly is the avoidance of production stoppages due to unexpected machine failure as well as to enhance the ways of detecting failures.

4.4.1 Time Domain Analysis

The time domain is measurement of the vibration signal as a function of time and can be used for mechanical fault detection. The most commonly used parameters of the vibration signal levels are the peak values (PV), root mean square (RMS), crest factor and kurtosis (Alguindigue 1993). The time domain analysis is used to process the collected vibration signals by an accelerometer attached to the machine, component or rig. There are indicators called “condition indices” which are used to indicate whether the machine’s condition is acceptable or not.

Time domain methods are appropriate when the faults in the system produce wideband frequencies due to periodic impulses. Use of the waveform enables changes in the vibration signature allowing the faults to be detected, but it is often difficult to diagnose the source of faults. The condition indices are used to describe the machine’s condition and are expected to increase in the presence of faults and further increase as the fault severity increases. The procedure consists either of visual inspection of the time domain signal, or to analytically examine the time domain vibration signal and extract statistical parameters (Alguindigue 1993; Sait 2011).

Figure 4.5, shows the raw time domain waveform with the effect of varying degrees of installation shaft misalignment of planetary gearbox at (Healthy, 0.4mm, 0.7mm and 1.0mm respectively). The amplitude in Figure 4.5, does not give any clear information which makes the fault detection and fault locating very difficult. In general, time domain analysis is not

useful for the identification of the gear faults, and this method has had limited success for detecting localised defects in planetary gearboxes (Alguindigue 1993).

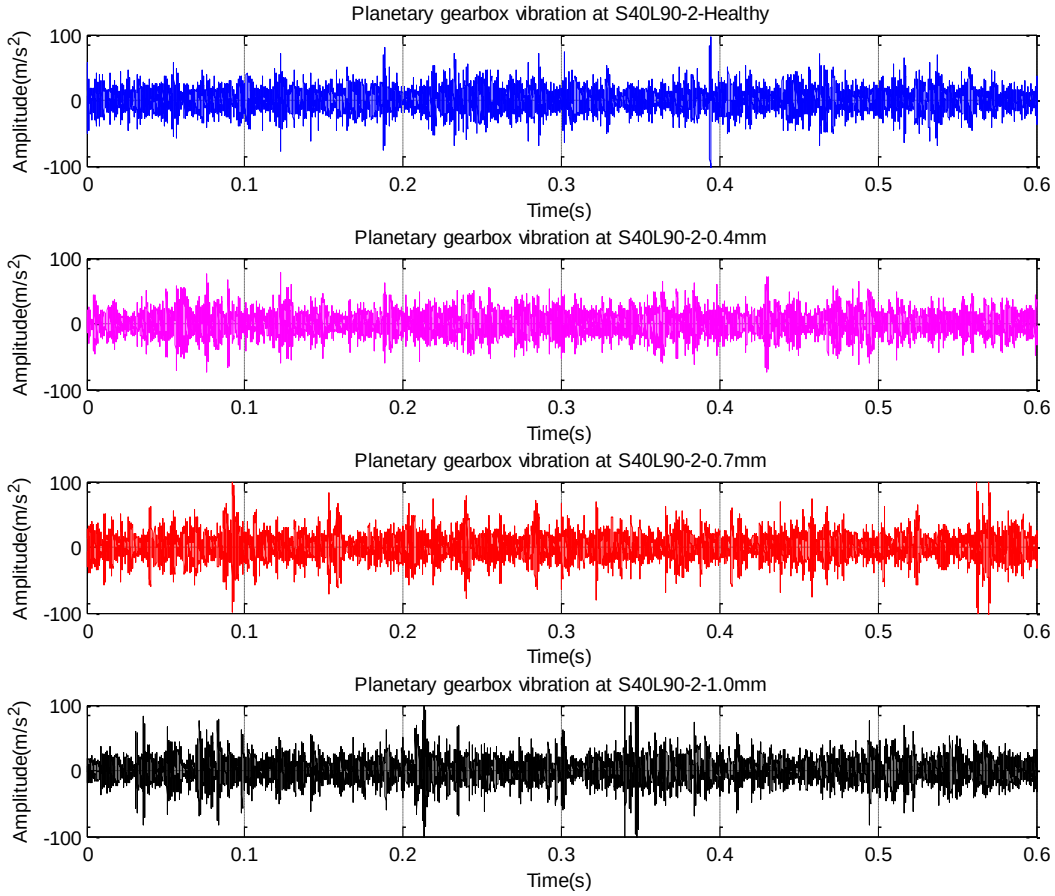

Figure 4.5 Waveform of the vibration signal for a planetary gearbox: healthy and with misalignment faults

4.4.1.1 Filters Classifications

A pass band filter is a device for passing only a band of frequencies; signal frequencies lying outside the pass band are removed or weaken. Filters fall into one of the following categories, based on the overall shape of their pass band (Zhang-Cheng and Jia-Sheng 2010). Generally, there are four types of filters, see Figure 4.6, low-pass filters which pass low frequency signals; high-pass filters which pass high frequency signals (up to infinity); band stop filters which reject signals occurring between two given frequencies (band-stop filters are also called notch filters when the stop band is narrow); and band-pass filters which pass only signals between two given frequencies, blocking lower and higher signals and are often

characterised as having a bandwidth that is symmetric around a centre frequency (Sait 2011; Ramsden July/2001).

The band-pass filter should be set where the effect of the bearing fault is predominant in the spectrum. It could be anywhere in the middle range of the spectrum where there are no other significant contributors except for background vibrations (Stack 2004).

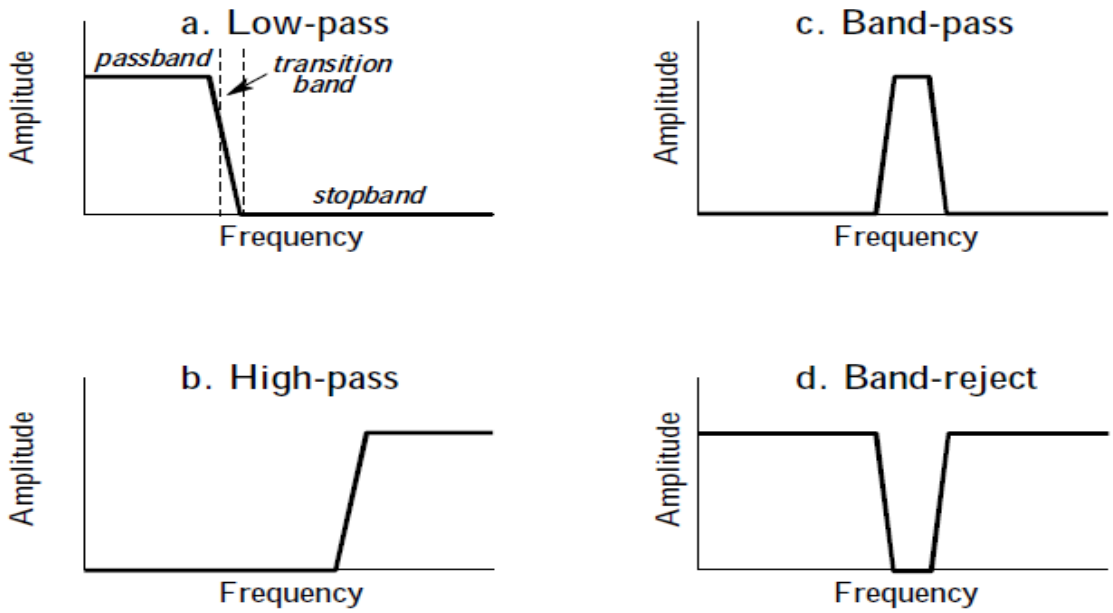

Figure 4.6 Type of filters reproduced from (Stack 2004)

The structure and the machine of which the bearing or gear are part will have natural frequencies or resonances that are very sensitive to excitation. It can happen that the bearing or gear fault will have a frequency that is close to one of these resonances and may well excite that resonance, thus the resonance will amplify the line spectrum, giving at least, a better signal or noise ratio, but there are drawbacks, for example;

1. The vibration level measured is very sensitive to the placement of the sensor and the measured values may represent the structural properties rather than the bearing condition.
2. If the resonances are very narrow or very lightly damped, they may contaminate the signal envelope. With low damping, the resonance may cause the pulse to "ring", broadening out the envelope of the pulses (Stack 2004).

4.4.1.2 Root Mean Square (RMS)

The RMS value is the square root of an average of squared values of the waveform. In a sinusoidal wave, the RMS value is 0.707 times the peak value of the wave. From the figure below it can be seen that it is the area under the curve. If the negative area under the curve is rectified by changing it into the positive area, the resultant wave will show a constant level and this level is proportional to the root mean square value (Steve Sabin 2006; Bruel.V 2009; M. P. Norton 2013).

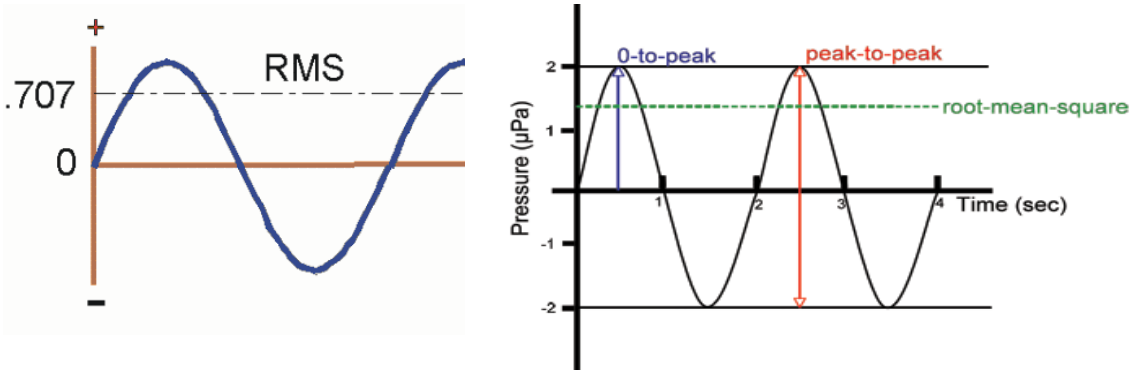

Figure 4.7 RMS and Peak-Peak Value reproduced from (Steve Sabin 2006; Bruel.V 2009; M. P. Norton 2013).

Determination of the RMS value of particular vibration amplitude of a certain signal is vitally important. The value of RMS of the amplitude of the acceleration can be expressed as (2010).

$$RMS = \sqrt{\frac{1}{N}\sum_{n=1}^{N}\left(x(n)-M\right)^2} \tag{4.1}$$

$$M = \frac{1}{N}\sum_{n=1}^{N}X(n) \tag{4.2}$$

where;

- N -is the number of samples taken from the signal.
- $x(n)$ -is the amplitude of the signal for the n sample.
- M -is the average amplitude of the N the sample.

4.4.1.3 Peak Value (peak –peak)

Peak Value (Peak-Peak) is the peak amplitude of the wave. Peak is the maximum distance the wave deviates from the zero or equilibrium point. Peak from zero to positive value is known as the positive peak and peak from the minimum value to zero is known as the negative peak as in Figure 4.7 .The vertical distance from positive peak and negative peak is called peak to peak value. In a sinusoidal wave, positive peak distance and negative peak distance are exactly the same but this is not necessarily the case for every waveform (Stack 2004; 2010).

4.4.1.4 The Crest Factor

The Crest Factor (CF) can be defined as the peak-to-RMS ratio of the measured vibration see Equation (4.3) and Figure 4.8 it gives a first indication of bearing failure. The lower curve in the figure shows a typical trend for the CF as a bearing condition deteriorates. At the beginning healthy component shows a relatively constant ratio of peak to RMS value. As a localised fault develops, the resulting short bursts of vibration increase the peak level substantially but have little influence on the RMS level, therefore the CF increases (Bruel.V 2009). As the fault develops, the peak level will typically grow to a certain limit and, as the gears deteriorate further, more spikes will be generated in the vibration signal and the RMS value increases relatively (Bruel.V 2009; M. P. Norton 2013).

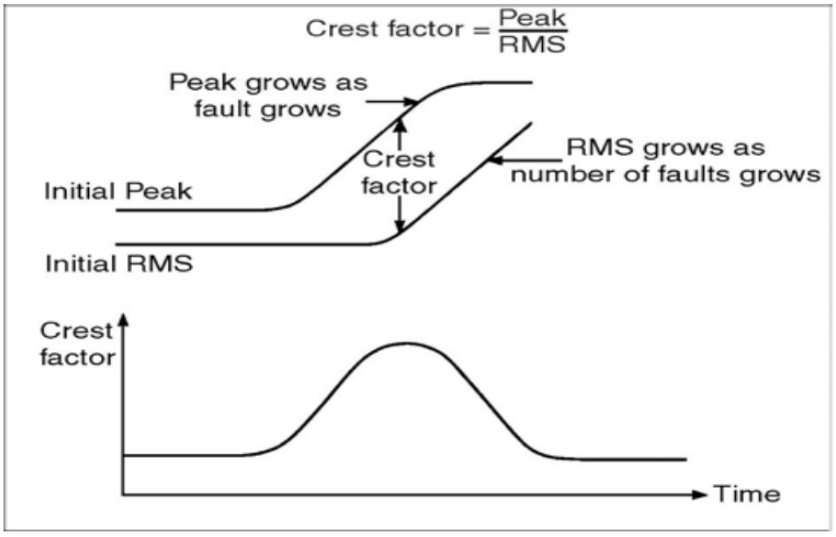

Figure 4.8 The crest factor principles reproduced from

$$CF = \frac{Peak*value}{RMS} \tag{4.3}$$

4.4.1.5 Kurtosis

The kurtosis is a statistical calculation of signal, (see Equation 4.4). The kurtosis is a statistical measure of the number of peaks in a signal and their amplitudes, the more and sharper the peaks in a signal the greater the value of the kurtosis (Bruel.V 2009).

$$kurtosis = \frac{1}{N}\ enhance\ the / [\frac{1}{N}\ RMS\ ]^4 \tag{4.4}$$

where: the symbols have the same meaning as previously;

- M -is the amplitude of the signal for the N the sample.
- is the number of samples taken in the signal.
- $x(n)$ - is the amplitude of the signal for the nth sample.

4.4.2 Time Synchronous Averaging

Time synchronous averaging (TSA) is a technique that attempts to enhance the raw vibration signal by reducing the effects of noises or removing unwanted frequencies that may be generated by other components. The components can be from within the same machine or the external environment, for example other machines.

The implementation of a TSA algorithm for planetary gearbox is relatively straightforward. McFadden was the first to introduce this technique (Eric Bechhoefer 2009; Jing 2011). The equations for TSA are Equation (4.5) and Equation (4.6) below:

$$x(t) = x_n(t) + h(t) \tag{4.5}$$

The TSA of the signal is:

$$A(t) = \frac{1}{N}\sum_{i=0}^{N-1} x(t + iT_c\ ) \tag{4.6}$$

where: $A(t)$-is the averaged signal and N -the number of the average segments

TSA is a fundamentally different process from the process typically used to obtain the Fast Fourier Transform (FFT) which is often limited to a single sample. TSA results in a time domain signal with significantly lower noise than would result with a single sample, and it would be better if the FFT was computed from the averaged time signal (Clara. 2009; Eric Bechhoefer 2009). The key is to sample the signal using a trigger that is synchronised with the signal itself. The average is thus the sum of many samples of the same section of the signal and the averaging process gradually eliminates random noise because the random noise is not coherent with the trigger. Only signal synchronous with the trigger will persist in the averaged calculation, see Figure 4.9

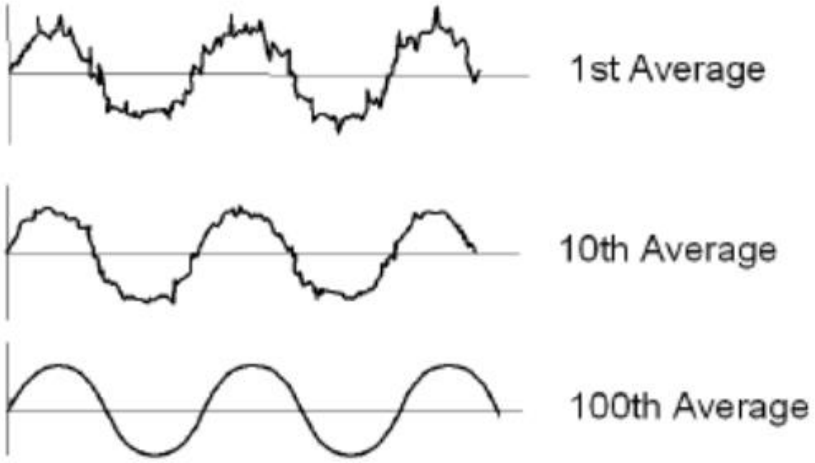

Figure 4.9 Illustration of the effect of time synchronous sample reproduced from (Clara. 2009)

4.4.3 Frequency Domain Analysis

Frequency domain analysis is related to frequencies of the rotating components, usually given in revolution per minute (rpm) or Hertz (Hz). Frequency domain data is gained by converting time domain data using the (Jing 2011; Heckbert. Jan,1998).

Fourier Transform and Fast Fourier Transform

Fourier transform (FT) of the function $f(x)$ is the function $f(\omega)$:

$$F(\omega) = \int_{-\infty}^{\infty} f(x) e^{-i\omega x} \, d_x \tag{4.7}$$

And the inverse Fourier transform is;

$$F(x) = \frac{1}{2\pi} \int_{-\infty}^{\infty} f(\omega) e^{i\omega x} \, d_{\omega} \tag{4.8}$$

where: that : $i = \sqrt{-1}$ and $e^{i\theta} = \cos\theta + i\sin\theta$

A Fourier transform pair is often written:

$$f(x) \leftrightarrow F(\omega) or \; F(x) = F(\omega) \tag{4.9}$$

Where: F-is the Fourier transform operator (Heckbert. Jan,1998).

4.4.4 Hilbert Transform

The Hilbert Transform (HT) is an integral transformation and has played a significant role in vibration analysis. It has been used to directly examine instantaneous attributes of the vibration signal for both phase and amplitude. It allows rather complex signals and systems to be analysed in the time domain (Patel 2012; Heckbert. Jan,1998).

The HT of function f (t) is defined by an integral transform:

$$H\left[f(t) \right] = \frac{1}{\pi} \int_{-\infty}^{\infty} \frac{x(t)}{t-\tau} \, dt \tag{4.10}$$

Where: $(t \; and \; \tau)$ The time and transformation parameters respectively.

The HT is equivalent to a filter in which the amplitudes of the spectral components are unchanged, but subject to a phase shift of $-\pi/2$

In machinery, the presence of local faults will, inevitably, modulate the measured signal which makes demodulation necessary. This can be accomplished by using the HT to form a complex time domain signal. Following Patel, et al., we have(Patel 2012):

$$A[f(t) = f(t) + iH[f(t)] \tag{4.11}$$

$$A[f(t)] = a(t)e^{i\varphi t} \tag{4.12}$$

where: $i = \sqrt{-1}$, $a(t)$, is the envelope of $A[f(t)]$ representation estimate of the modulation in the signal.

$$a(t) = \sqrt{f^2(\mathrm{t}) = H^2[f(t)]} \tag{4.13}$$

$$\varphi(t) = \arctan \frac{H[f(t)]}{x(t)} \tag{4.14}$$

4.4.5 Empirical Mode Decomposition

The empirical mode decomposition (EMD) algorithm first proposed by Huangcan was used to decompose a signal into the sum of functions named intrinsic mode functions (IMFs) which have the same number of zero crossings and extreme and is symmetric with respect to the local mean. The principle of EMD is to decompose the signal waveform into a series of Intrinsic Mode Functions (IMFs) indicating different time-scale features (A.O. Boudraa 2006).

The EMD equation is Equation () (Hui 2006; Qiuhua Du 2007):

$$\mathrm{X}(\mathrm{t}) = \sum_{i=1}^{n} c_i(t) + r_n(t) \tag{4.15}$$

where: $c_i(t)$ and $r_n(t)$ are the intrinsic mode function and residual function respectively.

4.4.6 Joint Time – Frequency Analysis

Many methods of signal analysis have been used for fault diagnostics. The FFT is one of the most commonly used methods for obtaining the frequency-domain from the time domain for fault diagnosis. However, FFT-based methods are not suitable for non-stationary signal analysis because they cannot provide information on non-stationary components, it is therefore necessary to find a method for the analysis of non-stationary signals. Time-frequency analysis, including wavelet transforms, is a new and powerful signal processing technique used in the analysis of non-stationary vibration signals for CM (Cohen 1989). Wavelet analysis has characteristics that can expose more features of vibration signals and is a useful tool for on-line fault detection.

The most important characteristics compared to the FFT are that it is two dimensional, both frequency and time, so can give frequency-time localisation. The raw time series representing the vibration signal needs to be windowed to generate signals to which suitable transformations can be applied. The time-frequency approach is divided into two, depending upon the transform applied, either linear or quadratic (Kadambe and Boudreaux bartels 1992).

4.4.7 Short–Time Fourier Transform

The Short Time Fourier Transform (STFT) uses sliding time windows to capture the frequency characteristics as functions of time. Thus, spectra are generated at discrete instants of time. The time period between impacts can be used for diagnosis by relating it to various known bearing characteristics. Inherent drawbacks with the STFT are the limitation between time and frequency resolutions and that it requires large amounts of computation time and storage (Kadambe and Boudreaux bartels 1992; Zhang, Ge et al. 2002).

Gabor first introduced the STFT. He adopted the Fourier transform (FT) to analyse only a small section of signal. The STFT method assumes that the signal $x(t)$ is quasi-stationary, and analyses the signal by taking the FT of the windowed signal. For a signal $x(t)$, the STFT is defined as (Guo Ai-Huang 2001):

$$S_x(t,\omega) = \int_{-\infty}^{\infty} x(\tau)h(t-\tau)e^{-i\omega t}\ d\tau \tag{4.16}$$

Where: $h(t)$ - is the sliding time window used for the analysis.

The limitation of STFT is that it provides constant resolution with the same length of window. Moreover, there exists no orthogonal for the STFT, making it difficult to find a fast and effective algorithm to calculate the STFT (Guo Ai-Huang 2001).

4.4.8 Wigner-Ville Distribution

The Wigner-Ville distribution (WVD) has many fine properties, such as the real-valued property, time marginal condition, frequency marginal condition, time-shift invariant property, and frequency modulation invariant. Because of these properties, the WVD can

represent the energy changes of the signal and determine the relationship between the energy changes and time and frequency (Hui 2006).

If a continuous time analytic signal is $z(t)$, the WVD of $z(t)$ can be computed from the time domain or the frequency domain as below:

$$WVD_z(t,f) = \int_{-\infty}^{\infty} z\left(t+\frac{\tau}{2}\right) z^*(t+\frac{\tau}{2}) e^{-j2\pi f\tau} dt \tag{4.17}$$

or

$$WVD_z(f,t) = \int_{-\infty}^{\infty} Z\left(t+\frac{v}{2}\right) Z^*(f+\frac{v}{2}) e^{j2\pi v\tau} dv \tag{4.18}$$

Where: $z(f)$ - denotes the Fourier transform of $z(t)$.

$z*(t)$ and $z*(f)$ denotes, respectively, the complex conjugate of $z(f)$ And $z(t)$

4.4.9 Continuous Wavelet Transform

The Wavelet Transform (WT) is similar to the STFT in that it also provides a time-frequency map of the signal being analysed. The improvement that the WT makes over the STFT is that it can achieve high frequency resolution with sharper time resolution.

The wavelet transform is particularly appropriate for vibration signal analysis since it gives information about the signal both in frequency and time domains. The continuous wavelet transform (CWT) of a finite energy time domain signal $f(t)$ with wavelet $\psi(t)$ is defined by Equation (4.18) (Jing 2010; Patel 2012):

$$W_f(a,b) = \int_{-\infty}^{\infty} f(t)\psi_{a,b}(t)dt \tag{4.19}$$

$$\psi_{a,b}(t) = \frac{1}{\sqrt{a}}\psi\left(\frac{t-b}{a}\right) \qquad a,b\grave{o}R; a\neq 0 \tag{4.20}$$

Where: t - is time.

ψ - is the mother wavelet which possesses two characteristic parameter which are: a . The scale - b is the location or space which is varying continuously.

4.4.10 Conventional Bispectrum

The bispectrum analysis is a one of the higher order spectra (HOS), and has been widely used in industry and by researchers since the 1980s (Zhang 2002). McCormick and Nandi (1999) used HOS and pattern recognition to diagnose the faults of a rotating machinery set consisting of an electric motor and a gearbox. They reported that the success rate was as high as 95% (A. C. McCormick 1999).

Given a discrete time vibration signal $X(n)$ its discrete Fourier transform (DFT), $X(f)$ is defined to be;

$$X(f) = \sum_{k=\infty}^{\infty} X(n) e^{-j2\pi fn} \tag{4.21}$$

Equation (above can be written in terms of magnitude $|X(f)|$ and phase φ_f as following

$$X(f) = |X(f)| e^{-j\varphi_f} \tag{4.22}$$

From discrete Fourier transform (DFT) and according to (Young 1979; Collis 1998) , the conventional bispectrum $B(f_1, f_2)$ can be defined in the frequency domain as :

$$B(f_1 + f_2) = E\left[X(f_1) X(f_2) X^*(f_1 + f_2)\right] \tag{4.23}$$

where:

$X^*(f)$ is the complex conjugate of $X(f)$ and $E[]$ is the statistical expectation operator.

f_1, f_2 , and $f_1 + f_2$ are three individual frequency components.

The definition of squared bicoherence used in Equation (), was chosen because it is bounded between 0 and 1 which is useful for comparing the degree of nonlinearity or coupling effects between different signals.

$$b^2(f_1, f_2) = \frac{\left|B(f_1, f_2)\right|^2}{E\left[\left|X(f_1)X(f_2)\right|^2\right]E\left[\left|X(f_1)X(f_2)\right|^2\right]} \quad (4.24)$$

A value of near 0 means an absence of interactions between components. Furthermore, based on the amplitude of the bicoherence nonlinear interactions can be detected and the degree of interaction can be measured between the coupling components. If the bicoherence is close to 1 there are nonlinear interactions between components of the frequency spectrum.

If the frequency components at f_1, f_2 and $f_1 + f_2$ are independent components, each frequency will be described by statistically independent random phases distributed over $(-\pi, \pi)$.Upon statistical averaging denoted by the expectation operator $E[\,]$. In Equation (4.24), the bispectrum will tend towards zero due to the random phase mixing effect. In this way random noise can be suppressed significantly.

4.4.10.1 Modulated Signal Bispectrum (MSB), and MSB-Estimation

Equation (4.25), includes only the presence of nonlinearities from the harmonically related frequency components (f_r, f_m) and $f_1 + f_2$.It overlooks the possibility that the occurrence of $f_1 - f_2$ might be due to the nonlinearity between f_r *and* f_m. Because of this, it is not adequate to describe amplitude modulated (AM) vibration signals such as those that are generated in planetary gearboxes. To improve the performance of the conventional bispectrum in characterising planetary gearbox signals, a new variant of the conventional bispectrum, the modulation signal bispectrum (MSB) was examined as in Equation (4.25) (Stack, Harley et al. 2004; Binqiang Chen 2012; Gaballa M Abdalla 2014):

$$B_{MS}(f_r, f_m) = E\left[X(f_r + f_s)X(f_r - f_s)X^*(f_m)X^*(f_m)\right] \quad (4.25)$$

where: $X(f)$, and its complex conjugate $X^*(f)$ are the Fourier transform of the signal sequence.

And a normalised version of Equation (4.25) can be introduced as:

$$B_{MS}(f_1, f_2) = E\left[X(f_r + f_s)X(f_r - f_s)\frac{X^*(f_m)X^*(f_m)}{|X(f_m)||X(f_m)|} \right] \quad (4.26)$$

From Equation (4.25) the amplitude of $X^*(f_m)/|X(f_m)|$ which relates to carrier component f_m is unity. Thus the amplitude of the MSB peaks is determined purely by the magnitude effect of sideband components (Fengshou Gu 2009; Gaballa M Abdalla 2014).

Equation (4.26) shows that through the operation of vector averaging in the frequency domain, MSB can extract the combinations of components at the meshing frequency, the lower sideband and the higher sideband. In the meantime, other components including random noise that does not meet the phase relationship will be suppressed. In this way the modulation effects in a vibration signal can be represented more accurately and reliably (Gaballa M Abdalla 2014).

4.4.10.2 Sideband Estimator using MSB

Because the vibration signals from mechanical faults in planetary gearboxes contain a series of sideband components which appear mainly around the supply component. A bispectrum slice at the supply frequency will be sufficient to characterise these sidebands for fault detection and diagnosis and by setting f_2 in Equation (4.24) to a constant frequency value such as the fundamental. $f_m = f_s = 50Hz$, the MSB slice at supply frequency can be expressed as;

$$B_{MS}(f_r, f_m) = E\left[X(f_r + f_s)X(f_r - f_s)X^*(f_m)X^*(f_m) \right] \quad (4.27)$$

In the diagnosis of PG faults, it is the amplitude of the sidebands or modulators that is useful for both detection and diagnosis. However, the magnitude of $B_{MS}(f_r, f_m)$ from Equation (4.27) is a combination of sideband and supply components. The diagnosis results will be influenced by the amplitude at supply frequency, i.e. the results are too sensitive to load conditions (Alwodai, Shao et al. 2013; Gaballa M Abdalla 2014; Xiange, Abdallaa et al. 2015).

Considering that the amplitude of the supply frequency is predominant in the vibration signals and can be identified easily in the frequency domain, an MSB slice based sideband

estimator Equation(4.27) shows that through the operation of vector averaging in the frequency domain, the MSB can extract the combination of components at the meshing frequency, the lower sideband and the higher sideband. In the meantime, random noise and other interfering components not meet the necessary phase relationship will be suppressed significantly. In this way the modulation effects in acoustic signal can be represented more accurately and reliably.

To examine the modulating components alone, rather than that of the combination with the meshing component, a MSB sideband estimator (MSB-SE) can be used according to Equation (4.28);

$$B_{MS}^{SE}\left(f_r, f_m\right) = E\left[\frac{X\left(f_r + f_s\right)X\left(f_r - f_s\right)X^*\left(f_m\right)X^*\left(f_m\right)}{|X\left(f_m\right)|^2}\right] \tag{4.28}$$

Because the magnitude in Equation ((4.29) is normalised, the magnitude of the MSB-SE is only the product of the lower and upper sidebands, which reflects the modulating component due to the presence of faults. In addition, MSB coherence (MSBC) defined in Equation (4.29) can estimate the influences of random components and hence confirm the reliability of the MSB peak detected.

$$b^2{}_{MS}\left(f_r, f_m\right) = \frac{|B_{MS}\left(f_r, f_m\right)|^2}{PS(f_m)E\left[\left|X\left(f_m + f_r\right)\left(f_m - f_r\right)\right|^2\right]} \tag{4.29}$$

MSB coherence has boundaries [0 1]. Where 1 means that the magnitude of the MSB is due to modulation effects, a zero value means that the MSB magnitude is mainly due to random noise. The value of the MSBC will indicate the reliability of MSB peaks. In addition, for a given measurement environment, the background noise will be much the same. The increase of MSBC can be an indicator of modulation degree and used for detecting the presence of modulations (Gaballa M Abdalla 2014; Xiange, Abdallaa et al. 2015).

4.5 Summary

In order to achieve high performance in detecting and diagnosing various faults in planetary gears using the above techniques, it is important to choose suitable CM systems and procedures such as online or offline vibration monitoring, online or offline performance monitoring, centred on the criticality of the plant and the relative importance of the faults that could develop. It should also concentrate on continually improving the CM system so as to accomplish the desired results successfully and efficiently.

The mechanism of CM involves a mix of sensors and signal processing tools that ensures the constant provision of sensor signals representing the condition of system components based on approaches including: acoustics, oil analysis, strain measurement, thermography, and vibration analysis, which is one of the most important approaches used for CM of machines.

Vibration analysis is very useful in industry for effective CM and helps achieve and maintain good operating conditions and efficient machines. Vibration data is presented in the time domain, frequency domain and joint time-frequency domain, as shown in Section 4.3. Each of these can be used to process the vibration signal for gear fault detection and diagnosis. However, there remain many problems with the detection and diagnosis of incipient faults in; for example, planetary gears and this thesis will investigate the modulation signal bispectrum (MSB) as an advanced analytical technique which may be able to overcome these problems.

CHAPTER FIVE

THE EXPERIMENTAL SYSTEM AND INTRUMENTATION

This chapter begins by providing general information and then summarising the specifications of the test rig that is developed based on a planetary gearbox and experimental requirements for verification of the proposed techniques. It then goes on to describe the instrumentation for measuring both vibration and relative operating parameters in Section 5.2, speed, temperature, and power supplies. Finally, Section 5.4 explains the general procedures to perform various experiments for fault severity and location diagnosis.

5.1 Specifications of the Test Rig

5.1.1 Introduction

Planetary gearboxes are widely used for power transmission systems and have received extensive attention, particularly regarding tooth breakage which is a common failure in, for example, wind-turbine planetary gear transmission systems. Planetary gears are described in Chapter 2, where it is made clear that the early detection and diagnosis of faults is important to prevent unexpected or catastrophic breakdowns (Mauricel. Adams 2001).

This test rig platform was used to simulate a real rotating machinery gearbox fault common in industry (broken tooth and misalignments). The CM method was to collect and analyse gearbox vibration measurements in order to detect and diagnose the gearbox fault.

5.1.2 Planetary Gearbox Test Rig Description

The planetary gearbox (PG) test rig used in this study that provided and upgraded by student to be suitable for planetary gearbox with Centre for Efficiency and Performance Engineering Group (CEPE) is shown in Figure 5.1, and a schematic diagram is shown in Figure 5.2. It consists of a two stage helical gearbox manufactured by David Brown Radian Ltd, a PG manufactured by STM Power Transmission Ltd, a three phase induction motor produced by Brook Crompton, and a load system consisting of two flexible couplings and a DC generator which acted as the load on the system. The AC induction motor is powered by 3-phase power supply (11 kW, 1465 rpm and four poles) and is flanged in a cantilever type arrangement to the helical gearbox. A two stage helical gearbox with a 3.6 contact ratio was used in the tests. The input shaft is driven by the AC motor which had a maximum speed of 1465 rpm. The motor speed was controlled by a speed controller and the maximum speed actually used was 580 rpm ≈40%.The speed of shaft rotation was decreased by the 3.6 ratio of the helical gearbox to 203rpm. It was then increased to 1460 rpm by the 7.2 ratio of the planetary gearbox, so that the flexible coupling between the planetary gearbox and the DC-generator rotated at 1460 rpm. An incremental optical encoder with range 10 Hz to 2 kHz was used to measure the instantaneous angular speed (IAS). It was installed at the end of the induction motor shaft and provided one pulse for each complete revolution. It was connected directly to the data acquisition system (DAS).

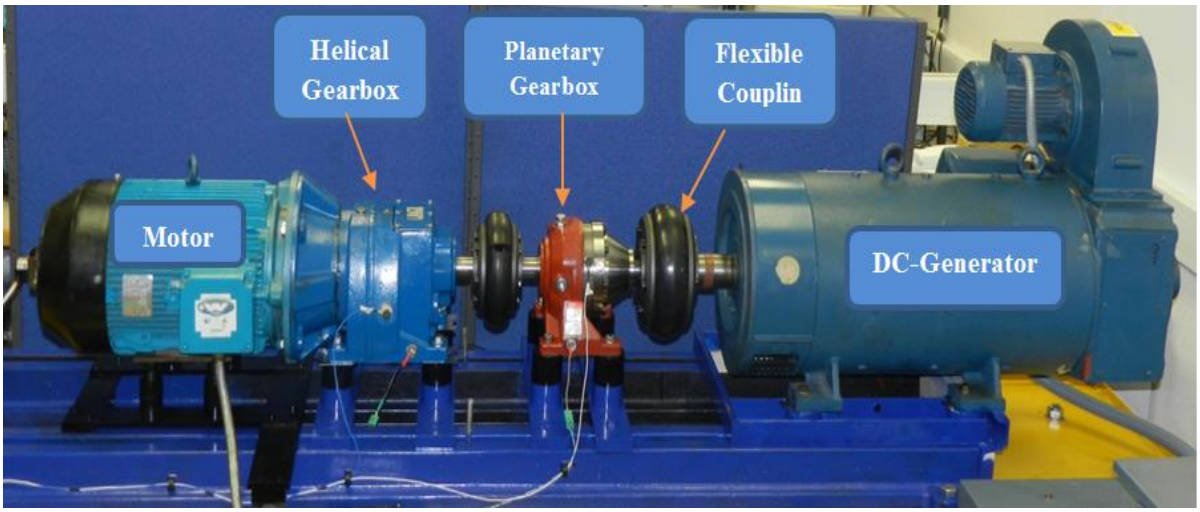

Figure 5.1 Planetary gearbox test rig

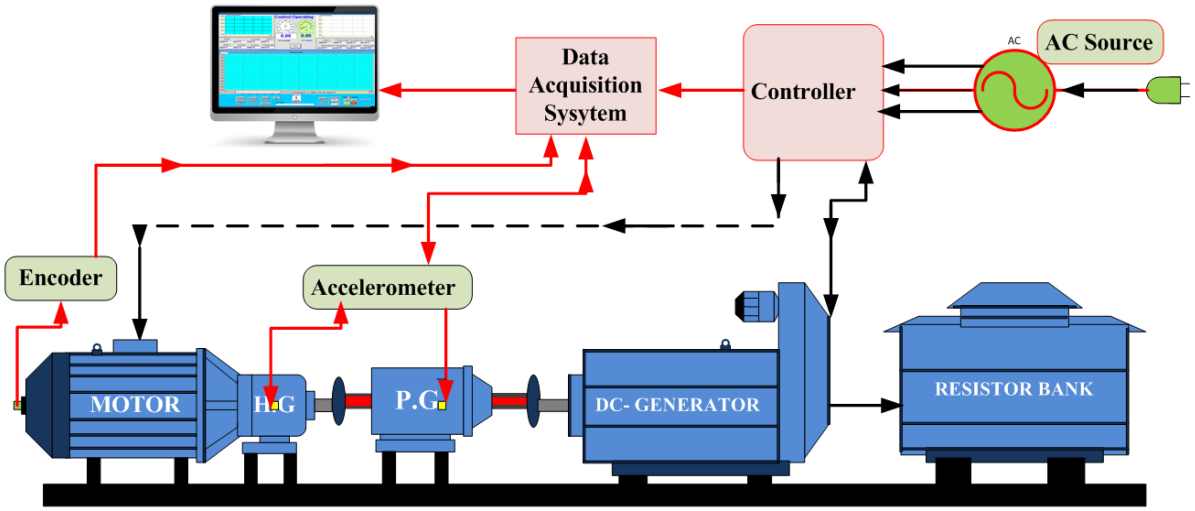

Figure 5.2 Schematic diagram of planetary gearbox test facility

The vibration of the test gearbox was measured by an accelerometer (Type PCB 338C04) with sensitivity of 100mV/g, and frequency response range from 1 Hz to 20 kHz. The accelerometer was mounted on the side of the planetary gearbox housing.

Figure 5.2 is a schematic diagram of the planetary gearbox facility showing the positions of the encoder and accelerometers. To change the speed of the drive motor, a digital variable speed controller was inserted between the AC power line source and the motor. The

controller can be programmed to any specific shaft rotation speed between 0 and 1465 rpm and load between 0% and 100 %.

5.1.3 AC Induction Motor

The drive was a four pole AC induction motor provided by Brook Crompton UK Ltd. The motor was powered by a three phase power supply and was flanged in a cantilever type arrangement to the helical gearbox. The motor is shown in Figure 5.3 and specifications presented in Table 5.1 (Al-Arbi 2012).

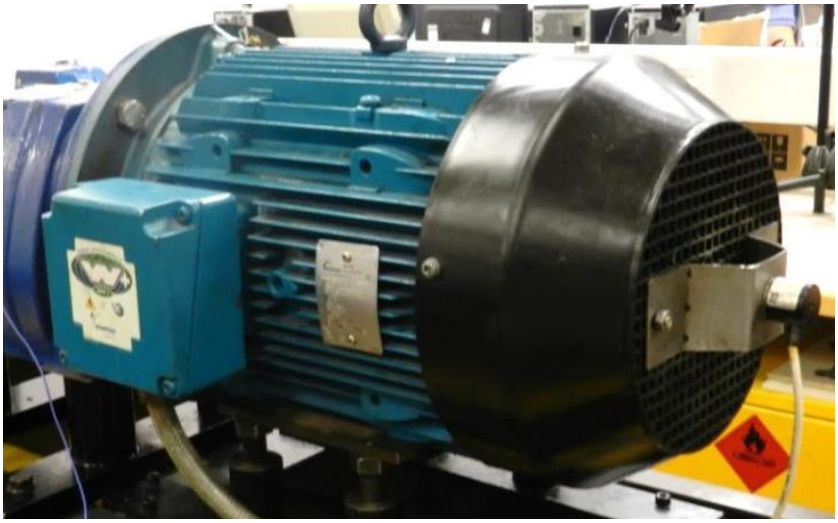

Figure 5.3 Three-phase 11 kW brook crompton induction motor

Table 5.1 Brook crompton induction motor specifications

Classification	**Induction**
Phase No.	3
Poles No.	4-Pair
Rated power	11 kW
Rated voltage	415 V
Current	22A @ Full Load
Rated speed	1465 rpm @full Load
Winding	Y Star To Δ delta
Stator slots Number	48
Rotor slots Number	40

5.1.4 Fenner Tyre Couplings

Figure 5.4 shows the FenaFlex Tyre Couplings used in this test rig. Two couplings were used, the first, the F80 FX10 assembly, joined the helical gearbox shaft with input planetary gearbox shaft and the second, the F100 FX10 joined the output shaft of planetary gearbox to the DC generator.

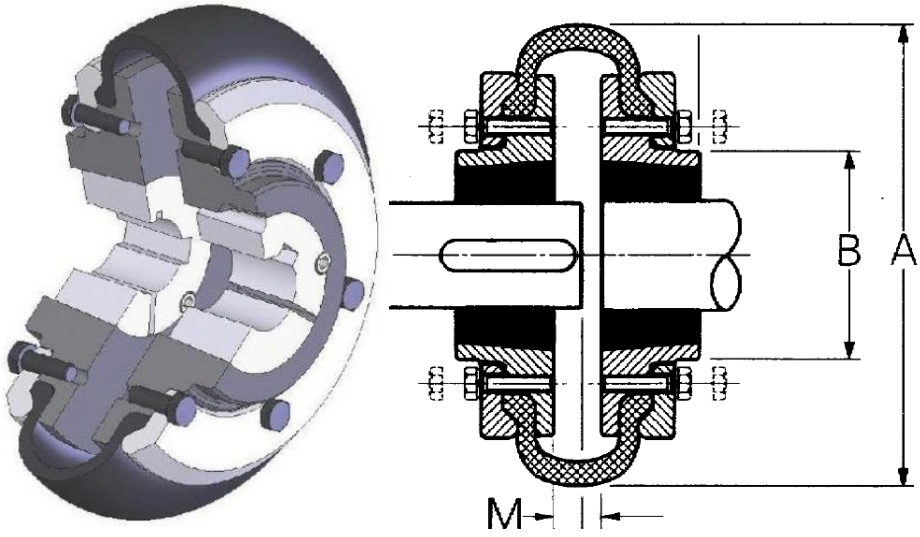

Figure 5.4 Fenner fenaflex tyre couplings reproduced from (ETRA 2015)

These couplings were highly elastic, lubrication free and could tolerate large degrees of misalignment in all planes. They also offered the advantages of simple installation and inspection without disrupting the drive. These couplings have good shock absorbing properties and reduce vibration and torsional oscillations. Additional manufacturer's information is listed and summarised in Appendix E (FPT 2015).

5.1.5 Two Stage Helical Gearbox

The photograph and schematic shown in Figure 5.5 are for the two-stage helical gearbox manufactured by David Brown Radian Ltd used in this test to reduce the drive shaft speed by a ratio of 3.678. The placement of combined motor gearboxes on AC machines has been driven by end users who require a convenient, compact design that comes as a complete package, without the need for additional mechanical components between motor and gearbox. The need to drive low-speed loads that require a high-torque has been a factor, because as any given power, torque in an AC motor is inversely proportional to speed it is

more efficient to use stepdown gearboxes for driving lower-speed loads at higher torque values. Thus, most motors now come as a motor gearbox combination that saves having to couple the motor up to a gearbox supplied separately. The motor is usually flange-mounted and mates directly to the gearbox front flange plate (Lane 2011).

5.1.5.1 Characteristic frequencies

The characteristic frequency for the helical gear box can be calculated for the first, second and third shaft rotational frequencies as follows :($f_{r1,}$ $f_{r2,}$ $f_{r3,}$), and the meshing frequencies fm1, fm2 for the first and second stages respectively.

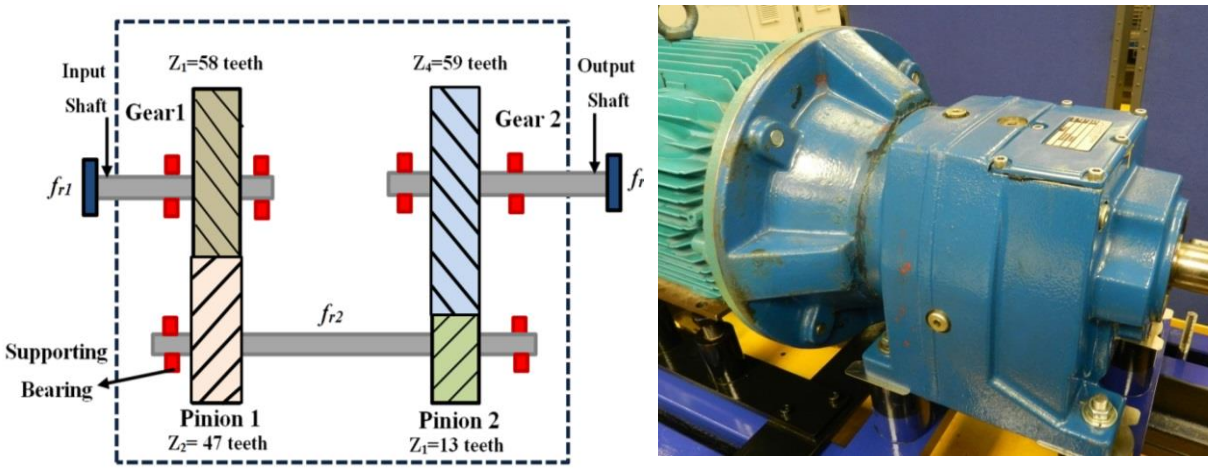

Figure 5.5 Two stage helical gearbox

The first speed f_{r1} is 40% of 1460 =586 rpm

$$f_{r1} = \frac{Rotor\ Mechanical\ Speed}{60\sec} = \frac{586rpm}{60\sec} \approx 9.76Hz \tag{5.1}$$

$$f_{r2} = f_{r1}.(\frac{z_1}{z_2}) = 9.76 * \frac{58.00}{47.00} = 12.00\ Hz \tag{5.2}$$

$$f_{r3} = f_{r2}.(\frac{z_3}{z_4}) = 12.00 * (\frac{13.00}{59.00}) = 2.64\ Hz \tag{5.3}$$

Mesh frequencies for the first and second stage can be calculated as:

$$f_{m1} = f_{r1}.z_1 = 9.76*58.00 = 566.08Hz \quad (5.4)$$

$$f_{m2} = f_{r2}.z_3 = 12.00*(13.00) = 156.00Hz$$

The second speed f_{r2} is 30 % of 1465 = 439.5 rpm

$$f_{r1} = \frac{Rotor.Mechanical.Speed}{60\sec} = \frac{439.5rpm}{60\sec} \approx 7.325\ Hz \quad (5.5)$$

$$f_{r2} = f_{r1}.(\frac{z_1}{z_2}) = 7.325*\frac{58.00}{47.00} = 9.039\ Hz \quad 5.6)$$

$$f_{r3} = f_{r2}*(\frac{z_3}{z_4}) = 9.039*(\frac{13.00}{59.00}) = 1.98\ Hz \quad (5.7)$$

Mesh frequencies for the first and second stage can be calculated as:

$$f_{m1} = f_{r1}.z_1 = 7.325*58.00 = 424.85Hz \quad (5.8)$$

$$f_{m2} = f_{r2}.z_3 = 9.039*(13.00) = 117.51Hz \quad (5.9)$$

The third speed, f_{r3},is 20 % of 1465 = 293 rpm

$$f_{r1} = \frac{Rotor.Mechanical.Speed}{60\sec} = \frac{293rpm}{60\sec} \approx 4.883Hz \quad (5.10)$$

$$f_{r2} = f_{r1}.(\frac{z_1}{z_2}) = 4.883*\frac{58}{47} = 6.026Hz \quad (5.11)$$

$$f_{r3} = f_{r2}.(\frac{z_3}{z_4}) = 6.026*(\frac{13}{59}) = 1.327Hz \quad (5.12)$$

Mesh frequencies for the first and second stage can be calculated as:

$$f_{m1} = f_{r1}.z_1 = 4.883*58.00 = 283.214Hz \quad (5.13)$$

$$f_{m2} = f_{r2}.z_3 = 6.026*(13.00) = 78.338Hz \quad (5.14)$$

where,

$Z1$ = number of teeth on the pinion gear at the first stage ($Z1 = 58$).

$Z2$ = number of teeth on the driven gear at the first stage ($Z2 = 47$).

$Z3$ = number of teeth on the pinion gear at second stage ($Z3 = 13$).

$Z4$ = number of teeth of the driven gear at second stage ($Z4 = 59$).

f_{m1} = mesh frequency of the 1st gear pair.

f_{m2} = mesh frequency of the 2nd gear pair.

5.1.6 Planetary Gearbox

The planetary gearbox was manufactured by STM Power Transmission Ltd. As can be seen in Figure 5.6 it consists of three planet gears. The planet carrier is floating which means that it was fixed to the output shaft by means of canter line which allowed it to move axially as required. A wear planet prevents the carrier from moving further than the sun gear in one direction and it could not move further on the splines than the engagement space available.

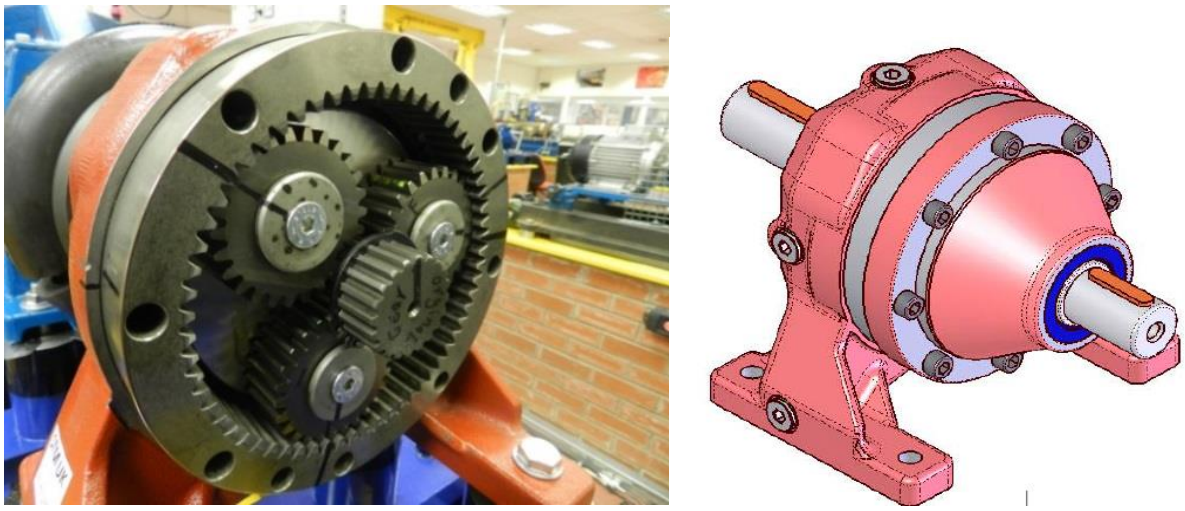

Figure 5.6 The planetary gearbox

The planet gears are hardened and use the inside of the planet gear as the inner bearing race. Loose needle bearings are then inserted between the planet gear and the planet gear shaft with the shaft itself being the other race of the bearing, as shown in Figure 5.7.

Figure 5.7 Planet gear with loose needle bearing

5.1.6.1 Planetary Gearbox Characteristic Frequencies

The planetary gearbox in this study is one where the gear wheel or ring is standstill, as seen in Figure 5.8 and the sun gear is moving.

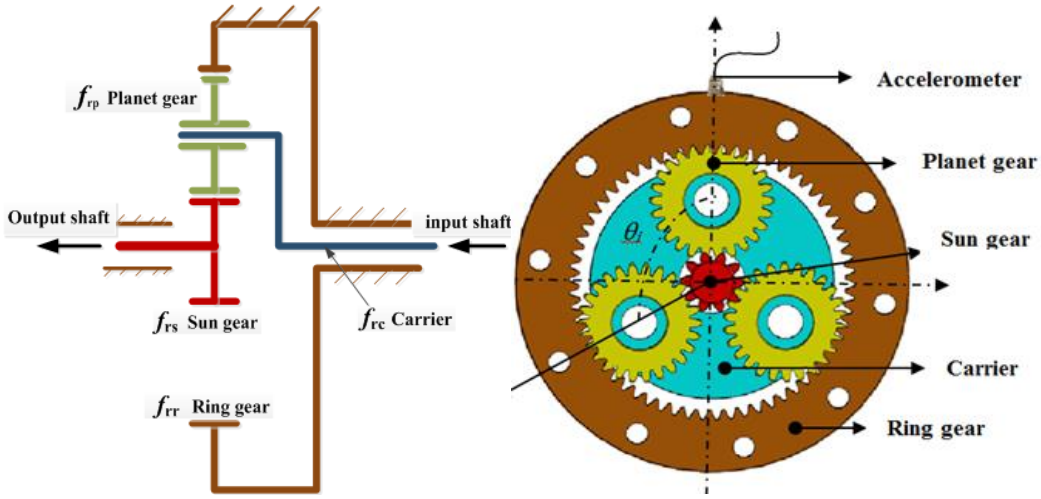

Figure 5.8 Schematic of planetary gear set with the standstill ring gear

5.1.7 DC Generator

The DC generator/motor used in this study and shown in Figure 5.9 enables different loads to be applied to the planetary gearbox test ring. The DC motor that provides the load to the AC motor is not controlled by a DC drive. Instead, the DC motor converts the mechanical energy supplied to electrical energy which is dissipated as heat in a resistor bank. The field current of the DC motor is controlled by a simple DC drive connected to two supply phases which

are configured to supply a current pre-set by a potentiometer which allows the test rig to operate from 0 to 100% load on the AC motor.

In the DC generator there is a small air gap between the armature part and the stator and the magnetic field remains strong through the current field core as seen in Figure 5.9. The field circuit is low-current with many coil turns generating the magnetic field. The field current only increases slightly with a large increase in the DC motor of generator power. The manufacturing specifications are listed in Table 5.2.

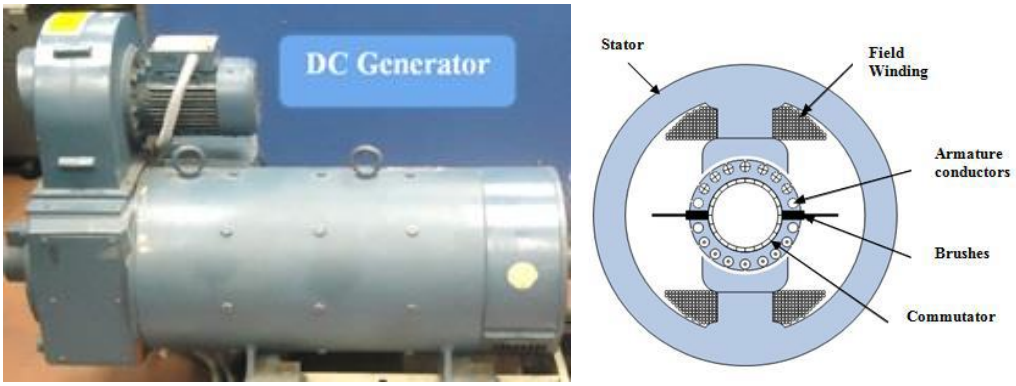

Figure 5.9 DC-Generators (mechanical load) reproduced from (Searle 1997).

Table 5.2 DC-generator specification

Description	
Generator No	G63801N
Size	SD 200XLC
Power	85 kW
Max. Speed	1750 rpm
Duty type	S1
Ins. Class	F
Mass	482 Kg

5.1.8 DC Motor Power Resistors

The DC motor resistor bank, see Figure 5.10, is matched to the DC motor. The maximum acceptable current is 200 A at 250 VDC, and this power rating is more than adequate for this

test rig. A schematic of the resistor bank with covers removed can be seen in Figure 5.10 (Lane 2011).

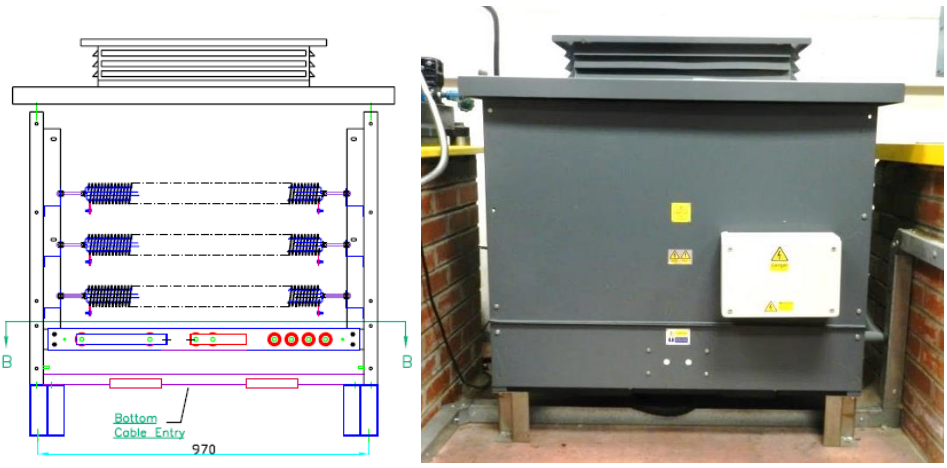

Figure 5.10 Resistor bank view

5.2 Vibration Measurement Sensors

5.2.1 Accelerometer

The piezoelectric (p-e) accelerometer is the transducer usually used for the measurement of vibration. P-e accelerometers have a high sensitivity which is good for the measurement of low amplitude vibration signals as they occur with incipient faults. These accelerometers have a wide frequency range from 1 Hz up to more than 20 kHz. The p-e accelerometer is small, durable and stable, with a linear response over a wide frequency range, properties which make it very suitable for use with gearboxes and gear meshing processes (Mark Senldge 1987).

The p-e accelerometer is composed of three main parts; the base, the p-e crystal and a seismic mass .When placed between the accelerometer base and the seismic mass, the p-e crystal functions as a spring. When vibration occur the accelerometer base moves relative to the seismic mass, and the crystal is subject to a force which produces a charge proportional to the applied force. According to Newton's second law of motion F= ma, but here the mass is constant so the charge is directly proportional to the acceleration. Because the accelerometer is rigidly attached to the vibrating surface the measured acceleration is equal to that of the surface, on which the accelerometer is mounted. For signal measurement and/or recording, an internal or external charge amplifier must be used. The internal charge

amplifier (ICP) accelerometer is now more common and the one usually used for long distance signal transmission (Mark Senldge 1987).

The present research work used an ICP accelerometer, PCB model 338C04. Here a low output impedance transducer, consisting of a built-in integrated circuit converted the charge signal into a voltage signal. Because the mass of the accelerometer was small it does not affect the surface movement significantly. Also its frequency range was wide enough for the gearbox vibration measurement. The environmental conditions on and around the gearbox were well within the limits specified by the manufacturer. Due to the microelectronics being inbuilt, there was an upper limit on working temperature of 90^0C. Table 5.3, presents the detailed specification of the accelerometer, and Figure 5.11, a photograph of the ICP accelerometer.

Table 5.3 Accelerometer Specifications

Parameter	**Performance**
Sensitivity	100 mv/g
Sensitivity tolerance	±10%
Frequency Range (±5%)	0.3 Hz to 12 kHz
Resonant Frequency	≥35 kHz
Non-linearity	≤1%
Transverse Sensitivity	≤5%
Overload limit (shock)	±5000gpk
Temperature Range (operation)	-53 to +93^0C
Output voltage	8 to 12 VDC

Figure 5.11. PCB Model 338C04

When mounting an accelerometer it is critical to consider sensor location for its accessibility, temperature, and whether its movement genuinely represents what is intended to be measured. Just as important is the mounting of the accelerometer. Figure 5.12 shows six measurement mountings for accelerometers and the corresponding frequency responses. To avoid unwanted distortion of the signal, the accelerometers were rigidly attached to their respective surfaces via a screw-threaded brass stud glued to the casing with ceramic cement. The upper frequency limit is imposed by resonance effects in the accelerometer, its mounting and the surface on which the accelerometer was mounted (Company 2007).

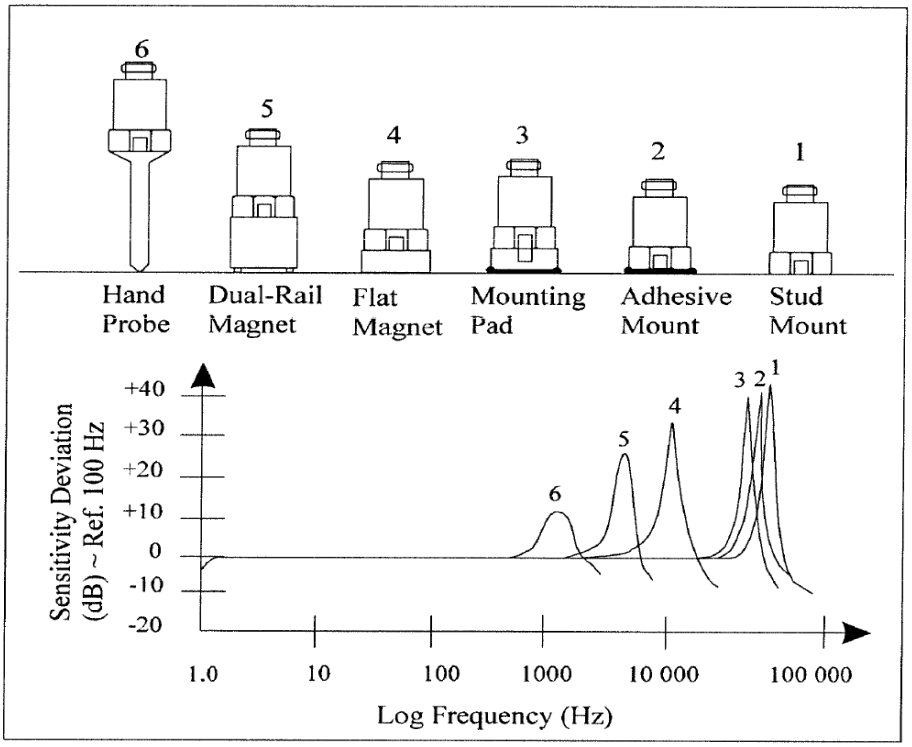

Figure 5.12 Accelerometer mountings and frequency responses reproduced from (Company 2007).

Characteristics of Accelerometer sensors

- ***Sensitivity***

A p-e accelerometer can be regarded as the charge source or the voltage source with high impedance. Consequently, charge sensitivity and voltage sensitivity are used to describe the relationship between acceleration and output(Johannes Wagner 2012).

- ***Frequency Response***

Measurement of frequency response requires mechanical excitation of the transducer. The acceleration is kept constant over the frequency range by means of a feedback signal coming from a reference accelerometer.

- ***Transverse Sensitivity***

Transverse sensitivity is the ratio of the output due to acceleration applied perpendicular to the sensitive axis divided by the basic sensitivity.

- ***Maximum Acceleration***

For charge output accelerometers the maximum acceptable acceleration is determined solely by the construction of the sensor. If the recommended maximum acceptable acceleration is exceeded by, for example, dropping the sensor on the floor, it will usually still function but recalibrating is recommended. Continuous vibration should not exceed 25 % of the stated limits to avoid wear. When highest accuracy is required, acceleration should not be higher than 10 % of the limit (Johannes Wagner 2012).

5.2.2 Incremental Rotary Encoder

The test rig was equipped with a high quality Hengstler incremental miniature optical encoder type RI32-0/100ER with a solid 5mm diameter shaft, see Figure 5.13, this was connected to the shaft rotor by a torsional rigid rubber coupling. The encoder was used to measure instantaneous angular speeds (IASs) over the range of 10 Hz to 2 kHz, with an output voltage of 5V, input high ≥2.5V, low ≤0.5V, and produced 100 pulses per revolution. The encoder was mounted on the end of the induction motor shaft to measure the motor speed and identify characteristic frequencies of gearbox vibration. No amplification of the measured IAS signal was required. The encoder was directly connected to the computer via the DAS system (Rohs 2014).

Figure 5.13 Hengstler RI32-0/100ER shaft reproduced from (Rohs 2014)

A detailed specification of the encoder is given in Table 5.4.(Rohs 2014).

Table 5.4 Shaft encoder specifications

Parameter	Performance
Supply Voltage	5VDCor10 to 30VDC
Max. pulse frequency	5V=300 kHz , 10-30V=200kHz
Current consumption	30mA , 40mA(5V DC)
Maximum shaft loading	Radial 10N, Axial 5N
Absolute max speed	4000 rpm
Operation temperature	-10C^o to + 70C^o
Shock resistance	100g

5.2.3 Data Acquisition System (DAS)

The data acquisition system used in the planetary gearbox test rig was a type PD2-MF-16-500/16L. Five of the available channels were used to measure the signals from the planetary gearbox, motor and speed encoder. The accelerometers were each connected to the DAS by a coaxial BNC cable to reduce noise. Usually, transducers such as accelerometers produce a voltage output proportional to the amplitude of the measured signal. The data acquisition card receives all the signal measurements which are then transmitted to the computer. The data acquisition control programme was developed in Lab-windows. The important DAS specifications are presented in the Table 5.5.

Table 5.5 DAS specification

Parameter	Performance
No. of Channels	16 differential , 16 single ended
Data resolution	16 bits
Sampling rate (maximum)	100 kHz
Max working voltage	12 V

Figure 5.14 shows how the signals collected from the planetary gearbox test rig were connected to the DAS channels: encoder (shaft speed and angular speed) to the first and second channels, the accelerometer on the helical gearbox to the third channel, the accelerometer on the planetary gearbox to the fourth channel, and current signal from the test rig to the fifth channel.

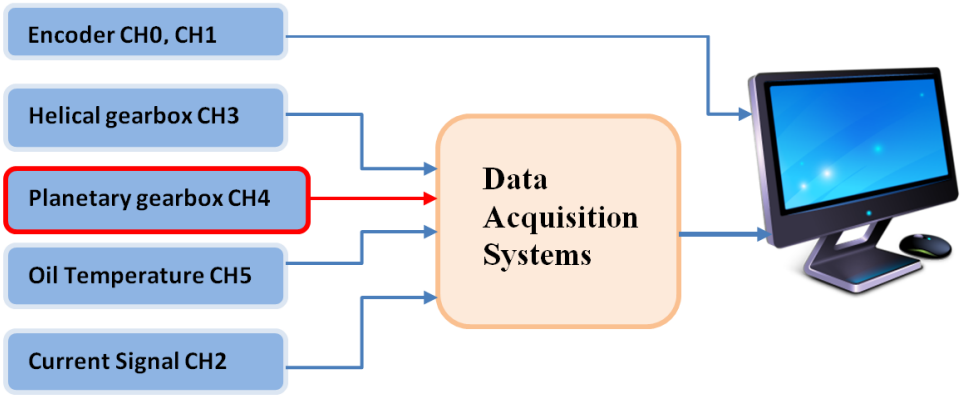

Figure 5.14 Signals measurement schematic diagram

5.3 The Test Rig Control Panel

The variable speed controller used for controlling the rotational speed of the system and load conditions is shown in Figure 5.15.

Figure 5.15 The test rig control panel

The control panel allowed the simulation of operating conditions (different speeds and different loads) so that in each test run the faults would be subject to exactly the same conditions. This is explained below.

- Set the DC generator motor load from 0% to 100%,and
- Set the AC induction motor speed between 0% and 40% of full motor speed.

Table 5.6 Shows the control panel functions as appeared in Figure 5.15

Armature current , Amps	Shows DC motor armature Amperes; the signal is obtained from DC motor current transformer output. Ranges between 0 and 200A max.
Field Current	Indicates the DC motor field current; the buffered output of the DC field controller gives the signal. Ranges between 0 and 5.0A max.
Operator touch screen	The touch screen permits the user to automatically start and record the system. Setting different load and speed conditions and times could also be done through the touch screen..

Switch On/Off Speed Control (Local Control Keys)	The yellow box has Green (Start) and Red (Stop) push buttons for operating the AC Drive Start/Stop. The drive front usually has a keypad but it can be placed on the test rig panel using a remote panel-mount kit. A series communication lead is used for connecting the keypad to the inverter drive(Lane 2011).

The parameters such as planetary gearbox oil temperature, vibration and speed were measured and recorded regularly from the PG test facility, for each test the raw data was acquired and displayed on a computer monitor in the form of plots across the screen as shown in Figure 5.16. This allows data to be examined before storing or recording it. Figure 5.16 and Table 5.7 shows the channels used in the test rig.

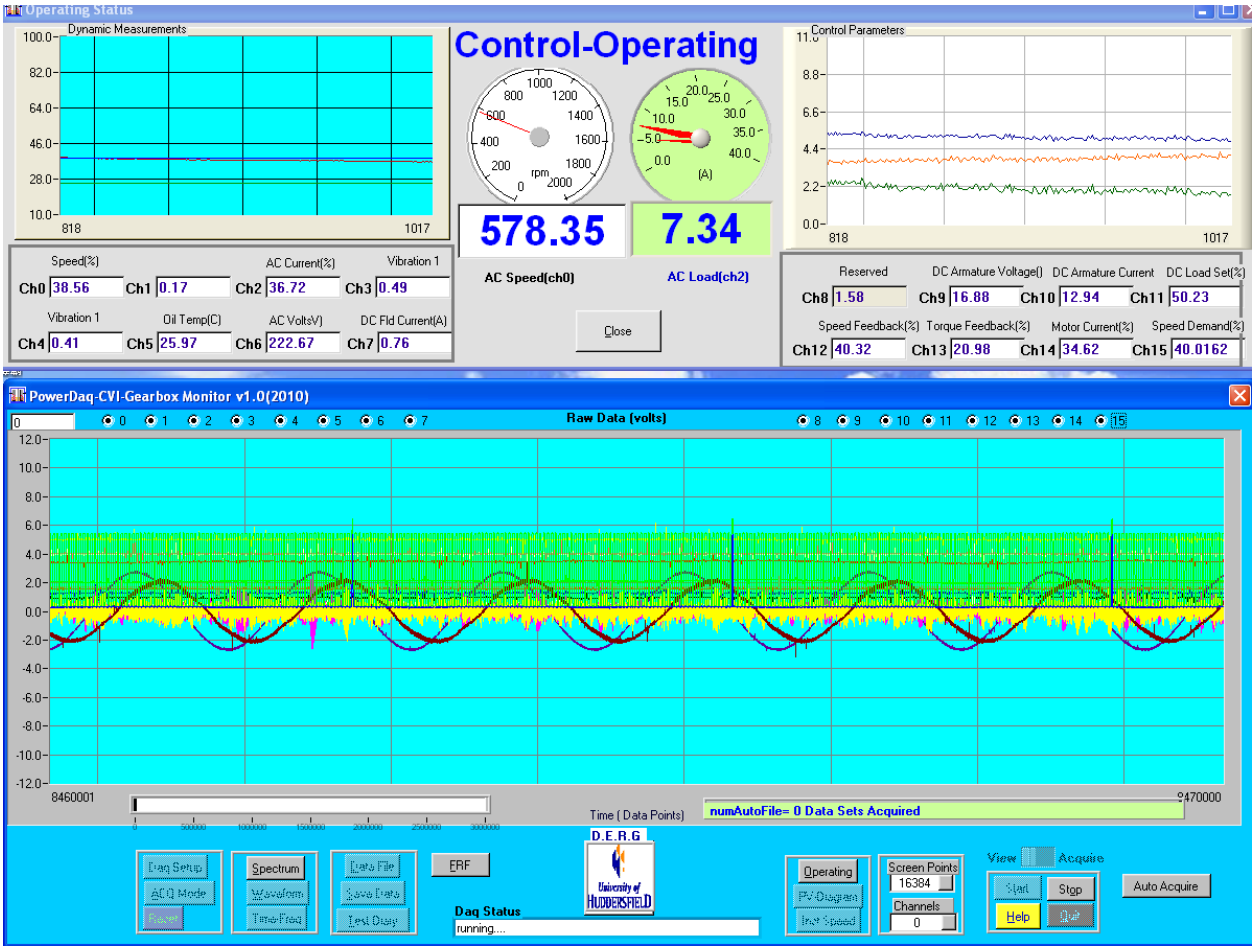

Figure 5.16 Raw data Acquired from test rig

Table 5.7 DQS channels

N°	CH0	Speed 1 from Encoder.
1.	CH1	Speed 2 from Encoder.
2.	CH2	AC Current
3.	CH3	Helical Gear box Vibration Gain X10
4.	CH4	Planetary Gear box Vibration no Gain.
5.	CH5	Planetary Gear box Oil temperature (CH 2 In Amplifier)
6.	CH6	AC Volts
7.	CH7	DC Field current
8.	CH8	……Not used ……
9.	CH9	*DC Armature Voltage*
10.	CH10	*DC Armature Current*
11.	CH11	*DC Load set (%)*
12.	CH12	*Speed feedback (%)*
13.	CH13	*Torque speed back (%)*
14.	CH14	*Motor Current (%)*
15.	CH15	*Speed demand (%)*

PLC CONTROLE

5.3.1.1 Speed Control

The block diagram of the experimental test rig is shown in Figure 5.17 and illustrates the major features of this test rig system, including the three–phase supply connected to the inverter to achieve speed control. The inverter changed the supply frequency according to the input speed set point and generated a new supply voltage for the AC induction motor. This voltage then drove the AC motor at the desired speed (Lane 2011).

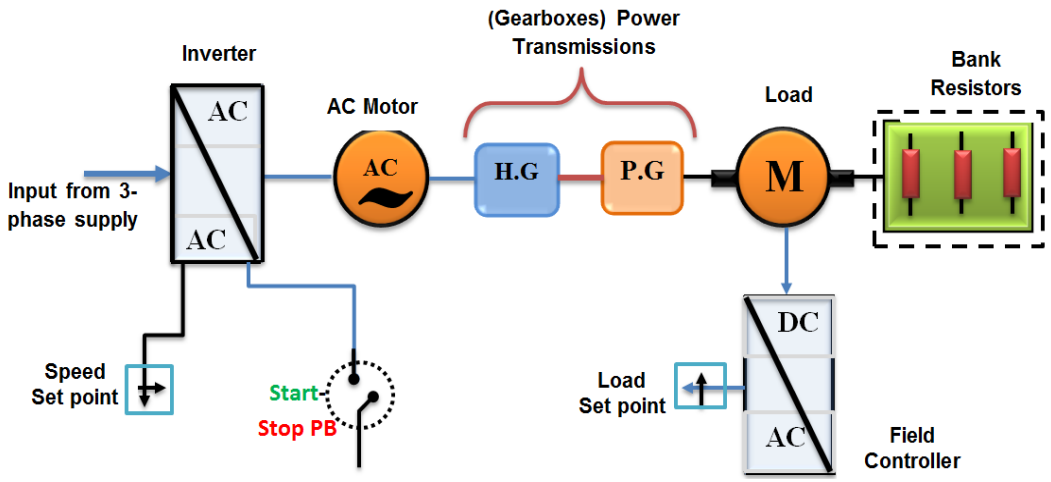

Figure 5.17 Block diagram of the experimental test rig

5.3.1.2 Load Control

The DC generator motor that provides the load to the AC motor dissipates the electrical energy it generates as heat in a resistor power bank. The field current of the DC motor is controlled by a simple DC drive connected to two supply phases which are configured to supply a current pre-set by a potentiometer. Consequently, this allows the test rig to operate from 0 to 100% of the maximum load on the AC induction motor (Lane 2011).

5.4 Data Collection Procedure

The tests were carried out at incremental speeds, 20%, 30% and 40% of the full speed of the AC motor (293, 439.5 and 486 rpm) and under different loads, zero load and 25%, 50%, 75% and 90% of the full load for each speed, see Figure 5.18, which is the Siemins touch screen control panel. Due to its high transmission ratio the planetary gearbox is running at 35% (513 rpm), 60% (879 rpm) and 80% (972 rpm) with respect to the AC motor speed.

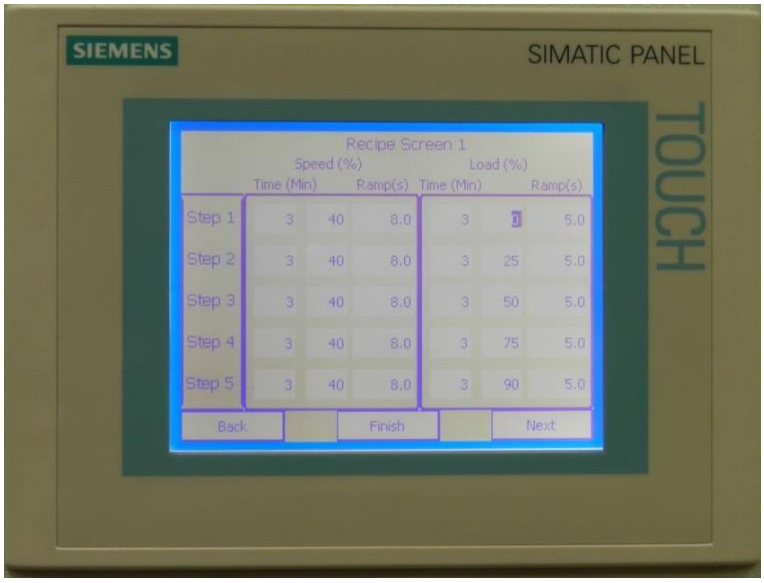

Figure 5.18 Control panel touch screen

The load and speed setting allows fault diagnosis to be examined at different loads and speeds which is the practical situation for many applications such as wind turbines. In addition, it considers that it may cause failures if operating the system in full operational conditions with fault inductions. The test rig was warmed up for one hour by running the AC motor at 40%, its maximum speed and a load of 90% of the full load. During this time it was

found that the temperature typically increased by 13.6^0C, from about 24.5^0C to about 38.15^0C, after which the temperature was stable. During the test the raw data is recorded at a specified sampling rate, data length and data resolution as in table.

Table 5.8 DAS setting in the experimental

No	Vibration-Power DAQ (PD2-MF-16-500/16L)
1.	Sampling rate = 100kHz
2.	Data length =$3x10^6$ Pts.
3.	Date resolution= 16 bits
4.	Time duration = 30 Sec

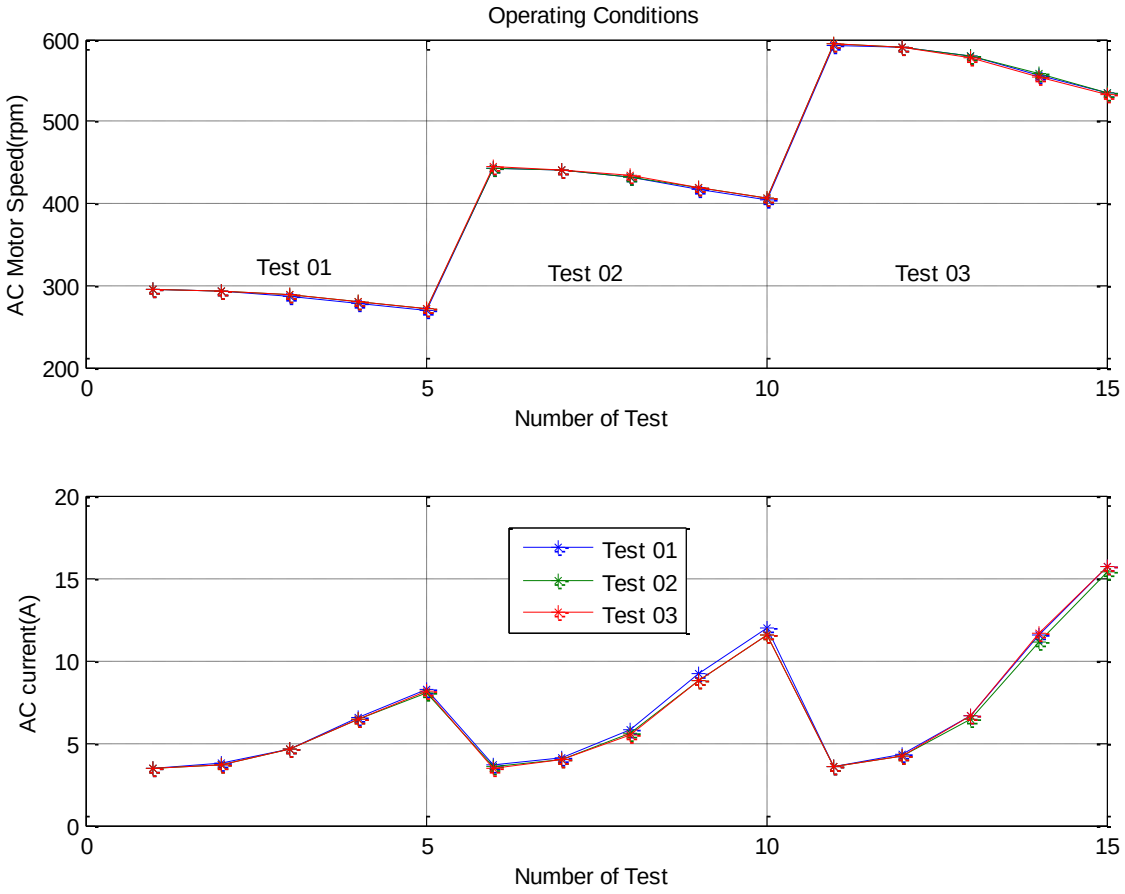

Figure 5.19 Each test repeated three times

In Figure 5.19, the three upper plots show the AC motor speeds for three trial runs for three operating conditions. Trial Run 1 is a plot of speed against load for an initial speed of 293 rpm as the load is progressively increased from zero to 90% in five steps. It shows that the speed decreased with increase in load. Each measurement was repeated six times to

demonstrate repeatability and reduce uncertainty. For Trial Run 2 and Trial Run 3 the initial speeds were set to 440 rpm and 486 rpm respectively and the load again increased in five steps from zero to 90%. For both plots the speed progressively decreased with increase in load.

The three plots in the lower section of Figure 5.19 shows the AC current as the load increased, and shows that for each initial condition (speed = 293rpm, 440rpm and 486 rpm) the current increased progressively with increase in load. The six plots in Figure 5.19 demonstrate the good reproducibility of the experimental measurements for each set of operating conditions.

The procedures followed in this experiment were:

I. The shaft encoder was mounted directly on the rear of the induction motor and the output cable was connected to the data acquisition channel, which was linked to the computer. One accelerometer was mounted directly on the case of the planetary gearbox.
II. Speed and load were selected and entered into the rig control panel before switching on. The software was put into view mode to ensure the signals were being received correctly, see Figure 5.16, then auto acquire data mode was activated.
III. All the raw vibration signals were collected from the accelerometers mounted on the gearbox casings and input to the DAS. This was repeated for each set of tests and the data stored as time domain signals on the computer under specified file names.
IV. MAT-LAB software codes were developed to process and analyse the signals recorded.
V. Vibration signals will also be studied for a better understanding of the characteristics of vibration signal in the planetary gearbox.
VI. The developed MATLAB code was used to process and analyse the recorded data.
VII. Each test in this study was repeated three times to ensure its repeatability, see Figure 5.19.
VIII. After collecting sufficient data, the rig was stopped and switched off at the mains.

5.5 Summary

Chapter five presented the test facilities and instrumentation used for measurement and data acquisition; including the induction motor, DC generator, helical gearbox and flexible couplings. The sensors, capable of measuring the parameters of interest, and their mountings on the test rig have been described in detail as seen in section 5.1. Although the planetary gearbox used in the test lab was from a wind turbine the seeded gearbox faults were as real and accurate.

Mat-lab software was used to develop a code, which calculates vibration raw signal on spectrum PS and modulation signal bispectrum MSB. The vibration signal was processed under baseline and different fault severity in sun and planet gears. Finally, all planetary gearbox data (healthy and fault) were compared with baseline.

CHAPTER SIX

MISALIGNMENT DIAGNOSIS OF A PLANETARY GEARBOX

This chapter describes the diagnostics of planetary gearboxes misalignment, one of the major operating problems that can arise due to variable operating conditions and differences in elastic deformations in the system. The effect of varying degrees of planetary gearbox installation misalignment is investigated using the spectrum analysis of the vibration measurements, in particular the modulation signal bispectrum (MSB). The result shows that shaft misalignment can be detected and diagnosed. It is evident that MSB produces a more accurate diagnosis in that it gave a correct indication of the fault severity and location for all operating conditions used.

6.1 Introduction

The multiple load paths within planetary gearing means the power transmitted is divided between several planet meshes and because of the use of smaller, stiffer components PGs have reduced noise, vibration and improved efficiency. As shown in the general review paper by Leia, et al, (Lei, Lin et al. 2014), considerable work has been carried out investigating vibration characteristics for monitoring various faults including gear pitting, crack and wear. However, it is noticeable that little research has been done in developing monitoring for misalignment, which is deemed as the second most commonly observed fault source in rotor systems (Patel 2009; Yong Gui 2013). Both AM and FM effects need to be taken into account in developing vibration signal models, and the effects on spectrum structure needs to be examined when analysing the measured signals for fault detection and diagnosis, see Chapter 2.

This research attempts to fill at least some of these gaps by investigating the effect of varying degrees of misalignment on the vibration spectra of a PG system, and to develop more reliable methods for diagnosing this fault. The modulation signal bispectrum (MSB), was used because it is particularly effective in capturing the weak modulations in PG signals for fault detection and diagnosis (Gu 2011). It was also used to better understand AM-FM effects on the vibration signals, and to enhance feature components for the detection and diagnosis of the misalignment at different speeds and loads, planetary gearbox vibrations and MSB Analysis.

6.1.1 Characteristic Frequencies for Diagnosis

A schematic of a PG is shown in Figure 6.1. A PG generally consists of three planet gears, one sun gear, ring gear and a carrier. The carrier is floating and fixed to the output shaft by means of splines which allow it to move axially as required.

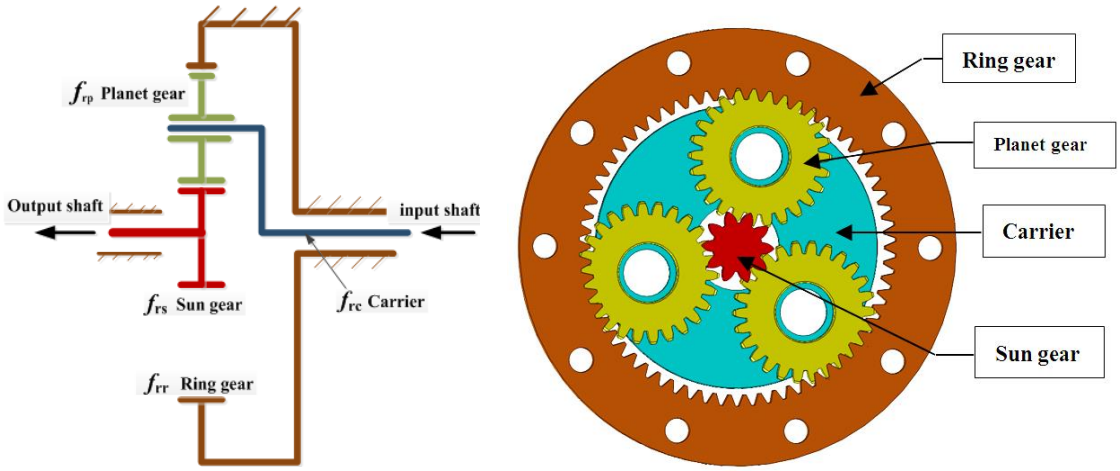

Figure 6.1 Schematic of a planetary gearbox with its standstill ring gear

According to this configuration, vibration characteristic frequencies for the case of error-free gears with the elastic deformation on tooth profile due to operating conditions are:

The carrier:

$$f_{rc} = \frac{f_{rs}}{i} = \frac{z_s}{z_r + z_s} f_{rs} \tag{6.1}$$

The planet gear:

$$f_{rp} = \frac{(z_p - z_r)z_s}{(z_r + z_s)z_p} f_{rs} \tag{6.2}$$

The meshing frequency:

$$f_m = (f_{rs} - f_{rc})z_s = \frac{z_r z_s}{z_r + z_s} f_{rs} \tag{6.3}$$

where: f_{rs} is the rotational speed of sun gear speed, ***i*** is the transmission ratio $= 1 + Z_r / Z_s$;

Z_r Z_p and Z_s, are the numbers of teeth for the ring, planet and sun gear respectively

In addition, considering that there are K planetary gears and due to the motion of the planetary gears, there will be a greater number of characteristic frequencies compared with a fixed shaft gearbox (Feng 2012).These will include:

Faults on the sun gear

$$f_{sf} = \frac{f_m}{z_S} = K(f_{rs-} f_{rc}) \tag{6.4}$$

Faults on the planet gear

$$f_{pf} = 2\frac{f_m}{z_p} = 2(f_{rc} + f_{rc}) \tag{6.5}$$

Faults on the ring gear

$$f_{rf} = \frac{f_m}{z_r} = Kf_{rc} \tag{6.6}$$

In general fault detection and diagnosis can be carried out by examining the change of these characteristic frequencies in the frequency domain. However, it is often very difficult to identify and quantify these components because of the effects of interferences between higher order of harmonics and the attenuation and distortion of different wave transfer paths. These components are often found in the frequency range around the meshing frequencies at which the characteristic components are modulated.

6.1.2 Vibration Characteristics at Meshing Frequency

When inevitable manufacturing errors and defects are taken into account, the vibration responses will be complicated modulation processes. As shown in the literature review, vibration sources induced by faults at a meshing location can be modelled as a combined process of AM and FM, with the gear pair meshing frequency or its multiples as the signal carrier frequency, and the characteristic frequency of the damaged gear or its multiples as the modulating frequency. In general, the signal can be expressed at meshing frequency f_m by;

$$X(t) = \sum_{h=0}^{H} a_h(t)\cos[2\pi h f_m t + b_h(t) + \theta_h] \tag{6.7}$$

where: H is the highest order of AM-FM harmonics to be considered.

The AM modulating components $a_h(t)$ for fault component f_f at are:

$$a_h(t) = c\sum_{n=0}^{N} A_{hn}\cos(2\pi n f_f t + \alpha_{hn}) \tag{6.8}$$

The FM component $b_h(t)$ is;

$$b_h(t) = \sum_{l=1}^{L} F_{hl} \sin(2\pi l f_f t + \varphi_{hl}) \tag{6.9}$$

where: C is a dimensionless constant depending on signal amplitude; θ_h, α_{hn} *and* φ_{hl} are the initial phases of the meshing components, AM components and FM components respectively. L, N are the highest order for AM and FM harmonics, respectively, to be considered in connection between AM and FM, only the first harmonic is considered in Equations (6.7), (6.8) and (6.9), which gives;

$$X(t) = [M_0 + M_1 \cos(2\pi f_f t + \alpha_{hn})]\cos[2\pi f_m t + F \sin(2\pi f_f t + \varphi_{hl}) + \theta_h] \tag{6.10}$$

By ignoring the high order components in approximating FM, $X(t)$ can be approximated as the superimposition of three components; the meshing component, *X1*, the sidebands to the AM, *X2*, and the sidebands to the FM, *X3* :

$$X(t) = X1 + X2 + X3 \tag{6.11}$$

where the meshing component is:

$$\mathrm{X1} = \frac{1}{2} M_0 \cos(2\pi f_m t + \theta) \tag{6.12}$$

Sidebands due to AM:

$$X2 = \frac{1}{4} M_1 \left\{ \cos\left[2\pi (f_m + f_f) t + \theta + \alpha \right] + \cos\left[2\pi (f_m - f_f) t + \theta - \alpha \right] \right\} \tag{6.13}$$

And sidebands due to FM

$$X3 = \frac{1}{4} M_0 F \left\{ -\cos\left[2\pi (f_m + f_f) t + \varphi + \theta \right] + \cos\left[2\pi (f_m - f_f) t - \varphi + \theta \right] \right\} \tag{6.14}$$

Thus the amplitude of sidebands is the vector sum of both AM and FM components. As the phases continuously change in a random manner, with operating conditions, the sideband components can be distributed asymmetrically around the meshing frequency. This is an important cause of sideband asymmetry, but the sensor position can also cause similar effects as shown by Dempsey, et al.(McFadden and Smith 1985), For example, the upper sideband

may disappear completely when the phase is opposite whereas the lower sideband would be doubled. This confirms that the sidebands can be asymmetrically distributed, and fluctuate substantially with operating conditions, including the presence of gear faults. These asymmetry effects will be increased by the differences that exist between vibration transmission paths from the same source to the same sensor. Thus, appropriate signal analysis methods need to be used to produce a reliable and accurate diagnostic feature.

6.1.3 Modulation Signal Bispectrum

As explain in Section 4.3.11, according to the definition of MSB in the frequency domain, the meshing frequency f_m and sideband f_r in a vibration signal can be correlated as;

$$B_{MS}(f_r, f_m) = E\left[X(f_r + f_s)X(f_r - f_s)X^*(f_m)X^*(f_m)\right] \quad (6.15)$$

where: $X^*(f)$ is the complex conjugate of the Fourier transform $X(f)$ of vibration signal $x(t)$; and $E[\,]$ is the statistical expectation operator, and the power spectrum of $x(t)$ is:

$$PS(f_m) = E\left[X(f_m)X^*(f_m)\right] \quad (6.16)$$

Equation (6.15) shows that through the operation of vector averaging in the frequency domain, the MSB can extract the meshing frequency, the lower sideband and the higher sideband. Components (including random noise) that do not meet the phase relationship will be substantially suppressed. In this way the modulation effects on the vibration signal can be represented more accurately and reliably (Abdalla, Tian et al. 2014).

To examine the modulating components alone, rather than in combination with the meshing component, a MSB sideband estimator (MSB-SE) can be used:

$$B_{MS}^{SE}(f_r, f_m) = E\left[X(f_r + f_s)X(f_r - f_s)X^*(f_m)X^*(f_m)/|X(f_m)|^2\right] \quad (6.16)$$

Equation (6.17) defines MSB coherence (MSBC). Because the magnitude in Equation 6.17) is normalised, the magnitude of the MSB-SE is the product of only the lower and upper sidebands, which better reflects the modulating component in the vibration signal due to the presence of faults. In addition, MSBC can be used to estimate the influence of random components and hence determine the reliability of any MSB peaks detected:

$$b^2_{MS}(f_r, f_m) = \frac{|B_{MS}(f_r, f_m)|^2}{PS(f_m)E\left[\left|X(f_m + f_r)(f_m - f_r)\right|^2\right]} \quad (6.17)$$

MSBC has boundaries [0 1]. The value of unity means that the magnitude of the MSB arises from true modulation effects. A zero value means that the MSB magnitude is mainly due to the effects of random noise. Intermediate values of MSBC will indicate the reliability of MSB peaks. Because, for any given environment, the background noise will remain much the same, any increase in MSBC can be taken as an indication of the presence of modulations (Abdalla, Tian et al. 2014).

6.2 Test Facilities and Experimental Setups

6.2.1 Test Facility

The test rig facility is described in some detail in Chapter Five and shown again in Figure 6.2

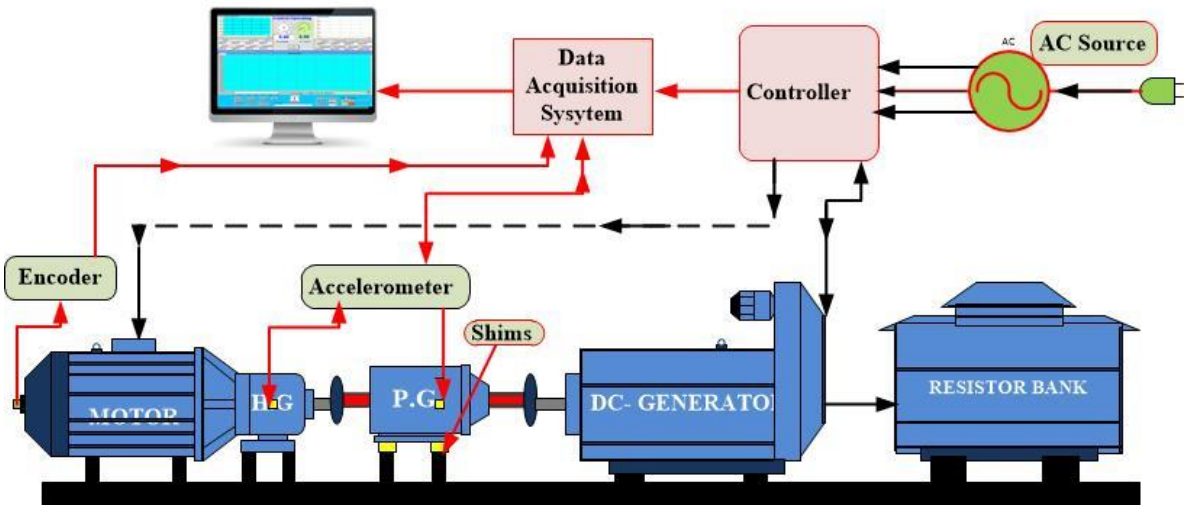

Figure 6.2 Schematic diagram of planetary gearbox test facility

6.2.2 Test Procedure

To examine the influence of the operating condition on fault diagnosis performance, tests were carried out with the AC motor at speeds 293 and 444 rpm and the planetary gearbox operating at 879 and 972 rpm, respectively. At each speed the system was operated under five loads (0%, 25%, 50%, 75% and 90%) of the full load. These operating conditions

allowed an exploration of different influences on the contents of the vibration spectra to aid the development of a reliable diagnosis method, see Section 5.3.

When all shafts in the system were aligned and checked using a dial-gauge, a baseline test was conducted to collect data under the designed operating conditions. The parallel misalignment or vertical offset on the planetary gearbox was introduced by adding shims underneath the installation legs. Three tests were carried sequentially with shim thicknesses of 0.4 mm, 0.7 mm and 1.0 mm respectively, to represent three degrees of misalignment fault severity (Abdalla, Tian et al. 2014).

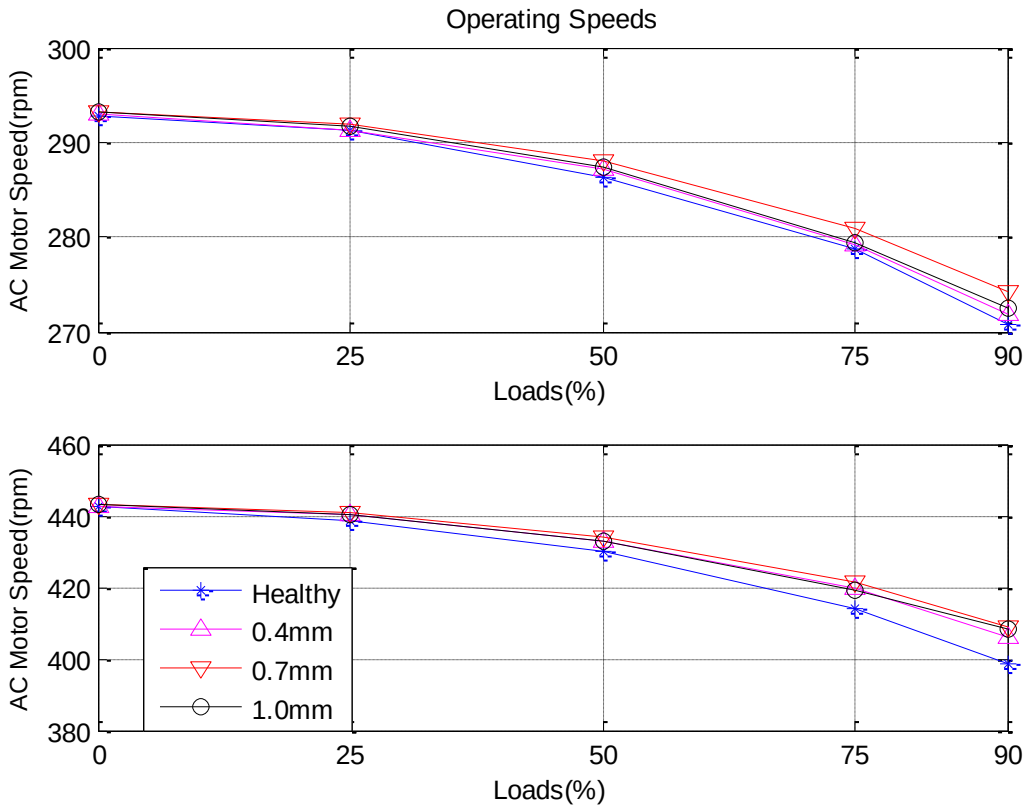

Figure 6.3 Repeatability of operating conditions

In Figure 6.3the plots show the AC motor speed as a function of load. In the upper window the initial speed was 293 Hz, and in the lower window, 444 Hz. The four plots in each window represent readings for the four misalignment conditions: healthy, with a 0.4 mm shim in place, with a 0.7 mm shim and a 1.0 mm shim. It shows that the speed decreased with increase in load. Each measurement was repeated six times to demonstrate repeatability of the measurements.

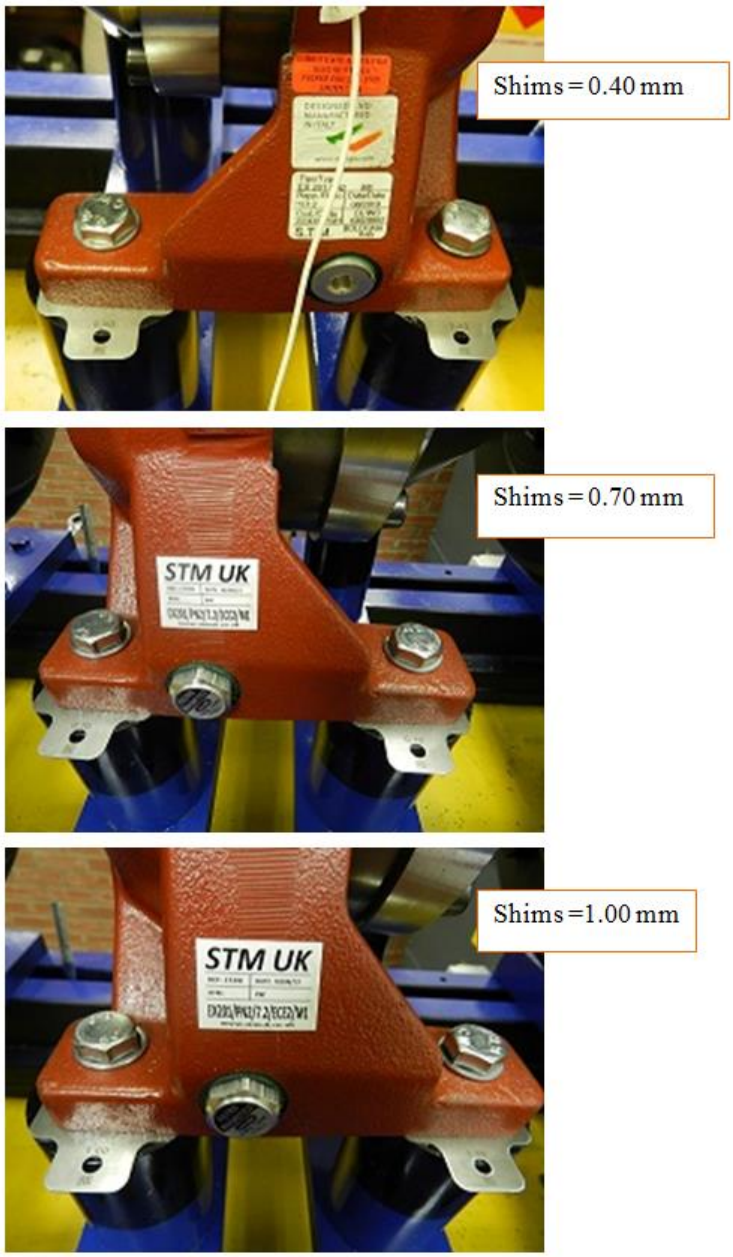

Figure 6.4 Configuration misalignment faults

6.2.3 Flexible Tyre Coupling

Flexible tyre couplings provided by the Fen Flex Tyre Couplings were used in this test rig; see Section 5.1.4 and Figure 5.4 and Figure 6.5. These exhibited the desirable features of an ideal flexible coupling and suitable taper locker fixing. The three degrees of shaft misalignment severity described above came within the acceptable range as listed in the manufacturer's manual, see Table 6.1.

Figure 6.5 Fenner tyre coupling reproduced from [168]

Table 6.1 Flexible coupling parameters

Size	Max. Speed (rev/min)	Torque (Nm)		Moment of inertia MR^2 (kgm^2)	Torsional Stiffness (Nm/°)	Maximum Misalignment (mm)	
		Nominal	Max.			Parallel	End float ±
F40	4500	21	64	0.00148	5	1.1	1.3
F45	**4500**	**37**	**110**	**0.00250**	**9**	**1.2**	**1.5**
F50	4500	53	160	0.00349	13	1.3	1.7
F60	4000	106	318	0.01030	26	1.6	2.0
F70	3600	162	487	0.01811	41	1.9	2.3
F80	3100	253	759	0.03679	63	2.1	2.6
F85	**3000**	**305**	**915**	**0.05015**	**76**	**2.2**	**2.8**
F90	2880	365	1096	0.06374	91	2.4	3.0
F100	2600	505	1517	0.11989	126	2.6	3.3
F110	2300	712	2137	0.16012	178	2.9	3.7
F120	2050	1182	3547	0.34302	296	3.2	4.0
F140	**1800**	**1881**	**5642**	**0.69452**	**470**	**3.7**	**4.6**
F160	1600	3113	9339	1.21767	778	4.2	5.3
F180	1500	5485	16455	2.01800	1371	4.8	6.0
F200	1300	8022	23508	4.03446	1959	5.3	6.6

6.3 Results and Discussion

The vibration signals that collected were processed by used both techniques MSB and power spectrum PS, the data was analysis by using the FFT with a Henning data window of 524288 points, which achieved a frequency resolution of 0.1362 Hz, so that the carrier frequency was sufficiently differentiated. In addition, the signals were for an average of 80 runs to obtain a more reliable spectrum by suppressing possible noise and interfering components for the MSB analysis.

6.3.1 Spectrum of Vibration Signals

Figure 6.6 (a) and (b) show the spectra in the low frequency range and around the 3rd harmonics of the meshing frequency for different load at the lower speed.

It can be seen that from Figure 6.6 (a), that the spectrum for the baseline is predominated by harmonics of f_{rs} and other components such as at f_{sf} and f_{rp} maybe visible under different load. Moreover, under the misaligned condition of 1.0 mm, spectral amplitude increase clearly at $2Xf_{rs}$ and $6Xf_{rs}$ but not $4X$, which is not fully consistent with the concept that the amplitudes of even harmonics should increase with the degree of misalignment. Additionally, the amplitude of these harmonics shows a slight decrease with increase in load. This is thought to be due to the effect of the nonlinear stiffness of the flexible couplings, which allows a smaller torsional oscillation at high static load. For a similar reason the amplitude at f_{rc} is very small because it undertakes a load 7.2 times of that at the sun gear shaft.

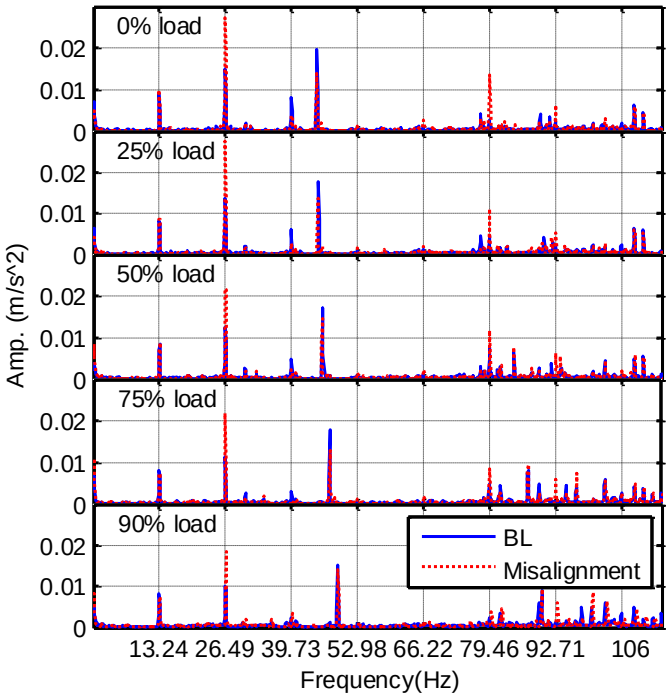

(a) Spectrum in the low frequency range

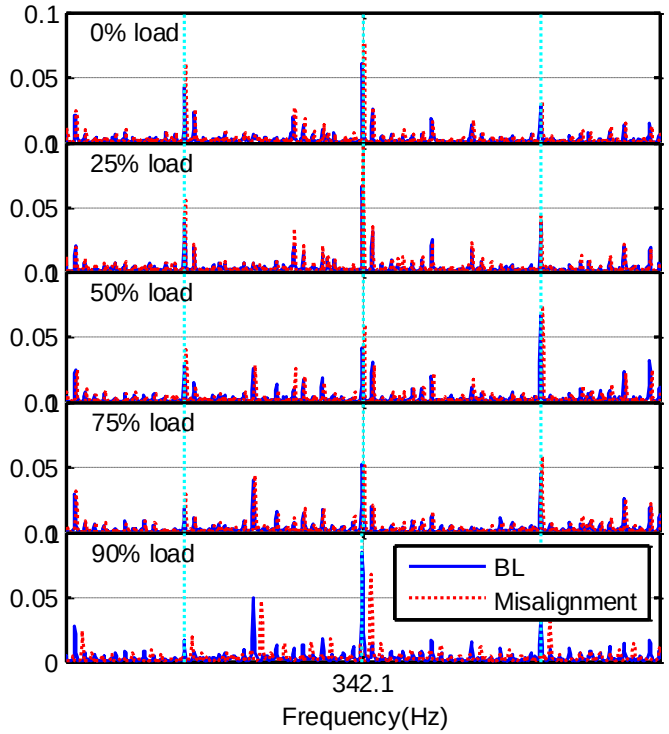

(b) Spectrum around 3rd meshing frequency

Figure 6.6 Vibration power spectra showing baseline and misalignment under different loads for initial drive speed of 440 rpm

In the meantime, the spectrum sections around $3Xf_m$ for the baseline case are generally higher than that of the low frequency range. Except for sidebands at ($3Xf_m \pm f_{rs}$), it is difficult to identify other sideband patterns, indicating the AM-FM effects. Moreover, the differences between the baseline and the misalignment are much smaller, compared to that of the low frequency range. This shows that the misalignment may cause a small effect on gear meshing processes due to the damping of key ways. In other words, this type of misalignment should be detected in the low frequency range (Abdalla, Tian et al. 2014).

Spectral amplitudes up to 10^{th} order of harmonics at all characteristic frequencies overviewed in section 2 are extracted from corresponding spectrum in both the low frequency range and that of different meshing frequencies. However, the spectral amplitudes of sideband obtained around meshing frequencies show inconsistent changes with the fault severity and operating conditions. This may indicate the adverse effect of AM–FM which may cause the sideband to oscillate in different conditions. On the other hand, as shown in Figure 6.7, the amplitude at f_{rs} from the low frequency range increases consistently with the degrees of misalignment, showing this spectral amplitude allows the misalignment to be diagnosed appropriately at the lower speed. However the amplitude could not make differences at the high load condition. This may be due to the influences of high background noise from the test system and the stronger vibration sources inside the gearbox (Abdalla, Tian et al. 2014).

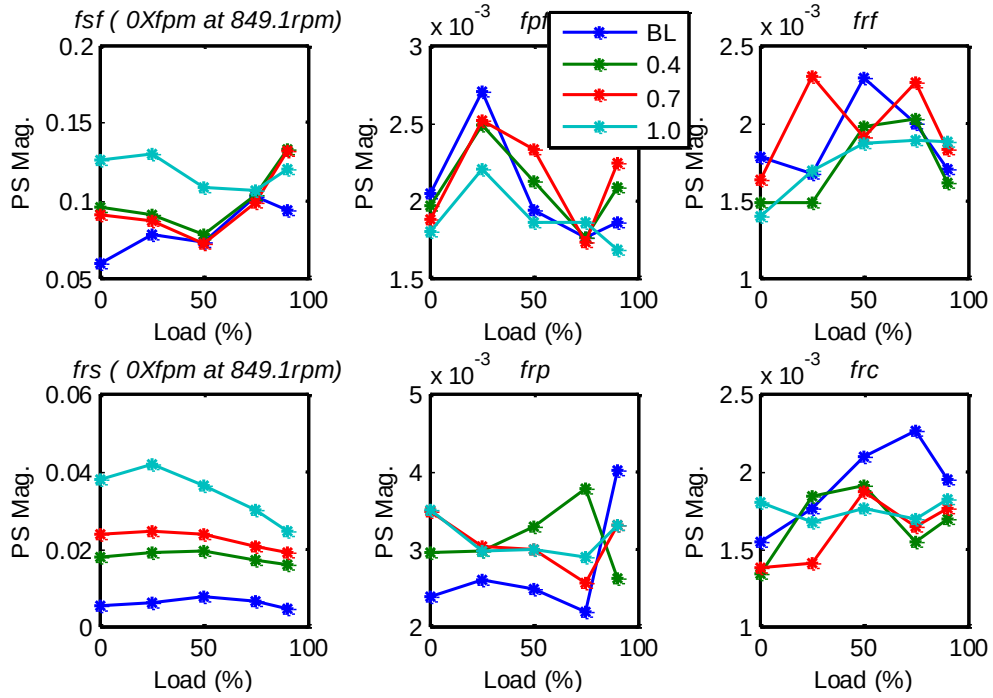

(a) Spectra amplitudes of characteristic frequencies at lower speed

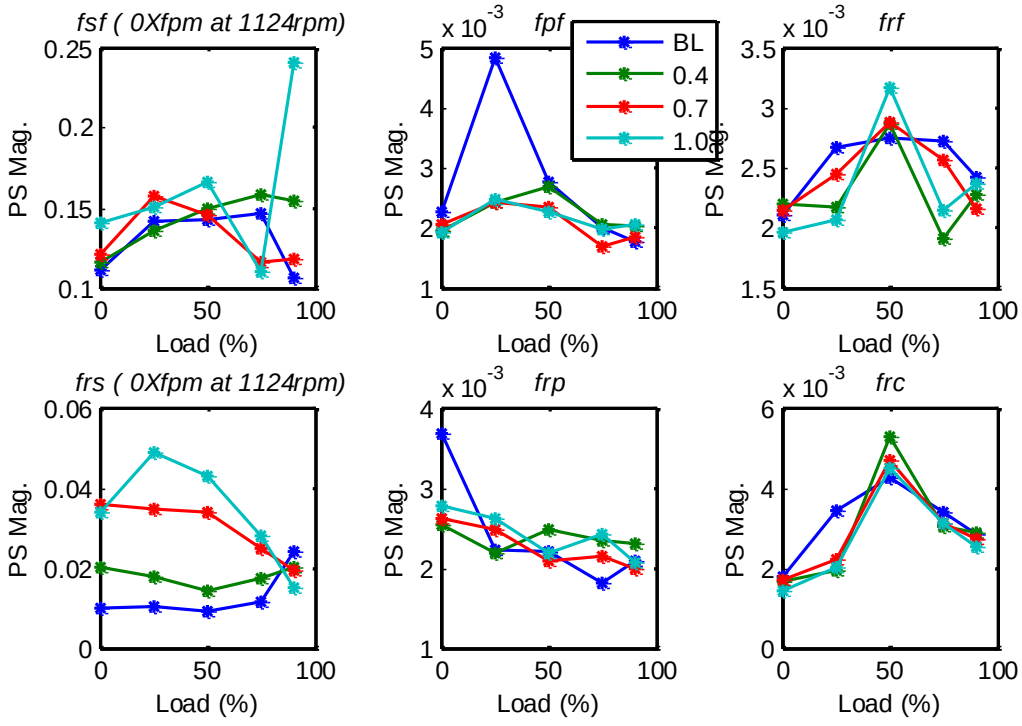

(b) Spectral amplitudes of characteristic frequencies at higher speed

Figure 6.7 Spectral amplitudes as a function of load at 849 and 1124 rpm for healthy and misalignment planetary gearbox

In addition, at the lower speed, amplitudes at f_{rf} and f_{rp} also show higher amplitudes under low loads, compared with that of baseline cases. These changes may lead to incorrect diagnosis results for faults that also occur or influence on the planetary gears.

6.3.2 MSB of Vibration Signals

To clarify possible misleading results from the power spectrum, MSB analysis is applied to corresponding signals. Figure 6.8, presents typical MSB results. It can be seen from the top row of Figure 6.8, that the increasing amplitude with the degree of misalignment is enlarged because MSB magnitude is able to exclude non-modulation components including the random noise. Meanwhile, MSB coherence as, shown in the bottom row, exhibit nearly unity amplitude which confirms the magnitudes are due to the effects of modulation.

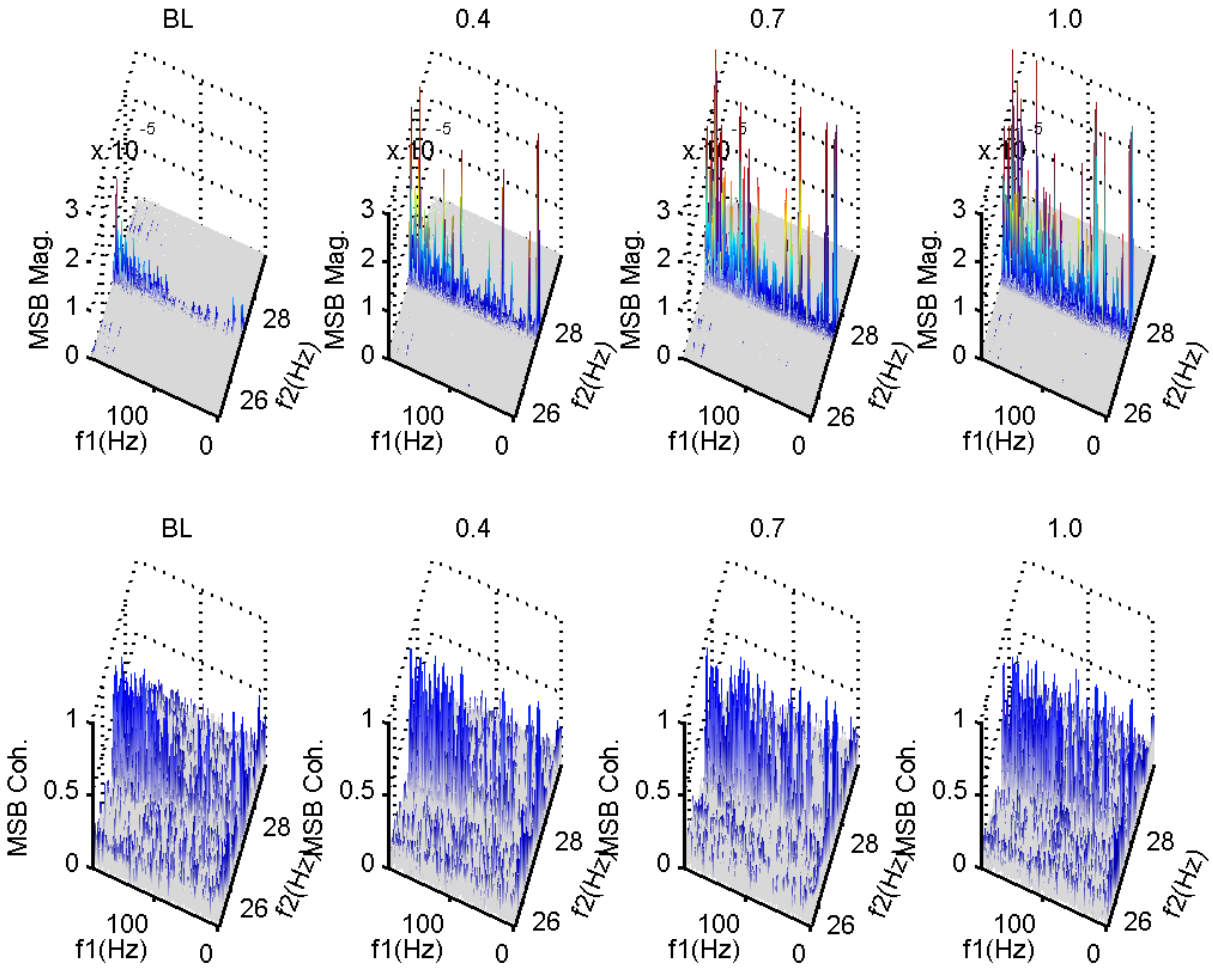

Figure 6.8 MSB results for different levels of misalignment for 849 rpm and 90% full load

6.3.2.1 MSB diagnostic result

To make a more accurate comparison, MSB amplitudes at the characteristic frequency are extracted in a similar way to the power spectrum, as shown in Figure 6.9. To benchmark diagnosis performance, MSB results are presented for the higher speed at which the PS may provide incorrect and misleading results. It can be seen that different degrees of misalignment under high loads for f_{rs} can be differentiated properly because of the MSB capability of suppressing noise and interferences. Unfortunately MSB-SE magnitude alone is also unable to make difference between the two higher degrees of misalignment at 0% load. This may be due to the highly unstable operation at low load conditions of the gearbox. Moreover, MSB coherence provides complementary information on the diagnosis results. As shown in the figure the amplitude at f_{rs} has amplitude more than 0.6. In particular, the amplitudes for misalignment cases are all higher than that of baseline (Abdalla, Tian et al. 2014).

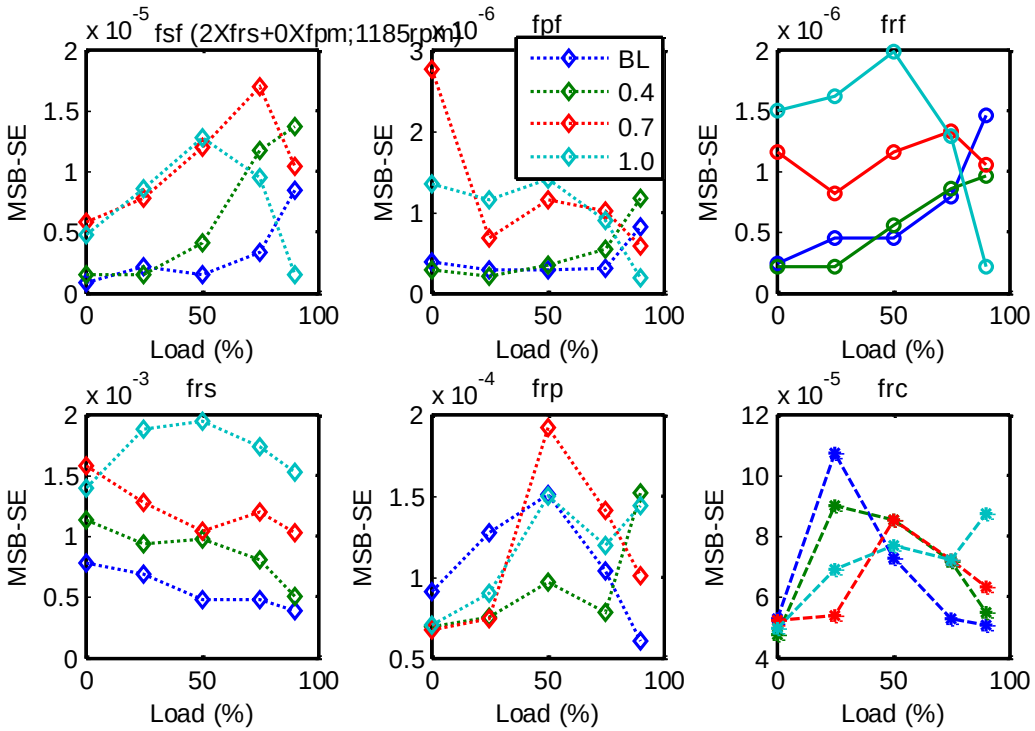

(a) MSB diagnostic results for high speed operation

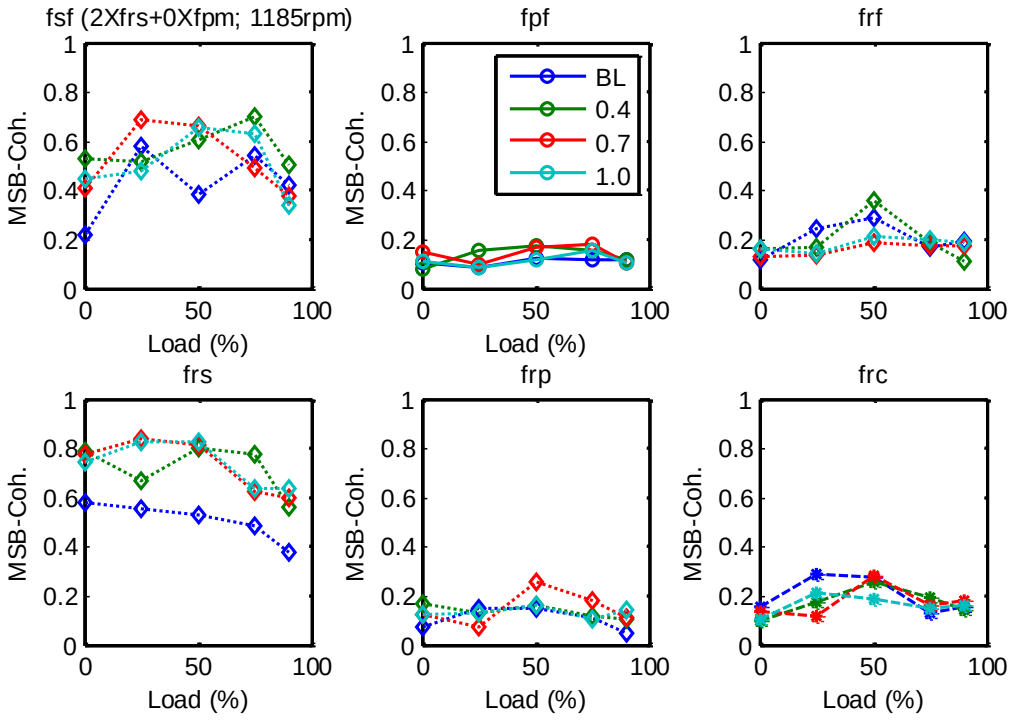

(b) MSB coherences for high speed operation

Figure 6.9 MSB as a function of load for different levels of misalignment for 1185 rpm

This shows that the levels of modulation degree is high and increases with misalignment. In the meantime MSB coherence also shows high amplitude at f_{rf}, this confirms that the increase in their magnitudes is mainly from modulation effects and hence the meshing process is abnormal, which is understandable as the misaligned shaft will inevitable influence the meshing quality. However, magnitude increases for characteristic components are associated with very low coherence amplitude. Therefore, these increases are still from the background noise rather than the effects from any faults (Abdalla, Tian et al. 2014).

6.4 Summary

In this chapter, the effect of varying degrees of misalignment of a planetary gearbox is investigated based on vibration measurements using the power spectrum and modulation signal bispectrum (MSB).

It has been shown that the misalignment can be diagnosed using the low frequency range of the vibration signal in which adverse effects due to co-occurrence of AM and FM are low compared with the components around the meshing frequencies. The power spectrum was

able to produce correct results only for some of the operating conditions. However, the MSB produces a more accurate diagnosis in that it gives a more reliable indication of the relative fault severity and location for the load applied. Vibrations from planetary gearbox show complicated spectrum patterns due to the combined effect of co-occurrence of AF and FM processes and noise. These will lead to high fluctuation in spectral amplitudes, causing difficulty in defining a stable diagnostic feature. MSB analysis provides a high performance in misalignment fault detection for selected modulation components with sidebands and provides stable diagnostic results. The MSB coherence provides valuable information on the quality of the MSB and can be an effective detector of modulation.

CHAPTER SEVEN

DIAGNOSIS OF SUN GEAR FAULTS

This chapter starts by the existence and characteristics of these sidebands by simulation studies. Then MSB is used to extract these sidebands accurately despite their contamination by random noise, the characteristic frequencies of faults in planetary gears, it then describes the fault to be seeded into the sun gear (representing a chipped or broken gear tooth), and then presents the test procedure for measuring the vibration response with and without the seeded fault. It is demonstrated that the residual sidebands resulting from the out-of-phase superposition of vibration waves from asymmetrical multiple meshing sources are much less influenced by gear errors than the in-phase sidebands in Section 7.4. Finally an experimental investigation is described which shows the effectiveness of this approach in detecting gear tooth faults by comparing the results with those obtained from the in-phase sidebands. Finally it is concluded the MSB should be able to produce accurate and consistent diagnosis of sun gear tooth faults.

7.1 Introduction

Many different signal processing methods in the time domain, frequency domain, time-frequency domain and advanced intelligent methods have been applied to analyse complicated vibration signals and provide accurate and reliable diagnostic features (C. Yuksel 2004; Samuel and Pines 2005; Lei, Lin et al. 2014). Considerable works have been carried out on the investigation of vibration characteristics for monitoring various faults including gear pitting, crack and wear. In addition, many different signal processing methods in the time domain, frequency domain, time- frequency domain and advanced intelligent methods have been applied to analyse the complicated vibration signal for defining accurate and reliable diagnostic features (McFadden 1985; McFadden 1991; Inalpolat 2009; Hong 2014). However, it has been found that most of this research developed diagnostic parameters related to fault dynamics based vibration components which have large amplitudes. Hong has shown that in-phase sideband components are especially useful for diagnosing different types of PG faults (Hong 2014) This chapter focuses on small sidebands present in the vibration spectrum but not usually very noticeable. It will show that these sidebands give reliable diagnostic information which is not influenced by, for example, manufacturing errors.

7.2 Residual Sidebands in Planetary Gearbox Vibrations

7.2.1 Characteristics of Residual Sidebands

According to the signal model developed in (McFadden 1985; Inalpolat 2009; Hong 2014), the spectrum for a tooth defect on the sun gear was simulated based on a typical industrial planetary gearbox whose key specification is provided in Chapter two Section 2.2.3 shows the spectrum in the frequency range up to the third harmonics of mesh frequency. It shows that spectrum lines with high amplitudes occur at $1f_m - 7f_{sf}$, $1f_m - 6f_{sf} + 1f_{rc}$, $1f_m - 5f_{sf} - 1f_{rc}$, and at $3f_m \pm 3f_{sf}$ and the peaks at $3f_m \pm 6f_{sf}$ $3f_m \pm 6f_{sf}$ (225 Hz and 147 Hz) become larger due to the constructive in-phase superposition of the three vibration waves measured at the fixed ring gear casing. This is in agreement with that predicted in (Hong 2014) for indicating the faults in sun gear. However, there are many other observable spectral components which

are not mentioned in (Hong 2014).In particular, the components which locate symmetrically around the 1st and 2nd mesh frequencies at $1f_m \pm 3f_{sf}$,$1f_m \pm 6f_{sf}$, $2f_m \pm 3f_{sf}$ and $2f_m \pm 6f_{sf}$ illustrated by the arrows, are clearly visible. These components are well-known features which are used widely for the fault diagnosis of fixed shaft gearboxes. In order to examine the usefulness of these sidebands in diagnosing faults in a planetary gearbox, they are named as residual sidebands in this study because they result from incomplete superimposition of out phase waves in the planetary gearbox. In contrast, the high amplitude sidebands such as those around the third mesh frequency at $3f_m \pm 3f_{sf}$ and $3f_m \pm 6f_{sf}$ are denoted as in phase sidebands (Gu, Abdalla et al. 2014).

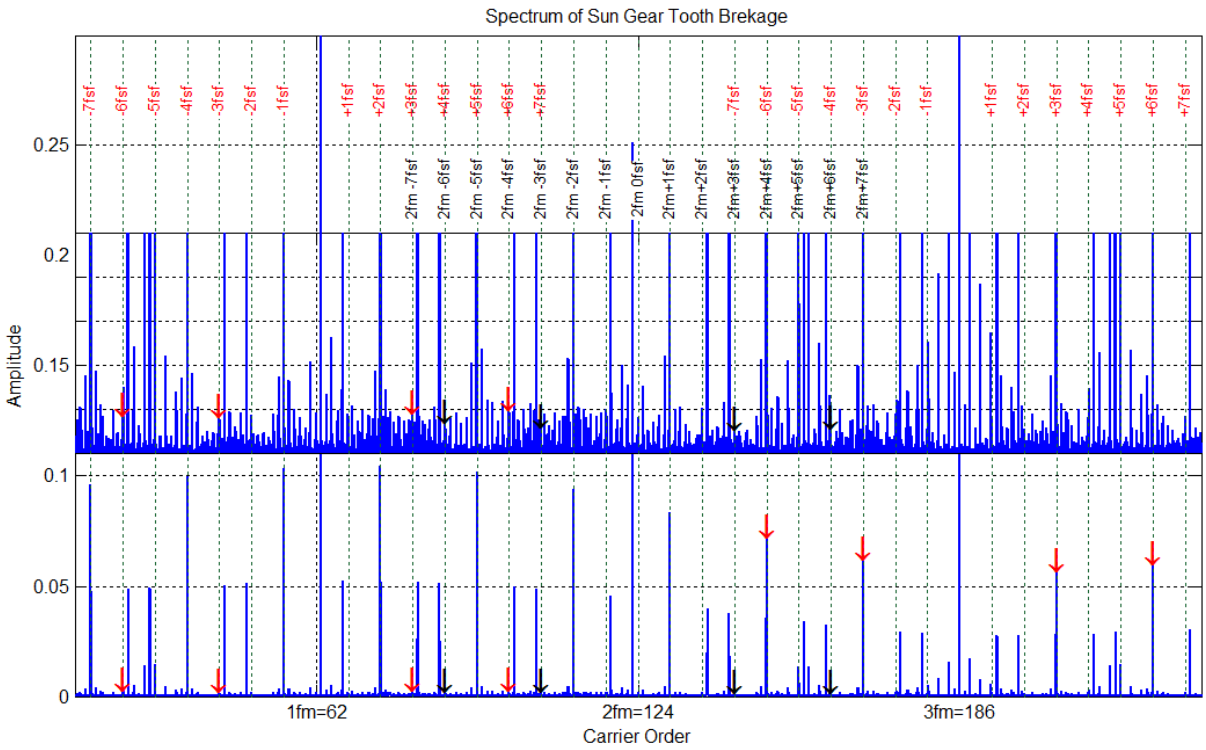

Figure 7.1 Spectrum for sun gear fault without error

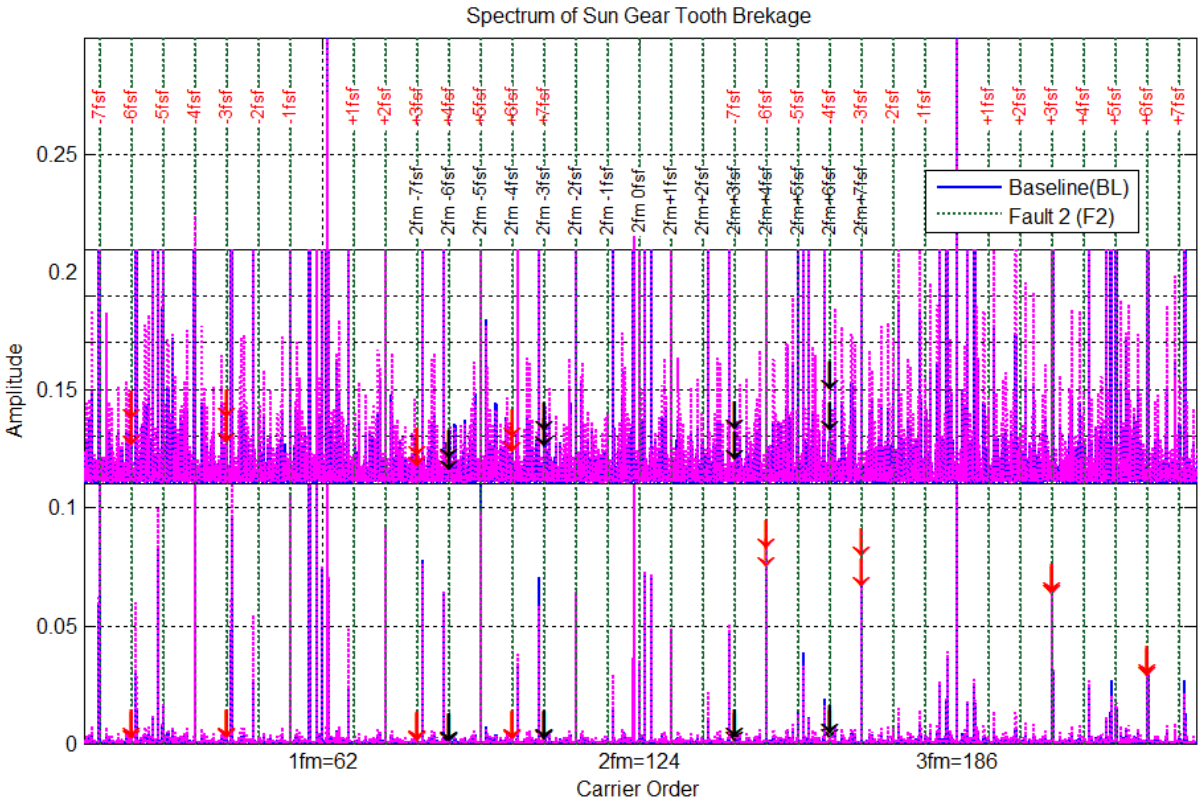

Figure 7.2 Spectrum for the case of sun gear fault with errors

It is easy to understand the existence of residual sidebands. The development of the existing theory such as (Hong 2014) predicts the existence of a fault component based on the assumption that apart from the fault the system is perfectly healthy. That is, without a fault, the vibration signal will have zero amplitude for the residual sidebands, however, for many reasons, including manufacturing errors, the symmetrical assumption does not hold true. Consequently, superimposition will result in non-zero residual sidebands, and at many frequencies, as shown in the magnified spectrum in Figure 7.2. In practice, the system can never be symmetrical because of unavoidable errors which mean that both the residual sidebands and the in-phase sidebands in the measured signals will have non-zero values.

To examine the usefulness of these residual sidebands for fault diagnosis, three simulations were carried out with increasing magnitude of tooth breakage: healthy baseline (BL), Fault 1 (F1) and Fault 2 (F2). Figure 7.3 shows a comparison between two different cases. The in-phase components clearly show differences between the two cases. Obviously, the differences of the in-phase sidebands around $3f_m$ (186Hz), which are illustrated by the

distance between the two arrows at the same spectral lines, can be used to differentiate the two cases, in the meantime, the residual sidebands, illustrated by the arrows in the magnified spectrum, show significant differences between the two cases. Therefore, both types of sideband can be good indicators for differentiating the faults.

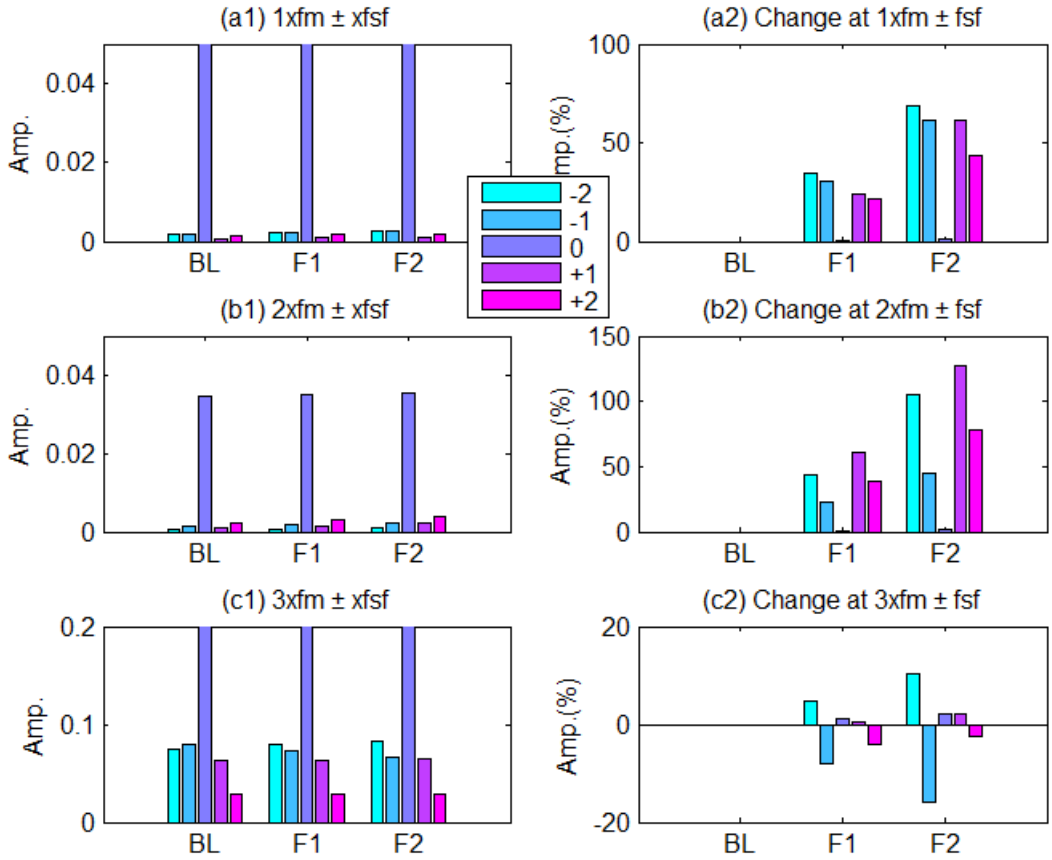

Figure 7.3. Comparison of sideband changes with seeding of tooth fault

To show the performance of using the residual sidebands for diagnosing the faults, the amplitudes at these sidebands are extracted from the spectrum and compared with those of the in-phase sidebands at the third harmonics (Gu, Abdalla et al. 2014).

Figure 7.3 shown that the residual sidebands around the first and second harmonics of the mesh frequencies increase monotonically with fault severity whereas, the in-phase sidebands at the third mesh frequency exhibit non-uniform change. Moreover, the relative changes of the residual sidebands are about five times as large as those of the in-phase sidebands. This means that the residual sidebands are much better for detecting and diagnosing the tooth fault than the in-phase sidebands. This is mainly because the in-phase superimposition

accumulates the effect of manufacturing errors simultaneously whilst accumulating the effect of faults over three gear sets. For the small sideband amplitudes due to a fault, the in-phase sideband will show a relatively small change, either an increase or decrease depending on the agreement of phases between the sidebands due to errors and those due to the fault. On the other hand the effect of errors is minimised at the residual sidebands; any small changes due to faults will show significant corresponding changes. Therefore, the residual sidebands can potentially produce a result consistent with fault severity and hence a more correct diagnosis.

7.3 Experimental Setups

7.3.1 Introduction

In Chapter two Section 2.2.3 shows a common planetary gearbox, generally consists of three planet gears all of the same size and meshed with one sun gear and ring gear. As previously described, the carrier is floating and affixed to the output shaft by means of splines which allow it to move axially as required for uniform load sharing between the three planetary gears. In this research an industrial planetary gearbox, is fully detailed and is listed in the Chapter two Section 2.23, the focus of the fault diagnosis study.

As shown by many previous studies, detection and diagnosis of gear faults can be achieved by examining the change of fault characteristic frequencies around the mesh frequency, f_m, and its harmonics. Given that there are K planetary gears moving with the carrier, characteristic frequencies around the meshing frequency are calculated for three typical fault cases, a fault on the sun gear, on the planet gear and on the ring gear (Lei, Lin et al. 2014),for three typical fault cases, which includes a fault on the sun, planet and ring gear as the equations in Chapter six Section 6.1.1.

As shown in (McFadden 1985; McFadden 1991; Hong 2014), only some of the expected sidebands will be apparent in the vibration spectrum when a planetary gearbox has a fault, because of the constructive superposition effects that occur when there is vibration wave superposition of signals from the three gear sets. Other sidebands are hard to see because of destructive superposition and, hence, have been neglected by previous studies.

7.3.2 Test Procedure for Sun Gear

The test was carried out with the AC motor running at three speeds 293 rpm, 439.5rpm and 486 rpm (20%, 30% and 40% of full speed). Because of the given transmission ratios the planetary gearbox will have corresponding speeds of 486, 879 and 972 rpm (40%, 60% and 80% of its full speed). At each speed the system is operated under five loads (0%, 25%, 50%, 75% and 90% of the full load). These operating conditions will allow an exploration of different influences on vibration signal content in order to develop a more reliable diagnosis method. As previously described, the test rig was run until the temperature was stable before measurements were made.

7.3.3 Sun Gear Fault Simulation

From the review of PG common failures, Section 2.2.3, tooth failure can be particularly damaging. Here, the tooth damage was produced by removing a percentage of the tooth face on the gear in the width direction. The sun gear tooth fault (F1) as seen in Figure 7.4 was made to simulate a real fault that can occur during operation.

Figure 7.4 Sun gear tooth fault F1

Sun gear fault (F2), seen in Figure 7.5, was also meant to simulate a real fault mechanism that could occur during operation. The same procedure for measuring the vibration was followed as for the seeded misalignment fault, see Section 5.3.

Figure 7.5 Sun gear tooth fault F2

7.4 Diagnostic Results and Discussion of Sun Gear Fault

7.4.1 Spectrum of Vibration Signals

Figure 7.6, shows typical vibration spectra for the sun gear with and without tooth faults. It can be seen that three distinctive peaks close to the first three mesh frequencies appear at. $f_m + f_{rc}$, $2f_m - f_{rc}$ and $3f_m$, which agree with prediction. However, there are also many distinctive peaks between two mesh frequencies. For example, the components at $2f_m - 6f_{sf} - 1f_{rc}, 2f_m + 7f_{sf}$ are not expected to appear in a healthy planetary gearbox. Therefore, based on the simulation studies in the Section7.2 above, these peaks indicate that the gearbox has significant manufacturing errors. It means that the diagnosis based on the in-phase sideband may not be accurate which can be demonstrated by examining the changes at $3f_m \pm 3f_{sf}$ and $3f_m \pm 6f_{sf}$ between the three cases.

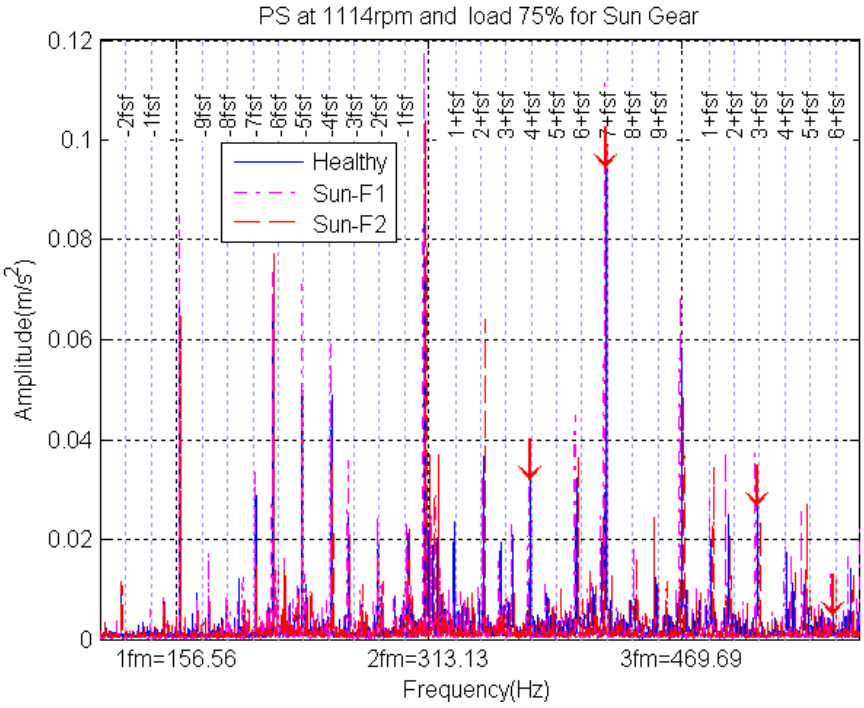

Figure 7.6 Sun gear vibration spectrum, healthy and with F1 and F2 tooth faults

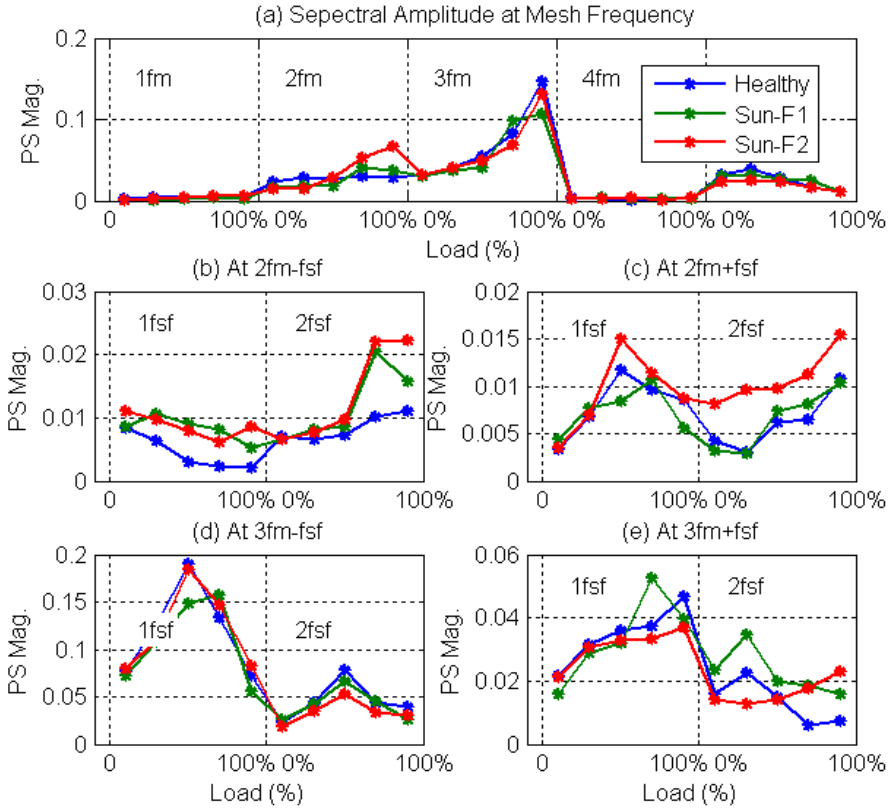

Figure 7.7 Spectral amplitudes of sidebands at mesh frequencies, fm, fsf, and harmonics, for sun gear, healthy and with F1 and F2 tooth faults

To examine the changes of the residual sidebands, their amplitudes, including those at the in-phase components were extracted and are presented in Figure 7.7. Because of the attenuation of the vibration transfer function, the spectrum shows very low amplitude below $1f_m$, which the general feature of acceleration responses, the residual sidebands is also around $1f_m$ are not explored because of their low signal to noise ratios. Based on the changes of these sidebands, it can be found that the amplitudes of the second order residual sidebands around $2f_m$ and those at $2f_m$ may be good indicators for the fault severity as their amplitudes show an increasing change which agrees with the fault severities at high load conditions.

In contrast, the amplitudes of other sidebands and meshing components exhibit high fluctuations between fault cases and loads. Hence, they cannot be used for obtaining a consistent diagnostic result. Especially, the in-phase sidebands around $3f_m$ show high amplitudes but with little relative changes between fault cases, showing that they are not good indicators for these faults.

In general, the residual sidebands show better diagnostic results, compared with the in-phase sidebands. However, as shown Figure 7.7 (b) and (c) these residual sidebands still cannot differentiate F1 from the baseline definitively.

7.4.2 MSB of Vibration Signals

Analysis was applied to the vibration signals Figure 7.8, shows typical MSB results for the three sun gear tests under 75% of full load. To show the clear change of the residual sidebands around mesh frequency $2f_m$ = 313.1 Hz, MSB and its corresponding coherence results are presented in the bifrequency domain in the region of $f_c \le 2f_m \pm 1 = 313 \pm 1Hz$ and $f_s < 100Hz$ to include the sidebands up to $6f_{sf}$. It can be seen in Figure 6.14 that the magnitude of many MSB peaks increase with the fault severities. In particular, peaks at bifrequencies $(2f_m, 5f_{sf})$ and $(2f_m, 5f_{rc})$ show very distinctive amplitudes which vary consistently with the faults. However, these two peaks are also the in-phase sidebands and are influenced more by errors, which will be shown in further content, therefore, they are not considered in this study. Instead it is the residual sidebands at $(2f_m, 3f_{sf})$ (313Hz, 46.8Hz)

and $(2f_m, 6f_{sf})$ (313Hz, 93.6Hz) that are of interest. As illustrated by the size of the arrows, although these sidebands have small amplitude, they show consistent changes with the size of faults. Furthermore, these small amplitudes are fully supported by high amplitudes of their corresponding coherence (Gu, Abdalla et al. 2014).

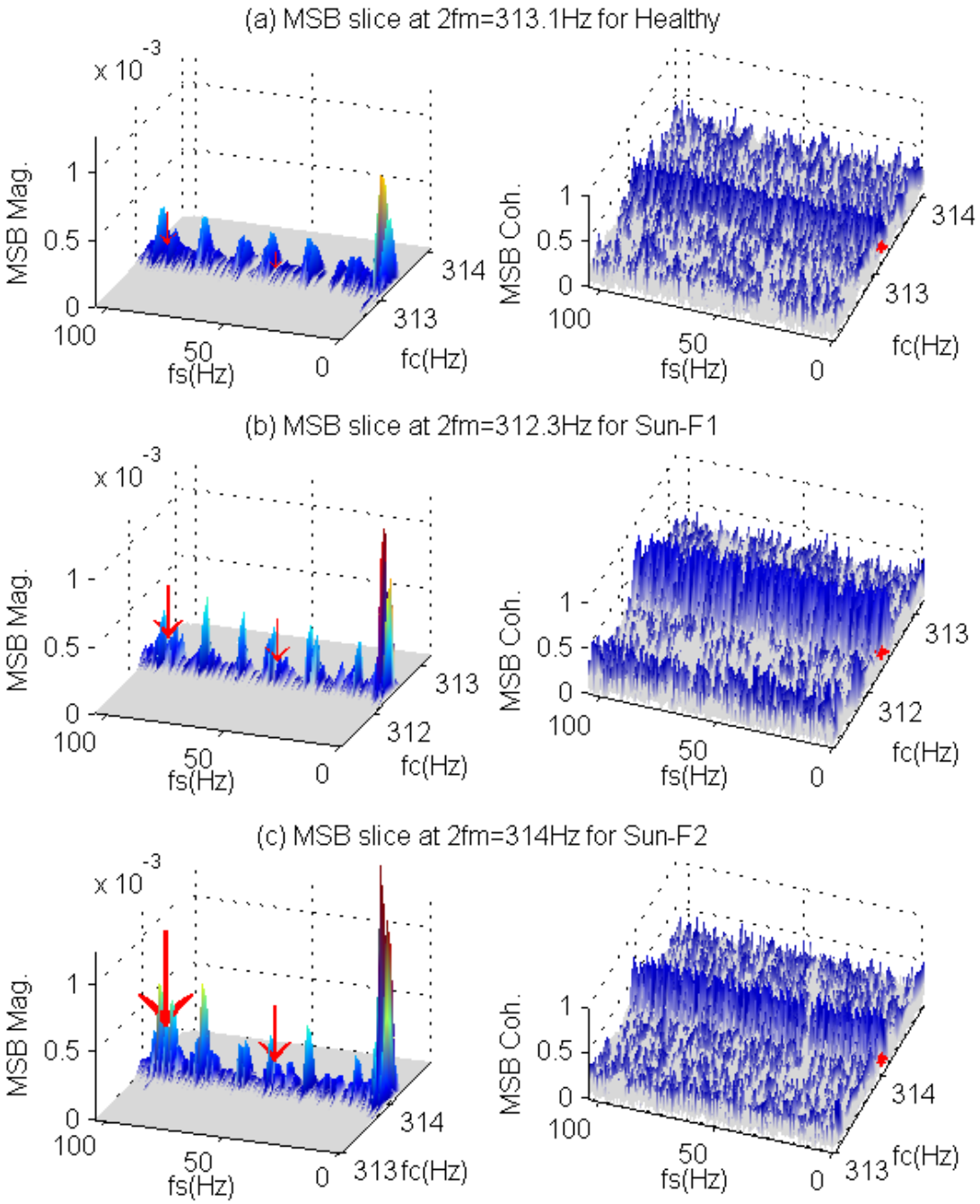

Figure 7.8 MSB results for sun gears, healthy and with tooth faults F1 and F2

Moreover, these changes can show a clear difference between the F1 and F2 faults and the baseline which could not be separated by the spectral amplitude shown in Figure 7.7. This demonstrates that MSB analysis provides a more accurate sideband estimate because of its noise suppression.

7.4.3 Diagnosis of Sun Gear Fault

To explore the performance of the residual sidebands obtained by MSB analysis, the peak values at the corresponding characteristic frequencies for PG fault diagnosis were extracted from the MSB results and presented in Figure 7.9 (a). From the results of residual sidebands obtained from the MSB slice at $2f_m$, it can be seen that the amplitudes at f_{sf} increased with increase in load. Moreover, as the load increased the differences in MSB-SE values between the three test cases became greater. Therefore, they can be used for fault diagnosis.

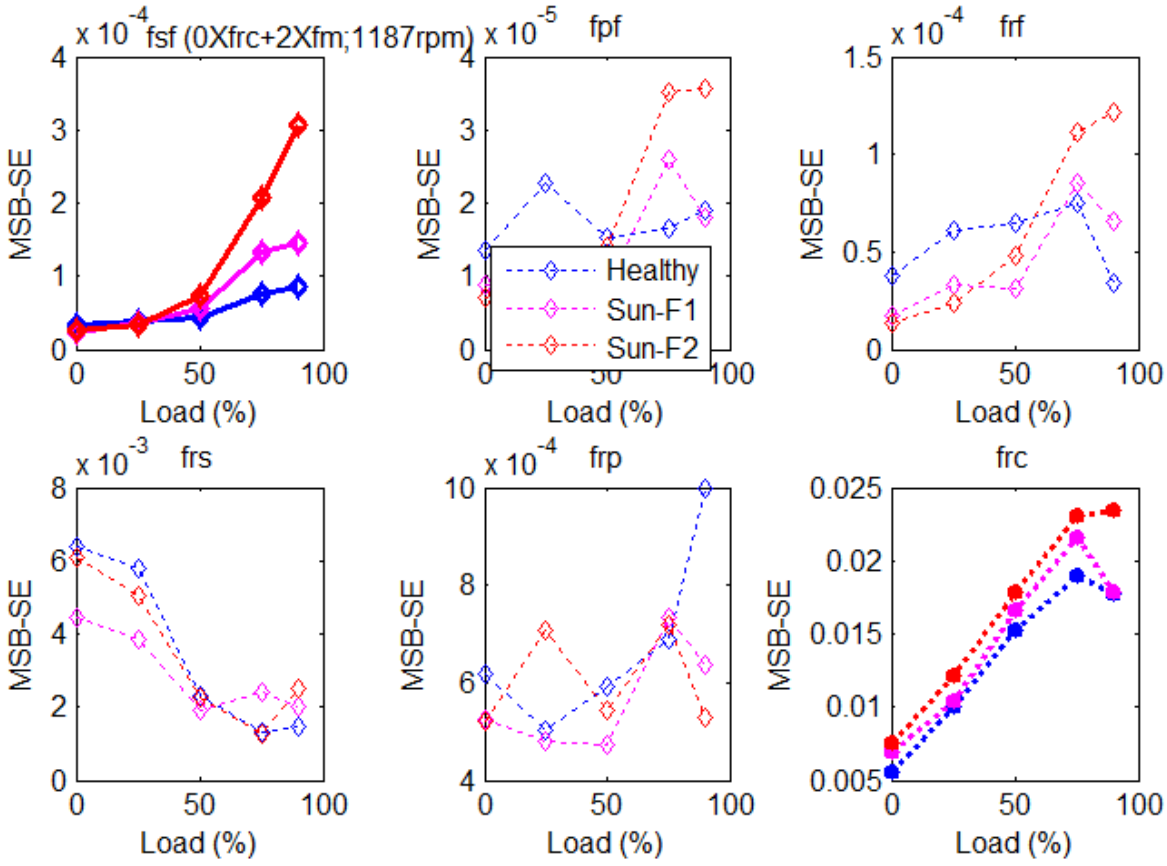

(a) Results from the sidebands around $2f_m$

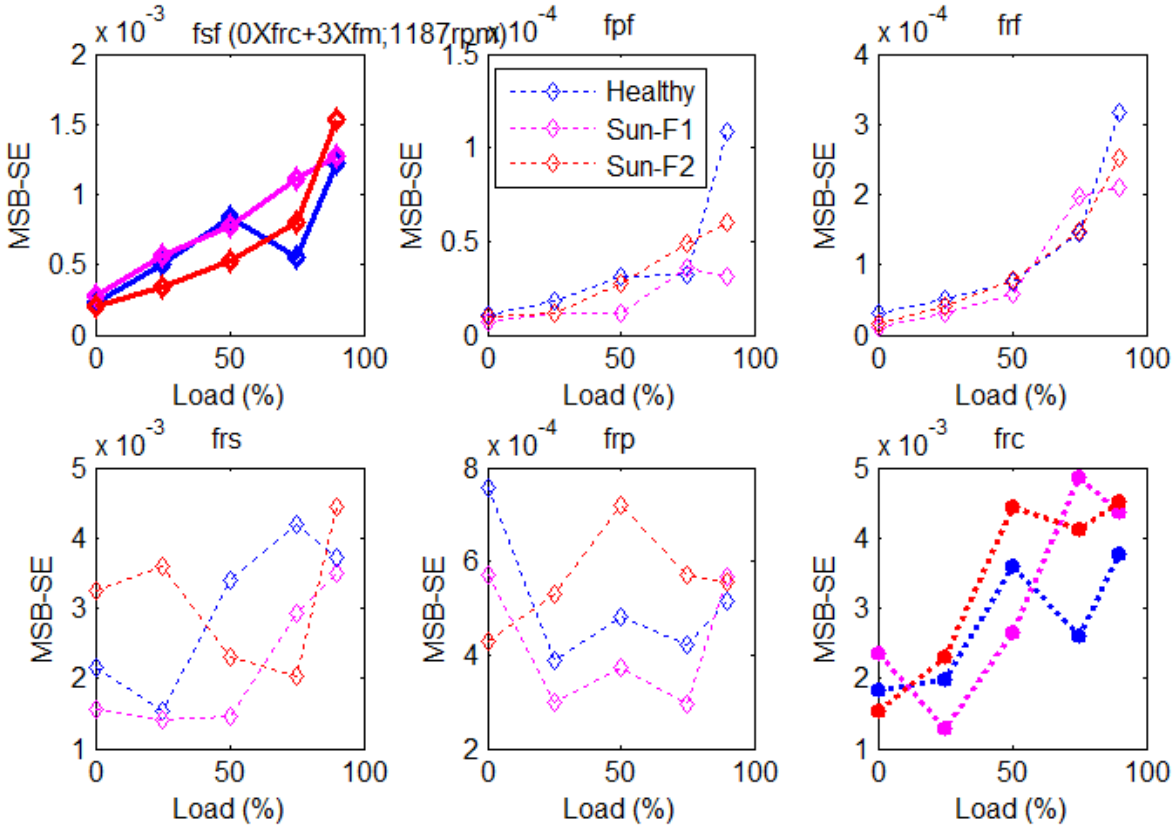

(b) Results from the in-phase-sidebands around $3f_m$

Figure 7.9 MSB as a function of load for different levels of tooth fault at 1185 rpm

The MSB results for f_{rc} also show similar results to those for f_{sf}. This may show that a fault on the sun gear may also cause changes in carrier dynamics. However, the amplitudes of both healthy and F1 show a clear drop at high load, which suggests that these sidebands are influenced by errors as are the in-phase sidebands.

For comparison, the results from in-phase sidebands around $3f_m$ are presented in Figure 7.9 (b). The plot of the amplitudes at f_{sf} reveals that these in-phase sidebands cannot indicate the incremental changes caused by the faults consistently, which agrees with that from the simulation (Gu, Abdalla et al. 2014).

7.5 Summary

An effective new method is proposed for sun gear fault detection in PGs, based on an accurate estimation of residual sidebands using a modulation signal bispectrum (MSB). The residual sideband resulting from the out-of-phase superposition of vibration signals from asymmetrical multiple meshing sources is much less influenced by inherent gear errors than that of the in-phase sidebands. Thus the MSB can produce accurate and consistent detection and diagnosis of faults in the sun gear; both simulation and experimental studies were shown in Section 7.3.1. The commonly used in-phase sidebands have higher amplitudes but include gear error effects, consequently leading to poor diagnostic results.

The residual sidebands of the planetary gearbox result from the imperfect superposition of the vibrations from multiple meshing sources which are asymmetrical in nature. Although the amplitudes of the residual sidebands are relatively small, compared with those of the in-phase they are much less influenced by inherent and inevitable PG gear errors. Using the MSB these small sidebands can be estimated with a good degree of accuracy, producing more accurate and consistent detection of sun gear faults. The results have shown that this sideband based method provides correct diagnostic results for different magnitudes of sun gear faults.

CHAPTER EIGHT

DIAGNOSIS OF FAULTS ON PLANET GEARS

This chapter starts with background of planet gear faults and then, test procedure for planet gear with the experimental test rig see section 8.2. The residual sideband resulting from the out-phase superposition of vibration waves from asymmetrical multiple meshing sources are much less influenced by gear errors than that of the in-phase sidebands. Therefore, with the accurate estimation by modulation signal bispectrum (MSB), they can produce accurate and consistent diagnosis.

8.1 Introduction

The industrial plant is well-contributed economically when the machines and equipment are effectively maintained. The gear performance declines if it is subjected to a defect like pitting, bending fatigue cracks, abrasive wear or scuffing. It is not possible to transmit the motion power as required in such circumstances; hence, it is not possible to avoid fatal defects. Due to ineffective maintenance action, there are nearly 24% of gearbox failures and faults in gearboxes cause 60% of gear related failures. Therefore, it is essential to realise the importance of gearbox condition monitoring to reduce failure and make sure operations run smoothly.

As shown in chapter 7 section 7.1 and 7.2 the test rig and the test procedure is the same, however the fault has been created in planet gears to simulate what might happen in the real industry field with different fault severity.

8.2 Experimental Setups

8.2.1 Introduction

As explained in chapter seven and Chapter two Section 2.2.3 shown, a common planetary gearbox, generally consists of three planet gears all of the same size and meshed with one sun gear and ring gear. In this research an industrial planetary gearbox, as full information is listed in the Chapter two Section 2.23, the focus of the fault diagnosis study.

As shown by many previous studies, detection and diagnosis of planet gear faults can be achieved by examining the change of fault characteristic frequencies around the mesh frequency, f_m, and its harmonics. Given that there are K planet gears moving with the carrier, characteristic frequencies around the meshing frequency are calculated for three typical fault cases, a fault on the sun gear, on the planet gear and on the ring gear (Lei, Lin et al. 2014),for three typical fault cases, which includes a fault on the sun, planet and ring gear as the equations in Chapter six Section 6.1.1.

8.2.2 Test Procedure for Sun Gear

The same test procedure in Chapter seven Section 7.2.2.The test was carried out with the AC motor running at three speeds 293 rpm, 439.5rpm and 486 rpm (20%, 30% and 40% of full speed). Because of the given transmission ratios the planetary gearbox will have corresponding speeds of 486 rpm, 879 rpm and 972 rpm (40%, 60% and 80% of its full speed).

At each speed the system is operated under five loads (0%, 25%, 50%, 75% and 90% of the full load). These operating conditions will allow an exploration of different influences on vibration signal content in order to develop a more reliable diagnosis method. As previously described, the test rig was run until the temperature was stable before measurements were made.

8.2.3 Planet Gear Fault Simulation

The planetary gearbox is a critical mechanism in the transmission systems of wind turbines and helicopters etc. Tooth failures in planetary gear sets will cause great risk to wind turbine operations. In this research study the severity of two faults were shown by removing small parts of the tooth face width as described in Chapter two Section 2.2.3. The planet gear tooth fault (F1) as shown in Figure 8.1 was made to simulate the real fault mechanism during operation times and by following the same procedure in chapter five section 5.3, the raw data was collected and recorded from all sensors of the fault signal to investigate the effect of the operating conditions (different rotating frequencies of the shaft and different loads).

Figure 8.1 Planet gear tooth fault F1

The planet gear tooth fault (F2) was made to simulate the real fault mechanism during operation times as shown in Figure 8.2. The tooth damage on the sun and planet gears was produced by removing a percentage of the tooth face on the gear in the width direction.

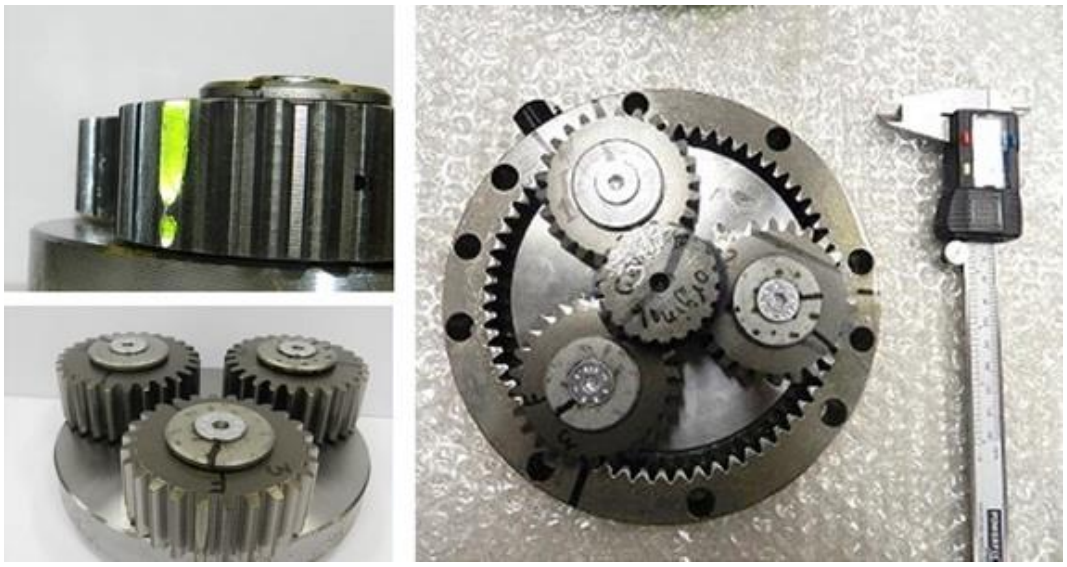

Figure 8.2 Planet gear tooth fault F2

8.3 Diagnostic Results and Discussion of Planet Gear Fault

8.3.1 Spectrum of Vibration Signals

From the discussion and diagnostic results Chapter seven the Section 7.4, the conclusion can be made that the residual sideband based method is reliable for planetary gearbox diagnosis. To evaluate its performance further, the method is applied to the datasets from the planet gear test. Figure 8.3 shows the spectrum of the vibration for the three cases of planet gear fault. Compared with the spectrum in Figure 7.6 Chapter seven Section 7.4.1, it exhibits clear differences, particularly the spectrum amplitudes at $2f_m - 6f_{sf} - 1f_{rc}$, $2f_m + 7f_{sf}$ are significantly lower. This shows that this set gear may have a lower error distribution; nevertheless, the results from conventional spectrum based method cannot give a correct diagnostic result to be consistent with the fault severities induced as explained.

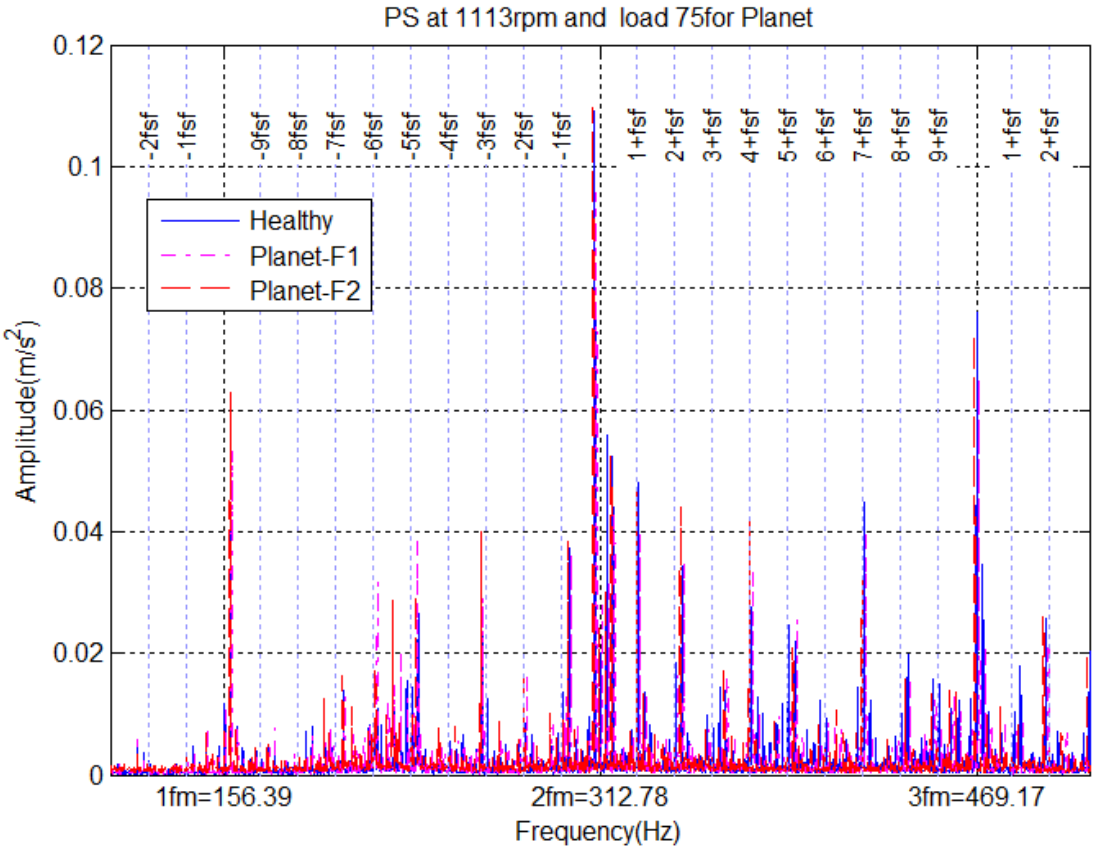

Figure 8.3 Spectrum for different fault cases of the planet gear

8.3.2 Diagnosis of Sun Gear Fault

Figure 8.4 presents the MSB based diagnostic results obtained from the residual sideband at $1f_m$, rather than $2f_m$ for the sun gear fault case. This is because these sidebands exhibit more of the features of residual sidebands, i.e. lower amplitude and less sensitive to the gear error. In addition, they also have less interfering components compared with those around $2f_m$. As shown in Figure 8.4, the MSB peaks at planet gear fault frequency f_{pf} show results which increase with fault severities and loads, resulting in correct diagnosis. In the meantime, the sidebands at f_{rp} also exhibit an increasing change which may be a secondary feature for the fault on the planetary gear (Gu, Abdalla et al. 2014).

On the other hand, the in-phase sidebands around $3f_m$ are able to separate the more severe fault because the gear error is less than that of the sun gear fault case, however, they cannot separate the smaller fault. This proves further that the residual sideband has more reliable diagnostic information than that from the in-phase-sidebands(Gu, Abdalla et al. 2014).

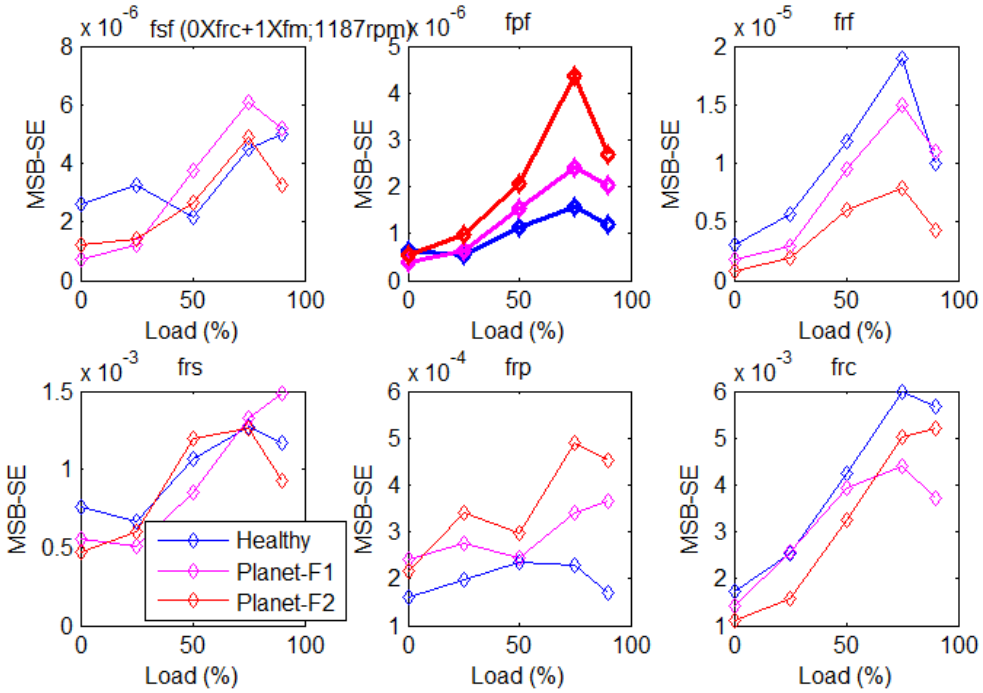

(a) Results from the residual sidebands around $1f_m$

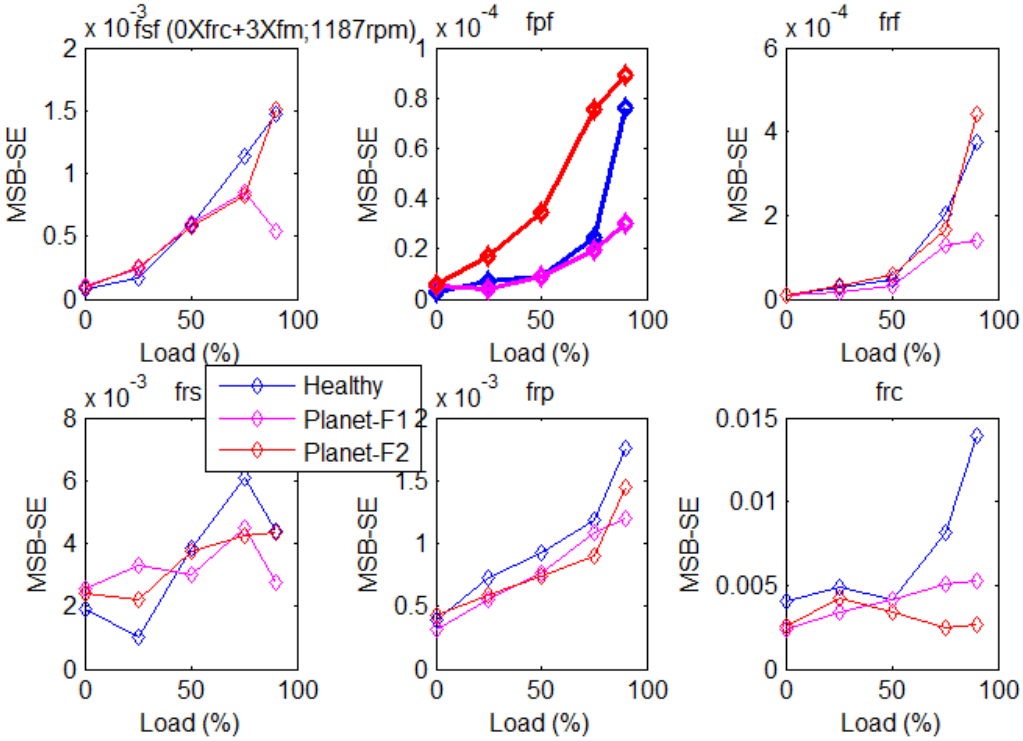

(b) Results from the in-phase sidebands around $3f_m$

Figure 8.4 MSB diagnosis results for different planet gear faults

On the other hand, the in-phase sidebands around $3f_m$ are able to separate the more severe fault because the gear error is less than that of the sun gear fault case, however, they cannot separate the smaller fault. This proves further that the residual sideband has more reliable diagnostic information than that from the in-phase-sidebands(Gu, Abdalla et al. 2014).

8.4 Summary

A new method proposed for the fault diagnosis of planetary gearboxes based on an accurate estimation of residual sidebands using a modulation signal bispectrum (MSB) is affected for fault detection. Moreover, the residual sideband resulting from the out-phase superposition of vibration waves from asymmetrical multiple meshing sources is much less influenced by gear errors than that of the in-phase sidebands. Therefore, with the accurate estimation by MSB, they can produce accurate and consistent diagnosis, which are evaluated by both simulating and experimental studies as shown in Chapter Seven Section 7.3.1. However, the

commonly used in-phase sidebands have high amplitudes but include gear error effects, consequently leading to poor diagnostic results.

The residual sidebands of the planetary gearbox result from the imperfect superposition of the vibrations from multiple meshing sources, which are asymmetrical in nature. Although the amplitudes of the residual sidebands are relatively small, compared with that of in-phase one, they are much less influenced by investible planet gear errors. Using the modulation signal bi-spectrum these small sidebands can be estimated with a good degree of accuracy, subsequently, producing more accurate and consistent diagnostic results of planet gear faults. The results have shown that this sideband based method provides correct diagnostic results for different sizes of planet gear faults.

CHAPTER NINE

CONCLUSIONS AND FUTURE WORK

This chapter reviews the objectives of this research programme and its achievements. The achievements are comparable to the objectives listed in Chapter 1. Next, the chapter describes the contributions to knowledge made by this research. Finally, the conclusions arising from this research for the condition monitoring of planetary gearboxes using modulated signal bispectrum analysis are given and recommendations for future work are listed.

9.1 Conclusion

The vibration signal from a planetary gearbox fault is non-stationary, which means that the signal frequency and amplitude change with time. So that time or frequency domain analysis will on their own - not be sufficient to detect planetary gearbox faults accurately and early. On the other hand, MSB analysis can be used for diagnostic investigation of planetary gearbox vibration signals where faults have an amplitude modulating effect on the characteristic frequencies of the gearbox.

9.1.1 Review of the Objectives and Achievements

- **Objective 1**: To familiarise and understand planetary gearbox structures and basic dynamics, and then establish a planetary gearbox test rig capable of reviewing gear vibration fundamentals and gear common failure modes.
- **Achievement 1**: The maintenance methods and their impact have been reviewed in Chapter1, Section 1.1; Section1.4 summarised and list the main aims and objectives. The understanding of planetary gearbox structure has been discussed and reviewed in Chapter 2, Section2.2. In the same chapter Section 2.3 discussed the vibration sources in the planetary gearbox.
- **Objective 2**: Review existing condition monitoring and vibration signal analysis techniques and assess the performance of generally used diagnostic techniques in terms of early fault detection of planetary gearbox.
- **Achievement 2:** Chapter 4, Section 4.2 reviewed the common condition monitoring techniques and in Section 4.3 described the conventional signal processing of planetary gearbox.
- **Objective 3**: To familiarise vibration measurements based on the planetary gearbox test rig, which includes gaining full skills of gear fault creation, experiment implementation and data processing.
- **Achievement 3**: The planetary gear box test rig facility and data acquisition software were presented in full detail and specifications in Chapter 5. The planetary gearbox supplied and manufactured by STM Power Transmission Ltd, was as presented in Figure

2.15,Chapter 2, consisting of three planet gears, sun gear, ring gear and carrier. The technical specifications of the planetary gearbox are given in Table 2.2. The planet carrier is floating and fixed to the output shaft by means of splines which allow it to move axially as required as discussed in chapter 2, Section 2.2.

- **Objective 4**: To measure vibrations from the planetary gearbox for evaluating vibration gearbox fault diagnosis methods. Also to investigate the influences of common faults, such as shaft misalignment and gear tooth defects with different severities in both the sun and planet gears.
- **Achievement 4**: The Planetary gearbox experimental tests were carried out under different operating conditions. The experiments were repeated with different levels of fault severity and the data collected. All data was collected during repeated experiments with and without simulation faults in Chapter 5, Section 5.3. From, misalignment and gear faults with different severity in both sun and planet gear on planetary gearbox fault diagnosis.
- **Objective 5**: To gain an understanding of the existing mathematical models for the dynamic analysis of planetary gearboxes. Subsequently, to establish a more realistic dynamic model and simulate vibration responses under different fault conditions and with inclusion of manufacturing errors in order to acquire an in depth understanding of vibration characteristics.
- **Achievement 5:** Chapter 3 has presented a mathematical model of PG box with three planet, one ring and one sun gear; see Section 3.4, to simulate the vibration signals produced by the gears. Detection, diagnostics and localisation of PG tooth fault have been investigated numerically. Detailed comparisons of numerical results, have shown that fault characteristic frequencies can be obtained after considering the gear manufacturing errors Additionally, it must be noted that the presence of sidebands in the vibration signal of the PG become more prominent and much more complex when manufacturing errors are taken into consideration. The planetary gearbox fault characteristic frequencies for gears (sun, planet, and ring gears) are different.
- **Objective 6**: To apply conventional signal analysis techniques, for example, power spectrum and time synchronous average (TSA), and then exploit advanced signal

processing methods such as MSB and improved MSB such as the MSB-based sideband estimator (MSB-SE), to obtain fault information in measured signals with noise and interferences.

- **Achievement 6**: Chapter 6, Section 6.3.1, descripted and discussed misalignment of planetary gearboxes as one of the major operating problems that can arise due to variable operating conditions and differences in elastic deformations in the system. The effect of varying degrees of installation misalignment of the planetary gearbox is investigated using spectral analysis of the vibration measurements, in particular the modulation signal bispectrum (MSB).In section 6.3, the result shows the misalignment can be detected and diagnosed. It is shown that MSB produces a more accurate diagnosis in that it gave a correct indication of the fault severity and location for all operating conditions used.
- **Objective 7**: To investigate and obtain a set of vibration features for detection and diagnosing different gearbox faults including shaft misalignments, sun gear faults and planet gear faults under different loads.
- **Achievement 7**: Chapter7 Section7.3, the chapter demonstrates the existence and characteristics of these sidebands by simulation studies. MSB is used to extract these sidebands accurately despite their contamination by random noise due to their small amplitudes. An experimental investigation is described which shows the effectiveness of this approach in detecting gear tooth faults by comparing the results with those obtained from the in-phase sidebands as seen in section 7.3. Finally it is concluded the MSB should be able to produce accurate and consistent diagnosis of sun and planet gear tooth faults.
- **Objective 8**: To provide guidelines and recommendation for future research work in this field.
- **Achievement 8**: After four years of research on planetary gearboxes a numbers of suggestions are highlighting and listed as future work, see Section 9.2 in Chapter 9. Especially, use of the model developed in Section 3.3, to predict the dynamic characteristics of a rotor with eccentricity, misalignment and mass imbalance, using a wireless sensor to measure the corresponding acceleration signals. This study would investigate the differences between signals due to eccentricity, misalignment and mass

imbalance and combinations of these faults to gain a better understanding of the effect of other vibration sources on the vibration recorded on a PG, Section 2.3, there needs to be experimental work with different kinds of faults.

9.1.2 Conclusion on Planetary Gearbox misalignment and gear Faults

Vibrations from the planetary gearbox show complicated spectrum patterns due to the combined effect of co-occurrence of AF and FM processes and noise, which often lead to large fluctuations in spectral amplitudes, making it difficult to define stable diagnostic features. MSB analysis has a high performance in suppressing random noise and in selecting modulation components with sidebands which are less asymmetric and this enables more stable diagnostic results to be obtained. Moreover, complementary information that is supplied by MSB coherence measurements ensures the quality of MSB magnitude and that it is an effective detector of modulation.

It has been shown that misalignment can be diagnosed from analysis of a low frequency range of the measured vibration signal, in which spectral fluctuations due to the AM-FM effect are relatively low. However, MSB produces a more accurate and reliable diagnosis in that it gives a correct indication of the fault severity and location for all operating conditions. In contrast, the power spectrum can produce correct results for only some of the operating conditions.

MSB can estimate with a high degree of accuracy, the small sidebands present in a PG and has been shown to produce more accurate and consistent diagnostic results for faults of different severities seeded into the sun and planet gears within a PG.

9.1.3 Novel Feature Summary

This research project presents a set of novel aspects on planetary gearbox systems with three planets that have not been considered by previous researchers. The following provides a summary of these aspects of novelty:

- **The First Novel Aspect:**

  The author could find no report of research that investigated the effect of varying degrees of misalignment on vibration spectra of a planetary gearbox system in order to develop more reliable methods for diagnosing the fault see Chapter six Section 6.3, The MSB, which is particularly effective in capturing the weak modulations in planetary gearbox signals for fault diagnosis, was used to understand the AM-FM effects and to enhance feature components for the detection and diagnosis of the misalignment at different speeds and loads

- **The Second Novel Aspect:**

  The detection and diagnosis of misalignment using MSB analysis is entirely novel. This method allows more stable diagnostic results to be obtained. Moreover, complementary information obtained from the MSB coherence ensures the magnitude of the MSB is an effective detector of modulation sees Chapter six Sections 6.3.2.

- **The Third Novel Aspect:**

  Fault diagnosis of a planetary gearbox based on MSB analysis and which focuses on the small sidebands usually not so noticeable in the spectrum is entirely novel see Chapter seven Section 7.2. However, it has been shown that these sidebands contain reliable diagnostic information which is not influenced by inherent manufacturing errors. This study demonstrated the existence and characteristics of small sidebands by simulation studies.

- **The Fourth Novel Aspect:**

  The residual sidebands are relatively small compared with those of the in-phase sidebands, but they are much less influenced by invisible gear errors. The author believes that, by using the MSB, these small sidebands can be estimated with a good degree of accuracy and hence produce more accurate and consistent diagnostic results see Chapter seven Section 7.4. Both simulating and experimental results have shown that this sideband based method provides correct diagnostic results for different fault severity on both the sun and planet gears of a PG**.**

- **The Fifth Novel Aspect:**

  The author believes that, the application MSB to a PG signal for detection and diagnosis of gears faults has not been undertaken before. The research work presented in this thesis is believed to be the first to explore the application of MSB to the detection and diagnosis the gear faults with different severities in PG see Chapter seven Sections 7.4.2, Chapter eight Section 8.3.

9.1.4 The Contributions to Knowledge through this Research work

- **The First contribution:**

  The author believes that misalignment of planetary gearboxes as one of the major operating problems that can arise due to variable operating conditions and differences in elastic deformations in the system. Therefore, the effect of varying degrees of installation misalignment of the planetary gearbox has been considered Chapter six Sections 6.3.2.

- **The Second Contribution:**

  As appears in publications, the author, one of a team working on combination fault diagnosis method based on MSB-SE see the publication, is developed for monitoring faults on both bearing and gear in a planetary gearbox. MSB analysis is effective in suppressing random noise and decomposing the nonlinear modulation components in the measure vibration signals. Thus, the sideband amplitudes extracted by MSB-SE, relating to characteristic frequencies have more reliable information on the fault which causes the sidebands. The method was verified with experimental data from a planetary gearbox with combined gear and bearing faults. The diagnostic results show not only the types of the combination faults: defects in bearing inner race and tooth breakages of sun gear can be separated, but also the severity of the two faults can be estimated successfully under high load conditions which has not been undertaken before.

9.2 Recommendation of Future Work on Planetary Gearbox

The author suggests the subsequent objectives to continue this research:

Recommendation 1: Apply different types of misalignment such as angular misalignment; see Section 2.2.3.4, to gain a better understanding of the effect of misalignment on PG systems.

Recommendation 2: Use the model developed in Section 3.3, to predict the dynamic characteristics of a rotor with eccentricity, misalignment and mass imbalance. Use a wireless sensor to measure the corresponding acceleration signals. This study would investigate the differences between signals due to eccentricity, misalignment and mass imbalance and combinations of these faults.

Recommendation 3: Use different types of sensors such as a combination of an accelerometer and an acoustic microphone and compare data collected from both.

Recommendation 4: To gain a better understanding of the effect of other vibration sources on the vibration recorded on a PG, Section 2.3 demonstrates there needs to be experimental work with different kinds of faults.

Recommendation 5: Combine faults in PG components and then investigate conventional and advanced techniques to detect and diagnose the faults using only one sensor.

Recommendation 6: A one stage PG was used for this research, this could be extended to combined or multi stage planetary gearbox. As a result, MSB-SE techniques could be used for two stage PG fault detection.

Recommendation 7: The advanced analysis technique MSB-SE used for the spur gears in a one stage PG could be extended to include different kinds of the gears system such as bevel and worm gears, with different gear faults at different levels of severity.

References

Chang, K. (2010). "Accurate alignment saves energy and costs." http://machinedesign.com/mechanical-drives/dont-let-shafts-be-afterthought Retrieved 15-01-20-016, 2016.

Chang, K. (2010). "How is Machine Vibration Described." http://reliabilityweb.com/index.php/articles/how_is_machine_vibration_described/ Retrieved 10/11/2013, 2013.

Jing, Y., Yip, L.,Makis, V. (2013). "Discovery of Sound in the sea ,Introduction to Signal Levels." http://www.dosits.org/science/advancedtopics/signallevels/ Retrieved 05/02/2014, 2014.

Jing, Y., Yip, L.,Makis, V. (2015). n"https://www.myodesie.com/wiki/index/returnEntry/id/3000#Planetary Gears. ." Retrieved Oct, 2015.

Chang, K. (2015). "Modulation and Demodulation 16." from http://www.talkingelectronics.com/Download%20eBooks/Principles%20of%20electronics/CH-16.pdf.

A. Bhatia, B. E. (2012). "Basic Fundamentals of Gear Drives." PDHonline Course M229 (4 PDH).

A. C. McCormick, A. K. N. (1999) "Bispectral and trispectral features for machine condition diagnosis." IEE Proceedings - Vision, Image and Signal Processing **146**, 229-234.

A.O. Boudraa, J. C. C., and Z. Saidi . (2006). "EMD-Based Signal Noise Reduction." International Journal of Signal Processing **1**(1): 33-37.

Abdalla, G., X. Tian, et al. (2014). "Misalignment diagnosis of a planetary gearbox based on vibration analysis."

Abousleiman, V. and P. Velex (2006). "A hybrid 3D finite element/lumped parameter model for quasi-static and dynamic analyses of planetary/epicyclic gear sets." Mechanism and Machine Theory **41**(6): 725-748.

Adams, M. L. (2009). Rotating machinery vibration: from analysis to troubleshooting, CRC Press.

Al-Arbi, S. (2012). Condition Monitoring of Gear Systems using Vibration Analysis, University of Huddersfield.

Alguindigue, I. E., Loskiewicz-Buczak, A,Uhrig, R. E. (1993). "Monitoring and diagnosis of rolling element bearings using artificial neural networks." Industrial Electronics, IEEE Transactions on **40**(2): 209-217.

Alwodai, A., Y. Shao, et al. (2013). Inter-turn short circuit detection based on modulation signal bispectrum analysis of motor current signals. Automation and Computing (ICAC), 2013 19th International Conference on, IEEE.

Ambarisha, V. K. and R. G. Parker (2007). "Nonlinear dynamics of planetary gears using analytical and finite element models." Journal of sound and vibration **302**(3): 577-595.

Anaheim. (2015). "Gearboxes Guide." from http://www.anaheimautomation.com/manuals/forms/gearbox-guide.php#sthash.rPcpceQR.Vs3HL64Y.dpbs.

Antony, G. (1988). "Gear vibration–investigation of the dynamic behavior of one stage epicyclic gears." AGMA technical paper.

August, R. and R. Kasuba (1986). "Torsional Vibrations and Dynamic Loads in a Basic Planetary Gear System." Journal of Vibration, Acoustics, Stress, and Reliability in Design **108**(3): 348-353.

Bahk, C.-J. and R. G. Parker (2011). "Analytical solution for the nonlinear dynamics of planetary gears." Journal of Computational and Nonlinear Dynamics **6**(2): 021007.

Bajrić, R., D. Sprečić, et al. (2011). "Review of vibration signal processing techniques towards gear pairs damage identification." International Journal of Engineering & Technology IJET-IJENS **11**(04): 124-128.

Bartelmus, W. and R. Zimroz (2009). "Vibration condition monitoring of planetary gearbox under varying external load." Mechanical Systems and Signal Processing **23**(1): 246-257.

Bartelmus, W. and R. Zimroz (2011). "Vibration spectra characteristic frequencies for condition monitoring of mining machinery compound and complex gearboxes." Prace Naukowe Instytutu Górnictwa Politechniki Wrocławskiej. Studia i Materiały **133**(40): 17-34.

Binqiang Chen , Z. n., ChuangSun,Bing Li. (2012). "Fault feature extraction of gearbox by using overcomplete rational dilation discrete wavelet transform on signals measured from vibration sensors." Mechanical SystemsandSignalProcessing **33**: 275–298.

Bodas, A. and A. Kahraman (2004). "Influence of carrier and gear manufacturing errors on the static load sharing behavior of planetary gear sets." JSME International Journal Series C **47**(3): 908-915.

Bonanomi, A. (2015). "Disc Couplings Improve Product Performance." http://www.powertransmissionworld.com/disc-couplings-improve-product-performance/ Retrieved 05-03-2016, 2016.

Botman, M. (1976). "Epicyclic gear vibrations." Journal of Engineering for Industry **98**(3): 811-815.

Broberg, P., A. Runnemalm, et al. (2013). "Improved corner detection by ultrasonic testing using phase analysis." Ultrasonics **53**(2): 630-634.

Bruel.V, K. (2009). "Detecting faulty rolling-element bearings." http://www.bksv.co.uk/doc/BO0210.pdf Retrieved 05/11/2013, 2013.

C. Yuksel , A. K. (2004). "Dynamic tooth loads of planetary gear sets having tooth profile wear." Mechanism and Machine Theory **39**: 697-715.

Chang, K. (2002). Modulation and Demodulation. RF and Microwave Wireless Systems, John Wiley & Sons, Inc.**:** 274-293.

Cheng Zhe, H. N., Gu Fengshou, Qin Guojun (2011). "Pitting Damage Levels Estimation for Planetary Gear Sets Based on Model Simulation and Grey Relational Analysis." CSME.

Clara., S. (2009). "Time Synchronous Averaging." Crystal Instruments: 5.

Cohen, L. (1989). "Time-frequency distributions-a review." Proceedings of the IEEE **77**(7): 941-981.

Collis, W. B., White, P. R,Hammond, J. K. (1998). "Higher-order spectra : The bispectrum and trispectrum " Mechanical Systems and Signal Processing **12**(3): 375-394.

Company, A. P. G. (2007). "PCB Piezotronics Vibration Division Accelerometer Installation and Operating Manual."

Cooley, C. G. and R. G. Parker (2012). "Vibration properties of high-speed planetary gears with gyroscopic effects." Journal of Vibration and Acoustics **134**(6): 061014.

Cornell, R. W. (1981). "Compliance and Stress Sensitivity of Spur Gear Teeth." Journal of Mechanical Design **103**(2): 447-459.

Crowther, A., V. Ramakrishnan, et al. (2011). "Sources of time-varying contact stress and misalignments in wind turbine planetary sets." Wind Energy **14**(5): 637-651.

Crowther, A., Ramakrishnan, V, Zaidi, N. A, Halse, Chris. (2011). "Sources of time-varying contact stress and misalignments in wind turbine planetary sets." Wind Energy **14**(5): 637-651.

Cunliffe, F., J. Smith, et al. (1974). "Dynamic tooth loads in epicyclic gears." Journal of Engineering for Industry **96**(2): 578-584.

Cunliffe, F., J. D. Smith, et al. (1974). "Dynamic Tooth Loads in Epicyclic Gears." Journal of Engineering for Industry **96**(2): 578-584.

D. Vijayaraghavan , D. E. B. (2005). "Effect of Misalignment on the Performance of Planetary Gear Journal Bearings." Resident at NASA/LeRC, Cleveland, Ohio(43606).

Davies, A. (2012). Handbook of condition monitoring: techniques and methodology, Springer Science & Business Media.

de Smidt, M. R. (2009). Internal Vibration Monitoring of A Planetary Gearbox, University of Pretoria.

Decker, H. J. and D. G. Lewicki (2003). "Spiral bevel pinion crack detection in a helicopter gearbox."

Dempsey, P. J., W. Morales, et al. (2002). "Investigation of spur gear fatigue damage using wear debris." Tribology & Lubrication Technology **58**(11): 18.

Dipl.-Ing. I. Boiadjiev, D.-I. J. W., Dr.-Ing. T. Tobie and Prof. Dr.-Ing. K.Stahl. (2015). "Tooth Flank Fracture – Basic Principles and Calculation Model for a Sub-Surface-Initiated Fatigue Failure Mode of Case-Hardened Gears." from http://www.geartechnology.com/articles/0815/Tooth_Flank_Fracture_-_Basic_Principles_and_Calculation_Model_for_a_Sub-Surface-Initiated_Fatigue_Failure_Mode_of_Case-Hardened_Gears.

Drury, C. G. and J. Watson (2002). "Good practices in visual inspection."

Eric Bechhoefer, M. K. (2009). "A Review of Time Synchronous Average Algorithms." Annual Conference of the Prognostics and Health Management Society: 10.

Eritenel, T. and R. G. Parker (2009). "Modal properties of three-dimensional helical planetary gears." Journal of Sound and Vibration **325**(1–2): 397-420.

ETRA. (2015). "Flexible Coupling Fenner Fenaflex." from http://tuotteet.etra.fi/en/g7996726/.

F Elbarghathi, T. W., D Zhen,F Gu,A Ball (2012). "Two Stage Helical Gearbox Fault Detection and Diagnosis based on Continuous Wavelet Transformation of Time Synchronous Averaged Vibration Signals." Journal of Physics: Conference Series **364**(1): 012083.

Fan, L., S. Wang, et al. (2016). "Nonlinear dynamic modeling of a helicopter planetary gear train for carrier plate crack fault diagnosis." Chinese Journal of Aeronautics.

Feng, Z., Zuo, Ming J.. (2012). "Vibration signal models for fault diagnosis of planetary gearboxes." Journal of Sound and Vibration **331**(22): 4919-4939.

Fengshou Gu, Y. S., Niaoqin Hu, Bruno Fazenda, Andrew Ball. (2009). "Motor Current Signal Analysis using a Modified Bispectrum for Machine Fault Diagnosis." 6.

FPT. (2015). "Drive couplings " Retrieved 11, 2015, from http://www.fptgroup.com/fenner.asp?title=Fenaflex-Tyre-Couplings&pageid=2672.

G-Redl. (2012). "Super Puma Down – II." from http://isambardkingdom.com/?m=201201.
Gaballa M Abdalla, X. T., Dong Zhen, Fengshou Gu and Andrew Ball (2014). "Misalignment Diagnosis of A Planetary Gearbox Based on Vibration Analysis." The 21st International Congress on Sound and Vibration.
Ganeriwala, S. N., Z. Li, et al. (2008). "Using Operating Deflection Shapes to Detect Misalignment in Rotating Equipment." Presented at IMAC XXVI February **4**: 7.
Ganguly, A., M. K. Kowar, et al. (2012). "Preventive Maintenance of Rotating Machines Using Signal Processing Techniques." **2**(2 May 2012): 35-40.
Geramitcioski, T. and L. Trajcevski (2002). Theoretical Improvement of the Planetary Gear Dynamic Model. DS 30: Proceedings of DESIGN 2002, the 7th International Design Conference, Dubrovnik.
Glatzel, T., S. Sadewasser, et al. (2003). "Amplitude or frequency modulation-detection in Kelvin probe force microscopy." Applied Surface Science **210**(1): 84-89.
Gu, F., G. M. Abdalla, et al. (2014). "A Novel Method for the Fault Diagnosis of a Planetary Gearbox based on Residual Sidebands from Modulation Signal Bispectrum Analysis."
Gu, F., Y. Shao, et al. (2011). "Electrical motor current signal analysis using a modified bispectrum for fault diagnosis of downstream mechanical equipment." Mechanical Systems and Signal Processing **25**(1): 360-372.
Gu, F., Shao, Y,Hu, N,Naid, A,Ball, A. D. (2011). "Electrical motor current signal analysis using a modified bispectrum for fault diagnosis of downstream mechanical equipment." Mechanical Systems and Signal Processing **25**(1): 360-372.
Gui, Y., Q. Han, et al. (2014). "Detection and localization of tooth breakage fault on wind turbine planetary gear system considering gear manufacturing errors." Shock and Vibration **2014**.
Guo Ai-Huang, F. J.-M., and Fen Eng-Xin. (2001). "Time – Frequency Characteristic of Single-Mode Fibre Dispersion." **31**(4): 299-302.
Guo, Y. and R. G. Parker (2010). "Dynamic modeling and analysis of a spur planetary gear involving tooth wedging and bearing clearance nonlinearity." European Journal of Mechanics - A/Solids **29**(6): 1022-1033.
Guo, Y. and R. G. Parker (2010). "Purely rotational model and vibration modes of compound planetary gears." Mechanism and Machine Theory **45**(3): 365-377.
H. Dong, Y. W. a. D. W. (2015). "Dynamic Model and Load Sharing Analysis of Planetary Transmission." The 14th IFToMM World Congress.
Hanson, D. (2015). "Cyber Monday Advice: Don't Buy the Extended Warranty." Retrieved 15/10, 2015, from https://ricochet.com/dont-buy-the-extended-warranty/.
Harris, T. A. and M. N. Kotzalas (2006). Advanced concepts of bearing technology: rolling bearing analysis, CRC Press.
Harris., S. L. (1985). "Dynamic Loads on the Teeth of Spur Gears." Proceedings of the Institution of Mechanical Engineers **172**: 87-112.
Heckbert., P. (Jan,1998). "Fourier Transforms and the Fast Fourier Transform (FFT) Algorithm." Computer Graphics **3**: 463.
Heney, P. J. (2013). "What are Couplings for Power Transmission, Technical Summary." from http://www.motioncontroltips.com/author/motion-control-tips-editor/.
Hidaka, T., YoshioNohara, MinoruOSHITA, Jun-ichi (1977). "Dynamic behavior of planetary gear: 3rd report, Displacement of ring gear in direction of line of action." Bulletin of JSME **20**(150): 1663-1672.

Hong, L., J. S. Dhupia, et al. (2014). "An explanation of frequency features enabling detection of faults in equally spaced planetary gearbox." Mechanism and Machine Theory **73**: 169-183.

Hong, L., Dhupia, Jaspreet Singh,Sheng, Shuangwen (2014). "An explanation of frequency features enabling detection of faults in equally spaced planetary gearbox." Mechanism and Machine Theory **73**(0): 169-183.

Hui, L., Yuping, Zhang (2006). Bearing Faults Diagnosis Based on EMD and Wigner-Ville Distribution. Intelligent Control and Automation, 2006. WCICA 2006. The Sixth World Congress on.

IAEA-TECDOC (2007). "Implementation Strategies and ,Tools for Condition Based Maintenance at Nuclear Power Plants." International Atomic Energy Agency

Inalpolat, M. and A. Kahraman (2010). "A dynamic model to predict modulation sidebands of a planetary gear set having manufacturing errors." Journal of Sound and Vibration **329**(4): 371-393.

Inalpolat, M., Kahraman, A. (2009). "A theoretical and experimental investigation of modulation sidebands of planetary gear sets." Journal of Sound and Vibration **323**(3–5): 677-696.

Industries, S. (2015). "Internal Spur Gears." from http://www.exportersindia.com/satyam-industries-rajkot/internal-spur-gears-rajkot-india-1296537.htm.

Irene Hamernick, L., Inc. (2006). "Vibration Analysis for Condition Monitoring Pumps and Systems." Maintenance Minders: 62-63.

Jarchow, F. and R. Vonderschmidt (1981). Tooth-Forces in Planetary Gears. Proceedings of the International Symposium on Gearing and Power Transmissions.

Jardine, A. K. S., D. Lin, et al. (2006). "A review on machinery diagnostics and prognostics implementing condition-based maintenance." Mechanical Systems and Signal Processing **20**(7): 1483-1510.

Jing, Y., Makis, V. (2011). Wavelet analysis with time-synchronous averaging of planetary gearbox vibration data for fault detection and diagnostics. Computer Science and Automation Engineering (CSAE), 2011 IEEE International Conference on.

Jing, Y., Yip, L.,Makis, V. (2010). Notice of Retraction
Wavelet analysis with time-synchronous averaging of planetary gearbox vibration data for fault detection, diagnostics, and condition based maintenance. Mechanical and Electronics Engineering (ICMEE), 2010 2nd International Conference on.

Johannes Wagner , J. B. (2012). "Piezoelectric Accelerometers,Theory and Application." Metra Mess- und Frequenztechnik in Radebeul e.K.MMF.de: 46.

John, P. (2006). Shaft Alignment Handbook" Third Ed. . New York, Taylor& Francis Group.LLC.

Kadambe, S. and G. F. Boudreaux bartels (1992). "A comparison of the existence of `cross terms' in the Wigner distribution and the squared magnitude of the wavelet transform and the short-time Fourier transform." Signal Processing, IEEE Transactions on **40**(10): 2498-2517.

Kahraman, A. (1994). "Natural modes of planetary gear trains." Journal of Sound and Vibration **173**(1): 125-130.

Kahraman, A. (1994). "Planetary Gear Train Dynamics." Journal of Mechanical Design **116**(3): 713-720.

Kahraman, A. (2001). "Free torsional vibration characteristics of compound planetary gear sets." Mechanism and Machine Theory **36**(8): 953-971.

Kahraman, A., H. Ligata, et al. (2010). "Influence of ring gear rim thickness on planetary gear set behavior." Journal of Mechanical Design **132**(2): 021002.

Kahraman, A. and S. Vijayakar (2000). "Effect of Internal Gear Flexibility on the Quasi-Static Behavior of a Planetary Gear Set." Journal of Mechanical Design **123**(3): 408-415.

Kasuba, R., August, R (1984). "Gear Mesh Stiffness and Load Sharing in Planetary Gearing, ASME 4th Power Transmission Conference." Transactions of the ASME.

Keller, J. A. and P. Grabill (2003). Vibration monitoring of UH-60A main transmission planetary carrier fault. ANNUAL FORUM PROCEEDINGS-AMERICAN HELICOPTER SOCIETY, AMERICAN HELICOPTER SOCIETY, INC.

Kiracofe, D. R. and R. G. Parker (2007). "Structured vibration modes of general compound planetary gear systems." Journal of Vibration and Acoustics **129**(1): 1-16.

Komgom N. Christian , N. M., Aouni Lakis, Marc Thomas (2007). "On the Use of Time Synchronous Averaging, Independent Component Analysis And Support Vector Machines For Bearing Fault Diagnosis." First International Conference on Industrial Risk Engineering: 610-624.

Lane, M. (2011). Using the AC Drive Motor as a Transducer for Detecting Electrical and Electromechanical Faults, University of Huddersfield.

Lei, Y., J. Lin, et al. (2014). "Condition monitoring and fault diagnosis of planetary gearboxes: a review." Measurement **48**: 292-305.

Lei, Y. and M. J. Zuo (2009). "Gear crack level identification based on weighted K nearest neighbor classification algorithm." Mechanical Systems and Signal Processing **23**(5): 1535-1547.

Lei, Y., M. J. Zuo, et al. (2010). "A multidimensional hybrid intelligent method for gear fault diagnosis." Expert Systems with Applications **37**(2): 1419-1430.

Leondes, C. T. (2000). Computer-Aided Design, Engineering, and Manufacturing: Systems Techniques and Applications, Volume II, Computer-Integrated Manufacturing, CRC Press.

Lewicki, D. G., K. E. LaBerge, et al. (2011). "Planetary gearbox fault detection using vibration separation techniques."

Ligata, H. S., A.Kahraman, A. (2008). "An Experimental Study of the Influence of Manufacturing Errors on the Planetary Gear Stresses and Planet Load Sharing." Journal of Mechanical Design **130**(4): 041701-041701.

Lin, J. and R. Parker (1999). "Analytical characterization of the unique properties of planetary gear free vibration." Journal of Vibration and Acoustics **121**(3): 316-321.

Lin, J. and R. Parker (2000). "Structured vibration characteristics of planetary gears with unequally spaced planets." Journal of Sound and Vibration **233**(5): 921-928.

Lin, J. and R. G. Parker (2002). "Planetary Gear Parametric Instability Caused by Mesh Stiffness Variation." Journal of Sound and Vibration **249**(1): 129-145.

Lynwander, p. (1983). Gear Drive Systems: Design and Application. Gear Drive Systems: Design and Application. New York,USA, Marcel Dekker, New York.

M.M.Mayuram, P. K. G. P. (2015). "GEAR FAILURE." from http://nptel.ac.in/courses/IIT-MADRAS/Machine_Design_II/pdf/2_6.pdf.

Ma, P. and M. Botman (1985). "Load sharing in a planetary gear stage in the presence of gear errors and misalignment." Journal of Mechanisms, Transmissions, and Automation in Design **107**(1): 4-10.

Mark Senldge, T. R. L. (1987). Piezoelectric Accelerometers and Vibration Preamplifiers,Theory and Application Handbook, Bruel & Kjaer Publications.

Márquez, F. P. G., A. M. Tobias, et al. (2012). "Condition monitoring of wind turbines: Techniques and methods." Renewable Energy **46**: 169-178.

Mauricel. Adams, J. (2001). Rotating Machinery Vibration From Analysis to Troubleshooting

New York, Marcel Dekker, Inc.

McFadden, P. (1987). "Examination of a technique for the early detection of failure in gears by signal processing of the time domain average of the meshing vibration." Mechanical Systems and Signal Processing **1**(2): 173-183.

McFadden, P. (1991). "A technique for calculating the time domain averages of the vibration of the individual planet gears and the sun gear in an epicyclic gearbox." Journal of Sound and Vibration **144**(1): 163-172.

McFadden, P. and I. Howard (1990). The detection of seeded faults in an epicyclic gearbox by signal averaging of the vibration, DTIC Document.

McFadden, P. and J. Smith (1985). "An explanation for the asymmetry of the modulation sidebands about the tooth meshing frequency in epicyclic gear vibration." Proceedings of the Institution of Mechanical Engineers, Part C: Journal of Mechanical Engineering Science **199**(1): 65-70.

McFadden , P. D. (1991). "A technique for calculating the time domain averages of the vibration of the individual planet gears and the sun gear in an epicyclic gearbox." Journal of Sound and Vibration **144**(1): 163-172.

McFadden , S. J. D. (1985). "An explanation for the asymmetry of the modulation sidebands about the tooth meshing frequency in epicyclic gear vibration." Institution of Mechanical Engineers **199**(1): 65-70

Meltzer, G. and Y. Y. Ivanov (2003). "Fault detection in gear drives with non-stationary rotational speed-part I: the time-frequency approach." Mechanical Systems and Signal Processing **17**(5): 1033-1047.

Mobley, R. K. (2002). An introduction to predictive maintenance, Butterworth-Heinemann.

N Tandona , A. C. (1999). "A review of vibration and acoustic measurement methods for the detection of defects in rolling element bearings." Tribology International **32**(8): 469–480.

Norton, M. P. and D. G. Karczub (2003). Fundamentals of noise and vibration analysis for engineers, Cambridge university press.

Odesie. (2015). "Gear Drives ", from https://www.myodesie.com/wiki/index/returnEntry/id/3000#Planetary.

Özturk, H. (2006). Gearbox Health Monitoring And Fault Detection Using Vibration Analysis. PhD, Dokuz Eylül.

P. Velex , M. A. (2006). "On the modelling of excitations in geared systems by transmission errors." Journal of Sound and Vibration **290**(3-5): 882–909.

Parker, R. G., J. Lin, et al. (2001). "Modeling, modal properties, and mesh stiffness variation instabilities of planetary gears."

Parker, R. G. and X. Wu (2010). "Vibration modes of planetary gears with unequally spaced planets and an elastic ring gear." Journal of Sound and Vibration **329**(11): 2265-2275.

Patel, R. K., Agrawal, S, Joshi, N. C. (2012). Induction motor bearing fault identification using vibration measurement. Engineering and Systems (SCES), 2012 Students Conference on.

Patel, T. H. and A. K. Darpe (2009). "Vibration response of misaligned rotors." Journal of Sound and Vibration **325**(3): 609-628.

Patel, T. H., Darpe, Ashish K (2009). "Vibration response of misaligned rotors." Journal of Sound and Vibration **325**(3): 609-628.

Paz, N. M., W. Leigh, et al. (1994). "The development of knowledge for maintenance management using simulation." IEEE Transactions on Systems, Man, and Cybernetics **24**(4): 574-593.

Qiuhua Du , S. Y. (2007). "Application of the EMD method in the vibration analysis of ball bearings." Mechanical Systems and Signal Processing **21**(6): 2634–2644.

R. Keith Mobley (2002). An Introduction to Predictive Maintenance. New York,USA, Butterworth-Heinemann is an imprint of Elsevier Science.

Ramsden, E. (July/2001). "An Introduction to Analog Filters." http://www.sensorsmag.com/sensors/electric-magnetic/an-introduction-analog-filters-1023.

Rao, S. S. (1995). Mechanical Vibrations,3rd Edition Addison-Wesley.

Roberto Mosse , L. E. S. (1996). Performance Monitoring,Indicators Handbook.

Rohs (2014). "Technical portal and online community for Design Engineers, Sensors & Transducers." 2082.

Saada, A. and P. Velex (1995). "An extended model for the analysis of the dynamic behavior of planetary trains." Journal of Mechanical Design **117**(2A): 241-247.

Sait, A., Sharaf-Eldeen, YahyaI (2011). A Review of Gearbox Condition Monitoring Based on vibration Analysis Techniques Diagnostics and Prognostics. Rotating Machinery, Structural Health Monitoring, Shock and Vibration, Volume 5. T. Proulx, Springer New York**:** 307-324.

Samuel, P. D. and D. J. Pines (2005). "A review of vibration-based techniques for helicopter transmission diagnostics." Journal of Sound and Vibration **282**(1–2): 475-508.

Searle, D. D. G. (1997). European Electric Motors, Drives and Controls. New Courtwick Way, Littlehampton, West Sussex,, Eurotherm Drives Ltd.

Shin, K. and J. Hammond (2008). Fundamentals of signal processing for sound and vibration engineers, John Wiley & Sons.

Smidt, M. R. d. (2009). Internal Vibration Monitoringof A Planetary Gearbox. MSC, **University of Pretoria**.

Stack, J. R., Habetler, T. G,Harley, R. G. (2004). "Fault classification and fault signature production for rolling element bearings in electric machines." Industry Applications, IEEE Transactions on **40**(3): 735-739.

Stack, J. R., R. G. Harley, et al. (2004). "An amplitude Modulation detector for fault diagnosis in rolling element bearings." Industrial Electronics, IEEE Transactions on **51**(5): 1097-1102.

Steve Sabin, R. C. (2006). "Understanding Discrepancies in Vibration Amplitude Readings Between Different Instruments." ORBIT **26**(Monitoring versus diagnostics): 18.

Sun, T. and H. Hu (2003). "Nonlinear dynamics of a planetary gear system with multiple clearances." Mechanism and Machine Theory **38**(12): 1371-1390.

Svetlitsky, V. A. (2012). Foundations of Engineering Mechanics ,Engineering Vibration Analysis: Worked Problems 1. Berlin Heidelberg, Springer Science & Business Media.

Tavakoli, M. S., Houser, D. R. (1986). "Optimum Profile Modifications for the Minimization of Static Transmission Errors of Spur Gears." Journal of Mechanical Design **108**(1): 86-94.

Walter Bartelmus, R. Z. (2011). "Vibration Spectra Characteristic Frequencies for Condition Monitoring of Mining Machinery Compound and Complex Gearboxes." Studia i Materiały **40**.

Wang, J., Y. Wang, et al. (2014). "Analysis of dynamic behavior of multiple-stage planetary gear train used in wind driven generator." The Scientific World Journal **2014**.

Wang, W. (2008). Condition-based maintenance modelling. Complex system maintenance handbook, Springer**:** 111-131.

Winter, H. and T. Placzek (1989). "Fundamentals of Gear Design by Raymond J. Drago (Butterworths, Stoneham MA, USA, 1988) 576 pages, hardcover, £E54.00." Journal of Synthetic Lubrication **6**(3): 256-256.

Wowk, V. (2000). Machinery Vibration Alignment. New York, McGraw Hill Professional.

Wu, B., A. Saxena, et al. (2004). An approach to fault diagnosis of helicopter planetary gears. AUTOTESTCON 2004. Proceedings, IEEE.

Wu, X. and R. G. Parker (2008). "Modal Properties of Planetary Gears With an Elastic Continuum Ring Gear." Journal of Applied Mechanics **75**(3): 031014-031014.

Wu, X. and R. G. Parker (2008). "Modal properties of planetary gears with an elastic continuum ring gear." Journal of Applied Mechanics **75**(3): 031014.

Xiange, T., G. M. Abdallaa, et al. (2015). Diagnosis of combination faults in a planetary gearbox using a modulation signal bispectrum based sideband estimator. Automation and Computing (ICAC), 2015 21st International Conference on.

Yesilyurt, I., Gu, Fengshou,Ball, Andrew D. (2003). "Gear tooth stiffness reduction measurement using modal analysis and its use in wear fault severity assessment of spur gears." NDT & E International **36**(5): 357-372.

Yong Gui , Q. K. H., Zheng Li , Zhi Ke Peng , Fu Lei Chu (2013). "The Fault Characteristics of Planetary Gear System with Tooth Breakage." Key Engineering Materials **569 - 570**: 489-496.

Young , K. a. E. J. P. (JUNE 1979). "Digital Bispectral Analysis and Its Applications to Nonlinear Wave Interactions." IEEE Transactions on Plasma Science **PS-7**(2): 120–131.

Yuksel, C. and A. Kahraman (2004). "Dynamic tooth loads of planetary gear sets having tooth profile wear." Mechanism and Machine Theory **39**(7): 695-715.

Zhang-Cheng, H. and H. Jia-Sheng (2010). "UWB Bandpass Filter Using Cascaded Miniature High-Pass and Low-Pass Filters With Multilayer Liquid Crystal Polymer Technology." Microwave Theory and Techniques, IEEE Transactions on **58**(4): 941-948.

Zhang, G., M. Ge, et al. (2002). "Bispectral analysis for on-line monitoring of stamping operation." Engineering Applications of Artificial Intelligence **15**(1): 97-104.

Zhang, G. C., Ge, M,Tong, H,Xu, Y,Du, R. (2002). "Bispectral analysis for on-line monitoring of stamping operation." Engineering Applications of Artificial Intelligence **15**(1): 97-104.

Zhou, X., W. Wu, et al. (2012). A contraction fixed point theorem in partially ordered metric spaces and application to fractional differential equations. Abstract and Applied Analysis, Hindawi Publishing Corporation.

APPENDIX A Preventive Maintenance

Chapter one begins with background to the industrial applications of condition monitoring. This is followed by a description of maintenance strategies and their application to planetary gearbox condition monitoring. The chapter then describes the advantages of planetary gears over parallel axis gears, followed by the motivation for this research programme and the overall aim and objectives of the research programme. Finally, the structure of the report is presented and the content of the remaining chapters is given.

A thorough comparison between advantages and disadvantages of preventive maintenance must be made to fully understand its importance.

Advantages: Preventive maintenance management consists of the following distinct advantages.

- ***Control of Management***. It is possible to plan preventive maintenance as a pre-active measure, as compared to repair maintenance, which is a reaction to failure. For pre-active measures, the equipment can be repaired when it is off-line as part of its normal working schedule. Whereas repair maintenance must take place when the machine fails.
- ***Overtime***. Reduction of overtime costs is possible by reducing surprise failures. Preventive maintenance tasks can be conveniently scheduled during normal working hours. However, repair maintenance may incur substantial overtime costs.
- ***Parts inventories***. Through preventive maintenance, the materials and components needed can be anticipated and made readily available. This means that organisations which use preventive maintenance require smaller amounts of stock compared to those who use repair maintenance.
- ***Standby equipment***. In the case of breakdowns, there is a strong emphasis upon the presence of standby equipment. This is mainly due to an increase in production demand and the low availability of equipment. For preventive maintenance, some backup is required, but it reduces the costs and investment.
- ***Quality***. It is possible to ensure better product quality and far fewer production breakdowns with preventive maintenance than with repair maintenance. Control

limits allow for management of tolerance, and with improved product quality and productivity there is a corresponding increase in net revenues.

- ***Cost–benefit relationship***. The application of a preventive maintenance programme can greatly assist organisations to increase profitability by better management of maintenance costs. Such a programme provides a three-way balance between production revenues, and corrective and preventive maintenance.

Disadvantages There are also certain disadvantages associated with preventive maintenance.

- ***Potential damage***. High reliability equipment is usually serviced by low reliability personnel. Due to negligence, incorrect procedures or ignorance, the equipment may be damaged every time such individuals interact with it. An extreme example of inappropriate preventive maintenance was the disaster at the Three Mile Island nuclear power plant.
- ***Infant mortality***. There is a small but real probability that new components will be defective. Quality assurance for replacement parts is not always appropriate.
- ***Parts use***. The useful life of the part would be terminated if it is not replaced at the planned preventive maintenance schedule. If failure occurs, more parts would need to be replaced(Mobley 2002).

APPENDIX B Basic Layout of a Planetary Gearbox

The planetary gearbox supplied and manufactured by STM Power Transmission Ltd, as presented in. consists of three planet gears, sun gear, ring gear and carrier. The technical specifications of the planetary gearbox are given in

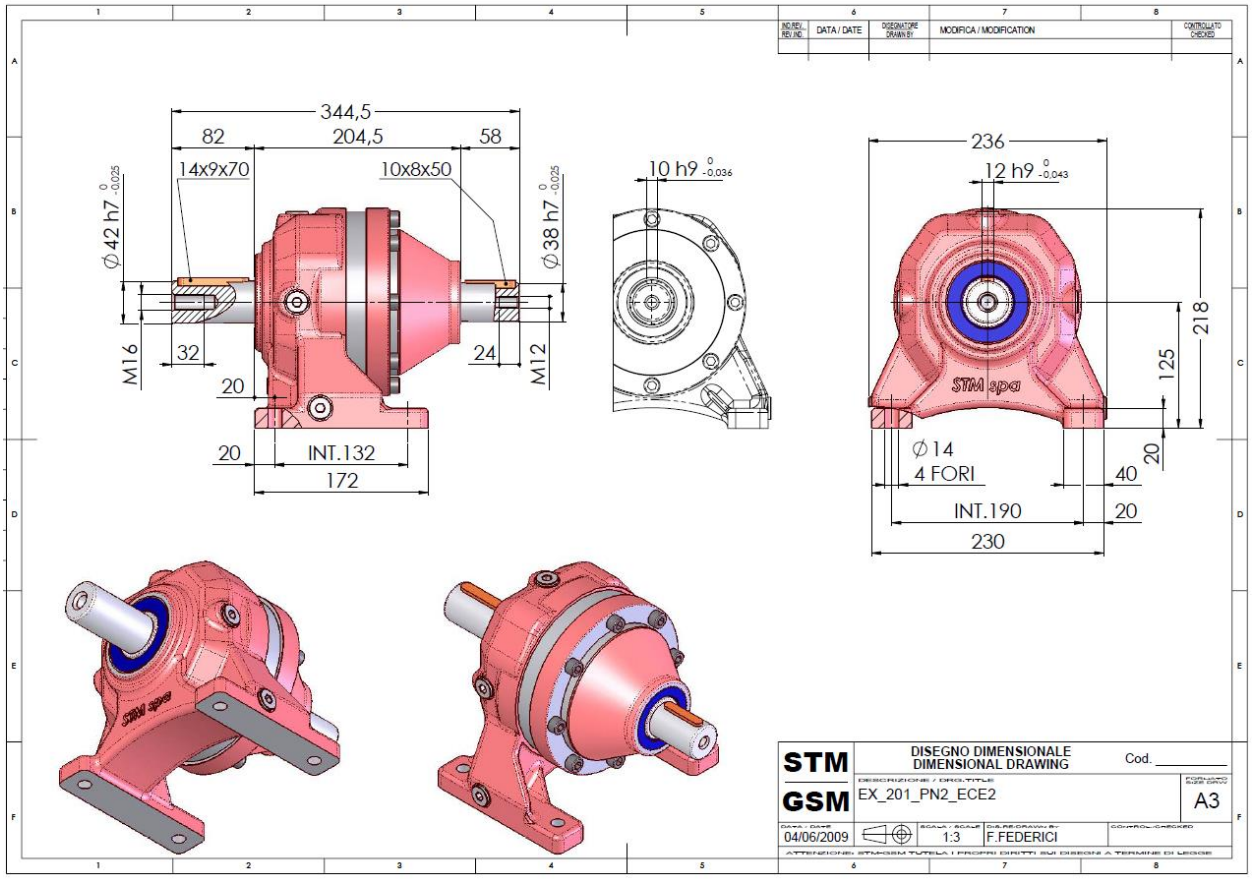

Figure B 1 STM Planetary gearbox

The planet carrier is floating and fixed to the output shaft by means of splines which allow it to move axially as required. The planet gears are hardened and use the inside of the ring gear as the inner bearing race. Loose needle bearings are then inserted between the planet gear and the planet gear shaft with the shaft itself being the other race of the bearing.

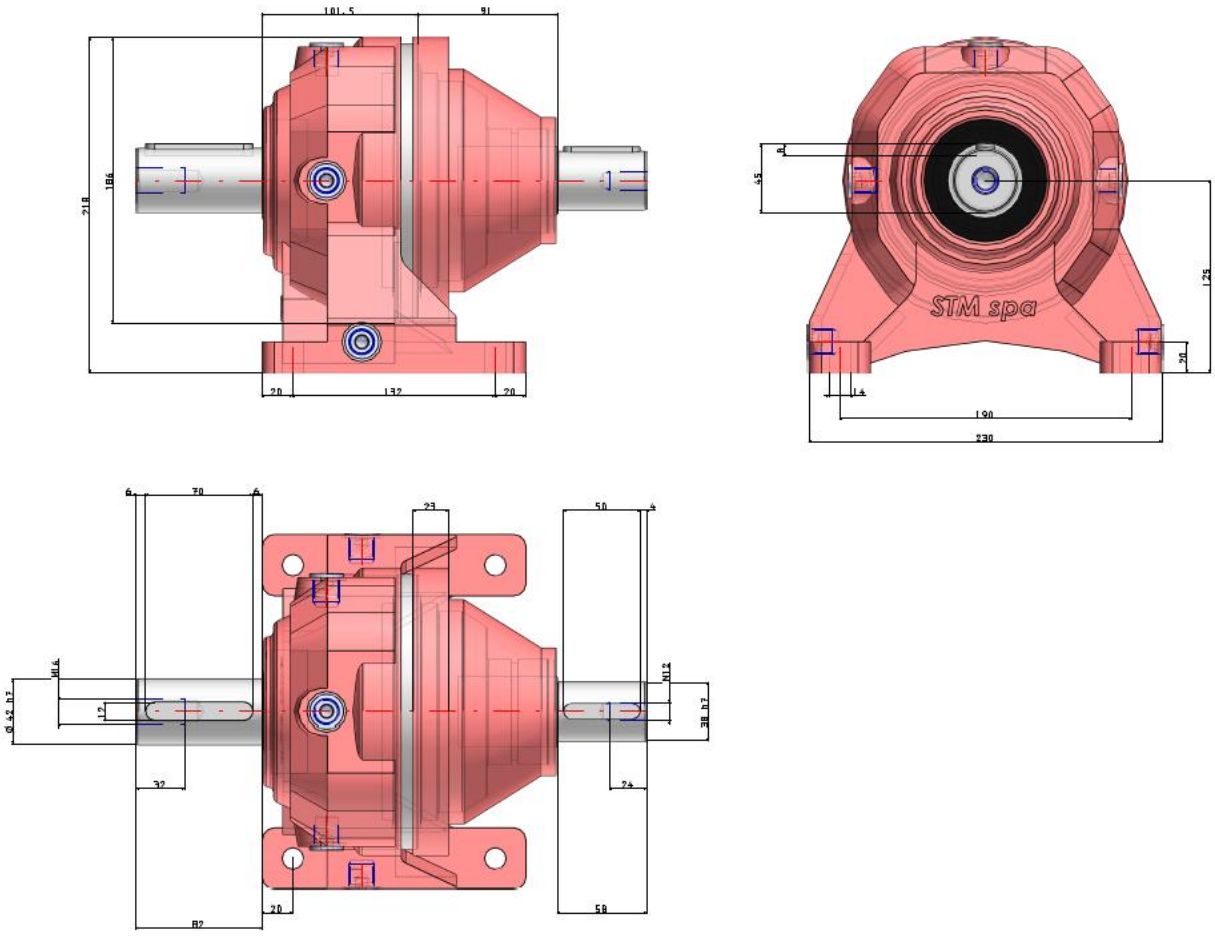

Figure B 2 STM Planetary gearbox

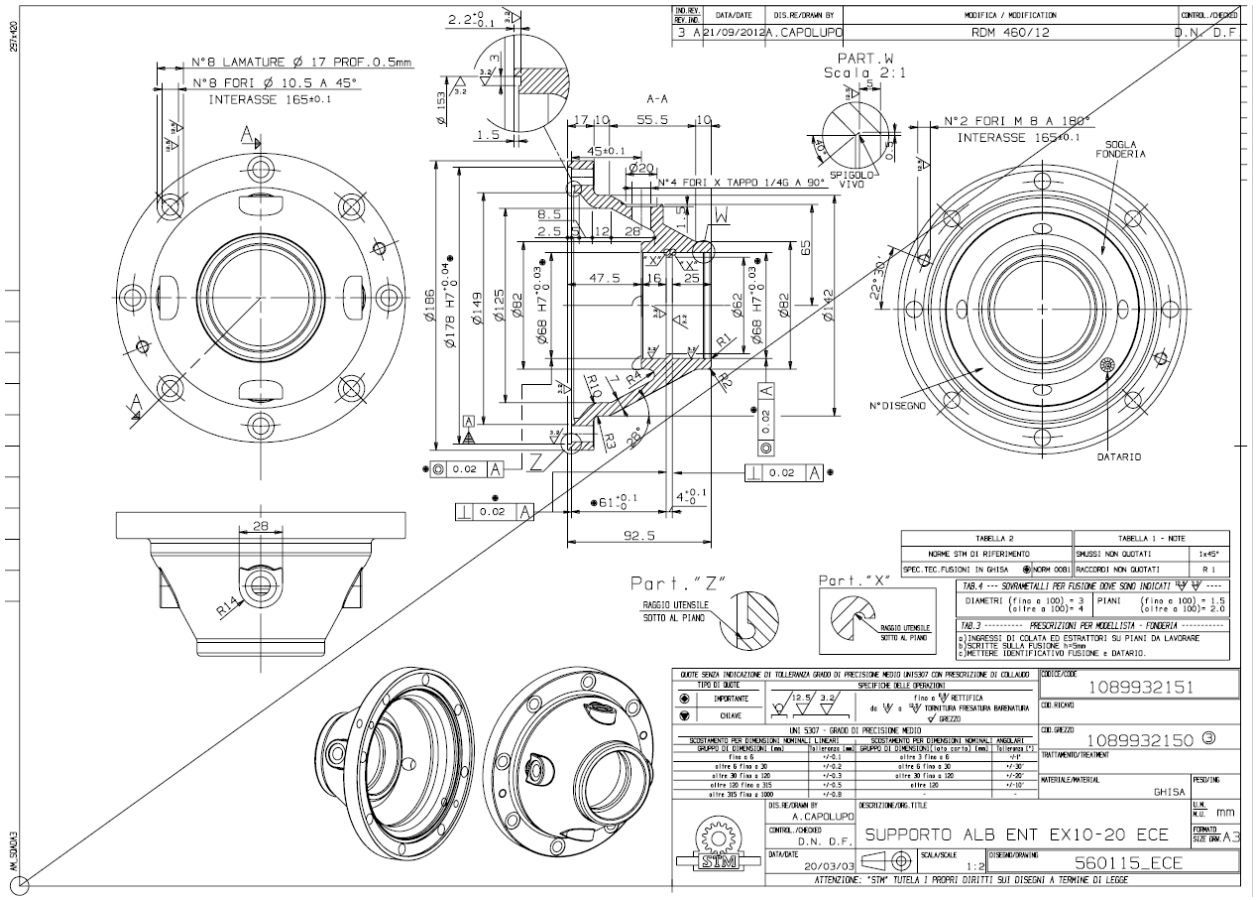

Figure B 3 Drawing for Gearbox Housing

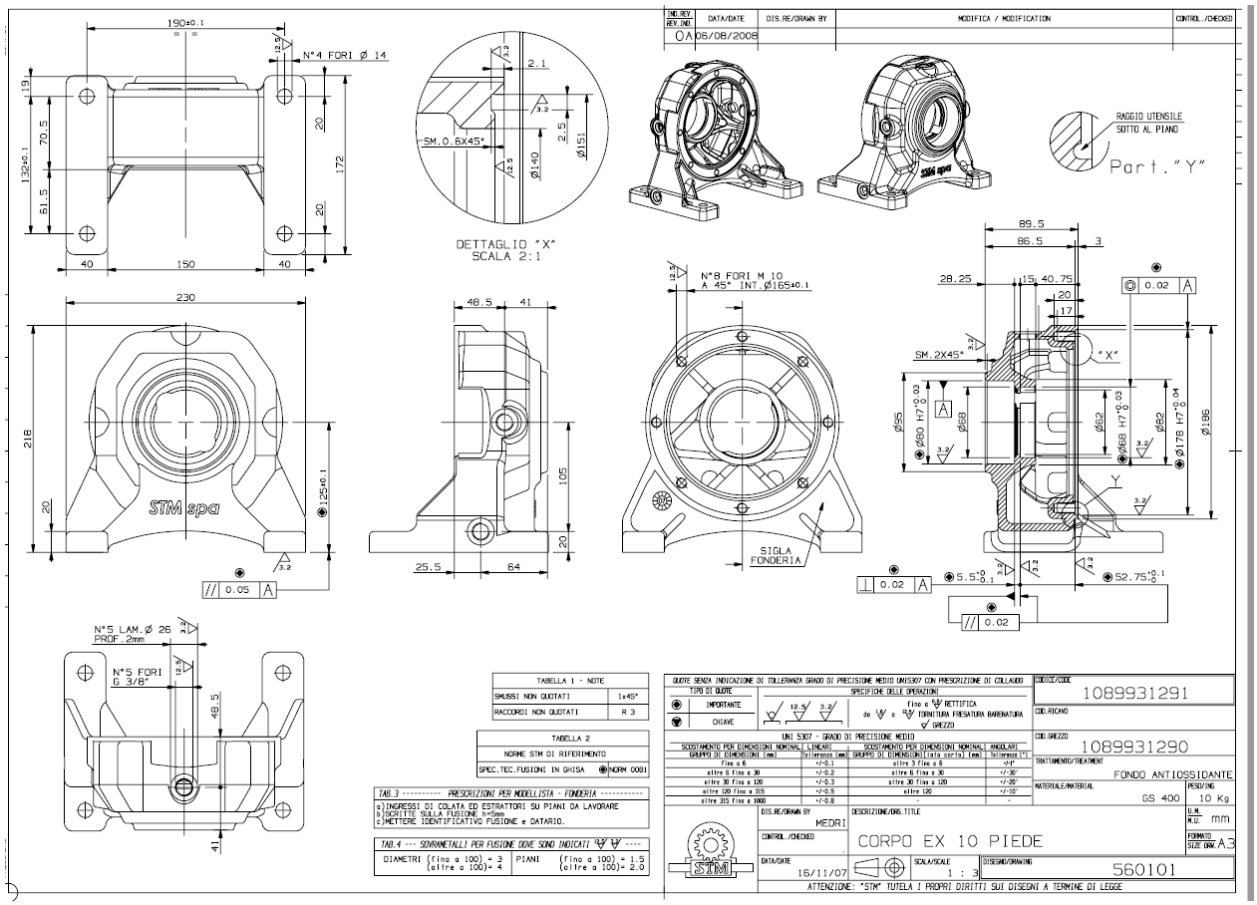

Figure B 4 Drawing for Gearbox Housing

APPENDIX E Coupling Specification

The Fen flexes Tyre Couplings is used in this test rig. Two couplings were used, the first, the F80 FX10 assembly, joined the helical gearbox shaft with input planetary gearbox shaft and the second, the F100 FX10, joined the output shaft of planetary gearbox to the DC generator These couplings have good shock absorbing properties and reduce vibration and torsional oscillations. Additional manufacturer's information is listed below:

FENNER TYRES	For adverse operating conditions Neoprene rubber compounds are used, for instance, grease or oil contaminations which can be used for temperatures between15O C^o and + 70O C^o for ambient temperature ranges in between -50 C^o to +50 C^o .Fenner tyres available as natural rubber compounds are used.
TORQUE-BORE RANGE	The range comprises of bore diameters up to 190 mm and torque capacity up to 12606 Nm.
MISALIGNMENT	Can handle angular, parallel and axial displacements separately as well in any combination. Angular misalignment can be adjusted up to 4^o, parallel misalignment up to 6 mm and end float up to 8mm.
TORSIONALLY SOFT	The complete system is protected because it pillows against damaging shock loads and increases the life of machinery and avoids major breakdowns.
INSTALLATION	Assembling does not need skilled labours or special tools. A straight edge across the diameter of flanges is placed in order to inspect alignment. The split flexible tyre is placed in the flanges and

	tightening of the screws in the correct position takes place.
DAMPING	Reduces vibration oscillations produced in internal combustion engines,. Fenner Tyre coupling dampens this destructive vibration and the amplitude of which increases greatly at critical points in the speed
MAINTENANCE	Only timely visual inspection is needed. No lubrication is needed as there are no moving parts.
EASY ELEMENT REPLACEMENT	The flexible element can be replaced by loosening the clamping screws and then replacing the tyre with a newer tyre. The coupling flanges, driven machine or driver need not be displaced.
ENVIRONMENT	Fenner Tyre coupling in the form of Neoprene or natural rubber can be used for majority of situations. It is recommended to use F.R.S. tyre in areas having fire hazard so as to permit electricity flow and prevent build-up of static electricity(ETRA 2015; FPT 2015).

APPENDIX C Gear Mass and Moment of Inertia

- **Calculation of gear dimensions** Assume pressure angle 20º

By calculate Diametrical Pitch

Diametrical Pitch (P) = (N+2)/OD

For Sun gear =0.4067, Planet gear=0.4516, Ring gear= 0.4671.

http://www.gizmology.net/gears.htm

- **Calculation of Moment of Inertia**

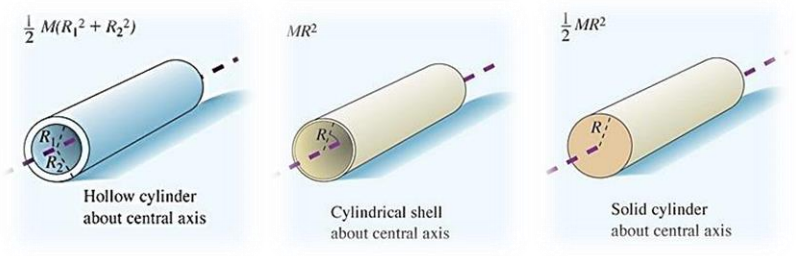

Figure C.5 Calculation of Moment of Inertia

- For carrier

I_c Is identified as thick walled cylindrical tube and contact with input shaft

$$I_c = (I_c + I_{shaft}) = \frac{1}{2} m_c (r_o^2 + r_i^2) + (\frac{1}{2} m_{sh} r_{sh}^{\ 2}) \quad \text{(C1)}$$

$$= \frac{1}{2} 2[(65/1000)^2 + (20/1000)^2] + \frac{1}{2} 1.4 \times (21/1000)^2$$

$$I_c = 4.9337 \times 10^{-3} \ \text{kg.m}^2$$

- For ring gear

$$I_r = m_r r^2 \qquad = 1.64 \times (64.54/1000)^2 \quad \text{(C2)}$$

$$I_r = 7.04535 \times 10^{-3} \ \text{kg.m}^2$$

- For sun gear with the output shaft

$$I_s = (I_{sun} + I_{shaft}) = (\frac{1}{2} m_s r_s^{\ 2} + \frac{1}{2} m_{sh} r_{sh}^{\ 2}) \quad \text{(C3)}$$

$$= (\frac{1}{2} \times 0.28 \times (14.5/1000)^2 + \frac{1}{2} \times 1 \times (19/1000)^2$$

$$I_s = 2.09935 \times 10^{-4} \ \text{kg.m}^2$$

- For planet

$$I_{pn} = \frac{1}{2} m_p (r_o^2 + r_i^2) \qquad \text{(C4)}$$

$$= \frac{1}{2} \times 0.34 \times (31/1000)^2 + (13.55/1000)^2$$

$$I_p = 1.9 \times 10^{-4} \qquad \text{kg.m}^2$$

- ***Matrix Format System:***

Vibration differential equation for a rotational and translational model with *N* planet can be expressed as:

$$M\ddot{q} + C\dot{q} + Kq(t) = F(t) \qquad \text{(C5)}$$

Where;

M , is the mass matrix. C , is the damping matrix. K , is the stiffness matrix. $\ddot{q}, \dot{q}, q$, are the acceleration, velocity and displacement of the vibration motion, $F(t)$ is the force vector of externally applied load or torque (Lin and Parker 1999; Inalpolat and Kahraman 2010).

The inertia matrix;

$$M = \left\{ \frac{I_c}{r_c^2}, \frac{I_r}{r_r^2}, \frac{I_s}{r_s^2}, \frac{I_p}{r_{p1}^2}, ..., \frac{I_p}{r_{pN}^2}, m_c + Nm_p, m_r, m_s, m_{p1}, ..., m_{pN}, m_c + Nm_p, m_r, m_s, m_{p1}, ..., m_{pN} \right\}^T$$

$$q = \left\{ \theta_c, \theta_r, \theta_s, \theta_{p1}, ..., \theta_{pN}, x_c, x_r, x_s, x_1, ..., x_p, y_c, y_r, y_s, y_{p1}, ..., y_{pN} \right\}^T \qquad \text{(C6)}$$

The matrices are defined in as follow:

$$K = \begin{bmatrix} K_{11} & K_{12} & K_{13} \\ & K_{22} & K_{23} \\ Symmetric & & K_{33} \end{bmatrix} \qquad \text{(C7)}$$

Where the stiffness matrix K_{11}, K_{22} and K_{33} has to be symmetric as follow;

$$K_{11}=\begin{bmatrix} \sum_{i=1}^{N} K_{pi}(t) & 0 & 0 & 0 & \cdots & 0 \\ & 0 & 0 & 0 & \cdots & 0 \\ & & \sum_{i=1}^{N} K_{pi}(t) & K_{sp1} & \cdots & K_{spN} \\ & & & K_{sp1}+K_{rp1} & \cdots & K_{spN}+K_{rpN} \\ \textit{Symmetric} & & & & \cdots & K_{spN}+K_{rpN} \end{bmatrix} \quad \text{(C8)}$$

$$K_{12}=\begin{bmatrix} \sum_{i=1}^{N} K_{pi}(t)\sin\psi_i & 0 & 0 & 0 \\ 0 & 0 & 0 & 0 \\ 0 & 0 & -\sum_{i=1}^{N} K_{rpi}(t)\sin\psi_{ri} & -\sum_{i=1}^{N} K_{spi}(t)\sin\alpha_s \\ 0 & K_{rp1}(t)\sin\psi_{ri} & -K_{sp1}(t)\sin\psi_{si} & K_{rp1}(t)\sin\alpha_r - K_{sp1}(t)\sin\alpha_s \\ \vdots & \vdots & \vdots & \vdots \\ \vdots & \vdots & \vdots & \vdots \\ 0 & K_{rpN}(t)\sin\psi_{rN} & K_{spN}(t)\sin\psi_{sN} & K_{rpN}(t)\sin\alpha_r - K_{spN}(t)\sin\alpha \end{bmatrix}$$

$$\begin{bmatrix} \cdots & 0 \\ \cdots & 0 \\ \cdots & -\sum_{i=1}^{N} K_{spN}(t)\sin\alpha_s \\ \cdots & K_{rpN}(t)\sin\alpha_r - K_{spN}(t)\sin\alpha_s \\ \vdots & \vdots \\ \vdots & \vdots \\ \cdots & K_{rpN}(t)\sin\alpha_r - K_{spN}(t)\sin\alpha_s \end{bmatrix} \quad \text{(C9)}$$

$$K_{13}=\begin{bmatrix}
\sum_{i=1}^{N} K_{pi}(t)\cos\psi_i & 0 & 0 & -K_{p1}(t) & \cdots & -K_{pN}(t) \\
0 & 0 & 0 & 0 & \cdots & 0 \\
0 & 0 & -\sum_{i=1}^{N} K_{spi}(t)\cos\psi_{si} & -K_{spi}(t)\cos\alpha_s & \cdots & -K_{spN}(t)\cos\alpha_s \\
0 & -K_{rpi}(t)\cos\psi_{ri} & K_{spi}(t)\cos\psi_{si} & -K_{rp1}(t)\cos\alpha_r\ -K_{sp1}(t)\cos\alpha_s & \cdots & -K_{rpN}(t)\cos\alpha_r\ -K_{spN}(t)\cos\alpha_s \\
\vdots & \vdots & \vdots & \vdots & & \vdots \\
\vdots & \vdots & \vdots & \vdots & & \vdots \\
0 & -K_{rpN}(t)\cos\psi_{rN} & K_{spN}(t)\cos\psi_{sN} & -K_{rpN}(t)\cos\alpha_r\ -K_{spN}(t)\cos\alpha_s & \cdots & -K_{rpN}(t)\cos\alpha_r\ -K_{spN}(t)\cos\alpha_s
\end{bmatrix} \tag{C10}$$

$$K_{22}=\begin{bmatrix}
\sum_{i=1}^{N} K_{pi}(t)\sin^2\psi_i-\sum_{i=1}^{N} K_{pi}(t)\cos^2\psi_i+k_c & 0 & 0 & -K_{pi}(t)\cos\psi_i & \cdots & -K_{pN}(t)\cos\psi_N \\
\sum_{i=1}^{N} K_{rpi}(t)\sin^2\psi_{ri} & 0 & K_{rp1}(t)\sin\psi_{ri}\sin\alpha_r & \cdots & K_{rpN}(t)\sin\psi_{rN}\sin\alpha_r \\
K_{spi}(t)\sin^2\psi_{si}+k_s & K_{sp1}(t)\sin\psi_{si}\sin\alpha_s & \cdots & K_{spN}(t)\sin\psi_{sN}\sin\alpha_s \\
K_{rp1}(t)\sin\alpha_r\sin\alpha_r\ -K_{sp1}(t)\sin^2\alpha_s+k_{p1}+k_p & \cdots & -K_{rpN}(t)\sin\alpha_r\sin\alpha_s\ -K_{spN}(t)\sin^2\alpha_s+k_{pN}+k_p \\
\text{Symmetric} & & & \cdots & -K_{rpN}(t)\sin\alpha_r soc\alpha_r\ -K_{spN}(t)\sin^2\alpha_s+k_{pN}+k_p
\end{bmatrix} \tag{C11}$$

$$K_{23}=\begin{bmatrix} 0 & 0 & 0 & -K_{pi}(t)\cos\psi_i \\ 0 & -\sum_{i=1}^{N} K_{rpi}(t)\sin\psi_{ri}\cos\psi_{ri} & 0 & K_{sp1}(t)\sin\psi_{si}\sin\alpha_s \\ 0 & 0 & -\sum_{i=1}^{N} K_{spi}(t)\sin\psi_{si}\cos\psi_{si} & K_{sp1}(t)\sin\psi_{si}\sin\alpha_s \\ -K_{pi}(t)\sin\psi_i & K_{rpi}(t)\cos\psi_{ri}\sin\alpha_s & -K_{spi}(t)\cos\psi_{Si}\sin\alpha_s & K_{rp1}(t)\cos\alpha_r\sin\alpha_s + K_{sp1}(t)\cos\alpha_s\sin\alpha_s \\ \vdots & \vdots & \vdots & \vdots \\ \vdots & \vdots & \vdots & \vdots \\ -K_{pN}(t)\sin\psi_N & K_{rpN}(t)\cos\psi_{rN}\sin\alpha_s & -K_{spN}(t)\cos\psi_{SN}\sin\alpha_s & K_{rpN}(t)\cos\alpha_r\sin\alpha_s + K_{spN}(t)\cos\alpha_s\sin\alpha_s \end{bmatrix}$$

$$\begin{bmatrix} \ldots\ldots & -K_{pN}(t)\cos\psi_N \\ \ldots\ldots & K_{spN}(t)\sin\psi_{sN}\sin\alpha_s \\ \ldots\ldots & K_{spN}(t)\sin\psi_{sN}\sin\alpha_s \\ \ldots\ldots & K_{rpN}(t)\cos\alpha_r\sin\alpha_s + K_{spN}(t)\cos\alpha_s\sin\alpha_s \\ \vdots & \vdots \\ \vdots & \vdots \\ \ldots\ldots & K_{rpN}(t)\cos\alpha_r\sin\alpha_s + K_{spN}(t)\cos\alpha_s\sin\alpha_s \end{bmatrix} \quad \text{(C12)}$$

$$K_{33}=\begin{bmatrix} -\sum_{i=1}^{N} K_{pi}(t)\sin^2\psi_i - \sum_{i=1}^{N} K_{pi}(t)\cos^2\psi_i + k_c & 0 & 0 & -K_{pi}(t)\sin\psi_i \\ & \sum_{i=1}^{N} K_{rpi}(t)\cos^2\psi_{ri} + k_r & 0 & -K_{rp1}(t)\sin\psi_{ri}\sin\alpha_r \\ & & -\sum_{i=1}^{N} K_{spi}(t)\cos^2\psi_{si} + k_s & -K_{sp1}(t)\cos\psi_{s1}\cos\alpha s \\ & & & K_{rp1}(t)\cos\alpha_r soc\alpha_s + K_{sp1}(t)\cos^2\alpha_s + k_p \\ \textit{Symmetric} & & & \end{bmatrix}$$

$$\begin{bmatrix} \ldots\ldots & -K_{pN}(t)\sin\psi_N \\ \ldots\ldots & -K_{rpN}(t)\sin\psi_{rN}\sin\alpha_r \\ \ldots\ldots & -K_{spn}(t)\cos\psi_{sN}\cos\alpha s \\ \ldots\ldots & K_{rpN}(t)\cos\alpha_r soc\alpha_s + K_{spN}(t)\cos^2\alpha_s + k_p \\ \ldots\ldots & K_{rpN}(t)\cos\alpha_r soc\alpha_s + K_{spN}(t)\cos^2\alpha_s + k_p \end{bmatrix} \quad \text{(C13)}$$

- The damping matrix C can be derived by the same way;

$$K = \begin{bmatrix} C_{11} & C_{12} & C_{13} \\ & C_{22} & C_{23} \\ Symmetric & & C_{33} \end{bmatrix} \tag{C14}$$

Where the stiffness matrix C_{11}, C_{22} and C_{33} has to be symmetric as follow;

$$C_{11} = \begin{bmatrix} \sum_{i=1}^{N} C_{pi}(t) & 0 & 0 & 0 & \ldots\ldots & 0 \\ & 0 & 0 & 0 & \ldots\ldots & 0 \\ & & \sum_{i=1}^{N} C_{pi}(t) & C_{sp1} & \ldots\ldots & C_{spN} \\ & & & C_{sp1}+C_{rp1} & \ldots\ldots & C_{spN}+C_{rpN} \\ Symmetric & & & & \ldots\ldots & C_{spN}+C_{rpN} \end{bmatrix} \tag{C15}$$

$$C_{12} = \begin{bmatrix} \sum_{i=1}^{N} C_{pi}(t)\sin\psi_i & 0 & 0 & 0 \\ 0 & 0 & 0 & 0 \\ 0 & 0 & -\sum_{i=1}^{N} C_{rpi}(t)\sin\psi_{ri} & -\sum_{i=1}^{N} C_{spi}(t)\sin\alpha_s \\ 0 & C_{rp1}(t)\sin\psi_{ri} & -C_{sp1}(t)\sin\psi_{si} & C_{rp1}(t)\sin\alpha_r - C_{sp1}(t)\sin\alpha_s \\ \vdots & \vdots & \vdots & \vdots \\ \vdots & \vdots & \vdots & \vdots \\ 0 & C_{rpN}(t)\sin\psi_{rN} & C_{spN}(t)\sin\psi_{sN} & C_{rpN}(t)\sin\alpha_r - C_{spN}(t)\sin\alpha \end{bmatrix}$$

$$
\begin{bmatrix}
\cdots\cdots & 0 \\
\cdots\cdots & 0 \\
\cdots\cdots & -\sum_{i=1}^{N} C_{spN}(t)\sin\alpha_s \\
\cdots\cdots & C_{rpN}(t)\sin\alpha_r - C_{spN}(t)\sin\alpha_s \\
\vdots & \vdots \\
\vdots & \vdots \\
\cdots\cdots & C_{rpN}(t)\sin\alpha_r - C_{spN}(t)\sin\alpha_s
\end{bmatrix}
\tag{C16}
$$

$$
C_{13} = \begin{bmatrix}
\sum_{i=1}^{N} C_{pi}(t)\cos\psi_i & 0 & 0 & -C_{p1}(t) \\
0 & 0 & 0 & 0 \\
0 & 0 & -\sum_{i=1}^{N} C_{spi}(t)\cos\psi_{si} & -C_{spi}(t)\cos\alpha_s \\
0 & -C_{rpi}(t)\cos\psi_{ri} & C_{spi}(t)\cos\psi_{si} & -C_{rp1}(t)\cos\alpha_r \; -C_{sp1}(t)\cos\alpha_s \\
\vdots & \vdots & \vdots & \vdots \\
\vdots & \vdots & \vdots & \vdots \\
0 & -C_{rpN}(t)\cos\psi_{rN} & C_{spN}(t)\cos\psi_{sN} & -C_{rpN}(t)\cos\alpha_r \; -C_{spN}(t)\cos\alpha_s
\end{bmatrix}
$$

$$
\begin{bmatrix}
\cdots\cdots & -C_{pN}(t) \\
\cdots\cdots & 0 \\
\cdots\cdots & -C_{spN}(t)\cos\alpha_s \\
\cdots\cdots & -C_{rpN}(t)\cos\alpha_r \; -C_{spN}(t)\cos\alpha_s \\
\vdots & \vdots \\
\vdots & \vdots \\
\cdots\cdots & -C_{rpN}(t)\cos\alpha_r \; -C_{spN}(t)\cos\alpha_s
\end{bmatrix}
\tag{C17}
$$

$$C_{22}=\begin{bmatrix}
\sum_{i=1}^{N} C_{pi}(t)\sin^2\psi_i-\sum_{i=1}^{N} C_{pi}(t)\cos^2\psi_i+c_c & 0 & 0 & -C_{pi}(t)\cos\psi_i \\
 & \sum_{i=1}^{N} C_{rpi}(t)\sin^2\psi_{ri} & 0 & C_{rp1}(t)\sin\psi_{ri}\sin\alpha_r \\
 & & C_{spi}(t)\sin^2\psi_{si}+c_s & C_{sp1}(t)\sin\psi_{si}\sin\alpha_s \\
 & & C_{rp1}(t)\sin\alpha_r\sin\alpha_r & -C_{sp1}(t)\sin^2\alpha_s+c_{p1}+c_p \\
Symmetric & & &
\end{bmatrix}$$

$$\begin{bmatrix}
..... & -K_{pN}(t)\cos\psi_N \\
..... & K_{rpN}(t)\sin\psi_{rN}\sin\alpha_r \\
..... & K_{spN}(t)\sin\psi_{sN}\sin\alpha_s \\
..... & -K_{rpN}(t)\sin\alpha_r\sin\alpha_s \;\; -K_{spN}(t)\sin^2\alpha_s+k_{pN}+k_p \\
..... & -K_{rpN}(t)\sin\alpha_r soc\alpha_r \;\; -K_{spN}(t)\sin^2\alpha_s+k_{pN}+k_p
\end{bmatrix} \qquad \text{(C18)}$$

$$C_{23}=\begin{bmatrix}
0 & 0 & 0 & -C_{pi}(t)\cos\psi_i \\
0 & -\sum_{i=1}^{N} C_{rpi}(t)\sin\psi_{ri}\cos\psi_{ri} & 0 & C_{sp1}(t)\sin\psi_{si}\sin\alpha_s \\
0 & 0 & -\sum_{i=1}^{N} C_{spi}(t)\sin\psi_{si}\cos\psi_{si} & C_{sp1}(t)\sin\psi_{si}\sin\alpha_s \\
-C_{pi}(t)\sin\psi_i & C_{rpi}(t)\cos\psi_{ri}\sin\alpha_s & -C_{spi}(t)\cos\psi_{Si}\sin\alpha_s & C_{rp1}(t)\cos\alpha_r\sin\alpha_s+C_{sp1}(t)\cos\alpha_s\sin\alpha_s \\
\vdots & \vdots & \vdots & \vdots \\
\vdots & \vdots & \vdots & \vdots \\
-C_{pN}(t)\sin\psi_N & C_{rpN}(t)\cos\psi_{rN}\sin\alpha_s & -C_{spN}(t)\cos\psi_{SN}\sin\alpha_s & C_{rpN}(t)\cos\alpha_r\sin\alpha_s+C_{spN}(t)\cos\alpha_s\sin\alpha_s
\end{bmatrix}$$

$$\begin{bmatrix}
..... & -C_{pN}(t)\cos\psi_N \\
..... & C_{spN}(t)\sin\psi_{sN}\sin\alpha_s \\
..... & C_{spN}(t)\sin\psi_{sN}\sin\alpha_s \\
..... & C_{rpN}(t)\cos\alpha_r\sin\alpha_s+C_{spN}(t)\cos\alpha_s\sin\alpha_s \\
\vdots & \vdots \\
\vdots & \vdots \\
..... & C_{rpN}(t)\cos\alpha_r\sin\alpha_s+C_{spN}(t)\cos\alpha_s\sin\alpha_s
\end{bmatrix} \qquad \text{(C19)}$$

$$C_{33}=\begin{bmatrix} -\sum_{i=1}^{N} C_{pi}(t)\sin^2\psi_i-\sum_{i=1}^{N} C_{pi}(t)\cos^2\psi_i+c_c & 0 & 0 & -C_{pi}(t)\sin\psi_i \\ & \sum_{i=1}^{N} C_{rpi}(t)\cos^2\psi_{ri}+c_r & 0 & -C_{rp1}(t)\sin\psi_{ri}\sin\alpha_r \\ & & -\sum_{i=1}^{N} C_{spi}(t)\cos^2\psi_{si}+c_s & -C_{sp1}(t)\cos\psi_{s1}\cos\alpha s \\ & & & C_{rp1}(t)\cos\alpha_r soc\alpha_s+C_{sp1}(t)\cos^2\alpha_s+c_p \\ \mathit{Symmetric} & & & \end{bmatrix}$$

$$\begin{matrix} \ldots\ldots & -C_{pN}(t)\sin\psi_N \\ \ldots\ldots & -C_{rpN}(t)\sin\psi_{rN}\sin\alpha_r \\ \ldots\ldots & -C_{spn}(t)\cos\psi_{sN}\cos\alpha s \\ \ldots\ldots & C_{rpN}(t)\cos\alpha_r soc\alpha_s+C_{spN}(t)\cos^2\alpha_s+c_p \\ \ldots\ldots & C_{rpN}(t)\cos\alpha_r soc\alpha_s+C_{spN}(t)\cos^2\alpha_s+c_p \end{matrix}\Bigg] \quad \text{(C20)}$$